Technische Universität München

Fakultät für Medizin

Effects of the loss of *Sfrp1* in the stromal compartment on the hematopoietic system

Franziska Hettler

Vollständiger Abdruck der von der Fakultät für Medizin der Technischen Universität München zur Erlangung des akademischen Grades einer

Doktorin der Naturwissenschaften (Dr. rer. nat.)

genehmigten Dissertation.

Vorsitzender: Prof. Dr. Heiko Lickert

Prüfende der Dissertation: 1. apl. Prof. Dr. Robert A. J. Oostendorp

2. TUM Junior Fellow Dr. Matthias Heinig

Die Dissertation wurde am 27.09.2021 bei der Technischen Universität München eingereicht und durch die Fakultät für Medizin am 07.06.2022 angenommen.

Table of contents

List of Abbreviations

ABL	abelson tyrosine kinase
ACK	ammonium chloride-potassium bicarbonate
AGM	aorta-gonadal mesonephros
ALCAM	activated leukocyte cell adhesion molecule
ALL	acute lymphocytic leukemia
AML	acute myeloid leukemia
ANGPT1	angiopoietin 1
ANOVA	analysis of variance
APC	adenomatous polyposis coli
BCR	B cell antigen receptor
BFR/BS	bone formation rate per bone surface
BH	Benjamini-Hochberg multiple testing correction
BM	bone marrow
BMSCs	bone marrow stromal cells
bp	base pair
BrdU	bromodeoxyuridine
BSA	bovine serum albumin
BV	bone volume
CBA	cytokine beads assay
CBP	cAMP-response element-binding protein (CREB)-binding protein
cDNA	complementary DNA
CE	critical exon 2
CFU	colony-forming unit
CFU-Fs	colony-forming unit fibroblasts
CLL	chronic lymphocytic leukemia
CLP	common lymphoid progenitor cells
CM	conditioned medium
CML	chronic myelogenous leukemia
CMP	common myeloid progenitor cells
Col1	collagen 1
CRD	amino-terminal cysteine-rich
CRE	CRE recombinase
Ct	threshold cycle
CTGF	connective tissue growth factor
CTNNB1	catenin Beta 1
CTSK	cathepsin K

CTX-I	C-terminal telopeptide of type I collagen
CXCL12	chemokine (C-X-C motif) ligand 12
CXCR4	alpha-chemokine receptor specific for stromal-derived-factor-1
DAPI	4.6-diamino-2-phenylindole dihydrochloride
DEGs	differentially expressed genes
DESeq2	DEG analysis based on the negative binomial distribution
DKK	dickkopf-related protein family
DMEM	dulbecco's Modified Eagle Medium
DMF	dimethylformamid
DMSO	dimethyl sulfoxide
DNA	deoxyribonucleic acid
DNase	desoxyribonuklease
dNTP	2'-Desoxyribonucleosid-5'-triphosphat
DPBS	dulbecco's phosphate buffered saline
dsDNA	double-stranded deoxyribonucleic acid
DYRKs	dual specificity YAK1-related kinases
E.coli	*Escherichia coli*
E13.5	embryonic day 13.5
ECs	endothelial cells
EDTA	ethylenediaminetetraacetic acid
EIF-3	eukaryotic initiation factor-3
EL	embryonic liver
ELISA	enzyme linked immunoabsorbent assay
EMP	erythromyeloid progenitors
env	envelope
ER	endoplasmic reticulum
ERAD	endoplasmic-reticulum-associated protein degradation
ES	embryonic cells
ESC	embryonic stem cells
et al.	et alii
EVI	receptor EVI (Wls/GPR177)
EZH2	enhancer of zeste homolog 2
FACS	fluorescence activated cell sorting
FCS	fetal calf serum
FDR	false discovery rate
FL	fetal liver

FLP	flippase
FLT3L	FMS-related tyrosine kinase 3 ligand
FS	forward scatter
FZD	frizzled
g	gram
G-CSF	colony stimulating factor
gDNA	genomic DNA
GFP	green fluorescent protein
GMP	granulocyte-monocyte precursor
GO	gene ontology
Gy	gray (1 Gy=1 J/kg)
HAT	histone acetyltransferase
HBSS	hank's buffered salt solution
HCl	hydrochloric acid
HEPES	4-(2-hydroxyethyl)-1-piperazineethanesulfonic acid
HM	hydrophobic motif
HRP	horseradish peroxidase
HS	horse serum
HSCs	hematopoietic stem cells
i.h.	intra-hepatic
i.v.	intravenous
IF	immunocytofluorescence
IFN-γ	Interferon-γ
IL-11	Interleukin-11
IL-12p70	Interleukin-12p70
IL-6	Interleukin-6
IL-7	Interleukin-7
IMDM	Iscorve's modified Dulbecco's medium
IRES	internal ribosomal entry site
IT	intermediate-term repopulating
IVC	individually ventilated cages
kb	kilobases, 1000 base pairs
kDa	kilodalton
KIT	tyrosine-protein kinase KIT or CD117
KM	Knochenmark
KO	Knock-out

L	Liter
LB	lysogeny broth
LDL	lipoprotein
Lin	lineage
LMPP	lymphoid primed multipotent progenitors
LN	lymph node
logFC	logFoldChange
LPL	lipoprotein lipase
LPS	lipopolysaccharide
LSC	leukemic stem cells
LSK	$Lin^{-}SCA\text{-}1^{+}Kit^{+}$
LT-HSCs	long-term hematopoietic stem cells
LT-HSZs	hämatopoetische Stammzellen
LTC-IC	long-term culture-initiating cell
MAR	mineral apposition rate
MCP-1	Monocyte Chemoattractant Protein-1
MDS	myelodysplastic syndrome
MEFs	mouse embryonic fibroblasts
MEP	megakaryocyte-erythrocyte precursor
$MgCl_2$	magnesium chloride
min	minutes
ml	milliliter
mM	millimolar
MPD	myeloproliferative disorder
MPP or MPs	multipotent progenitor cells
mRNA	messenger ribonucleic acid
MS/BS	mineral surface per bone surface
MSCs	mesenchymal stromal cells
MSPCs	mesenchymal stem and progenitor cells
MSZs	mesenchymale Stromazellen
MVs	myeloische Vorläufer
n	number
NaB	di-sodium tetraborate
NaCl	sodium chloride
NES	nuclear exporting signal
NFAT	nuclear factor of activated T-cells

NGF	nerve growth factor
Nkd	protein naked cuticle
NLS	nuclear localization signals
NTR	carboxy-terminal netrin
OBCs	osteoblastic lineage cells
OD	optische Dichte
OPN	osteopontin
Osx-Cre	*Osx1-GFP::Cre*
P/S	penicillin/streptomycin
p	passage
P1NP	procollagen type I propeptide
PB	peripheral blood
PCA	principle component analysis
PCP	planar cell polarity
PCR	polymerase chain reaction
PDGFRA	platelet-derived growth factor subunit A receptor
PFA	Paraformaldehyde
Ph	Philadelphia chromosome
pH	pondus Hydrogenii
PI	propidium-jodid
PKC	protein kinase
PTK7	protein tyrosine kinase
PTN	pleiotrophin
PVDF	polyvinylidene difluoride
PW	pulse width
RER	rough endoplasmic reticulum
RNA	ribonucleic acid
RNAseq	ribonucleic acid sequencing
ROR	tyrosine kinase-like orphan receptor
rpm	rounds per minute
Rspo	R-spondin
RT-qPCR	real-time quantitative PCR
RYK	receptor tyrosine kinase
s.c.	subcutaneous
SA	senescence-associated
SCF	stem cell factor

scRNA	small cytoplasmatic ribonucleic acid
SD	standard deviation
SDS-PAGE	sodium dodecyl sulphate–polyacrylamide gel electrophoresis
SER	smooth endoplasmic reticulum
SFRP1	Secreted frizzled-related protein 1
SFRP2	Secreted frizzled-related protein 2
SP	spleen
SPECS	secretome protein enrichment with click sugars
SPF	specific-pathogen-free
SS	sideward scatter
ST-HSCs	short-term hematopoietic stem cells
TCF	T-cell factor
TCF/LEF	T cell factor/lymphoid enhancer factor
TMM	trimmed mean of M-values
TNF	tumor necrosis factor
TPO	thrombopoietin
TRAP	tartrate-resistant acid phosphatase
Tris	2-Amino-2-(hydroxymethyl)-propane-1,3-diol
Tween 20	poly(oxyethylen)n-sorbitan-monolaurate
UG	urogenital ridges
UV	ultra violet
V	volt
VCAM-1	vascular cell adhesion protein 1
VCP	valosin-containing protein
WB	western blot
WBC	white blood cells
WIF-1	WNT inhibitory factor-1
WNT3a	wingless-type MMTV integration site family member WNT3a
WNT5a	wingless-type MMTV integration site family member WNT5a
WT	wildtype
X-Gal	β D- galactopyranoside
ZPF	Zentrum für präklinische Forschung
µCT	micro-CT
µg	microgram
µl	microliters
µm	micrometer

1. Introduction

1.1. Hematopoiesis

Blood is a fundamental organ for the human body that has several important tasks, such as delivering nutrients and oxygen to tissues, evenly distributing body heat, transporting of hormones and other messenger substances. Furthermore, blood cells defend organisms against pathogens and initiate the first phases of wound healing. The blood system consists of different cells, including erythrocytes, platelets, T and B lymphocytes, natural killer cells, granulocytes, monocytes and dendritic cells (Orkin & Zon, 2008). The development of the cellular components of the blood is called hematopoiesis (Boulais & Frenette, 2015; Jagannathan-Bogdan & Zon, 2013). This developmental process is structured as a hierarchy, atop are hematopoietic stem cells (HSCs), from which all other blood cells develop (Orkin & Zon, 2008).

Historically, hematopoiesis was already found to mainly take place in the bone marrow (BM) in 1868 (Neumann, 1868). The stem cell concept was proposed a few years later by Ernst Haeckel (Haeckel, 1877), who stated that: "The name ‘stem cell’ seems to me the most simple and appropriate one, because all other cells stem from it …" (Haeckel, 1877; Maehle, 2011). The developmental division of the cellular components of the blood from embryo to adult into primitive and definitive was described first in erythropoiesis (Rifkind, Chui, & Epler 1969), and later for hematopoiesis (reviewed by (Galloway & Zon, 2003)).

1.1.1 Embryonic hematopoiesis

In the mouse embryo, the hematopoiesis starts with the formation of primitive red blood cells, this includes an erythroid progenitor. The erythroid progenitor cells occur for the first time in blood islands in the extra-embryonic yolk sac on day 7.5 of embryonic development (E7.5) (Medvinsky, Rybtsov, & Taoudi, 2011; Orkin & Zon, 2008; Palis et al., 1999; Palis & Yoder, 2001). The primitive erythrocytes have a nucleus and are large compared to the definitive erythrocytes. In primitive hematopoiesis, a few white blood cells are also produced, like the first macrophages and megakaryocytes. Erythromyeloid progenitors (EMPs) also emerge in the yolk sac, but can also be found to differentiate in the fetal liver (Cumano & Godin, 2007; Frame, McGrath, & Palis, 2013). The circulation of the cells between intra- and extra-embryonic tissues starts at E8.5. At this time point, progenitors from all lineages can already be identified in the blood (Palis et al., 1999).

Definitive hematopoiesis takes place in different regions of the embryo, which contains HSCs which differentiated into all mature lineages (McGrath et al., 2015). The first definitive HSCs, which have the ability to engraft in irradiated WT-recipients and regenerate the whole hematopoiesis can be isolated on day E10.5 from the aorta-gonadal mesonephros (AGM) region as well as the placenta and the yolk sac (McGrath et al., 2015; Müller et al., 1994). From day E11.5 - 12.5, the HSCs migrate into the fetal liver (FL), expand and differentiate into progenitor cells until birth via the bloodstream (de Bruijn et al., 2002; Medvinsky et al., 2011). From day E16.5 to the first two weeks after birth, the HSCs migrate from the liver into the bone marrow (Cumano & Godin, 2007; Dzierzak & Speck, 2008; Ma et al., 1998; Pietras, Warr, & Passegué, 2011). After colonization, using various cytokines and chemokines, such as the chemokine signaling pathway of CXCR4-CXCL12, HSCs switch their cell division and proliferation activity to a quiescent cellular state (Bowie et al., 2007; Kim, Saunders & Morrison, 2007; Laird, von Andrian, & Wagers, 2008; McGrath et al., 2011; Wilson et al., 2008).

1.1.2 Adult hematopoiesis

HSCs are a heterogeneous and at the same time rare population of functionally undifferentiated cells. The bone marrow provides a suitable growth environment in which the HSCs can self-renew and differentiate themselves. This is important for maintaining blood cell homeostasis in the blood of adults. Moreover, HSCs self-renew or self-maintain to fully regenerate the functional tissue after injury, inflammation, cancer and during aging (Boulais & Frenette, 2015; Geiger, de Haan, & Florian, 2013; Loeffler & Roeder, 2002; Schreck et al., 2014). HSCs reside in the bone marrow surrounded by other cells within the microenvironment, also called niche. In the niche, most HSCs are in a dormant state, also known as G0 state. Normally, the dormant HSCs are recruited slowly to prevent premature stem cell exhaustion. HSCs can be rapidly activated and enter the cell cycle by extrinsic signals (Boulais & Frenette, 2015; Essers et al., 2009; Schofield, 1978; Takizawa & Manz, 2017; Wilson et al., 2008).

1.1.3 Stem cell hierarchy

The process of differentiation from HSC population to mature lineages can be tracked by subsequent patterns of acquisition or loss of surface markers by flow cytometry and fluorescently labelled monoclonal antibodies. In each hierarchical step, like differentiation, proliferation and self-renewal, the HSCs express specific proteins or carbohydrates on their cell surface (cell surface markers; Figure 1) (Doulatov et al., 2012; Galloway & Zon, 2003; Schreck et al., 2014).

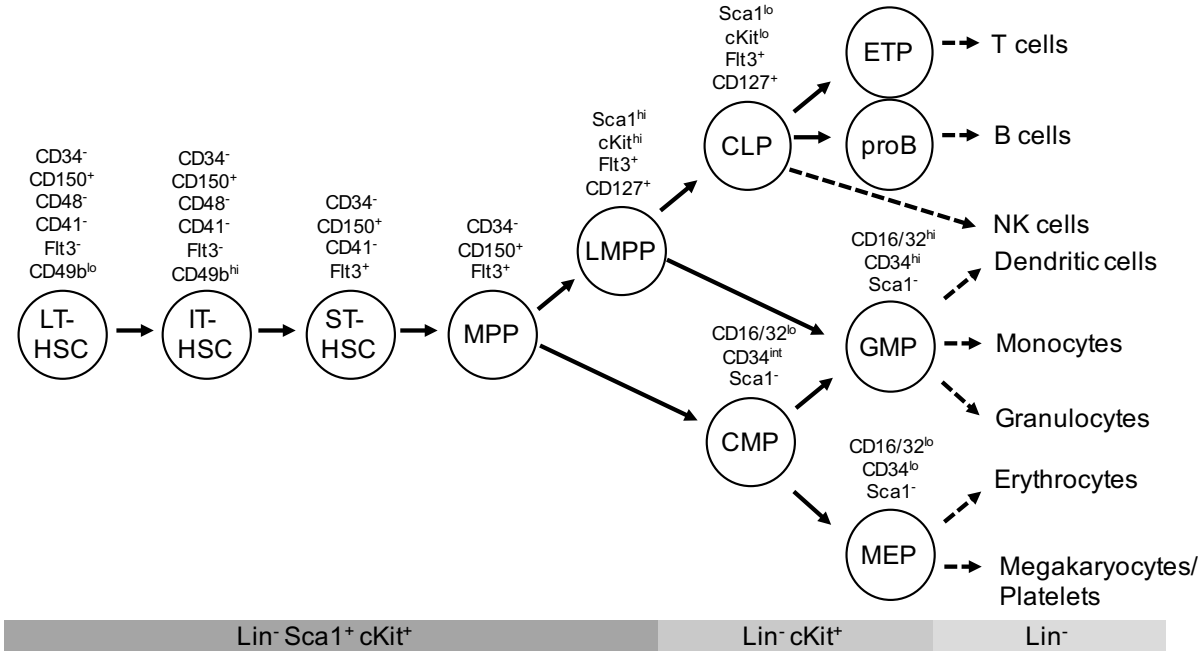

Figure 1. Hematopoietic hierarchy model in the mouse. In the hematopoietic system, long-term HSCs (LT-HSCs) give rise to intermediate-term HSCs (IT-HSCs) and short-term HSCs (ST-HSCs). The differentiation of HSCs gives rise to multipotent progenitors (MPPs) which differentiate into common myeloid progenitors (CMPs) and lymphoid primed multipotent progenitors (LMPPs). Cell differentiation continues into mature lineages. The differentiation from HSC population to mature lineages can be analyzed by cell surface markers (scheme modified based on (Doulatov et al., 2012)).

Mouse HSCs can be sub-classified into multipotent long-term repopulating (LT-) HSCs, intermediate-term repopulating (IT-) HSCs, and pluripotent short-term repopulating (ST-) HSCs. The LT-HSCs are lineage-negative (Lin^{-}), c-Kit^{+}, Sca-1^{+} (LSK), $CD48^{-}$, $CD34^{-}$, $CD150^{+}$ (Doulatov et al., 2012; Ikuta & Weissman, 1992; Kiel et al., 2005; Osawa et al., 1996; Schreck et al., 2014). LT-HSCs form an identical copy of themselves, with all their stem cell properties, and the more differentiated ST-HSC (Morrison & Kimble, 2006; Shizuru, Negrin, & Weissman, 2005; Weissman, Anderson, & Gage, 2001). The ST-HSC has a shorter life span, increasingly loses its ability of self-renewal and can differentiate into multipotent progenitor cells (MPP). The further differentiation into common lymphoid (CLP) or common myeloid progenitor cells (CMP), through different transcription factor activity, leads to all mature blood cell types (Seita & Weissman, 2010; Shizuru et al., 2005; Weissman et al., 2001). T and B lymphocytes, natural killer cells and the antigen-presenting dendritic cells arise from the CLP. The CMP differentiate either to granulocyte-monocyte precursor (GMP) cells or to megakaryocyte-erythrocyte precursor (MEP) cells. The GMP differentiate into granulocytes, monocytes and dendritic cells and the MEP into erythrocytes and platelets (Shizuru et al., 2005; Weissman et al., 2001).

1.2. Microenvironment of hematopoietic stem cells

The majority of the HSCs are located in "the bone marrow niche", first termed by Schofield in 1978 (Schofield, 1978). The adult bone marrow niche is a heterogeneous structure which contains different cell types like the hematopoietic lineage, neural and vascular cells, as well as endothelial cells (ECs) and non-hematopoietic multipotent bone marrow stromal cells (BMSCs). Different investigators demonstrated that HSCs are in cell-cell interaction with BMSCs (Crippa & Bernardo, 2018; Méndez-Ferrer et al., 2010), ECs (Li et al., 2003; Mendelson & Frenette, 2014; Ohneda et al., 1998), endosteal arterioles (Kunisaki et al., 2013) and osteoblasts (OBCs) (Calvi et al., 2003; Taichman & Emerson, 1998; Taichman, Reilly, & Emerson, 2000; Zhang et al., 2003). The cell-cell interaction of the HSCs and the niche cell populations regulate the balance of self-renewal and differentiation of the stem cells, along with signaling molecules and the extracellular matrix (Boulais & Frenette, 2015; Fröbel et al., 2021; Lo Celso & Scadden, 2011; Ohlstein et al., 2004; Schofield, 1978; Schreck et al., 2014; Wilson & Trumpp, 2006).

Consequently, it was shown that HSCs are supported by primary endothelial cells, which promote the maintenance and differentiation of HSCs *in vitro* (Li et al., 2003; Ohneda et al., 1998). Different investigators demonstrated that OBCs promote the expansion of primitive human hematopoietic cells *in vitro* (Taichman & Emerson, 1998; Taichman et al., 2000), as well as promoting the engraftment of HSCs *in vivo* (El-Badri et al., 1998).

Furthermore, it was demonstrated that BMSCs have the potential to differentiate into multiple lineages, like osteogenic- and chondrogenic-, as well as adipogenic-lineages (Chamberlain et al., 2007; Gazit et al., 2008; Morrison & Scadden, 2014) and support the homeostasis of the HSCs (Crippa & Bernardo, 2018). BMSCs can derive from both mesenchymal and neuroectoderm sources (Isern et al., 2014) and in the adults, they are a part of the bone marrow stroma (Pittenger et al., 1999).

The “International Society for Cellular Therapy” defined human BMSCs as “plastic-adherent when maintained in standard culture conditions, […] express CD105, CD73 and CD90, and lack of expression of CD45, CD34, CD14 or CD11b, CD79a or CD19, and HLA-DR surface molecules” and “must differentiate to osteoblasts, adipocytes and chondroblasts *in vitro*” (Dominici et al., 2006). Furthermore, it was shown that BMSCs express the vascular cell adhesion protein 1 (VCAM-1) (Short et al., 2001), platelet-derived growth factor subunit A receptor (PDGFRA) (Houlihan et al., 2012; Morikawa et al., 2009), activated leukocyte cell adhesion molecule (ALCAM or CD166) (Bowen et al., 1997) and SCA-1 (Houlihan et al., 2012). The BM endosteal cell subpopulations can be identified by expression of ALCAM and SCA-1 (Nakamura et al., 2010).

OBCs are enriched in the $CD45^-CD31^-Ter119^-ALCAM^+SCA\text{-}1^-$ population. However, immature mesenchymal cells are enriched in the $CD45^-CD31^-Ter119^-ALCAM^-SCA\text{-}1^+$ segment. These $SCA\text{-}1^+$ cells maintain the long-term repopulating activity and dormant phase of the HSCs (Nakamura et al., 2010).

Studying BMSCs has been shown to be a perilous undertaking. The term BMSCs in itself is already controversial (Bianco, Robey, & Simmons, 2008). Furthermore, Stagg et al. demonstrated that the BMSC surface maker expression changes in different *in vitro* conditions (Stagg et al., 2006). Also, the transcriptome of *in vitro* cultured BMSCs differs from freshly isolated BMSCs (Chen et al., 2016). Therefore, the functions of BMSCs *in vitro* are not necessarily the same as those cells *in vivo*. To characterize BMSCs, meticulous analyses must therefore be performed to couple their *in vitro* and *in vivo* behavior. In addition, BMSCs are heterogeneous *in vivo*, as was recently demonstrated in several single cell RNA sequencing (scRNA-seq) analyses.

Dolgalev & Tikhonova reanalyzed and combined recent studies of scRNA-seq of non-hematopoietic compartments of the niche from Baccin et al. (Baccin et al., 2020), Baryawno et al. (Baryawno et al., 2019), Tikhonova et al. (Tikhonova et al., 2019), Wolock et al. (Wolock et al., 2019) and Zhong et al. (Zhong et al., 2020) (Dolgalev & Tikhonova, 2021). All things considered, they reanalyzed over 30.000 cells and defined 14 clusters of subpopulations including arteriolar, arterial and sinusoidal endothelial cells (ECs), adipo- and osteo-mesenchymal stem and progenitor cells (MSPCs), mature and immature osteoblasts (OBCs), chondrocytes, fibroblasts, myofibroblasts, pericytes, smooth muscle cells, Schwann cells and cycling cells (Dolgalev & Tikhonova, 2021). The subpopulations in the niche contribute differently to the regulation of the HSC function.

HSCs are activated by hematological stress and ensure a faster entering of MPPs to the blood stream (Kiel et al., 2005; Morrison & Scadden, 2014; Sugiyama et al., 2006; Wilson et al., 2007). An alteration in the niche cell population could lead to alternated HSCs behavior (Birbrair & Frenette, 2016; Ho & Méndez-Ferrer, 2020), as well as to the development of leukemic stem cells (LSCs). During disease development, HSCs accumulate transforming mutations, undergo clonal selection and finally become LSCs. LSCs interact and modulate niche cells by generating a leukemic niche that supports the rapid developing disease. Consequently, the modified niche co-evolves with the malignant cells (Barcellos-Hoff, Lyden, & Wang, 2013; Baryawno et al., 2019; Geyh et al., 2013; Medyouf et al., 2014; Waclawiczek et al., 2020).

1.2.1 Regulatory signals from the components of the BM microenvironment

In a lifecycle, HSCs divide about five times as a reaction to hematopoietic stress (Wilson et al., 2008). The numerous regulatory signals from the microenvironment, like growth factors and cytokines, interact with HSCs to maintain the balance between dormancy and activation of HSCs.

BMSCs express granulocyte colony-stimulating factor (G-CSF), interleukin 6 (IL-6), interleukin 11 (IL-11), FMS-related tyrosine kinase 3 ligand (FLT3L) and stem cell factor (SCF) (Audet et al., 2002; Ding et al., 2012; Negahdaripour, Nezafat, & Ghasemi, 2016; Paul et al., 1990; Rafii et al., 1997; Yang et al., 2020). Furthermore, scRNA-seq studies confirmed the expression of the chemokine (C-X-C motif) ligand 12 (*Cxcl12*) in a subset of BMSCs, designated CXCL12-abundant reticulocytes (CAR cells) (Baccin et al., 2020; Baryawno et al., 2019; Tikhonova et al., 2019). However, *Scf* is also expressed by OBCs and BMSCs and maintain the long-term repopulation activity of HSCs (Ding et al., 2012; McCarthy, Ledney, & Mitchell, 1977; Mercier, Ragu, & Scadden, 2011). Furthermore, OBCs express osteopontin (OPN), thrombopoietin (TPO), angiopoietin 1 (ANGPT1) and CXCL12 to maintain the repopulation activity of HSCs (Mosteo et al., 2021). However, ANGPT1 and CXCL12 are also expressed by BMSC (Baryawno et al., 2019).

The niche factors SCF, as well as CXCL12 are essential for the maintenance of HSCs. The loss of CXCL12 and SCF in OBCs and BMSCs by a conditional mouse model showed no effect on HSCs. However, the depletion of these two cytokines in the ECs by a conditional mouse model demonstrated an impairment of the HSC maintenance (Ding & Morrison, 2013; Ding et al., 2012).

Oostendorp et al. generated two HSC supportive murine cells lines, UG26-1B6 and EL08-1D2. These cell lines support the maintenance of murine adult BM and human cord blood HSCs. UG26-1B6 support HSCs in co-cultures for four weeks, which successfully engrafted in recipient animals (Oostendorp et al., 2002; Oostendorp et al., 2005). Further studies showed that in a non-contact setting UG26-1B6 maintain HSCs (Buckley et al., 2011; Oostendorp et al., 2005). Furthermore, the secreted factors nerve growth factor (NGF) and collagen 1 (Col1) was identified to stimulate the HSC survival in a serum free medium (SFM) *in vitro* (Wohrer et al., 2014).

Ledran et al. identified secreted frizzled-related protein 1 (SFRP1), SFRP2, pleiotrophin (PTN) and wingless-type MMTV integration site family member (WNT5A), as well as Cathepsin K (CTSK) to be overexpressed in HSC supportive murine stromal cells, EL08-1D2 and UG26-1B6, in comparison to non-supportive cells (Ledran et al., 2008).

Hausinger et al. demonstrated that CTSK is important to maintain HSCs and the lymphopoiesis in both, *in vitro* and *in vivo* (Hausinger et al., 2021). SFRP1 is required for the cycling activity and maintenance of HSCs and hematopoietic progenitor cells (Renström et al., 2009). SFRP2, PTN and WNT5A are also necessary for the maintenance of HSCs (Istvanffy et al., 2011; Ruf et al., 2016; Schreck et al., 2017). The four proteins, SFRP1, SFRP2, PTN and WNT5A, are essential in the WNT signaling pathway. However, they keep HSCs dormant, limit their activation and prevent the HSCs from becoming exhausted (Istvanffy et al., 2011; Renström et al., 2009; Ruf et al., 2016; Schreck et al., 2017).

1.3. WNT signaling pathway

The bone marrow microenvironment secrete molecules like WNT4, WNT5A, WNT10B, which are members of the WNT signaling pathway. In addition, the microenvironment expresses WNT-factor-binding antagonists such as the Dickkopf-related protein family (DKK) and the secreted frizzled-related proteins (SFRPs) (Schreck et al., 2014). Of these families, DKK1 and SFRP1 were reported to regulate cycling activity and maintenance of HSCs (Fleming et al., 2008; Renström et al., 2009). Importantly, the promotor activity of the *Sfrp1* gene, and to a lesser extent of other WNT antagonists, is inhibited by hypermethylation in several types of leukemia and cancer (Jost et al., 2008; Seeliger et al., 2009; Wang et al., 2010). WNT5A was identified to indirectly regulate the hematopoietic cells by the regulation of osteoblast differentiation (Baksh, Boland, & Tuan, 2007; Sesler & Zayzafoon, 2013), as well as regulating the actin cytoskeleton of HSCs (Schreck et al., 2017).

The members of the WNT signaling pathway regulate several processes of preventing senescence, survival, differentiation, proliferation and quiescence of the HSCs and embryonic development (Boulais & Frenette, 2015; Dijksterhuis, Petersen, & Schulte, 2014; Reya & Clevers, 2005; Schreck et al., 2014; Willert et al., 2003). During embryogenesis, the WNT signal induces the formation of stem cells to mature blood cells (Woll et al., 2008). The WNT signaling pathway and its signals can affect the hematopoiesis and lymphopoiesis (Jrid et al., 2020; Luis et al., 2012; Reya & Clevers, 2005; Reya et al., 2003; Staal, Luis, & Tiemessen, 2008) and is essential for the self-renewal of hematopoietic stem cells, as well as neoplastic stem cells (Reya et al., 2003; Zhao et al., 2007). Alterations of the WNT signaling pathway can have strong oncogenic outcomes (Peifer & Polakis, 2000; Zhao et al., 2007) such as multiple solid cancers (Reya & Clevers, 2005; Zhao et al., 2007).

The WNT family involves 19 different secreted cysteine-rich glycoproteins known in vertebrates (Reya & Clevers, 2005; Staal et al., 2008) which bind to frizzled (FZD) receptors of the target cell and induce either the canonical or the non-canonical WNT pathway (Staal et al., 2008). The difference is that the canonical pathway contains the protein β- and γ-catenin, while a non-canonical pathway works independently through other key intermediates depending on calcium ion release, protein kinase activity and small Rho family GTPases (Rao & Kühl, 2010). Furthermore, it was described that the non-canonical pathway antagonizes the canonical pathway (Ishitani et al., 2003; Topol et al., 2003).

1.3.1 Canonical WNT signaling pathway

The most important factor in the canonical WNT signaling pathway is the accumulation of β-catenin in the cytoplasm and the subsequent translocation into the cell nucleus. Nuclear β-catenin acts as a transcriptional coactivator in different transcription complexes, also called the WNT enhanceosome (Fiedler et al., 2015), which governs transcription of WNT signaling gene targets (Komiya & Habas, 2008; Nygren et al., 2007; Patel et al., 2019; Reya & Clevers, 2005).

In the presence of WNT family agonists like the WNT family (WNT1, WNT3A, WNT6, WNT8 or WNT10A) (Greenbaum et al., 2013; James, 2013), the WNT transmembrane receptor Frizzled (FZD) and its co-receptors, low-density lipoprotein receptor-related protein 5 or 6 (LRP5/6) are activated.

The β-catenin destruction complex, which “includes the tumour suppressors AXIN and adenomatous polyposis coli (APC), the Ser/Thr kinases GSK-3 and CK1, protein phosphatase 2A (PP2A), and the E3-ubiquitin ligase b-TrCP” (Stamos & Weis, 2013) regulates the level of transcriptional co-activator β-catenin in the cytoplasm of a cell. It has been shown that there are mutations in the complex associated with the development of malignant disease (Stamos & Weis, 2013). First, AXIN binds to CK1 and GSK3. Afterwards, β-catenin joins the complex by binding to AXIN or APC (Kimelman & Xu, 2006). Then, β-catenin is phosphorylated by CK1 at position serine 45 and thereby prepares the phosphorylation of β-catenin by GSK3 at position threonine 41. As a result, β-catenin is phosphorylated at positions serine 33 and serine 37 by the GSK3, which generates a binding site for β-TRCP. Afterwards, the phosphorylated β-catenin (Serine 33, Serine 37, Serine 45 and Threonine 41) is recognized by β-TRCP and catalyzed by the $SCF^{\beta TRC}$ or the SCF^{Fbwx7} ubiquitin ligase complexes. The degradation of polyubiquitylated β-catenin is done by the 26S proteasome (Anthony et al., 2020; Hwang et al., 2005; Kimelman & Xu, 2006; Stamos & Weis, 2013).

Thus, the destruction complex mediates the destabilizing process of β-catenin and inhibits the expression of the WNT target genes (Figure 2, left) (Anthony et al., 2020; MacDonald, Tamai, & He, 2009; Patel et al., 2019; Rao & Kühl, 2010).

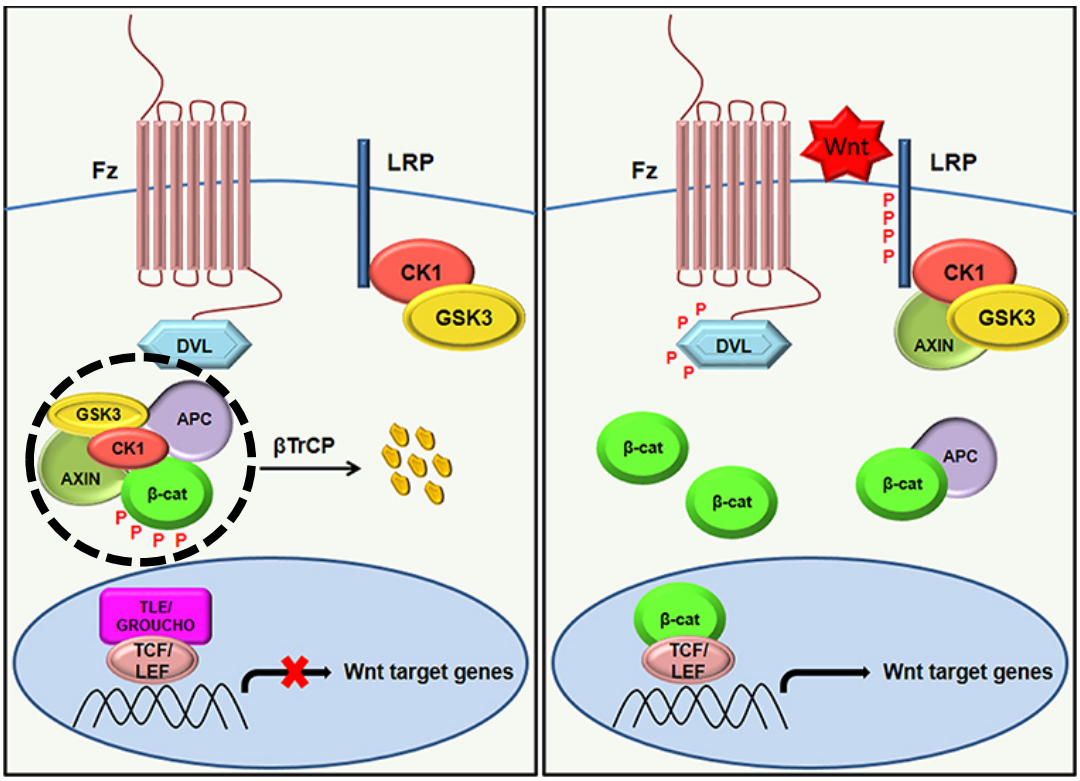

Figure 2. Model of canonical WNT pathway. (left) Scheme for the absence of a WNT ligand in the canonical WNT pathway. The β-catenin destruction complex (dashed line) regulates the level of β-catenin in the cytoplasm of a cell. **(right)** Scheme for the presence of a WNT ligand in the canonical WNT pathway. The β-catenin destruction complex is disrupted by binding of a WNT ligand to the LRP5/6 receptor. β-catenin can enter the nucleus and promotes the transcription of target genes (scheme adapted from (Patel et al., 2019)).

The activation, by binding of a WNT ligand to FZD, LRP5/6 and the cytoplasmic protein Disheveled (DVL) leads to the generation of a signalosome, which suppresses the function of the β-catenin destruction complex (Anthony et al., 2020; Parker & Neufeld, 2020). AXIN binds to DVL, which is the cytoplasmic tail of LRP5/6, and prevents the phosphorylation of β-catenin by GSK3. As a result, β-catenin accumulates in the cytoplasm (Anthony et al., 2020). In addition, β-catenin stabilization is amplified through other pathways, most notably the R-spondin (Rspo) pathway. In this pathway, Rspo activate the LGR receptors and their Znf3/Rnf43 ubiquitin ligase co-receptors. Rspo2 and Rspo3 are both expressed by the microenvironment (Desterke et al., 2020). The precise mechanism of canonical WNT signaling amplification still needs to be unraveled, but it is thought that activation of the Znf3/Rnf43 ubiquitin ligase activity enhances proteolytic degradation of components of the destruction complex.

The mechanism by which β-catenin gets from the cytoplasm to the nucleus is still unclear (Anthony et al., 2020). However, in the nucleus β-catenin binds to the DNA-bound T cell factor/lymphoid enhancer factor (TCF/LEF) and activate the expression of the WNT/TCF target genes (Hua et al., 2018; MacDonald et al., 2009; Nygren et al., 2007; Reya & Clevers, 2005; Staal & Clevers, 2000) (Figure 2, right), by recruiting the transcriptional coactivator proteins (CREB)-binding protein (CREBBP or CBP) or the closely related binding protein p300 (EP300) (Anthony et al., 2020; Hecht et al., 2000; Takemaru & Moon, 2000; Teo et al., 2005).

It was demonstrated that the canonical signaling through WNT3A, GSK3β, and β-catenin is required for the differentiation (Zechner et al., 2003), as well as maintaining the pluripotency in embryonic stem cells (ESCs) (Sato et al., 2004) and HSCs in a dose-dependent manner (Luis et al., 2011). The canonical WNT signaling pathway and β-catenin, as well as the transcriptional coactivator proteins CBP or p300 are essential for the regulation of proliferation and the maintenance, as well as differentiation of stem cells (Fleming et al., 2008; Giles, Peters, & Breuning, 1998; Muroyama, Kondoh, & Takada, 2004; Otero et al., 2004; Peng et al., 2014; Teo et al., 2005; van de Wetering et al., 2002).

1.3.2 Cross signaling with non-canonical WNT signaling pathway

The non-canonical WNT signaling pathway is β-catenin independent and can be separated into two pathways, “the planar cell polarity (PCP) pathway and the Ca^{2+}-dependent pathway” (Lutze et al., 2019). Both pathways can be activated in the presence of WNT ligands like WNT4, WNT5A, WNT5B and WNT11 which binds to non-canonical FZDs and their co-receptors, tyrosine kinase-like orphan receptor (ROR), receptor tyrosine kinase (RYK), or to the protein tyrosine kinase 7 (PTK7) receptor (Figure 3) (Patel et al., 2019; Staal et al., 2008).

The PCP pathway regulates the cell polarity through controlling the asymmetric cell division and asymmetric distribution of proteins within the cell (Sugimura & Li, 2010). The non-canonical WNT/calcium pathway controls the intracellular calcium levels in the cytoplasm and affects the gene transcription by the nuclear factor of activated T-cells (NFAT) (Ackers & Malgor, 2018; Staal et al., 2008; Wong et al., 2003).

The main stimulant for the non-canonical PCP pathway is WNT5A. WNT5A is expressed in stromal cells (Buckley et al., 2011), osteoblast-lineage cells (Maeda et al., 2012), as well as $B220^{+}$ lymphocytes (Liang et al., 2003). Our studies showed that WNT5A is upregulated in the HSC supportive stromal cell line UG26-1B6 (Buckley et al., 2011).

In young HSCs, WNT5A stimulates the non-canonical signaling pathway and thereby regulates the quiescence by controlling the small Rho GTPase Cdc42 activity. Due to the increased expression of WNT5A with increasing age, HSCs shift from canonical to non-canonical WNT signaling pathway (Florian et al., 2013). WNT5A promotes the maintenance of HSCs in the non-canonical pathway but can also inhibit the canonical pathway by promoting β-catenin degradation (Mikels & Nusse, 2006; Nemeth et al., 2007; Topol et al., 2003). Therefore, WNT5A interacts with ROR2 and leads to the activation or repression of the transcription of WNT target genes. Furthermore, the expression of WNT5A increased the level of ROR2. Yuan et al. demonstrated the WNT5A/ROR2 signaling inhibits the canonical pathway (Yuan et al., 2011).

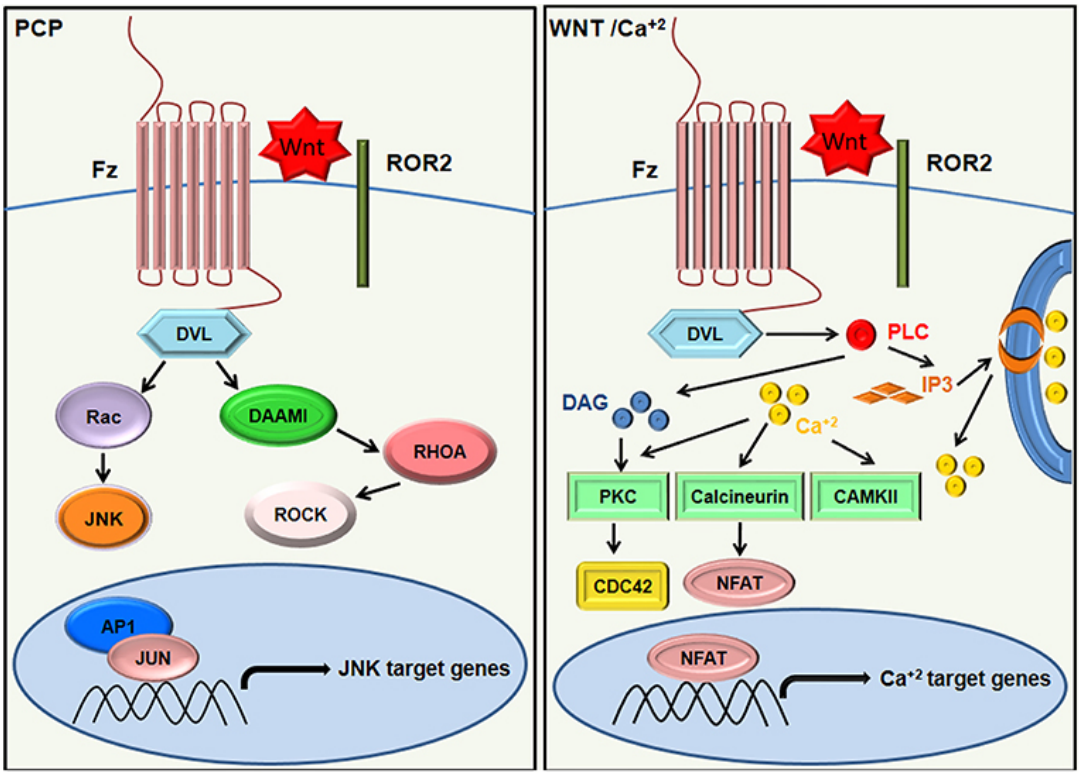

Figure 3. Non - Canonical WNT pathway. (left) Scheme for the non-canonical planar cell polarity (PCP) pathway. **(right)** Scheme for the non-canonical WNT/calcium pathway (scheme adapted from (Patel et al., 2019)).

1.3.3 Transcriptional coactivator proteins p300, CBP and the WNT enhanceosome

Eckner et al. identified the histone acetyltransferase (HAT) p300 as a transcriptional coactivator protein using protein-interaction assays with the adenoviral E1A oncoprotein (Eckner et al., 1994). p300 has a 63 % homology at the amino acid sequence and is closely related to the cAMP-response element-binding protein (CREB)-binding protein (CBP), which was identified as a protein interacting with CREB (Chrivia et al., 1993; Iyer, Ozdag, & Caldas, 2004; Partanen, Motoyama, & Hui, 1999).

The two proteins are particularly homologous in their HAT domain and bromodomain (Anthony et al., 2020; Liu et al., 2008; Zeng et al., 2008). Both proteins are involved in biological processes such as proliferation, differentiation, cell cycle, apoptosis, and DNA damage response (Anthony et al., 2020; Chan & La Thangue, 2001; Giles et al., 1998; Giordano & Avantaggiati, 1999; Goodman & Smolik, 2000; Iyer et al., 2004; Zhong & Jin, 2009).

The main function of a transcriptional co-regulator, such as p300 and CBP, is the interaction with an activator (transcription factor), such as E1A (Bannister & Kouzarides, 1995), E2F (Marzio et al., 2000), Jun (Bannister et al. , 1995), p53 (Avantaggiati et al., 1997; Chan & La Thangue, 2001; Lill et al., 1997), Smads (Pouponnot, Jayaraman, & Massagué, 1998), E6 (Patel et al., 1999) and BRCA1 (Pao et al., 2000) to increase the transcription of a target gene.

Several investigators identified different functions in the regulation of canonical WNT/β-catenin signaling in both, *in vitro* and *in vivo*, for CBP and p300 (Kahn, 2014; Kawasaki et al., 1998; Kung et al., 2000; Ma et al., 2005; Roth et al., 2003; Yao et al., 1998). Rebel et al. identified that CBP is crucial for HSC self-renewal, while p300 is important for the differentiation of hematopoietic cells (Rebel et al., 2002). Teo et al. proposed that in the WNT/β-catenin signaling pathway the balanced complex formation between β-catenin and either CBP or p300 regulates the differentiation and proliferation. The WNT/β-catenin/CBP complex promotes cell differentiation, whereas the WNT/β-catenin/p300 complex promotes cell proliferation (Figure 4) (Teo & Kahn, 2010; Teo et al., 2005).

CBP and p300 are transcriptional co-regulators and interact with a variety of transcription factors. Because of this, they play an important role in many cellular processes, such as proliferation, differentiation and apoptosis. Both, CBP and p300, show a tumor-suppressing effect in hematopoietic cells (Roth et al., 2003). CBP and p300 are part of what is called the WNT enhanceosome, which drives WNT target gene expression (Anthony et al., 2020). The enhanceosome is recruited by Pygo or β-catenin, which bind to LIM and SSDP core proteins and bridge to BCL9 and TCF/LEF. The complex is stabilized through ubiquitin-regulated Gro/TLE. Within this transcriptional complex, CBP or p300 target specific sequences, allowing their transcription (Anthony et al., 2020). Since CBP and p300 share their HAT domain and bromodomain which binds to the enhanceosome, there is a balance between CBP- and p300-directed transcription.

Mutations in these genes and a misbalance of the complex formations are the cause of deregulated WNT target gene transcription, which promote hematopoietic disorders and epithelial tumors (Emami et al., 2004; Gaythe et al., 2000; Goodman & Smolik, 2000; Kung et al., 2000; Ma et al., 2005; Oike et al., 1999; Teo & Kahn, 2010; Teo et al., 2005; Yao et al., 1998).

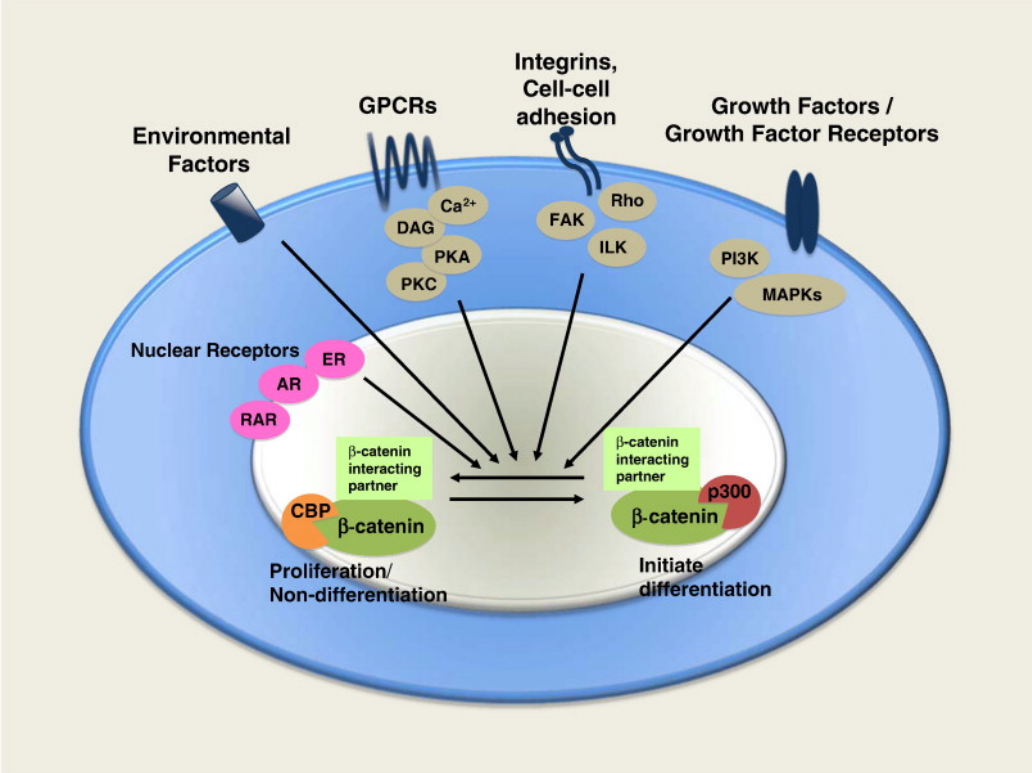

Figure 4. Regulation of proliferation versus differentiation. The WNT/β-catenin/CBP complex promotes differentiation, whereas the WNT/β-catenin/p300 complex promotes proliferation (scheme adapted from (Teo & Kahn, 2010)).

1.3.4 CBP/p300 pathway modulators

Therapeutics that specially target the canonical β-catenin co-activators CBP and p300 is an active field of investigation. Several molecules have been identified that target either CBP or p300, directly or indirectly, even if the two molecules have a homology of 63 % at the amino acid sequence.

Emami et al. identified ICG-001 that direct inhibits the interaction the TCF/β-catenin reporter and CBP, but not the p300/β-catenin interaction. ICG-001 thereby leads to differentiation of the cells (Emami et al., 2004). The potential for a therapeutic usage of CBP–β-catenin antagonist ICG-001 has been analyzed in several preclinical models of leukemia (Gang et al., 2014; He et al., 2014; Wend et al., 2013).

Another direct CBP and β-catenin antagonist is PRI-724, which increases the p300/ β-catenin usage and promotes stem cell differentiation. PRI-724 (C-82), a derivative of ICG-001, generated by Prism Pharma and Eisai Pharmaceuticals (Hirakawa et al., 2019), was previously used in a clinical study (phase I) in patients with solid tumors (El-Khoueiry et al., 2013). Both inhibitors have shown promise in studies aimed at unlocking their therapeutic potential as a drug for targeting cancer stem cells (Chan et al., 2015) for the treatment of endometriosis in preclinical models (Hirakawa et al., 2019).

Higuchi et al. identified YH249/250, the first direct p300/β-catenin antagonists, which has the ability to maintain pluripotency in ESCs (Higuchi et al., 2016) and stimulates the proliferation and survival of HSCs (Zhao et al., 2017). Furthermore, small-molecule antagonists of kinases (ID-8) and phosphatases (IQ-1) were identified to indirectly prevent the interaction of p300 and β-catenin, which tips the balance in favor of CBP to β-catenin in the enhanceosome (Hasegawa et al., 2012; Miyabayashi et al., 2007; Miyabayashi et al., 2008; Schenke-Layland et al., 2011).

The inhibitor ID-8 was identified to maintain human ESCs and promote expansion of long-term pluripotent cells by inhibiting the dual specificity YAK1-related kinases (DYRKs). ID-8 decreases the p300/ β-catenin interaction and indirectly increases the CBP/ β-catenin complex in human ESCs (Hasegawa et al., 2012).

1.3.5 PP2A-mediated modulation of the WNT enhanceosome

With regard to the involvement of p300 in cell proliferation and differentiation, Miyabayashi et al. have demonstrated that specific IQ-1 inhibitors indirectly prevent the interaction of β-catenin with p300, by binding the subunit PR72/130 of the serine/threonine phosphatase PP2A (He et al., 2014; Miyabayashi et al., 2007; Schenke-Layland et al., 2011). The molecule IQ-1 was identified to maintain murine ESCs and provide long-term pluripotent cell expansion by regulating the affinity of p300 for β-catenin and increase β-catenin/CBP usage through regulating the phosphorylation of p300 Ser-89 (Miyabayashi et al., 2007). Other studies demonstrated the increased expansion of murine cardiovascular progenitor cells (Schenke-Layland et al., 2011), as well as the lung epithelium of mouse embryos (Sasaki & Kahn, 2014). He et al. showed that the treatment with IQ-1 promotes the development of cancer cells into a cancer cell subpopulation with a drug resistance and highly tumorigenicity by increasing the CBP/ β-catenin complex (He et al., 2014).

IQ-1 inhibits the protein phosphatase PP2A, which regulates several processes, like intracellular signaling, gene expression, cell proliferation, cell death, and cell cycle activity (Janssens & Goris, 2001; Mumby & Walter, 1993).

The PP2A core enzyme contains a scaffold subunit (A or PR65 subunit) and a catalytic subunit (C subunit). Regulatory subunits, which include four types: B (B55 or PR55), B′ (B56 or PR61), B″ (PR48/PR72/PR130), and B‴ (PR93/PR110), binding to the PP2A core enzyme to form a complex (Figure 5A) (Dzulko et al., 2020; Shi, 2009).

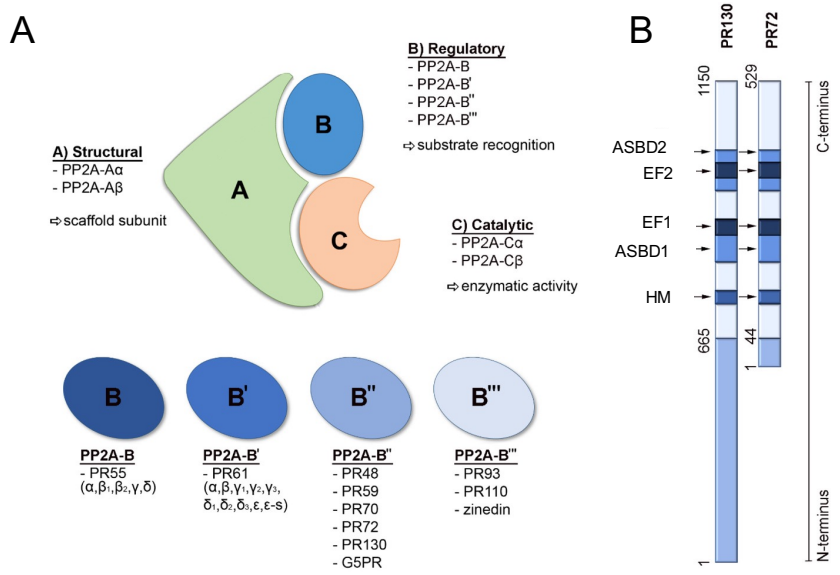

Figure 5. Serine/Threonine phosphatase PP2A and the B-type subunits PR72/PR130. (A) Structure of PP2A contains a scaffold subunit (A or PR65 subunit) and a catalytic subunit (C subunit), as well as a regulatory subunit, like B (B55 or PR55), B′ (B56 or PR61), B″ (PR48/PR72/PR130), and B‴ (PR93/PR110). **(B)** Structure of the subunit PR72 and PR130, which share the same C-terminus that includes two A subunit binding domains (ASBD1/2), two $Ca2^{+}$-binding EF-hand motifs (EF1/2), and a hydrophobic motif (HM; scheme adapted from (Dzulko et al., 2020)).

The subunit PR72/130 (Figure 5B) interact with the protein naked cuticle (Nkd) (Creyghton et al., 2005; Creyghton et al., 2006; Dzulko et al., 2020; Zeng et al., 2000). The subunit PR72/130 controls phosphorylation of p300 (Ser-89), which is important to increase the β-catenin/p300 interaction, in a protein kinase (PKC)-depended manner. The binding of IQ-1 with the subunit PR72/130 disrupts the PP2A/PR72/130/Nkd complex and prevents the interaction of β-catenin with p300 by decreasing the content of phospho-p300 (Ser89) and reduces the p300 complex-mediated differentiation (Figure 6) (Miyabayashi et al., 2007; Rieger et al., 2016).

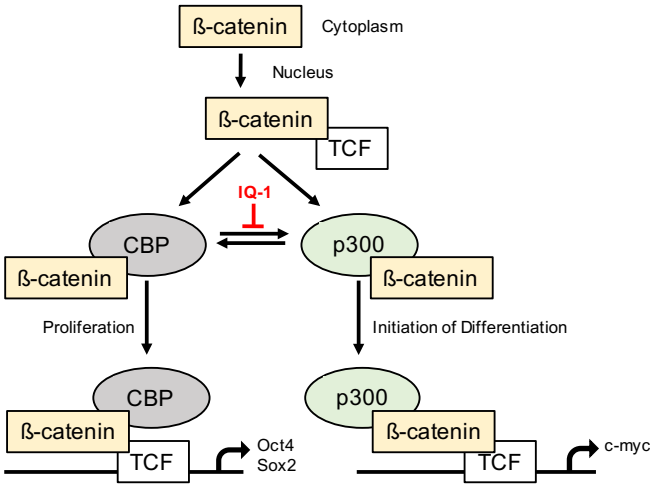

Figure 6. IQ-1 promotes maintenance of embryonic stem cells. Overview of the Wnt/β-catenin coactivator usage model. The β-catenin/CBP interaction is required for the cell proliferation, while the β-catenin/p300-is required for the differentiation of cells. IQ-1 inhibits the interactions of **β**-catenin with p300 (scheme modified based on (Miyabayashi et al., 2007)).

1.4. WNT signaling inhibitors

To guide HSC behavior, the WNT signaling pathways contains (co) receptors, ligands, and inhibitors to generate a balance (Kawano & Kypta, 2003; Luis et al., 2012). Some inhibitors bind directly to WNT ligands like WNT inhibitory factor-1 (WIF-1), some inhibitors bind to FZD receptors like secreted frizzle related proteins (SFRP) and some inhibitors bind WNT co-receptor LRP-5/6 such as Dickkopf homologues (DKK), a member of the Dickkopf (Dkk) family, as well as some inhibitors that interrupt the Frizzled signalosome assembly such as connective tissue growth factor (CTGF) (Hsieh et al., 1999; Kawano & Kypta, 2003). Since the focus of this thesis lies on SFRP1, its role as a WNT signaling mediator will be discussed in more detail.

1.4.1 Secreted frizzled-related protein 1

Secreted frizzled-related protein 1 (SFRP1) is a secreted glycoprotein member of SFRP family of WNT inhibitors in human and mouse. The SFRP family also includes SFRP-2, -3, -4 and -5 (Baharudin et al., 2020; Bovolenta et al., 2008; Kawano & Kypta, 2003). Much like the WNT family members, SFRP1 consists of a carboxy-terminal netrin (NTR) domain and an amino-terminal cysteine-rich (CRD) domain. As mentioned above, WNT ligands like WNT3A bind to FZD receptors and stimulate WNT signaling. In presence of a WNT inhibitor like SFRP1, SFRP1 can modulate WNT signaling pathway through binding to the WNT ligand (Figure 7A), by interact with cytoplasmic β-catenin (Figure 7B), or through binding to the FZD receptors (Figure 7C).

In the absence of SFRP1, the WNT ligand binds to the FZD receptor and promotes the cytoplasmic β-catenin accumulation followed by β-catenin translocation (Figure 7D). SFRP1 can bind directly to the WNT ligand by its NTR domain and prevent the binding of the WNT ligand to the FZD receptor (Figure 7A) (Baharudin et al., 2020; Chong et al., 2002; Lopez-Rios et al., 2008; Renström et al., 2009). Liang et al. showed that SFRP1 can also control WNT signaling by binding to cytoplasmic β-catenin, thereby interfering with binding of β-catenin with T-cell factor (TCF) in the nucleus. Additionally, this inhibition would block further WNT signaling activation (Figure 7B) (Liang et al., 2019). SFRP1 can also bind to the FZD receptor through its CRD domain, which is homologous to the WNT-binding site of FZD receptors, and thereby inhibit the WNT ligand/FZD receptor interaction (Figure 7C) (Agostino & Pohl, 2019; Agostino, Pohl, & Dharmarajan, 2017).

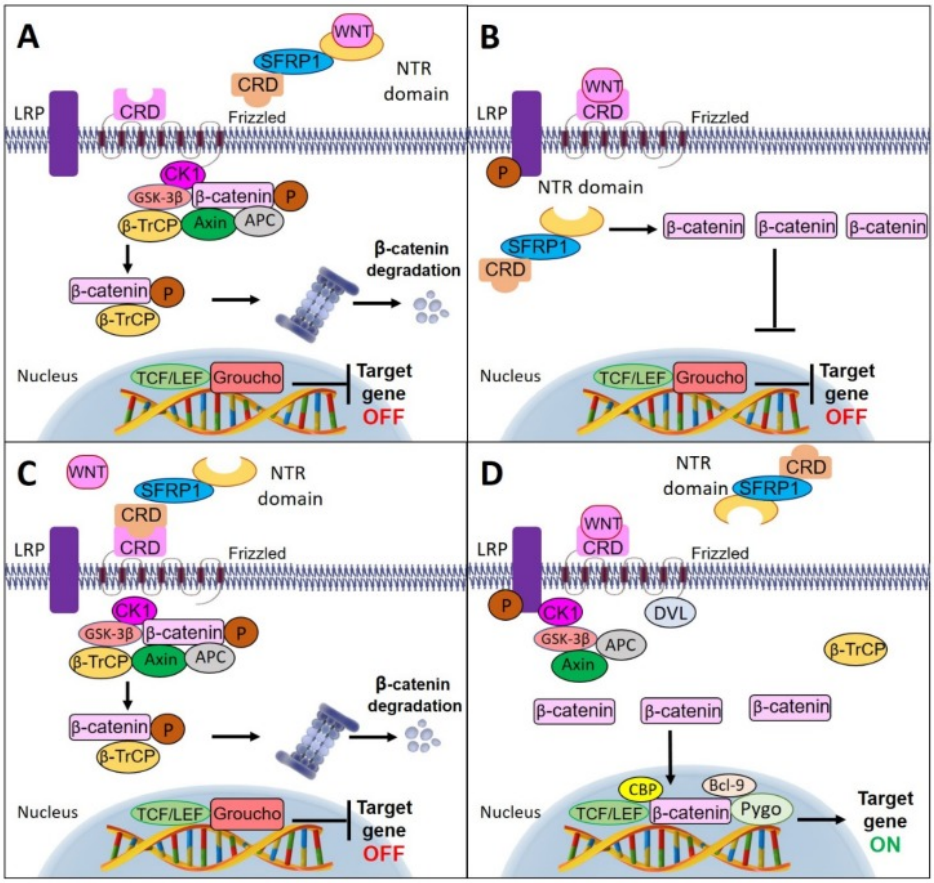

Figure 7. Involvement of SFRP1 in the WNT signaling pathway. (A) In the presence of SFRP1, it binds to the WNT ligand. **(B)** In the presence of SFRP1, it interacts with the cytoplasmic β-catenin. **(C)** In the presence of SFRP1, it binds to the FZD receptor. **(D)** In the absence of SFRP1, the WNT ligand binds to the FZD receptor (scheme adapted from (Baharudin et al., 2020)).

1.4.1.1 SFRP1 in bone marrow cells

The WNT inhibitor SFRP1 is expressed in the kidney (Leimeister, Bach, & Gessler, 1998; Yoshino et al., 2001), brain and skeleton (Häusler et al., 2004; Trevant et al., 2008), as well as bone marrow stromal cells (Dufourcq et al., 2008; Nakajima et al., 2009; Renström et al., 2009). SFRP1 stimulates neovessel formation (Goodwin & D'Amore, 2002), plays a role in the eye field (Kim et al., 2007), is important during cardiomyogenesis and hematopoiesis (Kwon et al., 2007; Naito et al., 2006) and in the adult skeleton (Bodine et al., 2004; Gaur et al., 2005; Gaur et al., 2006). Interestingly, *Sfrp1* expression is regulated by estrogen, and SFRP1 levels vary during the menstrual cycle and pregnancy (Yokota et al., 2008). For this reason, in my experimental work I mostly use male *Sfrp1* mutant mice.

Our group identified SFRP1 as a possible mediator of HSC regulation. We generated murine stromal cell lines which either supported or did not support hematopoiesis in culture (Oostendorp et al., 2002; Oostendorp et al., 2002a). The two most supportive stromal cells: EL08-1D2 and UG26-1B6 supported the long-term maintenance of HSCs from both murine adult bone marrow and human cord blood HSCs (Kunisaki et al., 2013; Oostendorp et al., 2002; Oostendorp et al., 2005). Gene expression comparison of these two HSC supportive stromal cell lines with non-supporting stromal cells, demonstrated that both *Sfrp1* (Ledran et al., 2008; Renström et al., 2009) and its related family member *Sfrp2* (Oostendorp et al., 2005) were over-represented in supportive stromal cells. In the bone marrow microenvironment, SFRP1 is expressed by mesenchymal stromal cells (MSCs) (Dufourcq et al., 2008) and osteoblasts (Dolgalev & Tikhonova, 2021; Nakajima et al., 2009). More recent single cell expression studies confirm that *Sfrp1* expression is mostly restricted to multipotent CXCL12-abundant reticulocytes (CAR cells).

SFRP1 is well known for its role in skeletal maintenance and it stimulates Runx2 for chondrocyte hypertrophy, differentiation of osteoblast and apoptosis of osteocytes (Bodine et al., 2004; Gaur et al., 2005; Gaur et al., 2006).

In hematopoiesis, it was demonstrated that microenvironmental expression of *Sfrp1* regulates cell cycling activity and maintenance of HSCs but decreases the number of MPPs *in vitro* (Nakajima et al., 2009; Renström et al., 2009). Yokota et al. identified SFRP1 in stromal cells as an estrogen inducible gene, which prevents lymphopoiesis. Furthermore, SFRP1 stabilized β-catenin in hematopoietic progenitors (Yokota et al., 2008).

1.5. Leukemia and the bone marrow microenvironment

In the hematopoietic system, HSCs that are mainly in quiescent state reside in the hematopoietic bone marrow microenvironment, which consists of several cell types. The extrinsic signals such as adhesion molecules, cytokines or growth factors from niche cells are critical to control the balance between HSC activation and quiescence. The niche also contributes to the maintenance of leukemic stem cells (LSCs). In the presence of leukemic cells, niche cells show an activated phenotype with a pro-inflammatory signature (Fröbel et al., 2021; Lutzny et al., 2013; Zambetti et al., 2016). However, the molecular events promoting this gene expression signature and how these expressed genes modulate the niche to support leukemic cells and protect leukemic cells against established therapies still have to be elucidated in detail.

HSCs exhaust after repeated stress and over time by enter into the cell cycle which is associated with DNA damage and mutations (Bakker & Passegué, 2013). After each cycle, replication stress persists (Flach et al., 2014; Walter et al., 2015). The accumulation of replication-stress-damaged HSCs can result in increased clonal hematopoiesis (Heyde et al., 2021) and malignant transformation over time (Welch et al., 2012).

Genetic changes in HSCs involving mutations in signaling molecules such as JAK2, RAS, FLT3 or KIT leading to human myeloid malignancies such as acute myeloid leukemia (AML) or chronic myelogenous leukemia (CML) and myelodysplastic syndrome (MDS) (Huntly & Gilliland, 2005; Milosevic & Kralovics, 2013; Rosnet et al., 1996; Woll et al., 2014). LSCs show similarities in regulating mechanisms like normal HSCs, such as self-renewal and differentiation (Kreso & Dick, 2014; Passegué et al., 2003; Reya et al., 2001). Aberrant function of disease-initiating LSCs expel the normal HSCs from their microenvironment (Colmone et al., 2008), which leads to remodeling the niche to a LSC supporting microenvironment (Asada, Takeishi, & Frenette, 2017; Korn & Méndez-Ferrer, 2017; Schepers, Campbell, & Passegué, 2015).

Raaijmakers et al. showed that the deficiency of *Dicer1* in the osteoprogenitors results in MDS initiation (Raaijmakers et al., 2010). In solid tumors, pre-tumorigenic alterations are connected to inflammation and inflammatory myeloid cell recruitment (Mishra et al., 2008). The microenvironment-mediated protection of LSCs contains cell growth signals from cytokines, chemokines, and adhesion molecules to leukemic cells (Ladikou et al., 2020). As a result, the microenvironment protects the LSCs from exposure to chemotherapeutic agents, which can lead to a renewed outbreak of leukemia after effective treatment (Houshmand et al., 2019). One obstacle to treat AML is chemotherapy resistance, which can be triggered by various factors (Kempf et al., 2021).

Kempf et al. demonstrated that the deficiency of the histone methyltransferase enhancer of zeste homolog 2 (EZH2) leads to an upregulation of target genes, whereby an advantage in cell growth occurs, which leads to a resistance against chemotherapy (Kempf et al., 2021). Furthermore, it was shown that samples from human B-cell lymphoma with simultaneous overexpression of USP9X and XIAP have increased chemotherapy resistance, which is rescued by inhibition of either USP9X or XIAP (Engel et al., 2016).

Leukemic cells might arise from genetically altered HSCs or transformed progenitors (Goardon et al., 2011; Reya et al., 2001). Furthermore, HSCs are more dependent than LSCs on signals from the niche for their survival and proliferation (Schepers et al., 2015). The WNT signaling pathway in hematopoietic cells and non-hematopoietic cells is important for the self-renewal of normal and malignant stem cells (Mangolini et al., 2018; Zhao et al., 2007). Indeed, the stimulation of β-catenin by BCR-ABL fusion oncogene was found to modulate both the blastic and the acute phase of CML *in vitro* and in *vivo* (Hu et al., 2016; Zhao et al., 2007). Additionally, Kode et al. demonstrated that AML and MDS patient also showed an accumulation of β-catenin in the nucleus of osteoblasts which results into an increased Notch signaling (Kode et al., 2014). Moreover, it was shown that the Notch2 activity in the MSCs is stimulated by tumor cells, activate the transcription of the complement factor C1q, which thereby inhibits the degradation of β-catenin by Gsk3 in CLL cells (Mangolini et al., 2018).

The transcriptional cofactors p300 and CBP are involved in the WNT signaling pathway. Alternations which leads to a loss of function mutation in these two factors can result in tumorigenesis (Iyer et al., 2004). Therefore, the role of p300 and CBP in hematopoiesis and the development of leukemia was investigated in mouse models. Yao et al. showed that the complete knockout of p300 and CBP in mice leads to an embryonic lethality (Yao et al., 1998), whereas, only the heterozygous CBP knockout mice develop hematopoietic malignancies (Kung et al., 2000). Cheng et al. demonstrated that only p300 acts as a tumor suppressor in the transformation of MDS to AML (Cheng et al., 2017). However, it was demonstrated in mouse models for CML and AML, LSCs become insensitive to both Notch- and TGF-β signaling (Krause et al., 2013; Santaguida et al., 2009). Lane et al. demonstrated in a MLL-AF9 AML transplantation model of a mouse that LSCs were independent of the WNT-derived signaling for localization within the bone marrow compared to healthy HSCs (Lane et al., 2011). Bhatia et al. investigated that the bone marrow stroma of CML patients has reduced ability to support the growth of normal long-term culture-initiating cells (LTC-IC) which is induced by malignant stromal macrophages (Bhatia et al., 1995).

Shirasaki et al. demonstrated that the irradiated NOD/SCID murine bone marrow microenvironment transplanted with CML cell-derived BCR-ABL-carrying myofibroblasts form a LSC environment for the proliferation of CML cells *in vivo* (Shirasaki et al., 2012). Schepers et al. showed that the interaction of LSCs with MSCs remodeled the osteoblastic lineage cells (OBCs) by modification of cytokine signaling pathways, which maintain LSCs in inducible BCR-ABL transgenic CML mice (Schepers et al., 2015). During disease development HSCs that accumulate transforming mutations undergo clonal selection and finally become LSCs. LSCs interact and modulate niche cells by generating leukemic microenvironment that supports the rapid developing disease (Figure 8A). On the other hand, it is also possible that mutations in the bone marrow microenvironment promote hematological malignancies (Figure 8B) (Asada et al., 2017). This statement is supported by the fact that leukemia develops in donor cells after allogeneic stem cell transplantation in patients (Hertenstein et al., 2005; Wiseman, 2011).

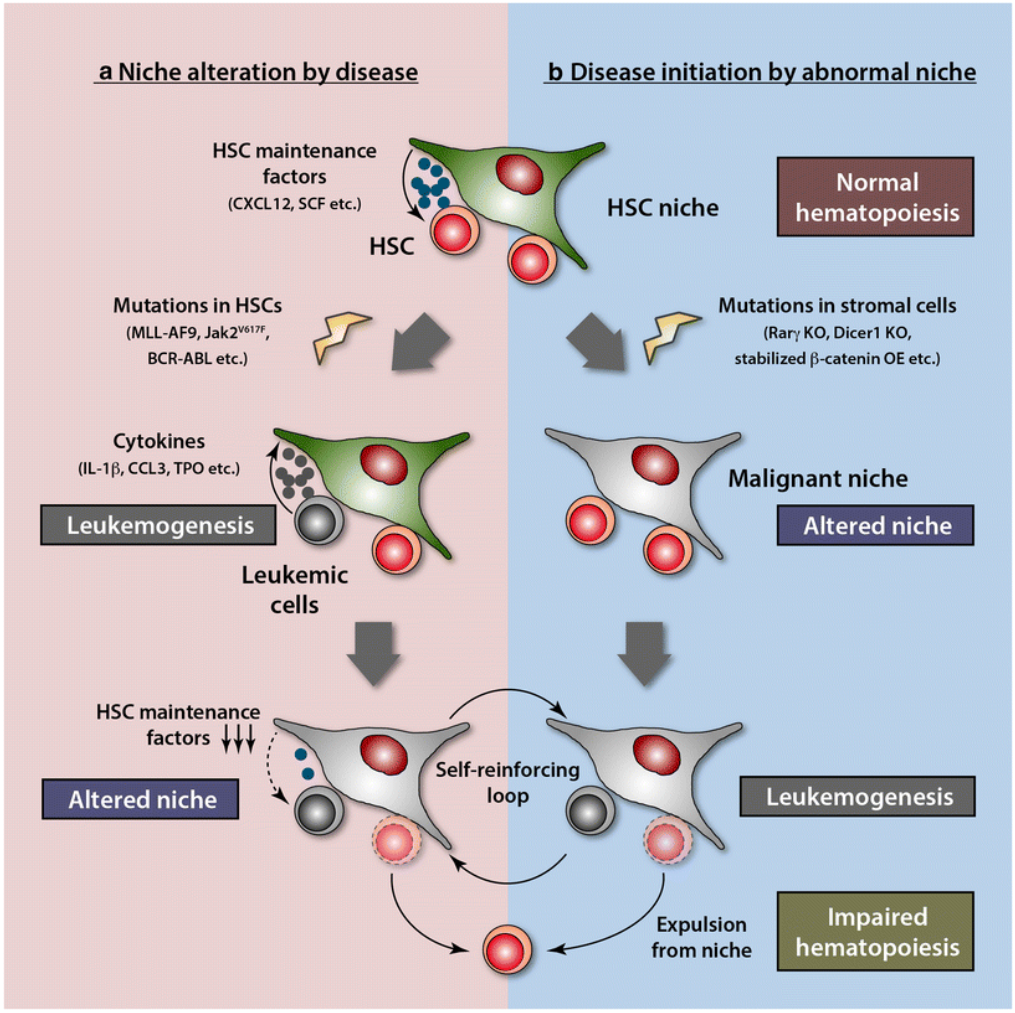

Figure 8. Interaction of leukemic stem cells and the microenvironment. (A) Interaction of leukemic stem cells with the HSC bone marrow microenvironment lead to alternations in the HSC niche and support of LSCs. **(B)** Alternations in the microenvironment initiate hematologic malignancies (scheme adapted from (Asada et al., 2017)).

1.5.1 SFRP1 and cancer

SFRP1 has been identified in many types of cancer as a tumor suppressor gene (Finch et al., 1997; Huang et al., 2007). In numerous human cancers, *SFRP1* expression is downregulated or prone to gene deletions (Figure 9) by either epigenetic silencing or chromosome deletions (Gumz et al., 2007; Takada et al., 2004). Deregulation of *SFRP1* expression leads to downmodulation of the WNT-associated pathways like cell proliferation, migration, fate determination, differentiation, and polarity (Baharudin et al., 2020; Vincent & Postovit, 2017).

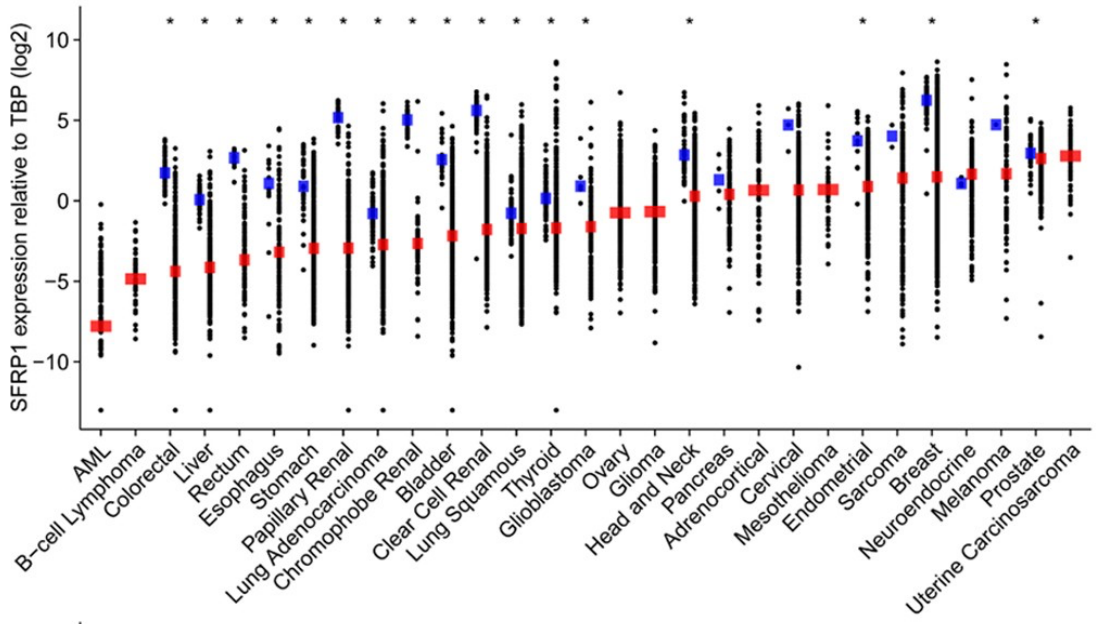

Figure 9. Expression levels of SFRP1 in normal and cancerous tissues in patients. Black data point represents the SFRP1 expression levels of patient samples. Blue bars show median expression for normal samples. Red bars show median expression for tumor samples (scheme adapted from (Vincent & Postovit, 2017)).

Downregulation or loss of the expression of *SFRP1* was found particularly in invasive carcinomas, such as in gastric cancer (To et al., 2001), cervical cancer (Ko et al., 2002), hepatocellular carcinoma (Huang et al., 2007), prostate cancer (Zi et al., 2005), renal cell carcinoma (Dahl et al., 2007; Gumz et al., 2007; Huang et al., 2007) and breast cancer (Bovolenta et al., 2008; Turashvili et al., 2006; Zhou et al., 1998). Ugolini et al. demonstrated that the SFRP1 expression was lost in 78 % of 90 breast cancers samples and 16 % of benign tumor samples (Ugolini et al., 1999).

Additionally, *SFRP1* gene expression also contributes to leukemogenesis, as it is also found to be epigenetically hypermethylated in acute myeloid leukemia (AML) (Jost et al., 2008; Reins et al., 2010), chronic lymphocytic leukemia (CLL) (Liu et al., 2006) and acute lymphocytic leukemia (ALL) (Reins et al., 2010; Román-Gómez et al., 2007), as well as myelodysplastic syndrome (MDS) (Reins et al., 2010). Other studies showed that the stable re-expression of SFRP1 could be a new therapeutic treatment strategy for cancers with downregulation or loss of the expression of *SFRP1* (Cooper et al., 2012; Gumz et al., 2007).

1.5.2 BCR-ABL fusion oncogene

As mentioned above, the BCR-ABL fusion oncogene is a good model to study WNT-dependent oncogenesis through the stimulation of β-catenin by BCR-ABL (1.5 Leukemia and the bone marrow microenvironment). CML is characterized by the observation that over 90 % of all leukemic cells bear the BCR-ABL fusion oncogene.

In normal cells, the Abelson tyrosine kinase (ABL) protein can be found in the nucleus and the cytoplasm of cells. The ABL protein stimulated proliferation, differentiation, survival, death, and migration in response to stress or other signals (Figure 10A) (Ren, 2005; Wang, 2014). ABL-deficient mice showed an increased rate of perinatal mortality, lymphopenia, and osteoporosis, as well as a decreased body size with abnormal development of spleen, head, and eye (Ren, 2005; Schwartzberg et al., 1991; Tybulewicz et al., 1991).

The B cell antigen receptor (BCR) protein is normally found as part of the B-cell receptor complex. BCR contains several modular domains and is involved in signaling pathway for B-cell development and survival through activation, proliferation, and differentiation as well as a proper immune response (Figure 10B) (Dal Porto et al., 2004; Liu et al., 2020). BCR-deficient mice showed a normal development, while the neutrophil respiratory was increased (Voncken et al., 1995).

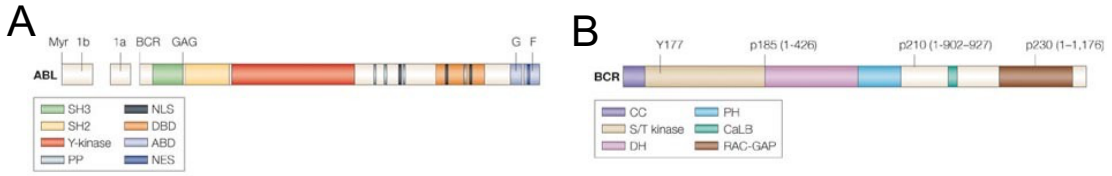

Figure 10. The Abelson tyrosine kinase (ABL) protein and B cell antigen receptor (BCR) protein. (A) Abelson tyrosine kinase (ABL) protein has two isoforms (1a and 1b), five domains (SH3, SH2, Y-kinase, DBD, ABD), four binding sites (PPs), three nuclear localization signals (NLSs) and one nuclear exporting signal (NES). The point at which ABL fuses with BCR is indicated. **(B)** The B cell antigen receptor (BCR) protein contains five domains (CC, S/T, DH, PH, RAC-GAP) and one binding site (CalB). The point in BCR that fuses with ABL is indicated (p185, p210, p230; scheme adapted from (Ren, 2005)).

The fusion protein BCR-ABL, is coded by the Philadelphia chromosome (Ph), which was first described in 1960 by Peter C. Nowell in Philadelphia. He described the Philadelphia chromosome as a minute chromosome present in malignant cells from chronic myelogenous leukemia (CML) patients, which was not found in normal leukocytes (Nowell & Hungerford, 1960a, 1960b). Rowley showed 1973, that the minute chromosome is a result of reciprocal translocation between the long arms of chromosomes 9 and 22 (Rowley, 1973). The exact breakpoints in the reciprocal translocation and RNA splicing generates BCR-ABL proteins with various molecular weights like $p185^{BCR-ABL}$, $p210^{BCR-ABL}$ and $p230^{BCR-ABL}$ (Ren, 2005). The $p210^{BCR-ABL}$ protein is characteristic for CML. In B-cell acute lymphoblastic leukemia (B-ALL), 33.3 % of the patients express $p210^{BCR-ABL}$ protein, whereas 66,6 % of the patients express $p185^{BCR-ABL}$ protein (Deininger, Goldman, & Melo, 2000).

Studies suggest that the developing of CML has two sides, including the effect of BCR-ABL in the cells and the interaction of these cells with the bone marrow microenvironment (Ren, 2005). To analyze the effect of BCR-ABL positive cells *in vivo* several mouse models were developed. The expression of BCR-ABL in murine bone marrow cells through a retroviral transfection and afterwards transplantation into mice stimulated a myeloproliferative disorder (MPD) (Daley, Van Etten, & Baltimore, 1990; Elefanty, Hariharan, & Cory, 1990; Kelliher et al., 1990). It was identified that the retroviral transduction of bone marrow cells with $p185^{BCR-ABL}$ established a B-cell acute lymphoblastic leukemia (B-ALL) with a shorter latency. However, the retroviral transduction of bone marrow cells with $p210^{BCR-ABL}$ established chronic myelogenous leukemia, which verifies the oncogenic activity of BCR-ABL (Li et al., 1999; Reckel et al., 2017).

1.6. Aim of the thesis

Our group has previously shown that HSC supportive murine stromal cells, EL08-1D2 and UG26-1B6, over represent the expression of *Sfrp1* in comparison to non-supportive cells (Ledran et al., 2008; Renström et al., 2009). The summary above states that the extrinsic expression of SFRP1 in the hematopoietic microenvironment is required for the cycling activity and maintenance of HSCs and hematopoietic progenitor cells (Renström et al., 2009). While *Sfrp1* is expressed at a low level by HSCs, high expression levels were described in osteogenic mesenchymal stromal cells within the bone marrow. Unpublished work from our group also shows that *Sfrp1* is expressed in some mature hematopoietic populations.

It is therefore likely that SFRP1 expressed by the osteogenic microenvironment or mature myeloid populations in the bone marrow are involved in the regulation of HSCs. In addition, since epigenetic downregulation and deletion of *SFRP1* has been described, including human leukemia, it is likely that downregulation of SFRP1 levels in niche cells promotes the development or the maintenance of leukemia, or both.

The aim of this thesis was to shed more light on how SFRP1 expression in specific osteogenic mesenchymal cells affects single HSCs and their function *in vitro* and *in vivo*. In addition, it was explored how deletion of *Sfrp1* in osteogenic mesenchymal cells promotes the development of leukemia.

To initiate these studies, *Sfrp1*$^{fl/fl}$ mice were developed to study cell lineage-specific *Sfrp1* deletion using Cre deletor strain (*Osx-GFP::Cre*). In these mice, stem cells were studied under steady state and under stress conditions, such as LPS stimulation. Furthermore, to study proliferation, differentiation, and self-renewal on the single cell level, a novel supportive culture system was developed for single HSCs. As a model of leukemogenesis, the development of BCR-ABL^{+} leukemia was studied in newborn mice with *Sfrp1* gene deletion in stromal cells.

2. Materials

2.1. Consumptions and utensils

Table 1. List of used consumption and utensils.

Utensils	Manufacturers
Aluminum foil for cold storage	VWR life science (USA)
Cell Culture Dish, 10 mm, growth-enhanced treated	TPP Techno Plastic Products AG (CH)
Cell Culture Flasks Cellstar 125 ml/250 ml/550 ml	Greiner Bio-One GmbH (DE)
Cell Culture Plates Cellstar 6, 12, 24, 48, 96 well	Greiner Bio-One GmbH (DE)
CL-Xposure film	Thermo Fisher Scientific Inc. (USA)
Cryogenic vial, 2 ml	Corning Inc. (USA)
Disposable bags	Carl Roth (DE)
Disposable UV cuvettes	Brand GmbH & Co KG (DE)
Eppendorf™ twin.tec™ LoBind 96-Well-PCR-Plate	Eppendorf AG (DE)
Filter Vacuum driven disposable bottle top filter Steritop	Millipore Co. (USA)
Filter 22 µm, 30 µm, 45 µm, 70 µm, 100 µm	BD™ Filcon, BD Bioscience (DE)
Filter tips TipOne 1-10 µl, 20 - 200 µl, 200 - 1000 µl	Starlab (DE)
Freezing container	Mr Frosty ™ - Thermo Fisher Scientific Inc. Cool Cell ® - Bio Cision (USA)
MACS LS cell separation columns	Miltenyi Biotec (DE)
MicroAmp® Fast 96-Well Reaction Plate	Applied Biosystems (USA)
Microcentrifuge safe-lock tubes, 1.5, 2 ml	Eppendorf AG (DE)
4-15 % Mini Protean® TGX Stain-Free™ Protein Gel	Bio Rad Laboratories GmbH (DE)
Monoject, blunt cannula needles	Kendall Healthcare (USA)

Mortar	Thermo Fisher Scientific Inc. (USA)
Needles, 100 Sterican, 27 Gauge	B. Braun Melsungen AG (DE)
Parafilm	Pechiney Plastic Packaging (USA)
Pestle	Thermo Fisher Scientific Inc. (USA)
Polylysine® Slides	Thermo Fisher Scientific Inc. (USA)
Polypropylene centrifuge tubes 15, 50 ml	Greiner Bio-One GmbH (DE)
PVDF-Membrane	Bio Rad Laboratories GmbH (DE)
Round-bottom 96 well plate	Nunc A/S (DK)
Serological Pipettes, 2, 5, 10, 25, 50 ml	Greiner Bio-One GmbH (DE)
S-Monovette Blood Collection System	Sarstedt AG & Co. (DE)
Superfrost Plus™ Adhesion Microscope Slides	Thermo Fisher Scientific Inc. (USA)
Super PAP PEN	Thermo Fisher Scientific Inc. (USA)
Syringes, U-40 Insulin, Omnifix, 1 ml	B. Braun Melsungen AG (DE)
Syringes single-use Omnifix 3/5/10 ml	B. Braun Melsungen AG (DE)

2.2. Machines and equipment

Table 2. List of used machines and equipment.

Machines and equipment	Name	Manufacturers
Animal Blood Counter	Counter Scil Vet Abc™	Scil vet academy (DE)
Autoradiography cassettes	Hypercassette™	GE Healthcare (USA)
Cell Incubator	Hera Cell 240	Heraeus Instruments (DE)
Cell sorter	MoFlo High Speed Astrios S1 ARIA IIIu	Beckman Coulter (DE) Beckman Coulter (DE) BD Bioscience (USA)
Centrifuges	Megafuge 3.0RS, Multifuge 3S Biofuge fresco	Heraeus Instruments (DE) Heraeus Instruments (DE) Heraeus Instruments (DE)

	Sigma 1-14	Sigma Laborzentrifugen GmbH (DE)
Counting chamber	Neubauer-improved	Paul Marienfeld GmbH (DE)
Developing machine	OTIMAX X-Ray Film Processor	PROTECT GmbH & Co. KG (DE)
Dissecting instruments	-	Fine Science Tools GmbH (DE)
ELISA Reader	Multiscan FC	Thermo Fisher Scientific Inc. (USA)
Fluorescence Microscope	Leica DM RBE	Leica, Wetzlar (DE)
Flow cytometer	CyAn ADP LxP8	Beckman Coulter (DE)
Gel Electrophoresis chamber	Biometra Minigel-Twin	Biometra GmbH (DE)
Hamilton Needle	KF 726S Needle (26S/51/2) 6pk 90139	Hamilton (CH)
Hamilton Syringe	type 710N, volume 100 µl, cannula size 22s ga	Hamilton (CH)
Homogenisator	SONOPLUS (HD 2070)	Bandelin electronic (DE)
Ice machine	S.-No:061244	Ziegra Eismaschinen (DE)
Laminar flow hood	ANTAES 48/72	BIOHIT (DE)
Linear accelerator	Mevatron KD2	Siemens (DE)
Microscope	CKX41 Axiovert 25 microscope	Olympus Corporation (Japan) Carl Zeiss (DE)
NanoDrop	NanoDrop™ 2000/c Spectrophotometer	Thermo Fisher Scientific Inc. (USA)
Photometer	SmartSpec™ Plus Spectrophotometer	Bio-Rad (USA)
Precision scales	PLJ 2100-2M	Kern & Sohn GmbH (DE)
QuadroMACS Separator	MACS	Miltenyi Biotec (DE)
Radiation Unit	Gulmay (Typ RS225) Buchler (Typ OB29/902-1)	Gulmay (USA) Buchler GmbH (DE)

Real-Time PCR System	StepOne Plus Real-Time PCR	Applied Biosystems (USA)
Stereomicroscope	Olympus SZ61 Modeel SZ2-ST	Olympus Corporation (Japan)
Stereomicroscope light	Olympus: SCHOTT KL200 S/N 015767	Olympus Corporation (Japan)
Thermal Cycler	PTC 100 Peltier	Bio-Rad (USA)
Thermomixer	comfort	Eppendorf AG (DE)
UV-light Gel-Doc	XR Imaging System	R&D Systems (DE)
Vortex	IKA MS1 minishaker	Werke & Co. (DE)
Water bath	Grant Instruments™ SUB Aqua Pro Water Bath	Fisher Scientific (UK)

2.3. Software

Table 3. List of used software.

Software	Company
AxioVision	Carl Zeiss MicroImaging GmbH
FlowJo, Version 8.8.6.	TreeStar Inc. FlowJo™ Software (for Mac), Ashland, OR: Becton, Dickinson and Company; 2019.
GraphPad Prism, Version 7.0e	Graphpad Software Inc.
Image J, Version: 2.0.0-rc-43/1.50e	Rasband, W.S., ImageJ, U. S. National Institutes of Health, Bethesda, Maryland, USA, https://imagej.nih.gov/ij/, 1997-2018.
Microsoft Excel, Version 2010	Microsoft Inc.
Microsoft Power Point, Version 2010	Microsoft Inc.
Microsoft Word, Version 2010	Microsoft Inc.
Photoshop, Version CS5 Extended 12.0x32	Adobe Inc.
Python, Version 3.8.0	Van Rossum, G. & Drake Jr, F.L., 1995. Python reference manual, Centrum voor Wiskunde en Informatica Amsterdam. Available at http://www.python.org

R	R Development Core Team (2008). R: A language and environment for statistical computing. R Foundation for Statistical Computing, Vienna, Austria. ISBN 3-900051-07-0, Available at http://www.R-project.org.
Step One Software, Version v.2.3	Thermo Fisher Scientific/ Applied Biosystems

2.4. Chemicals

Table 4. List of used chemicals.

Chemicals	Company
Agarose Neo Ultra-Qualität	Carl Roth (DE)
Alizarin Red S	Sigma-Aldrich (DE)
Calcein	Sigma-Aldrich (DE)
Dimethylformamid (DMF)	Sigma-Aldrich (DE)
Dimethyl sulfoxide (DMSO)	SERVA Electrophoresis GmbH (DE)
Diphtheria toxin	Merck Group (DE)
Di-Sodium-tartrate	AppliChem (DE)
Ethanol, 99.8 %	AppliChem (DE)
Ethidium bromide, 1 % solution	Carl Roth (DE)
Ethylenediaminetetraacetic acid (EDTA)	Carl Roth (DE)
Fast Red Violett LB Salt	Sigma-Aldrich (DE)
Glycerol	Sigma-Aldrich (DE)
Hygromycin B	Clontech (FRA)
Isofluran 100 %	CP-Pharma (DE)
Isopropanol	Sigma-Aldrich (DE)
Naphthol-AS-BI-Phospate	Sigma-Aldrich (DE)
Methanol	Sigma-Aldrich (DE)
Oil Red O	Sigma-Aldrich (DE)
Paraformaldehyde (PFA), neutral buffered, 10 %	Sigma-Aldrich (DE)

Polybrene	Sigma-Aldrich (DE)
Propidium-Jodid (PI)	Invitrogen (DE)
SlowFade Gold Antifade Reagent with DAPI	Invitrogen (DE)
Sodium Acetat	Sigma-Aldrich (DE)
Sodium tetraborate derahydrate	Sigma-Aldrich (DE)
SuperSignal® West Pico/Dura/Femto Extended Duration Substrate	Pierce Biotechnology (USA)
Triton X 100	Sigma-Aldrich (DE)
Trypan blue	Invitrogen (DE)
Tween 20	Carl Roth (DE)
UltraPure Dnase/Rnase-Free Distilled Water	Invitrogen (DE)
β-Mercaptoethanol	Invitrogen (DE)

2.5. Biological reagents

Table 5. List of used biological reagents.

Biological reagents	Company
Adipogenic Supplement	R&D Systems (DE)
Albumin Fraction V, ≥ 98 %, bovine (BSA)	Carl Roth (DE)
Borgal solution, 24 %	Virbac (DE)
Bradford Protein Assay	Bio Rad Laboratories GmbH (DE)
Cell Adhere™ Type I Collagene	Stemcell Technologies (DE)
Collagenase Type 1	Worthington Biochemical (USA)
Convenia®	Zoetis (DE)
Deoxyribonuclease I (DNase)	Sigma-Aldrich (DE)
Fetal calf serum (FCS)	PAA (DE)
Gelatin from bovine skin	Sigma-Aldrich (DE)
Gene RulerTM 1 kb Plus Ladder	Invitrogen (DE)
Horse serum (HS)	BioWhittaker (DK)
Human LDL	Stemcell Technologies (DE)

IQ-1 Inhibitor	Selleckchem (USA)
LB Agar	Carl Roth (DE)
LB medium	Carl Roth (DE)
Lipofectamine®2000	Invitrogen (DE)
Lipopolysaccharides (LPS) from *E. Coli*	Sigma-Aldrich (DE)
Metacam®	Boehringer Ingelheim(DE)
mIL-3, mIL-6, mIL-11	R&D Systems (DE)
mSCF	R&D Systems (DE)
Nerve Growth Factor (NGF)	R&D Systems (DE)
Osteogenic Supplement	R&D Systems (DE)
Penicillin/Streptomycin	Invitrogen (DE)
Precision Plus Protein Standards (Dual Color)	Bio Rad Laboratories GmbH (DE)
Protease Inhibitor	Thermo Fisher Scientific Inc. (USA)
Proteinase K	Thermo Fisher Scientific Inc. (USA)
Puromycin	Invitrogen (DE)
Ringer-Lactat-Solution	B. Braun Melsungen AG (DE)
Sodium Orthovanadate	Merck Group (DE)
Trypsin 10x	Invitrogen (DE)
Vista Green DNA Dye	Cell Biolabs (USA)

2.6. Buffers, medium and solutions

2.6.1 Purchased buffers, medium and solutions

Table 6. List of ordered buffer, medium and solutions.

Ordered buffer, media and solutions	Company
Adipogenic/Osteogenic Base medium	R&D Systems (DE)
ACK Lysing Buffer	Thermo Fisher Scientific Inc. (USA)
α-MEM plus GlutaMAX	Invitrogen (DE)
Ampicillin	Sigma-Aldrich (DE)

BIT 9500 Serum Substitute	Stemcell Technologies (DE)
Dulbecco's Modified Eagle Medium (DMEM)	Invitrogen (DE)
Dulbecco's phosphate buffered saline (DPBS)	PAA (DE)
Hank's Buffered Salt Solution, 10x (HBSS)	Invitrogen (DE)
HEPES	Invitrogen (DE)
Iscorve's Modified Dulbecco's Medium (IMDM)	Thermo Fisher Scientific Inc. (USA)
Minimum Essential Medium Eagle	Sigma-Aldrich (DE)
MethoCult™ GF M3434	Stemcell Technologies (DE)
Opti-Mem I Reduced Serum Medium	Invitrogen (DE)
Penicillin/Streptomycin (P/S)	Invitrogen (DE)
RIPA buffer	Pierce Biotechnology (USA)
SOC Medium	Sigma-Aldrich (DE)
2x TCL buffer	Quiagen Inc. (DE)
0.5 % Trypsin-EDTA (10x)	Invitrogen (DE)

2.6.2 Prepared buffers, medium and solutions

Table 7. List of self-made buffer, medium and solutions.

Self-made buffer, media and solutions	Composition
Alizarin Red solution	1mg/ml in deionized H_2O
Alkaline Solution (Comet Assay)	1.2 g NaOH
	0.2 ml EDTA Solution
	→adjust volumne to 100 ml with deionized H_2O
BBMM medium	325 ml IMDM + Glutamax
	150 ml FCS (not heat-inactivated)
	2,5 g BSA
	5 ml L-Glutamin
	2,5 ml Penicillin/Streptavidine (100x)
	1 ml β-Mercaptoethanol
Blocking Buffer (IF)	10 % FCS (heat-inactivated)
	0.1 % Triton-X
	89.9 % PBS

Blocking Buffer (WB)	1 x TBS
	0.1 % Tween 20
	5 % BSA or milk powder
Collagenase digestion buffer	2 ml DMEM with 10% FCS
	200 µl HBSS (10x)
	20 µl Collagenase Type II
	6 µl Dnase I (5mg/ml)
Destain solution	10 % Cetylpyridiumchloride
	10mM Sodiumphosphate
	→at pH 7.0
EDTA solution	0.5 M in deionized H_2O
	→at pH 8.0
Electrophoresis Running Solution (Comet Assay)	12 g NaOH
	2 ml EDTA solution
	→adjust volumne to 1 L with deionized H_2O
FACS buffer (500 ml)	500 ml DPBS
	0.5 % BSA
Freezing medium	10 % DMSO
	FCS (heat-inactivated)
Gelatin solution (1%, 500 ml)	5 g Gelatin powder
	500 ml deionized H_2O
HF2+ buffer (1 l)	10 % HBSS (10x)
	2 % FCS (heat-inactivated)
	0.1 % ml HEPES
	100 U/ml penicillin
	100 mg/ml streptomycin
	86 % deionized H_2O
Lysis Buffer (Comet Assay)	14.6 g NaCl
	20 ml EDTA Solution
	10 ml Lysis Solution (10x)
	10 ml DMSO
	→adjust volumne to 100 ml with deionized H_2O
	→at pH 10.0
MEF, NIH, Phoenix medium (500 ml)	445 ml DMEM (+L-glutamine)
	10 % FCS (heat-inactivated)
	100 U/ml penicillin
	100 mg/ml streptomycin

MSC media (500 ml)	α-MEM plus GlutaMAX
	10 % FCS (heat-inactivated)
	100 U/ml penicillin
	100 mg/ml streptomycin
	10 mM β-Mercaptoethanol
NaB buffer	0.01 M disodium tetraborate
	deionized H_2O
Oil Red O Stock solution	0.5 g Oil Red O
	100 ml Isopropanol
Phoenix media for transfection (500 ml)	445 ml DMEM (+L-glutamine)
	10 % FCS hi
10x Running Buffer	288 g Glycine
	60 g Tris
	20 g SDS pellets
	2 L H2O
Stroma media (500 ml)	α-MEM plus GlutaMAX
	15 % FCS (heat-inactivated)
	5 % HS (heat-inactivated)
	100 U/ml penicillin
	100 mg/ml streptomycin
	10 mM β-Mercaptoethanol
10x TBS	500 mM Tris
	1500 mM NaCl
	→adjust to pH 8 with HCl
Transfer buffer	500 ml 10x Running buffer
	1 L Methanol
	3.5 L H2O
TRAP buffer	1.64 g Sodium acetate
	23 g Di-Sodium-tartrate
	→adjust volume to 500 ml with deionized H_2O
	→at pH 5.0
TRAP-staining solution	40 mg Naphthol-AS-BI-Phosphate
	4 ml Dimethylformacid
	200 ml TRAP buffer
	240 mg Fast Red Violett LB Salt
	2 ml Triton X 100
	→first mix Naphthol-AS-BI-Phosphate and DMF, afterwards add the other reagents

2.7. Preparation and detection kits

Table 8. List of used kits.

Kits	Company
Annexin V Kit	BD Pharming (USA)
APC/FITC BrdU Flow Kit	BD Pharming (USA)
Cytometric Bead Array (CBA) KiT	BD Pharming (USA)
Comet Assay KiT	Cell Biolabs (USA)
Lineage cell depletion Kit (mouse)	Miltenyi Biotec (DE)
pHrodo™ *E.coli* Green BioParticles® Phagocytosis Kit	Thermo Fisher Scientific Inc. (USA)
Power SYBR Green PCR Master Mix	Applied Biosystems (USA)
Quanti Tect Reverse Transcription Kit	Quiagen Inc. (DE)
Qiagen® HiSpeed® Plasmid Maxi Kit	Quiagen Inc. (DE)
Qiagen® Spin Miniprep Kit	Quiagen Inc. (DE)
VWR Red Taq DNA Polymerase Master Mix	VWR life science (USA)
RNeasy Micro Kit	Quiagen Inc. (DE)
Senescence Cells Histochemical Staining Kit	Cell Signaling (USA)
Wizard® Genomic DNA Purification Kit	Promega (USA)

2.8. Primary and secondary antibodies

2.8.1 Primary antibodies flow cytometry

Table 9. List of used primary antibodies for flow cytometry.

Antigens	Clone	Fluorochrome	Volume/1*10^6 cells	Company
Anti-mouse CD3e	145-2C11	PE-Cy5.5	0.1 µl	ebioscience (USA)
Anti-mouse CD4	30-F11	PE-Cy5.5	0.1 µl	ebioscience (USA)

Anti-mouse CD8a	53-6.7	PE-Cy5.5	0.1 µl	ebioscience (USA)
Anti-mouse CD11b	M1/70	APC APC-eFluor®780	0.1 µl	ebioscience (USA)
Anti-mouse CD31 (PECAM-1)	390	APC	0.1 µl	ebioscience (USA)
Anti-mouse CD34	RAM34	FITC	0.1 µl	ebioscience (USA)
Anti-mouse CD45	30-F11	FITC PE PE-Cy5.5. PE-Cy7 eFluor®450 APC APC-eFluor®780	0.1 µl	ebioscience (USA)
Anti-mouse CD45R (B220)	RA3-6B2	PE-Cy7 PE-Cy5.5	0.1 µl	ebioscience (USA)
Anti-mouse CD117 (KIT)	2B8	APC PE	0.1 µl	ebioscience (USA)
Anti-mouse CD150	9D1	APC PE	0.1 µl	ebioscience (USA)
Anti-mouse CD166	eBioALC48	PE	0.1 µl	ebioscience (USA)
Anti-mouse Gr-1 (Ly-6G)	RB6-8C5	eFlour450®	0.1 µl	ebioscience (USA)
Anti-mouse SCA-1	D7	PE PE-Cy7	0.1 µl	ebioscience (USA)
Anti-mouse 67	SolA15	PE-Cy7	1 µl	ebioscience (USA)
Anti-mouse TER119	TER119	PE eFlour450®	0.1 µl	ebioscience (USA)

Biotinylated anti-mouse CD3e	145-2C11	-	0.1 µl	ebioscience (USA)
Biotinylated anti-mouse CD11b	M1/70	-	0.1 µl	ebioscience (USA)
Biotinylated anti-mouse CD48	HM48-1	-	0.1 µl	ebioscience (USA)
Biotinylated anti-mouse B220	RA3-6B2	-	0.1 µl	ebioscience (USA)
Biotinylated anti-mouse Gr1 (Ly-6G)	RB6-8C5	-	0.1 µl	ebioscience (USA)
Biotinylated anti-mouse TER-119	TER-119	-	0.1 µl	ebioscience (USA)

2.8.2 Primary antibodies immunofluorescence and western blot

Table 10. List of used primary antibodies for immunofluorescence.

Antigens	Catalog Nr.	Antibody species	Conc.	Company
Beta catenin (L54E2)	2677s	mouse	1:100	Cell Signaling (USA)
CBP	7389s	rabbit	1:50	Cell Signaling (USA)
gamma H2AX	05-636	mouse	1:50	Upstate/Millipore (USA)
p300 CT	05-257	mouse	1:100	Upstate/Millipore (USA)
phospho-p300 (Ser89)	PA5-12652	rabbit	1:100	Invitrogen (DE)
p-Beta Catenin (S33/37/T41)	9561s	rabbit	1:50	Cell Signaling (USA)
SFRP1	4690S	rabbit	1:100	Cell Signaling (USA)

2.8.3 Secondary antibodies flow cytometry

Table 11. List of used secondary antibodies for flow cytometry.

Reagents	Conjugate	Volume/1x10^6 cells	Company
Streptavidin	eFluor450®	0.1 µl	Invitrogen (DE)

2.8.4 Secondary antibodies immunoflourescence and western blot

Table 12. List of used secondary antibodies for immunofluorescence and western blot.

Antigens	Catalog Nr.	Antibody species	Fluorochrome	Conc.	Company
Mouse	A10036	Donkey	Alexa-Fluor 546	1:500	Thermo Fisher Scientific (USA)
Rabbit	A11010	Goat	Alexa-Fluor 546	1:500	Thermo Fisher Scientific (USA)
Mouse	A11001	Goat	Alexa-Fluor 488	1:500	Thermo Fisher Scientific (USA)
Rabbit	A32731	Goat	Alexa-Fluor 488	1:500	Thermo Fisher Scientific (USA)

2.9. Primer

2.9.1 PCR primer

Table 13. List of PCR primers for genotyping.

Name	Sequence 5´ → 3´
5HA_left	GGAGTCCCTATGGCACTTCA
CCE_right3	AGCTGCTGTGAGTACCTGAA
CE3_left	AAGACGAAGTTCCAGCCTCA
CE3_right	CTCCACAAGGTCACAGCTCA
Sfrp1 del left 4	GGAGTCCCTATGGCACTTCA
Sfrp1 del right 4	GCAGCAGGTGAAGAGAACTG
OSX CRE L	AGGCAGGTGCCTGGACAT
OSX CRE R	CTCTTCATGAGGAGGACCCT
OSX CRE Internal F	CTAGGCCACAGAATTGAAAGATCT
OSX CRE Internal R	GTAGGTGGAAATTCTAGCATCATCC

2.9.2 qPCR primer

Table 14. List of qPCR primers.

Name	Sequence 5´ → 3´
human Sfrp1-F	AATCCAGTCGGCTTGTTCTT
human Sfrp1-R	CTAATCTAAATGGCCCTTGCTTTAC
RT-qPCR EIF3-F	TGTCGGACAGCCAGCTAAAG
RT-qPCR EIF3-R	CCATGATGCTGGACACACTG
Gorasp2 Forward	CACTGGGTTCCCTGTACCAC
Gorasp2 Reverse	GATGCGACTCACAGAGACCA
Rpl39 Forward	ATTCCTCCGCCATCGTGCGCG
Rpl39 Reverse	TCCGGATCCACTGAGGAATAGGGCG

2.9.3 Universal RNA for qPCR

Table 15. List of universal RNA for qPCR.

Name	Company
Human Universal Reference Total RNA	Takara Bio Inc. (Japan)
Mouse Universal Reference Total RNA	Takara Bio Inc. (Japan)

2.10. Vectors

Table 16. List of used vectors.

Name	Factory
pLKO.1	(Renström et al., 2009)
sh*Sfrp1*	(Renström et al., 2009)
MIG	(Miething et al., 2003)
pMIG-p185 (BCR-ABL)	(Miething et al., 2003)

2.11. Bacteria

Table 17. List of used bacteria.

Name	Factory
DH5-α chemisch kompetente *E. coli*	Invitrogen (DE)

2.12. Cell lines

Table 18. List of used cell lines.

Name	Factory
NIH-3T3	(Littlefield, 1982)
NX (Phoenix) Eco 293T	(Pear et al., 1993)
UG26-1B6 pLKO.1	(Oostendorp et al., 2002a; Renström et al., 2009)
UG26-1B6 sh*Sfrp1*	(Renström et al., 2009)

2.13. Mice strains

Table 19. List of used mice strains.

Name	Factory
C57BL/6.J	Harlan Laboratories, Rossdorf, Germany
BL/6/SJL (Ly5.1)	Taconic Europe, Ry, Denmark
129S2/SvHsd	Harlan Laboratories, Rossdorf, Germany
129xBL/6	Breeding in ZPF: 129S2/SvHsd x C57BL6.J
129xLy5.1	Breeding in ZPF: 129S2/SvHsd x B6/SJL
129B6 *Sfrp1*$^{-/-}$	Breeding in ZPF: (Satoh et al., 2006)
C57BL/6.J *Sfrp1*$^{lox/lox}$	Breeding in ZPF
B6.Cg-Tg(Sp7-tTA,tetO-EGFP/cre)1Amc/J	Breeding in ZPF: (Rodda & McMahon, 2006)
C57BL/6.J *Sfrp1*$^{\Delta/+}$	Breeding in ZPF
C57BL/6.J *Sfrp1*$^{\Delta/\Delta}$	Breeding in ZPF

2.14. Human healthy and leukemic donor

Table 20. List of human healthy and leukemic donors.

Name	Diagnosis	Date of donation (Age)	Date of birth	Sex
Healthy 1	Healthy	2015/04 (31)	1983/09	male
Healthy 2	Healthy	2015/04 (35)	1980	male
Healthy 3	Healthy	2015/04 (26)	1989/03	male

Healthy 4	Healthy	2015/04 (47)	1967/12	male
Healthy 5	Healthy	2015/04 (35)	1979/06	male
Healthy 6	Healthy	2015/06 (41)	1973/12	male
Healthy 7	Healthy	2015/07 (26)	1989	male
Healthy 8	Healthy	2020/11 (40)	1980	female
Healthy 9	Healthy	2020/10 (26)	1994	female
Healthy 10	Healthy	2020/10 (53)	1967	female
Patient 1	AML from MDS	2006/07 (69)	1936/08	female
Patient 2	AML	2006/11 (71)	1935/02	male
Patient 5	AML	2007/09 (76)	1931/09	male
Patient 6	AML	2007/11 (69)	1938/06	female
Patient 7	AML	2008/01 (25)	1982/03	male
Patient 8	AML	2004/08 (64)	1940/05	male
Patient 9	CML	2004/11 (55)	1949/07	female
Patient 10	CML	2005/03 (57)	1947/07	female
Patient 14	AML	2011/06 (37)	1973/12	female
Patient 15	AML	2011/07 (54)	1957/07	female
Patient 17	AML	2011/10 (33)	1978/08	male
Patient 18	AML	2020/11 (40)	1980/02	male
Patient 19	AML	2020/08 (26)	1993/09	male
Patient 20	AML	2019/12 (35)	1984/04	male

3. Methods

3.1. Experimental procedure of mice

3.1.1 Generation of *Sfrp1* conditional knockout strain

For the analysis of the impact of stromal cell-secreted SFRP1 on the hematopoiesis we used a conditional knockout model where the *Sfrp1* gene is flanked by loxP sides (Sfrp1^{tm1a} mouse strain: "KO first") and crossed the newly generated *Sfrp1*$^{fl/fl}$ conditional mouse with a mouse line expressing CRE recombinase (CRE) under control of the *Sp7* (also known as *Osterix 1*, *Osx1*) promoter, which additionally harbors a reporter IRES GFP as a selectable marker (*Osx1-GFP::Cre* transgenic mouse line (B6.Cg-Tg(Sp7-tTA,tetO-EGFP/cre)1Amc/J)) (Rodda & McMahon, 2006).

In brief, the Sfrp1^{tm1a} mouse line *Sfrp1*$^{fl/fl}$ was generated using EUCOMM *Sfrp1* targeting vector (HTGR03001_Z_2_A0) in C57BL/6N embryonic stem cells (JM8A3.N1, clone HEPD0593_1_C09) (Pettitt et al., 2009) in collaboration with Dr. R. Naumann (Max Planck Institute of Molecular Cell Biology and Genetics (MPI-CBG), Dresden).

This mouse line contains an IRES:*lacZ* trapping cassette and a floxed promoter-driven targeting *neo* cassettes for the generation of a 'Knockout-first allele', when crossed with a FLP-*FRT* mouse (flippase (FLP) recombinase) (Sadowski, 1995) or *Cre-lox* mouse (Araki et al., 1997; Sauer & Henderson, 1988; Sternberg & Hamilton, 1981). This strategy is based on the identification of a 'critical' exon common to all transcript variants that, when deleted by CRE, induce a frame-shift mutation. The KO-first allele is flexible and offers wide reusability options like reporter knockouts, conditional knockouts, and null alleles (Skarnes et al., 2011) (Figure 11).

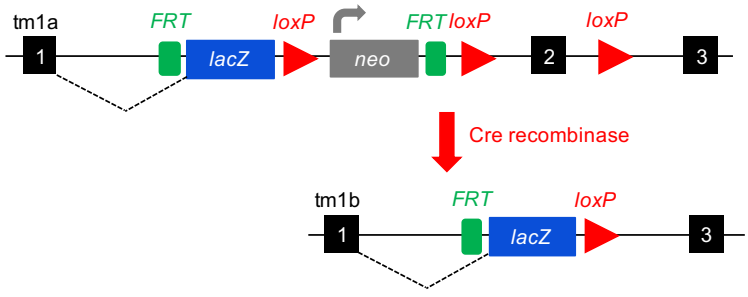

Figure 11. Knockout – first (KO-First) conditional allele strategy. The KO-First allele tm1a containing *FRT* (green), *loxP* side (red) flanked IRES:*lacZ* trapping cassette (blue) and a floxed promoter driven *neo* cassettes (grey) additional to the *loxP* side flanked critical exon 2. Production of reporter knockout by exposure to site specific Cre recombinase (tm1b) (Scheme adapted from (Skarnes et al., 2011)). The LacZ and Neo cassettes were deleted using crosses with the Flp mouse by our collaborators in Dresden. We then received the Sfrp1^{tm1a} KO first (*Sfrp1*$^{fl/fl}$), which were crossed with C57/BL6.J mice for use in Munich. These mice were then crossed with appropriate cell lineage-specific Cre deleter strains (*Osx1-GFP::Cre*).

3.1.2 Mouse strains used in this thesis

The activity of the transcription factor *Osx-Cre* (*Osx1-GFP::Cre*) is limited to osteoblast lineage cells, bone marrow stromal cells, osteocytes, hypertrophic chondrocytes, perivascular cells and adipocytes in the bone marrow (Chen et al., 2014; Rodda & McMahon, 2006). In all experiments, age- and sex- matched *Sfrp1*$^{+/+}$ (wildtype (WT)), *Sfrp1*$^{lox/lox}$ (WT), and *Osx1-GFP::Cre* (WT) mice were used as controls.

For the generation of fetal liver (FL) cells and mouse embryonic fibroblasts (MEFs) C57BL/B6.JCrl (BL6; CD45.2) mice were used. Additionally, 129B6 Sfrp1$^{-/-}$ (Satoh et al., 2006) were used for the generation of MEFs. For the repopulation assays, the F1 crosses of 129S2/SvPasCrl (129; CD45.2) and either B6.SJL-Ptprca Pepcb/BoyJCrl (Ly5.1; CD45.1) (129xLy5.1) or C57BL/B6.JCrl (BL6; CD45.2) (129xB6) were used as donor or recipient mice unless otherwise specified. These mice were ordered from Charles River Laboratories (Lyon, France, https://www.criver.com) at the age of 6 weeks.

All mice were kept in the Center of Preclinical Research (Zentrum für präklinische Forschung (ZPF)) under specific-pathogen-free (SPF) conditions in micro-isolators in individually ventilated cages (IVC), corresponding to Federation of European Laboratory Animal Science Associations (FELASA) recommendations. All experiments were approved by the Government of Upper Bavaria.

3.1.3 Genomic DNA isolation

The mice were marked at the age of three to four weeks using markings in the ears. The genomic deoxyribonucleic acid (gDNA) was isolated from small tissue samples of the mouse ear using Wizard® Genomic DNA Purification Kit (Table 8). In brief, the tissue was digested overnight in 300 µl of Nuclei Lysis Solution with 60 µl of a 0.5 M EDTA solution and 2 µl Proteinase K (200 µg/ml) at 55 °C and 800 rpm.

The following day, 100 µl of the Protein Precipitation Solution was added, followed by 20 sec of vortexing thoroughly and an incubation step on ice for 5 min. Afterwards the sample was centrifuged at 13,000 x *g* for 10 min. In the next step, the supernatant containing DNA was transferred to a new 1.5 ml microcentrifuge tube filled with 300 µl of 100 % isopropanol. After inverting the tube and centrifugation at 13,000 x *g* for 10 min, the isopropanol was carefully aspirated and the pellet was resuspended in 600 µl of 70 % ethanol, inverted and centrifuged again. The ethanol was removed followed by air-drying of the pellet for 60 min. Subsequently, the DNA was resolved with 100 µl DNA Rehydration Solution and stored at 4 °C.

3.1.4 Mouse genotyping for *Sfrp1* conditional mice

The mouse genotyping is based on polymerase chain reaction (PCR). For all PCRs, we used VWR Red Taq DNA Polymerase Master Mix (Table 8) containing Tris-HCl pH 8.5, $(NH_4)_2S0_4$, 1.5 mM $MgCl_2$, 0.11 % Tween®20, 0.22 mM of each dNTP, 0.11 units/µl VWR Taq DNA polymerase and stabilizer. The genotypes were determined by resulting PCR products. In order to determine the genotype of the mice as *Sfrp1* conditional (*Cre* negative but floxed) or deleted allele (*Cre* positive and *Sfrp1* knockout in stromal cells) of the critical exon 2 (CE), the following three PCR reactions are needed (Table 21).

Table 21. Content of PCR scheme for genotyping of *Sfrp1* conditional mice.

	5HAL - CCER	CE3	DEL
Master Mix	17.5 µl	14 µl	17 µl
Primer - F	1 µl	1.5 µl	1 µl
Primer - R	1 µl	1.5 µl	1 µl
Intern Control - F	-	1 µl	-
Intern Control - R	-	1 µl	-
gDNA	0.5 µl	1 µl	1 µl
Total Volume	20 µl	20 µl	20 µl

The CE3 PCR was performed to confirm *Cre* gene insertion. Furthermore, the 5HAL-CCE3R PCR as well as the Sfrp1_del PCR were performed to determine successful deletion of critical exon 2. All primers are listed in the Table 11. PCRs were run in a PTC 100 Peltier Thermal Cycler corresponding to the melting temperatures of each primer pair (Table 22).

Table 22. PCR program for genotyping of *Sfrp1* conditional mice.

	5HAL - CCER	CE3	DEL
Denaturation	94 °C for 3 min 94 °C for 20 sec	94 °C for 3 min 94 °C for 30 sec	94 °C for 3 min 94 °C for 20 sec
Annealing	57 °C for 1 min	64 °C for 1 min	59 °C for 20 sec
Extension	72 °C for 1 min 72 °C for 2 min	72 °C for 1 min 72 °C for 10 min	72 °C for 2 min 72 °C for 10 min
Hold	4 °C forever	4 °C forever	4 °C forever
Cycles (from step 2 - 4)	35 x	35 x	35 x

The PCR products were analyzed by an agarose gel electrophoresis (4.4 Generation and analysis of *Sfrp1* conditional mice). Therefore, the PCR products were loaded on a 1.5 % agarose gel containing ethidium bromide (0.5 µg/ml) and the gel was run in 0.01 M di-sodium tetraborate (NaB buffer). The electrophoresis was performed at 180 V for 60 min and the DNA fragments were visualized using the BioRad Gel-Doc XR Imaging System.

3.1.5 *In vivo* lipopolysaccharide treatment

For the study of hematopoietic stress, the mice were stimulated *in vivo* with lipopolysaccharide (LPS, Table 5), a component of gram-negative bacteria, whose recognition by blood cells induces immune reactions (Farhana & Khan, 2021). Eight- to ten-week-old *Sfrp1* conditional mice and control mice were intraperitoneally (i.p) injected with 1000 ng LPS. The control group was treated with HF2+ buffer. 24 h after treatment the peripheral blood (PB), bone marrow (BM), spleen (SP) and stromal cells were isolated and analyzed by flow cytometry. In some experiments, the primitive BM cells were studied in a repopulation assay and for colony formation with MethoCult™ methylcellulose-based medium (M3434).

3.1.6 *In vivo* IQ-1 inhibitor assay

In order to rescue the functionality of LT-HSCs and obviate spontaneous differentiation in *Sfrp1* conditional mice we inhibited catenin beta 1 (CTNNB1)-p300 binding with the specific inhibitor IQ-1 (Table 5) *in vivo*. Eight- to ten-week-old control and *Sfrp1* conditional mice were i.p injected with 14 µg (stock concentration 10 mg/ml) of the IQ-1 inhibitor for five days and analyzed 24 h after the last treatment. The control group was treated with HF2+ buffer. The PB, BM, SP and stromal cells were isolated and analyzed by flow cytometry. In some experiments, the primitive BM cells were studied in a repopulation assay and for colony formation with MethoCult™ methylcellulose-based medium (M3434).

3.1.7 Murine tissue extraction and preparation

In this study, we analyzed the mouse embryonic fibroblast (MEF), fetal liver (FL), peripheral blood (PB), bone marrow (BM), spleen (SP), lymph node (LN) and stromal niche cells.

3.1.7.1 Mouse embryonic fibroblast and fetal liver

MEFs were generated from embryos (E11.5 or E13.5) using a generic protocol (Durkin et al., 2013; Qiu et al., 2016) without trypsin digestion of the embryonic tissue. FL cells were isolated from embryos at E13.5. In brief, adult female mice (8 weeks) were bred with adult male mice (8 weeks) in the evening. The female mice were checked on the next morning for the appearance of a vaginal plug.

For isolation of MEFs and FLs the pregnant females were sacrificed with isoflurane (Table 4) and cervical dislocation. The uterus was isolated by careful opening the abdomen with forceps and scissors. The embryos within the uterine horns were placed into a new dish containing HF2+ buffer (Table 7), separated by using scissors and maternal tissues were removed. For the isolation of the FLs and the MEFs a stereomicroscope was used (Figure 12).

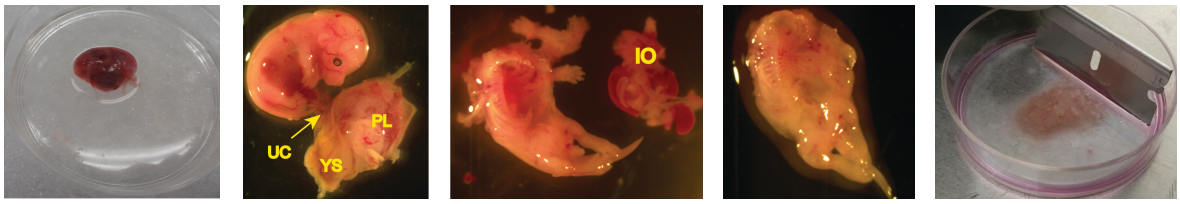

Figure 12. Process for isolation of FLs and MEFs. Left to right: embryos within the uterine horns; removing the yolk sac and placenta; removing head, FL and internal organs; moving the body to a new cell dish; cutting body into small pieces. PL - placenta; YS - yolk sac; UC - umbilical cord; IO - internal organs (scheme adapted from (Qiu et al., 2016)).

The bodies of the embryos (without the top of the head) were placed into a new dish containing HF2+ buffer. The FL from each fetus was removed using sterile forceps. Afterwards, the FL was squeezed, filtered through 30 µm cell strainer, digested with 1 % DNAse I (5 mg/ml, Table 5) for 30 min, washed with HF2+ buffer and used immediately for retroviral infection or stored for long-term storage in liquid nitrogen in freezing medium (Table 7). Subsequently, all internal organs of the embryo were removed. The body of the embryo was placed in a well of a 6-well plate and cut into small pieces using two 1 ml syringes (Table 1). During the procedure, a few scratches were cut into the plastic of the well, the embryo was covered with 2 ml MEF medium (Table 7) and cultured at 37 °C and 5 % CO_2 in a tissue culture incubator until MEF colonies were visible (after 3-4 days).

For passage, MEFs were counted and 1/3 was seeded together with 20 % of the cell and debris-free supernatant of the previous passage (3.2.1 Culture of adherent cells). For experiments, MEFs were collected between 80 % till 90 % confluence, cultured and used immediately for the generation of conditioned medium (CM) or stored for long-term storage in liquid nitrogen in freezing medium.

3.1.7.2 Peripheral blood

PB was obtained by the facial vein (during regeneration experiment) or taken directly from the heart (end of experiment) with a 1 ml syringe (Table 1). At the end of the experiment mice were sacrificed with isoflurane. The facial vein blood or heart blood were collected in a S-Monovette Blood Collection System (silicate-treated collecting tube) and the blood compositions were analyzed with an animal blood counter Scil Vet Abc™.

If serum was needed the collected blood samples were centrifuged by 2000 x *g* for 10 min at 4 °C. Afterwards the supernatant was collected and stored at -80 °C until further Cytometric Bead Array (CBA) analysis.

In order to analyze the composition of the white blood cells by flow cytometry, the red blood cells were lysed by the Ammonium-Chloride-Potassium (ACK) Lysing Buffer from Gibco™. In brief, either the remaining pellet after serum collection or the whole blood was transferred into a 15 ml polypropylene centrifuge tube containing 5 ml Gibco™ ACK Lysing Buffer and incubated on ice for 15 min. Afterwards, 5 ml HF2+ buffer was added to dilute the lysing buffer. The samples were centrifuged at 500 x *g* for 5 min to collect the white blood cells. The pellet was resuspended in 1 ml HF2+ buffer and stored at 4 °C for further flow cytometry analysis.

3.1.7.3 Bone and bone marrow

For characterization of the bone homeostasis and of the hematopoietic cells in the BM, the mice were sacrificed with isoflurane and cervical dislocation and the femurs and tibia of both hind legs, as well as the spinal column (only for the bone homeostasis analysis) were isolated. For bone homeostasis analysis, the femurs and tibia of both hind legs, as well as the spinal column were fixed with 4 % PFA for 48 hours. Afterwards the bones were washed three times with 1 x DPBS and stored in 50 % EtOH at room temperature. The bones were analyzed by Heike Weidner (Bone Lab, Dresden). To analyze the degree of bone mineralization, we injected mice with a calcium-binding fluorescent dye (Calcein, 6 mg/ml) five and two days before sacrifice.

For the hematopoietic cell analysis, the BM was flushed out the bones with HF2+ buffer. The flushed BM was resuspended by using Monoject™ Blunt Cannula Needle (16 G x 1-1/2", Covidien) and afterwards filtered through a 30 µm filter. Then the BM was pelleted at 500 x *g* for 5 min and resuspended in 1 ml HF2+ buffer. The BM cells were counted with a Neubauer improved cell counting chamber and stored at 4 °C. Unless otherwise described, these cells were used for flow cytometry and sorting analysis. The sorted cell compartments were used for real-time quantitative PCR (RT-qPCR), mouse colony-forming unit (CFU) assay, single cell culture (SCC) assay, cell cycle assay, apoptosis assay, DNA damage assay, repopulation assay and immunocytofluorescence staining.

3.1.7.4 Spleen and lymph node

For the analysis of the hematopoietic cells in the SP and LN, the mice were sacrificed with isoflurane and cervical dislocation. The SP and the LN were isolated, the size of the organs were measured, and the organs were weighed on a precision scale. Afterwards the SP and the LN were pressed and filtered through a 70 µm filter. The cells were homogenized using Monoject™ Blunt Cannula Needle (16 G x 1-1/2", Covidien) and again passed through a 30 µm filter with HF2+ buffer. Then the SP- and LN cells were spun down at 500 x *g* for 5 min and resuspended in 1 ml HF2+ buffer, counted with a Neubauer improved cell counting chamber and stored at 4 °C. Unless otherwise described, these cells were used for flow cytometry analysis.

3.1.7.5 Stromal niche cells

For the isolation of stromal niche cells, the flushed femur and tibia were cut into small pieces and ground with mortar and pestle. The resulting bone chips were washed in 1 x DPBS to remove loosely cells. The bone chips were incubated with 3 mg/ml type I collagenase and 15 µg/ml DNAse I (5 mg/ml, Table 5) dissolved in DMEM with 10 % FCS and 1 x HBSS for 90 min at 37 °C and 5 % CO_2 and carefully shaken from time to time. Afterwards, the digested bones were washed three times with HF2+ buffer. The stroma niche cells were filtered through a 30 µm filter, centrifuged at 500 x *g* for 5 min and resuspended in HF2+ buffer. The stromal niche cells were counted with a Neubauer improved cell counting chamber and stored at 4 °C. Unless otherwise described, these cells were used for flow cytometry and sorting analysis. The sorted cell compartments were used for RT-qPCR, CFUs, differentiations and immunocytofluorescence staining.

Additionally, the remaining mesenchymal stromal cells (MSCs) in the digested mouse compact bone were isolated as described previously (Zhu et al., 2010). In brief, the remaining bone chips were plated on a 0.1 % gelatin coated 10 cm^2 dish with MSC medium and cultured at 37 °C and 5 % CO_2 in a tissue culture incubator until colonies were visible (after 7-10 days). Adherent stroma colonies were washed with 1 x DPBS. For passage, cells were treated with 1 x Trypsin for 5 to 10 min at 37 °C when a 70 % - 80 % confluency (every 3-4 days) was reached and reseeded at a 1:3 ratio together with 20 % of the cell and debris-free supernatant of the previous passage (3.2.1 Culture of adherent cells). The cells were used immediately or stored for long-term storage in liquid nitrogen in freezing medium. For experiments, such as long-time culture, scratch assay, senescence, differentiation, cultured MSCs were used at passage 4. The remaining cells were frozen as pellets at -80 °C for further analysis such as western blot.

3.1.8 *In vivo* repopulation assay

In order to study alterations in hematopoietic stem cell behavior caused by the loss of *Sfrp1* in the bone marrow microenvironment, the repopulation assay is required to measure donor-derived blood cell regeneration *in vivo* in irradiated transplant recipient mice under controlled conditions.

For the adult *in vivo* repopulation assay, the CD45 congenic system (CD45.1 and CD45.2) was used to differentiate donor-derived cells and recipient cells and was performed as described previously (Marquez Romero et al., 2020; Renström et al., 2009; Schreck et al., 2017). For transplantations eight-to ten-week-old lethally irradiated recipient mice (8.5 Gy) received donor cells via intravenous (i.v.) injection in the tail vein. The transplanted adult mice received 8 mg of the long-term antibiotic Convenia® (80 mg/ml, Table 5) per kilo of bodyweight via subcutaneous (s.c.) injection. Furthermore, the mice were administered 1 mg/ml Borgal® solution (24 %, Table 5) for a total of three weeks post transplantation in drinking water.

For the MEF project, 20 harvested clones with at least one division from 129xLy5.1 (F1, CD45.1xCD45.2) donor cells were transplanted into 129xB6 (F1; CD45.2) recipients, together with 1 x10^5 BM cells and 5 x 10^5 spleen helper cells of 129xB6 mice. The analysis of the PB was performed five-, ten- and 16-weeks post transplantation by flow cytometry. 16 weeks post transplantation, mice were sacrificed (3.1.7 Murine tissue extraction and preparation) and BM was analyzed by flow cytometry. Mice were counted positive with ≥ 1 % donor engraftment in the myeloid and lymphoid lineage.

For the *Sfrp1* project, 100 sorted $Lin^-Sca\text{-}1^+Kit^+CD34^-CD150^+$ donor BM cells of *Sfrp1* conditional mice and control mice (CD45.2) were transplanted into 129xLy5.1 (F1; CD45.1xCD45.2), together with 1 x 10^5 BM cells and 5 x 10^5 spleen helper cells from 129Ly5.1 mice. The PB was analyzed in week four, eight, 12, 16, and 20 post transplantation by flow cytometry. 20 or 24 weeks after transplantation, mice were sacrificed and BM, SP, and PB were analyzed by flow cytometry. Mice were counted positive with ≥ 1 % donor engraftment in the myeloid and lymphoid lineage. Sorted BM cells were used for further analysis like immunocytofluorescence staining.

The newborn *in vivo* repopulation assay was used for the model of primary leukemia. In leukemia model of B6, 0.5 x 10^5, 2 x 10^5 and 4 x 10^5 BCR/ABL^+ FL cells, expressing green fluorescent protein (GFP) and in the *Sfrp1* conditional mice 0.5 x 10^5 BCR/ABL^+ FL cells were transplanted into newborn recipients.

The newborn recipient animals (first to fourth day after birth) from the *Sfrp1* conditional mice and B6 were irradiated lethally with 4.5 Gy (without mother) one day before the transplant. Therefore, the pups were separated from the parents. After radiation, newborn recipients receive oral pain treatment with 1 mg/kg Metacam® (1.5 mg/ml, Table 5). Since the newborn animals have no body hair in the first four days, the liver is clearly visible. The newborn recipients received the GFP^+ donor cells via intra-hepatic (i.h.) injection in 20 µl HF2+ buffer with Hamilton® syringes (Table 2).

After transplantation, the newborn recipients received again an oral pain treatment with 1 mg/kg Metacam® (1.5 mg/ml, Table 5). In addition, the newborn mice were given antibiotics (1 mg/ml Borgal) in breast milk for a total of three weeks. In the case of a complicated disease pattern and severe symptoms the animals were sacrificed and analyzed by flow cytometry.

3.1.8.1 Monitoring of transplanted mice

The irradiation of the animals represented a moderate stress (stress level 2), due to the fixation of the animals, injections and antibiotic administration as well as bleeding. The development of leukemia was expected about 8 to 10 weeks after transplantation in the BCR-ABL leukemia model with newborn recipient animal. This resulted in an infiltration of the GFP^+ leukemic cells in the BM, SP, LN and PB. If symptoms appear, the mice were sacrificed according to the criteria (stress level 3) in the score sheet of the application for animal experiments (Table 23 and Table 24).

Table 23. Criteria for the scoring of the mice in an experiment.

Monitoring		Score
Body weight	Weight loss < 5 %	0
	Weight loss 5-10 %	5
	Weight loss 11-19 %	10
	Weight loss > 19 %	20
Blood check	Leucocytes in PB< 15 x 10^3/µl	0
	Leucocytes in PB 15-30 x 10^3/µl	5
	Leucocytes in PB 30-50 x 10^3/µl	10
	Leucocytes in PB 30-50 x 10^3/µl	20

Side effect irradiation	No visible effects	0
	Diarrhea, mild dehydration (grade I, 3-6 % of body mass), paleness of skin and mucosa (due to anemia)	5
	Diarrhea (1-3 days), dehydration (grade II, 6-8 % of body mass)	10
	Diarrhea sustained (> 3 days), dehydration (grade II, 6-8 % of body mass, petechial bleeding, difficulty in breathing (due to anemia/ thrombocytopenia)	20
Behavior and posture	Normal behavior (sleeping habits, reaction to contact, social contacts, curiosity)	0
	Arched back, slightly limited movements or hyperkinetic, aberrant posture	5
	Strongly arched back, lethargy, separation from the group, coordination disorder	10
	Auto aggression, lateral position	20
Visual evidence of an infection	Leucocytes in PB	20
	Strong ascites, open abscess	

Table 24. Level of stress in an animal experiment.

Stress level	Valuation, consequence	Score
Stress level 0	No distress	0
Stress level 1	mild distress, careful surveillance	1 - 9
Stress level 2	Moderate distress, consult of person in charge	10 - 19
Stress level 3	serve distress, end of experiment	20

3.2. Experimental procedure of cell culture

3.2.1 Culture of adherent cells

The UG26-1B6 stromal cell line (Oostendorp et al., 2002; Oostendorp et al., 2005), the sorted MSCs and OBCs as well as the cells from the bone chips were cultured on 0.1 % gelatin-coated cell culture dishes. Therefore, the cell culture dishes were covered with 0.1 % gelatin and cultured for 30 min at 37 °C. The NIH/3T3 cells, Phoenix Eco cells and MEFs were cultured without 0.1 % gelatin-coated culture dishes.

The deep-frozen cryogenic vials containing cells in freezing medium (FCS, 10 % DMSO) were thawed with 5 ml suitable culture medium to dilute the cell toxic DMSO. The thawed or fresh isolated cells (3.1.7 Murine tissue extraction and preparation) were centrifuged for 5 min at 500 *x g* and cultured on the cell culture dishes containing a suitable culture medium and incubated at 37 °C (UG26-1B6 stromal cell line was cultured at 33 °C) with 5 % CO_2.

The culture confluence was checked by phase-contrast microscopy. If the cells reached an 80 % confluence, the culture supernatant was collected and centrifuged for 5 min at 500 x *g* at room temperature to pellet floating cells and debris. In the meantime, the adherent cells were washed two times with 1 x DPBS. Afterwards 1 x Trypsin was added for 5 to 10 min to detach adherent cells from the bottom of the culture dishes. The reaction was stopped by adding two volumes of culture medium containing fetal calf serum (FCS). The FCS in the medium contains a trypsin inhibitor, particularly α1-antitrypsin (protease inhibitor), and also a high concentration of other proteins, which attenuate the effect of trypsin on the cellular proteins. Then the cells were centrifuged for 5 min at 500 *x g*. For passage, cells were counted and cultured in fresh medium together with 20 % of the cell and debris-free supernatant of the previous passage. To freeze the pellet, it was resuspended in freezing medium and transferred into a labeled cryogenic vial with a maximum of 0.5 x 10^6 cells and frozen in a freezing container to ensure standardized controlled -1 °C/min cell freezing in a -80 °C freezer. The following day, cells were stored in liquid nitrogen.

3.2.2 Determination of cell number and cell vitality

To determine the number of living cells a Neubauer improved cell counting chamber and a 0.5 % trypan blue solution was used. The cells were resuspended in 1000 µl HF2+ buffer. Depending on the expected number of cells, the cells were diluted 1:100 (BM, SP, LN) or 1:10 (stromal cells). 20 µl of the cell suspension was diluted with the trypan blue solution in a ratio of 1:1. Around 20 µl of the cell/trypan blue mixture was introduced into the counting chamber by capillary force.

Living cells have an intact cell membrane, which prevents the trypan blue from entering the cytosol. Dead cells absorb the trypan blue and the cells appear blue under the microscope. To calculate the total number of cells per microliter of a sample, the four large squares placed at the corners are counted.

$$\text{Particles per µl volume} = \frac{Counted\ cells}{Counted\ surface\ (mm^2) \cdot Chamber\ depth\ (mm) \cdot Dilution}$$

3.2.3 Colony-forming unit fibroblasts

In order to evaluate the potential of MSCs to develop colony-forming unit fibroblasts (CFU-Fs), 500 to 1000 sorted (p0) or cultured (p3) cells were plated in a well of a 6-well plate covered with 2 ml MSC medium (Table 7). After three days (cultured MSCs) and ten days (sorted MSCs), the colonies were counted under the microscope.

3.2.4 Long term culture

The MSC long term culture (growth curve), was done as described previously (Stenderup et al., 2003). In brief, 10,000 cells/well were cultured on 0.1 % gelatin coated 6-well plate with MSC medium (Table 7) at 37 °C and 5 % CO_2 in a tissue culture incubator. The cultures were split when at least one of the wells was 80 % confluent. The cell numbers were determined with a Neubauer improved cell counting chamber. Cells were continuously reseeded at a density of 10,000 cells/well. If cell counts decreased below 10,000 cells, all cells were reseeded. Cell growth rate was determined by using the formula *log N/log 2*. *N* is the counted cell number divided by the number of cells which were initially seeded. A representative growth curve was generated by adding the cell growth rates at each passage. The cells were cultured as long as a statistical statement for the long-term culture could be made (at least two samples per genotype).

3.2.5 Scratch assay

The scratch assay is a method which mimics cell migration during wound healing and gives information about the behavior and potency of cells. The *in vitro* scratch assay was performed as described previously (Liang, Park, & Guan, 2007). In brief, 100,000 cells/well were seeded on 0.1 % gelatin coated 6-well plate in MSC medium (Table 7) at 37 °C and 5 % CO_2 in a tissue culture incubator in the late afternoon. The assay started at 100 % confluency the next morning. The cell monolayer was evenly scraped two times with the top of a 10 µl pipet tip in order to form a cross in the cell monolayer. Representative pictures were taken from the artificial scratch intersection after 0 h, 6 h, 12 h and 24 h by an Axiovert 25 microscope and an AxioVision software (Carl Zeiss). The area of the scratch was analyzed to calculate the migration rate by the software ImageJ.

3.2.6 Senescence assay

The senescence detection was performed with the Senescence β-Galactosidase Staining Kit (Cell Signaling Technology) which is based on an increase of β-galactosidase in lysosomes that cleave the 5-bromo-4-chloro-3-indolyl β D-galactopyranoside (X-Gal), resulting in a blue staining. Therefore, we used sorted MSC and OBCs at passage 1 or cultured MSCs from the bone chips at passage 4 and cultured 10,000 cells in a 12-well plate in MSC medium (Table 7) at 37 °C and 5 % CO_2 for one week without medium change. The staining of the cellular senescence was performed following the manufacturer's recommendation. In brief, the cells were washed twice with 1 ml 1 x DPBS and fixed for 6 to 7 min at room temperature using 1.5 ml 1 x Fixation Buffer. Meanwhile the staining mixture was prepared. The cells were washed with 1 x DPBS for three times, covered with 500 µl staining mixture per well and incubated overnight at 37 °C without CO_2 to ensure a pH 6. The cells were analyzed by calculating the percentage of blue stained cells expression β-galactosidase (senescent cells) against the non-blue (not senescent cells) under an Axiovert 25 microscope and an AxioVision software (Carl Zeiss).

3.2.7 Mesenchymal differentiation assays

Mesenchymal stromal cells (MSCs) are multipotent stem cells and have the potential to self-renew, and differentiate into adipogenic-, osteogenic-, and chondrogenic-lineages *in vitro* (Kfoury & Scadden, 2015; Méndez-Ferrer et al., 2010; Robert et al., 2020; Visweswaran et al., 2015). During this study, differences in spontaneously (only adipogenic differentiation) or induced adipogenic and osteogenic differentiation were observed in sorted (p1) and cultured (p4) confluent grown mesenchymal populations. For the induced adipogenic and osteogenic differentiation the StemXVivo Osteogenic/Adipogenic Base Media with supplements was used.

3.2.7.1 Adipogenic differentiation

For the spontaneous adipogenic differentiation, sorted MSCs were cultured till confluency up to passage 1 in MSC medium (Table 7) at 37 °C with 5 % CO_2. For the induced adipogenic differentiation, 10,000 MSCs were cultured in a 24-well plate with 1 ml MSC medium at 37 °C with 5 % CO_2. The following day, the cells were washed three times with 1 x DPBS and incubated with 500 µl of the 0.2 µm filtered StemXVivo® Osteogenic/Adipogenic Base Media containing the StemXVivo® Adipogenic Supplement (1:100) and Penicillin- Streptomycin (1:100). An Oil Red O staining was performed to illustrate the adipogenic differentiation, if characteristic lipid droplet formations occurred after 4 to 7 days.

3.2.7.1.1 Oil red O staining of adipogenic differentiated cells and measurement

The adipogenic differentiated cells were washed twice with 1 x DPBS and fixed with 10 % paraformaldehyde (PFA) at room temperature for 15 min. Afterwards, the fixed cells were washed again twice with 1 x DPBS and either stored in 1 x DPBS at 4 °C sealed with Parafilm® or immediately stained with the Oil Red O staining solution. Therefore, the concentrated Oil Red O stock solution was prepared by dissolving 0.5 g of the Oil Red O in 100 ml of 100 % isopropanol. The solution was incubated for 60 min at 56 °C in a water bath. Afterwards, the solution was diluted with distilled water to a 60 % isopropanol solution and passed through a 45 µm filter. The fixed and washed cells were covered with the 60 % Oil Red O solution for 10 min at room temperature under gently shaking conditions. The cells were washed three times with 1 x DPBS followed by a microscopically observation of the red stained vesicles. The staining was usable for a few days. Representative pictures were taken by using an Axiovert 25 microscope and an AxioVision software (Carl Zeiss). Afterwards, the absorbance was measured at 520 nm OD in a multiplate reader by extracting the Oil Red O solution from the red stained vesicles by adding 100 µl of 100 % isopropanol.

3.2.7.2 Osteogenic differentiation

For the induced osteogenic differentiation, 10,000 MSCs were cultured in a 24-well plate with 1 ml MSC medium at 37 °C with 5 % CO_2. The following day, the cells were washed three times with 1 x DPBS and incubated with 500 µl of the 0.2 µm filtered StemXVivo® Osteogenic/Adipogenic Base Media containing the StemXVivo® Osteogenic Supplement (1:20) and Penicillin- Streptomycin (1:100). The differentiation medium was changed once a week and after two weeks morphological changes and calcium depositions became visible. An Alizarin Red S staining was executed to illustrate the calcium deposition of the cuboidal formic osteogenic differentiated cells.

3.2.7.2.1 Alizarin red staining of osteogenic differentiated cells and measurement

The osteogenic differentiated cells were washed twice with 1 x DPBS and fixed with 10 % PFA at room temperature for 15 min. Afterwards, the fixed cells were washed twice with 1 x DPBS and either stored with 1 x DPBS at 4 °C sealed with Parafilm® or immediately stained with 40 mM Alizarin Red (pH = 4.2, Sigma-Aldrich) staining solution for 10 min at room temperature under gently shaking conditions. Afterwards, the cells were washed for three times with 1 x DPBS followed by microscopic observation of the red stained calcium deposition. The staining was stable for a few days. Representative pictures were taken by using an Axiovert 25 microscope and an AxioVision software (Carl Zeiss).

Afterwards, the absorbance was measured at 562 nm OD in a multiplate reader (Thermo Fisher Scientific) by extracting the Alizarin Red S solution from the calcium depositions by adding 100 µl of a destain solution (10 % cetylpyridinium chloride in 10 mM sodium phosphate, pH 7.0).

3.2.8 Generation of conditioned medium for culture of HSCs

Conditioned medium (CM) was prepared as described previously (Marquez Romero et al., 2020; Wohrer et al., 2014). In brief, 700,000 MEFs (passage 4) or 1,200,000 UG26-1B6 cells (passages 12-15) were cultured on a 10 cm^2 dish. For the UG26-1B6 stromal cell line the dish was coated with 0.1 % gelatin for 30 min at 37 °C. Twelve hours after culturing the cells in 8 ml MEF medium (MEFs, Table 7) or Stroma medium (UG26-1B6, Table 7) at 37 °C and 5 % CO_2 in a tissue culture incubator, the mitosis was inactivated with X-Ray-irradiation (Table 2). Subsequently, the cells were washed twice with 1 x DPBS and cultured in 12 ml serum-free medium from Stemcell Technologies containing 1:100 penicillin- streptomycin and 1:1000 β-mercaptoethanol at 37 °C (MEFs) or 33 °C (UG26-1B6). 40 µg/ml of low-density lipoprotein (LDL) was added where indicated. CM was harvested after 72 h, filtered through a 0.22 µm filter and either used immediately or stored at -20 °C.

3.2.9 Phoenix helper free retrovirus producer cell line cultivation

For the retrovirus infection experiments, the phoenix helper free ecotropic retrovirus producer line (Phoenix E cell line), which only infect mouse or rat cells, was used. The highly transfectable Phoenix E cell line is based on the 293T cell line with the ability to produce gag-pol and envelope proteins, which are essential for ecotropic virus production. Therefore, the 293T packaging cell line was co-transfected with three types of plasmids (envelope (env), packaging (gag-pol) and transfer (Murine Stem Cell Virus)) with selection markers. For the selection of the Phoenix E cell line, the drugs hygromycin B (gag-pol genes) and diphtheria toxin (env genes) were used (Pear et al., 1993).

The cells were treated for 7 days at the same time with 300 µg/ml hygromycin B (50 mg/ml, Invitrogen) for the gag-pol packaging genes and 2 µg/ml diphtheria toxin (1 mg, Sigma-Aldrich) for the envelope genes. For one week, the treated cells were split daily into 5 x 10^6 cells per 75 cm^2 cell culture flask in 10 ml selective medium including DMEM, 10 % FCS, 0.3 mg/ml hygromycin B and 2 µg/ml diphtheria toxin. Afterwards the cells (passage 0) were regrown in Phoenix medium, expanded to passage 3 and then stored for long-term storage in liquid nitrogen in freezing medium (FCS, 10 % DMSO). For virus production, the cells between passages 5 and 10 were used.

After thawing, Phoenix E cells were cultured in a 175 cm^2 cell culture flask. Phoenix E cells are very sensitive. Therefore, cells were treated with 1 x Trypsin for only 1 min at 37 °C when a 70 % to 80 % confluency (every 2-3 days) was reached and reseeded at a 1:4 ratio in Phoenix medium.

3.2.9.1 Retroviral transfection and infection of fetal liver cells

Transfection is the process of introducing foreign DNA into eukaryotic cells by chemical and physical methods. In the experiments, the cationic lipid-based reagents Lipofectamin^{TM}2000 (Life Technologies) were used to introduce the DNA into the fetal liver cells (E 13.5, B6). The cationic lipids form a complex with the negatively charged phosphates of the DNA (Kabanov & Kabanov, 1995; Labat-Moleur et al., 1996). Due to their positive charge and lipophilic structure, these complexes interact with the negatively charged and hydrophobic cell membrane by endocytosis (Gao & Huang, 1995).

For the transfection, 4 x 10^6 Phoenix cells were cultured on a 10 cm^2 dish in the late afternoon. The next morning, the cells were 70 % confluent. This is important to ensure the process of proliferation, the prerequisite for retroviral infection (Miller, Adam, & Miller, 1990). For each 10 cm^2 dish, two solutions were prepared (Table 25) and gently mixed.

Table 25. Composition of the solutions required for retroviral infection.

	Solution 1	**Solution 2**
Medium	500 µl OptiMem	1000 µl OptiMem
Supplements	20 µg DNA	40 µl Lipofectamin

After the incubation of 10 min at room temperature, both solutions were gently mixed and incubated for 40 min at room temperature. The phoenix cells were supplemented with 3.5 ml fresh phoenix medium without antibiotic (penicillin, streptomycin) per 10 cm^2 dish and 1.5 ml of the lipofectamin/DNA mixture was carefully added to the phoenix cells. After the incubation of 4 h at 37 °C and 5 % CO_2, the medium was exchanged with BBMM (Table 7) and the Phoenix E cells were cultured at 33 °C and 5 % CO_2. The retroviral supernatant was harvested after 24 h, 36 h, 48 h and filtered through a cell filter (0.45 µm) in order to remove any detached Phoenix E cells. Afterwards 8 µg/ml of the cationic polymer polybrene was added to the filtered viral supernatant to increase the infection efficiency (Davis et al., 2002). Additionally, rmIL-3 (10 ng/ml), rmIL-6 (10 ng/ml), rmSCF (50 ng/ml) were added to promote the retroviral-mediated gene transfer and to stimulate and regulate the migration and proliferation of the cells (Luskey et al., 1992).

3.2.9.2 Fetal liver infection

The murine FL cells were prestimulated for 24 h in BBMM medium (Table 7) containing growth factors (10 ng/ml rmIL-3, 10 ng/ml rmIL-6, 50 ng/ml rmSCF) at 37 °C and 5 % CO_2. Therefore, the cells were cultured in a very small density (4.5 x 10^6 cells/well) on 0.1 % gelatin coated 12-well plate. FL cells were infected with viral supernatants in a 12-well plate by spin infection (60 min, 33 °C, 1500 rpm) three to four times every 12 h. Therefore, the supernatant of the FL cells was collected separately from each approach and centrifuged for 5 min at 500 x *g*. The resulting pellet contains floating FL cells that were in the collected supernatant. The pellet was resuspended in the fresh filtered viral supernatant containing rmIL-3 (10 ng/ml), rmIL-6 (10 ng/ml), rmSCF (50 ng/ml) and polybrene (8µg/ml). The FL cells and the virus supernatant were evenly distributed on the 12-well plate. After each spin infection, the FL cells were incubated for 12 h at 37 °C and 5 % CO_2. 12 h after the last spin infection, the FL cells were harvested, resuspended in BBMM medium with 1 % DNAse I (5 mg/ml, Table 5) and incubated for 15 min at room temperature to prevent agglutination of FL cells. Afterwards the cells were washed with HF2+ buffer, centrifuged for 5 min at 500 x *g*, resuspended in HF2+ buffer, counted with a Neubauer improved cell counting chamber and stored at 4 °C. The infection efficiency of the cells was determined by flow cytometry, using green fluorescent protein (GFP) as a selectable marker. Then, the cells were prepared for the repopulation assay.

3.3. Experimental procedure of cell-based assays

3.3.1 Single cell culture assay

$CD34^-$ SLAM cells were sorted into the inner 60 wells of a round-bottomed 96-well plates preloaded with 100 µl of 0.25 nm filtered conditioned media (CM) and supplemented with two growth factors: rmSCF (100 ng/ml) and/or rmIL-11 (20 ng/ml), both from R&D Systems, additionally in some experiments supplemented with Collagen 1 (300 µg/ml) and nerve growth factor (NGF, 250 ng/ml). Immediately after sorting, the round-bottomed 96-well plates were centrifuged for 5 min at 200 x *g* and microscopically inspected for the presence of single cells. Every 24 h each well was inspected and cells were counted for clonal growth. After 5 days, the number of clone size was determined. The cells that had divided at least once (> 2 cells/well) were harvested and stained with antibodies for lineage markers, KIT and SCA-1 (Table 9). The cells were analyzed on a CyAn ADP Lx P8 and evaluated with FlowJo software (TreeStar). In some experiments, the harvested clones were studied in a repopulation assay and for colony formation with MethoCult™ methylcellulose-based medium (M3434).

3.3.2 Mouse colony-forming unit assay

The functional colony forming unit (CFU) assay quantifies multi-potential and lineage-restricted progenitors of the erythroid, granulocytic, monocyte/macrophage, and platelets using MethoCult^{TM} methylcellulose-based medium (Stemcell Technologies).

In brief, MethoCult^{TM} GF M3434 (Stemcell Technologies) is a semi-solid matrix and contains cytokines (rm SCF, rm IL-3, rh IL-6, rh EPO, rh insulin, human transferrin (iron-saturated)) for the support of optimal growth of BFU-E (burst-forming unit-erythroid), CFU-GM (CFU-granulocyte, macrophage), CFU-GEMM (CFU-granulocyte, erythrocyte, macrophage, megakaryocyte) of primitive mouse hematopoietic cells. The whole BM cells (2.5 x 10^4), sorted Lin^- cells (1 x 10^4) and sorted $CD34^-$ SLAM (1 x 10^3) were added to the methylcellulose, vortexed and cultured at 37 °C and 5 % CO_2 in a 35-mm dish. After an incubation time of 10 to 14 days, formed colonies were classified into CFU-GM, CFU-GEMM and BFU-E, and counted by an Axiovert 25 microscope and an AxioVision software (Carl Zeiss) at 100-fold magnification. After the colonies had been determined, the cells were removed from the semi-solid matrix using HF2+ buffer, stained for mature populations (Table 9) and analyzed using CyAn ADP Lx P8.

3.3.3 Cell cycle assay

To study differences in cell cycling (G0/G1, S, G2 and M phases) a PI/Ki-67 staining followed by flow cytometry analysis was performed. Therefore, the collagenase type I treated cells of the bone chips were used. The cells were fixed and the plasma membrane was permeabilized using the Cytofix/Cytoperm buffer of BrdU Flow Kit (Table 8) containing PFA and saponin (Jacob, Favre, & Bensa, 1991). The cells were washed twice with 1 x DPBS and stained with the anti-Ki-67 antibody for 16 h at 4 °C. Before flow cytometry analysis on CyAn ADP Lx P8, 1 µg/ml propidium iodide (PI) was added.

3.3.4 Apoptose assay

The loss of plasma membrane asymmetry is an early indication of apoptosis. In the case of apoptosis, the membrane phospholipid phosphatidylserine (PS) residues become visible. The FITC Annexin V Apoptosis Detection Kit I from BD-Biosciences was used to detect apoptosis by staining phosphatidylserine (PS) molecules which have translocated to the outside of the cell membrane. Therefore, 3000 $Lin^-Sca1^+Kit^+$ (LSK) cells were sorted and cultured for 48 h in a 12-well plate, prefilled with 2 ml medium. For the MEF project the cells were cultured in SFM 4GFs, MEF-CM 2GFs or MEF-CM 4GFs. For the Sfrp1 project the cells from *Sfrp1* conditional mice and control mice were cultured in HF2+ buffer.

After culture, LSK cells were harvested with HF2+ buffer. Each sample was stained with 500 µl Annexin buffer containing 0.1 µg/ml PI and 2 µl Annexin V - FITC for 15 min at 4 °C in the dark. Fluorescence staining of cells was analyzed on CyAn ADP Lx P8.

3.3.5 DNA damage assay

One reason for DNA damage can be cellular stress. For the study of various types of nucleic acid damage, the single cell gel electrophoresis (Comet Assay) from Cell Biolabs was used. Therefore, mature populations ($GR1^+CD11b^+$, $GR1^{med}CD11b^+$, $B220^+$) and primitive populations (LT-HCS) were sorted out of two to three pools of eight- to ten-week-old mice per experiment. In the beginning, the Lysis Buffer, Alkaline Solution and the Electrophoresis Running Solution was prepared. The OxiSelect^{TM}Comet Agarose was heated to 90°C for 20 min in a water bath and then cooled at 37°C for 20 min. Afterwards, 75 µl of the Comet Agarose was added to the OxiSelect^{TM}Comet Slide to generate a base layer. After 15 min at 4°C, the suspension cells were prepared with a total of 1 x 10^5 cells/ml. The cells and the Comet Agarose were mixed in a 1:10 ratio and 75 µl of the mixture was spotted onto the top of the base layer. After an incubation of 15 min at 4°C in the dark an alkaline electrophoresis was performed for 30 min at 1 volt/cm. Immediately, the slides were washed three times in cold H_2O for 2 min and one time in cold 70% ethanol for 5 min. The ethanol was removed by air-drying the slide, followed by adding 100 µl/well of (1:10,000 in TE Buffer) diluted Vista Green DNA Dye. After 15 min of incubation at room temperature, fluorescence images were recorded with constant settings on a Leica DM RBE fluorescent microscope (AxioVision software; Carl Zeiss). For each genotype and each condition, 30 - 40 random cells were recorded at 100-fold magnification. The DNA damage of the cells was then analyzed by measuring the shift between the comet head (nucleus) and the resulting tail (DNA damage).

3.3.6 Cytometric bead array

The BD^{TM} Cytometric Bead Array (CBA) Mouse Inflammation Kit from BD-Biosciences is a bead-based immunoassay and was used to analyze Interleukin-6 (IL-6), Interleukin-10 (IL-10), Monocyte Chemoattractant Protein-1 (MCP-1), Interferon-γ (IFN-γ), Tumor Necrosis Factor (TNF), and Interleukin-12p70 (IL-12p70) protein levels by flow cytometry in the blood serum. The CBA was performed according to the manufacturer's instructions. In brief, a serial dilution of the mouse inflammation standards from 1:2 to 1:256 (9 standards) was performed. The capture beads were mixed after determination of the number of assay tubes. For each assay tube, 3 µl of each capture bead was added to a single tube. Afterwards, 50 µl of the serum from each sample was added to the assay tube.

Immediately 18 µl of the capture beads and 18 µl of the PE detection reagent was added to each assay tube. The assay tubes were incubated at 4 °C overnight in the dark. The following day, the samples were washed with 300 µl Wash Buffer and centrifuged at 200 *x g* for 5 min. The supernatant was removed by aspiration and the pellet was resuspended with 300 µl Wash Buffer. The samples were analyzed by flow cytometry on CyAn ADP Lx P8.

3.3.7 Phagocytose assay

For the detection of phagocytosis, the retroviral infected GFP^+ FL cells and the pHrodo™*E.coli* GreenBioParticles® Phagocytosis Kit for flow cytometry from Invitrogen was used. The Escherichia coli particles are inactivated and not opsonized. The fluorescent labelled particles are highly sensitive for the detection of phagocytosis.

For the assay, the instructions of the manufacturer were followed. As a comparison, the retroviral infected GFP^+ FL cells were used. Therefore, mature populations ($GR1^+CD11b^+$ and $GR1^{med}CD11b^+$) were sorted out of two to three pools of eight- to ten-week-old mice per experiment. 100,000 cells of the sorted cell populations were pipetted to a 96 well round bottom plate (triple determination) and the samples were treated with 50 µg/ml pHrodo™ Green dye–labeled *E. coli* or 50,000 retroviral infected GFP^+ FL cells in 50 µl HF2+ buffer, mixed by pipetting and incubated for 3 h at 37 °C and 5 % CO_2. After the 3 h the samples were placed on ice to stop the reaction, washed with HF2+ buffer and centrifuged for 5 min at 500 *x g*. As a negative control the sorted cells were cultured without the pHrodo™ Green dye–labeled *E. coli´s* or GFP^+ FL cells. The samples were analyzed by flow cytometry on CyAn ADP Lx P8 and on a Leica DM RBE fluorescent microscope with an AxioVision software (Carl Zeiss).

3.4. Experimental procedure of flow cytometry and cell sorting

3.4.1 Lineage depletion

For the isolation of lineage negative cells from murine BM, the Lineage Cell Depletion Kit from Miltenyi Biotec was used following to the manufacturer's instructions. In brief, the BM cells were incubated with the Biotin-Antibody-Cocktail for 10 min at 4 °C. The Biotin-Antibody-Cocktail labels lineage positive antigens like CD5, CD45R (B220), CD11b, Anti-GR1 (Ly6G/C), and Terr-119 indirectly with a magnetic labeling system. Subsequently, the cells were washed with HF2+ buffer and the lineage positive cells were secondarily labeled with an anti-biotin Micro Beads antibody for 15 min at 4 °C. Afterwards, the cells were washed with HF2+ buffer, centrifuged at 500 x *g* for 5 min and the pellet was resuspended in 500 µl of HF2+ buffer. The separation was performed using a MACS Separator.

The MACS Column was placed in the MACS Separator. In the resulting magnetic field, the non-labeled lineage negative cell population could be passed through the column. In order to elute the lineage positive cell population, the MACS Columns were separated from the MACS Separator to remove the magnetic field.

3.4.2 Flow cytometry staining

The flow cytometry analysis of hematopoietic cells was performed in the PB, BM, SP and LN. For the mature population staining of BM, SP and LN, 2 x 10^6 cells were generally used. 5 x 10^6 cells of the whole BM cells were used to stain progenitors and HSCs. The analyzation of the blood cell composition and the collagenase-treated stromal cells was performed by using the whole cell pellet. For flow cytometry sorting of BM cells, lineage depleted BM cells (3.4.1 Lineage depletion) were used.

For the staining of surface markers, the resuspended cells were centrifuged at 500 x *g* for 5 min and incubated in 100 µl HF2+ buffer with primary (Table 7) and secondary antibodies (Table 11) for 60 min at 4 °C. Afterwards, the cells were washed with HF2+ buffer and centrifuged at 500 x *g* for 5 min. The cells then were resuspended in HF2+ buffer with 1 µg/ml propidium iodide (PI) and analyzed using flow cytometry on CyAn ADP Lx P8 (Beckman Coulter). For sorting of several cell populations, the cells were stained as described above, and sorted on MoFlo High Speed cell sorter and on an Astrios high speed cell sorter (Beckman Coulter).

3.4.3 Immunocytofluorescence staining

For immunocytofluorescence staining, LT-HSCs, LSK and MSC populations were sorted out a minimum of two eight- to ten-week-old mice per experiment. A total of 500 to 1,500 cells were spotted on poly-L-Lysin-coated slides. The cells were fixed with 4 % PFA for 5 min, after 30 min of incubation at 4°C. Then the cells were washed three to four times with 1 x DPBS and blocked with blocking buffer (Table 7) for 60 min at room temperature. In the meantime, the primary antibodies (Table 10) were diluted in blocking buffer. The cells were stained overnight at 4 °C in a humid chamber. The following day, the cells were washed three to four times for 10 min with blocking buffer. Meanwhile, the secondary antibodies (Table 12) were diluted in blocking buffer and the cells were stained at 4 °C in humid chamber overnight again. The following day, the cells were washed three times for 10 min with blocking buffer and one time for 10 min with 1 x DPBS. Further, SlowFade Gold Antifade Reagent with 4.6-diamino-2-phenylindole dihydrochloride (DAPI) from Invitrogen was added and slides were fully covered with coverslips.

Fluorescence images were recorded with constant settings on a Leica DM RBE fluorescent microscope (AxioVision software; Carl Zeiss). For each genotype and each condition 30 to 40 random cells were recorded at 100-fold magnification. The mean fluorescence intensity of the cells was then analyzed by using the digital image processing software ImageJ (NIH).

3.5. Protein detection via western blot

For the detection of a conditional knockout of *Sfrp1* in the *Osx-Cre* targets we used cultured MSCs (p4). Cultured MEF (p4) were used for the verification of antibodies from *Sfrp1*$^{-/-}$ mice.

3.5.1 Protein extraction

For the lysis of the cells, the pellets of the cells were resuspended in RIPA buffer (Pierce Biotechnology) supplemented with 1:100 proteinase inhibitor and 1:1000 sodium orthovanadate, a phosphatase inhibitor. The cells were incubated for 20 min on ice and vortexed every 5 min. Afterwards, the samples were sonicated two times for 10 sec, 40 cycles at 30 % power and then centrifuged for 20 min at 14,000 rpm at 4 °C. The supernatant of the sample (containing the protein) was transferred to new microcentrifuge safe-lock tube and the pellets were discarded.

3.5.2 Determination of protein content

The colorimetric determination of the protein content was measured by using Bio-Rad Bradford Protein Assay. 999 µl of the 1:5 in distilled water diluted Bio-Rad Protein Assay solution was transferred to a UV non-permeable cuvette and 1 µl of the extracted protein supernatant was added to the solution. The absorption was measured by a photometer at a wavelength of 595 nm, and a final concentration of 50 µg was calculated by means of a standard curve.

3.5.3 Protein separation via SDS-PAGE

The samples were prepared for the separation via sodium dodecyl sulfate (SDS) protein gel electrophoresis (SDS-PAGE). Therefore, the protein was diluted with a 4 x loading dye and buffer to reach a final volume of 50 µg in 40 µl per sample. The components were incubated for 10 min at 95 °C and then loaded on a 4 - 15% Mini Protean® TGX Stain-Free™ Precast gel placed in an electrophoresis chamber which was filled with 1 x running buffer. The gel was run at the beginning at 60 V for 10 min and then at 120 V for about 50 min until the sample reached the bottom of the gel.

3.5.4 Electro blotting

The separated proteins were blotted by a wet transfer onto polyvinylidene difluoride (PVDF) membranes (0.45 µm, Millipore). The methanol activated PVDF membrane was placed towards the anode so that the migrating negatively charged proteins can be transferred to it. The transfer takes place under constant cooling at a constant current of 1000 mA in Transfer Buffer. The duration of the transfer depends on the molar mass of the proteins to be transferred (about 1 min per kDa).

3.5.5 Protein detection

After the protein was successfully blotted to the membrane, it was washed three times with 1 x Tris - buffered saline - Tween 20 for 5 min. Afterwards the membrane was blocked, depending on further used antibody, with 5 % bovine serum albumin (BSA) or 5 % skim milk powder in 1 x TBS-T for 60 min at room temperature. The primary antibody was diluted (Table 10) in the block solution and incubated over night at 4 °C on a shaker. The following day, the membrane was washed three times with 1 x TBS-T for 5 min and then the membrane was incubated with the horseradish peroxidase (HRP)-coupled secondary antibody (Table 12) in block solution for 60 min. Before detection solution was added to the membrane, it was washed twice with 1 x TBS-T and once with TBS. The developer solutions Super Signal West (Pico, Dura and Femto) from Pierce were used to visualize the proteins. The luminescence was visualized via X-ray films and an OPTIMAX X-Ray Film Processor developing machine. In order to visualize more than one protein on a blot, the antibodies were stripped from the membrane. Therefore, the membrane was incubated with a destaining solution for 10 min. Then, the protein detection procedure was started from the beginning (blocking of the membrane). Comparison of protein content (visualized on X-ray films) from the different genotypes was determined by using the digital image processing software ImageJ.

3.6. Gene expression analysis via real time quantitative PCR

Real time quantitative PCR (RT-qPCR) was performed to detect differences of the gene expression in stroma cell populations of the *Sfrp1* conditional mice compared to the controls. Therefore, MSC populations were sorted out of eight- to ten-week-old mice.

3.6.1 RNA isolation

For the RT-qPCR the MSC cells were sorted in HF2+ buffer and the RNA were either directly isolated or the cell pellet was frozen at -80 °C. The total RNA purification from the small samples was performed using the RNeasy Micro Kit (for cell numbers < 5 x 10^5, Table 8) and RNeasy Mini Kit (for cell numbers > 5 x 10^5, Table 8) from Quiagen according to the manufacturer's instructions. In brief, sorted and pelleted cell populations were lysed in 300 µl RLT buffer (RNeasy Mini Kit) or 350 µl RLT Plus buffer (RNeasy Micro Kit) containing guanidine-thiocyanate and 1:100 β-mercaptoethanol. To ensure effective disruption, the cells were resuspended several times, homogenized by vortexing and passing the QIAshredder spin column. The homogenized samples were diluted with one volume of 70 % ethanol and mixed well by pipetting to optimize the binding conditions to the silica-based membrane of the RNeasy spin column (RNeasy Mini Kit) or RNeasy MinElute spin column (RNeasy Micro Kit). The spin columns were placed in a 2 ml collection tube and centrifuged for 15 sec at 8000 *x g.* The flow-through was discarded and the columns were washed by using 700 µl RW1 buffer, either two times with 500 µl RPE buffer (RNeasy Mini Kit) or in addition to the 500 µl RPE buffer, one time with 500 µl 80 % ethanol (RNeasy Micro Kit). Afterwards, the columns were air dried with open lids by centrifugation for 5 min at full speed since remaining ethanol might interfere the last step. Finally, the total RNA was eluted in 30 µl (RNeasy Mini Kit) or 14 µl (RNeasy Micro Kit) H_2O under low-salt conditions and immediately stored on ice or at -80 °C for further processing.

3.6.2 Reverse transcription

After total RNA purification, the reverse transcription into cDNA, with additional elimination of genomic DNA was processed using QuantiTect® Reverse Transcription Kit from Qiagen. All steps were performed on ice. In brief, the prepared components for the genomic DNA elimination as well as for the reverse-transcription were prepared as described in Table 26. RNA concentration was determined with NanoDrop™ 2000/c spectrophotometer (Thermo Fisher Scientific).

Table 26. Pipette scheme for genomic DNA elimination reaction and reverse-transcription master mix.

Genomic DNA elimination mixture	Reverse - transcription master mix
1 µl gDNA Wipeout Buffer (7x)	1 µl Quantiscript Reverse Transcriptase
1 µg RNA sample	4 µl Quantiscript RT Buffer (5x)
Variable RNase free water	1 µl RT Primer Mix
14 µl total volume	6 µl total volume

For the genomic DNA elimination, the gDNA elimination mixture was incubated for 2 min at 42 °C. Afterwards the reverse-transcription master mix was added to the template RNA and the mixture was incubated for 15 min at 42 °C, followed by 3 min at 95 °C to inactivate the Quantiscript Reverse Transcriptase. The cDNA was used immediately for RT-qPCR or stored at -20 °C.

3.6.3 Real time quantitative PCR

In the RT-qPCR, the amplification of the cDNA and at the same time the quantification of the PCR progress was recorded in real time using fluorescent labeling. Therefore, the Power SYBR Green PCR Master Mix from Applied Biosystems was used, following the manufacturer's instructions. The SYBR Green dye binds to double-stranded (ds) DNA. The components for the RT-qPCR master mix are10 µl Power SYBR Green PCR Master Mix, 0.1 µl Primer (forward and reverse each), 8.77 µl H_2O and 0.3 µl ROX RefDye (1:50). 19 µl of the master mix were pipetted to a 96-well plate and 1 µl of each sample was added to a well (triple determination). The fluorescent signal was detected by Applied Biosystem Step One Plus Real-Time PCR System and reflects the amount of dsDNA product generated during PCR.

Table 27. PCR program for gene expression analysis via qPCR.

Phase	Temperature & Time
Denaturation	50 °C for 2 min 95 °C for 5 min
Annealing	95 °C for 15 sec
Extension	58 °C for 20 sec 72 °C for 30 sec
Hold	4 °C forever
Cycles (from step 3-5)	40 x

To normalize the resulting data of the gene expression, housekeeping genes are used as reference genes. These genes have a constant expression level independent from the cell type and condition (Kouadjo et al., 2007; Thorrez et al., 2008). The gene expression in mouse tissue was analyzed by calculating the ΔCT value relative to the housekeeping genes golgi reassembly stacking protein 2 (Gorasp2) and ribosomal protein L39 (RPL39). For the gene expression in human tissue, the housekeeping gene eukaryotic initiation factor 3 (eIF3) was used.

Additionally, to compare the results of different plates of RT-qPCRs among each other, the data were normalized by mouse or human universal reference cDNA and the ΔΔCT value was calculated.

3.7. Gene expression analysis via RNA sequencing

3.7.1 RNA isolation

For the RNA sequencing (RNAseq) 800 to 1000 MSCs were sorted in a well of a 96-well PCR plate (Eppendorf), prefilled with 5 µl 1 x TCL buffer (Quiagen) containing 1:100 β-mercaptoethanol. After sorting, the 96-well PCR plate was covered with an aluminum foil for cold storage (VWR) and centrifuged for 1 min at 50 x *g*. Immediately after centrifugation, the cells were placed on dry ice and then stored at -80 °C until further usage.

The total RNA purification from the MSCs and the reverse transcription into cDNA were performed by Rupert Oellinger (TUM, AG Rad) as described previously (Picelli et al., 2013).

3.7.2 Library preparation and RNAseq from niche cell populations

The library preparation for bulk 3'-sequencing of poly(A)-RNA from niche cell populations was done as described previously (Parekh et al., 2016). Briefly, barcoded cDNA of each sample was generated with a Maxima RT polymerase (Thermo Fisher) using oligo-dT primer containing barcodes, unique molecular identifiers (UMIs) and an adapter. 5' ends of the cDNAs were extended by a template switch oligo (TSO). All samples were pooled, and the cDNA was amplified with primers binding to the TSO-site and the adapter. cDNA was tagmented with the Nextera XT kit (Illumina) and 3'-end-fragments finally amplified using primers with Illumina P5 and P7 overhangs. In comparison to Parekh et al. the P5 and P7 sites were exchanged to allow sequencing of the cDNA in read1 and barcodes and UMIs in read2 to achieve a better cluster recognition. The library was sequenced on a NextSeq 500 (Illumina) with 65 cycles for the cDNA in read1 and 16 cycles for the barcodes and UMIs in read2. RNA sequencing has been performed in a collaboration with Rupert Oellinger (TUM, AG Rad).

3.8. Experimental procedure of bacterial techniques

3.8.1 Transformation

In the experiments, heat shock competent *E. coli* bacteria (DH5a, Invitrogen) were used, which have the ability to absorb free extracellular genetic material. In the first step of the procedure, the competent bacteria and the MIG empty vector control and MIG-p185BCR/ABL vector (Miething et al., 2003) were slowly thawed on ice.

The two vectors carry both an ampicillin resistance gene (Amp) and a gene encoding green fluorescence protein (GFP) for use as a selectable marker. After 2 µl of the vector was added to the competent cells, the competent cells/DNA mixture was incubated on ice for 30 min. For the heat shock, the competent cells/DNA mixture was incubated for 30 sec at 42 °C and placed on ice. After 250 µl of the microbial growth SOC medium was added to increase the transformation efficiency of *E. coli* (Hanahan, 1983), the mixture was incubated at 37 °C for 1 h by 225 rpm. In the following step, 50 µl and 100 µl of the mixture was spread on two separated preheated 10 cm^2 LB agar (Carl Roth) plates with appropriate antibiotic (100 µg/ml ampicillin) and subsequently incubated at 37 °C without CO_2 overnight.

3.8.2 Isolation of the plasmid

For the plasmid isolation, single bacterial clones were picked from a LB agar plate or a glycerol stock. Then, the LB medium containing ampicillin (100 µg/ml) was inoculated with resistant clones. The liquid cultures were incubated over night for 12 h to 16 h at 37 °C without CO_2 by 700 rpm to produce the necessary bacterial clones (cell mass) for the isolation of sufficient amounts of DNA. Depending on the required amount of DNA, 5 ml (Qiagen® Spin Miniprep Kit) or 250 ml (Qiagen® HiSpeed® Plasmid Maxi Kit) of the LB medium were used according to the Qiagen manufacturer's instructions. After the bacterial cells were harvested by centrifugation at 2000 x *g* for 10 min at 4 °C and purification of DNA, the DNA was eluted with distilled water. The concentration of the DNA was photometrically determined by NanoDrop™ 2000/c spectrophotometer and stored at -20 °C. The resulting DNA was analyzed by sequencing. The glycerol stocks were prepared from 600 µl of the liquid bacterial culture with 400 µl 85 % glycerol and stored at -80 °C.

3.8.3 Sequencing

Sequence analyses of the plasmid was carried out by Eurofins Genomics in Ebersberg.

3.9. Experimental procedure of histological methods

For the histological examinations, the tumors from *Sfrp1* conditional mice treated with MIG-$p185^{BCR/ABL}$ were fixed for 2 days in 4 % PFA and afterwards stored in 1 x DPBS. The histological analysis was carried out in the pathology department by Dr. Katja Steiger. For the analysis, the tumor was first embedded in paraffin and the finished paraffin block was then cut with a rotary microtome. The sections were then deparaffinized, stained with hematoxylin and eosin. The histological slices were evaluated at a 40-fold magnification.

3.10. Computational methods and data

3.10.1 RNA sequencing analysis

The minor murine reference genome release GRCm38.p6 including all haplotypes and patches was used as reference for mapping the raw read data with Dropseq tools v1.13 (Macosko et al., 2015). Gencode annotation release M19 was used to determine read counts per gene resulting in a *genes x samples* count matrix.

To start bioinformatic analysis, we developed a pipeline for filtering of these RNAseq results in python. Initially, we combined the count table, which we received from our collaborators AG Rad, according to the cell count, fused both Run1 and Run2 to a mean Run by calculating the mean (average) of the given data set and built an integer. Afterwards, we sorted the table of the read counts according to genotypes and split the samples (columns) in respect to the culture flag (primary, culture). We only used primary samples for the subsequent steps. Next, we removed all transcripts with a low gene count. Namely those with a read count under 10.

After removing features with consistently low counts (median <10), we normalized the raw count data using the trimmed mean of M-values (TMM) (Robinson & Oshlack, 2010) normalization method, as implemented in the edgeR (Robinson, McCarthy, & Smyth, 2010) package. DESeq2 (Love, Huber, & Anders, 2014) approaches with Benjamini-Hochberg multiple testing correction (BH or the false discovery rate (FDR)) (Benjamini & Hochberg, 1995) was used to select the differentially expressed genes (DEGs) from the normalized gene expression data. Genes were defined as differentially expressed if demonstrating a $-1.0 \leq \log2FC \geq 1.0$ and a p-value ≤ 0.05 between the respective comparison groups. The final list of DEGs was derived from DESeq2 by calculating the mean log2FC and combining the respective p-Values using Fisher's method (Fisher, 1948).

Functional enrichment analysis of the DEGs was performed using enrichGO from the clusterProfiler (Yu et al., 2012), which identify overrepresented biological GO categories. Furthermore, PANTHER classification system version 10.0 (Mi et al., 2016) was used, based on the GO database (version 1.2), with default settings for mice using the annotation dataset ‘GO biological process complete’.

3.10.2 Statistical analysis

In each experiment, the statistical tests were performed by using GraphPad Prism (GraphPad Software, La Jolla, CA). The statistical tests are indicated in the figure legends. A *p* value less than or equal to 0.05 was considered to be statistically significant. Data are presented as mean ± SD. Grubbs' test was used to determine significant outlier (significance level ≤ 0.01). All analyses for the RNAseq were performed in python and the R statistical environment.

4. Results

Hematopoietic stem cells (HSCs) reside in the microenvironment of the bone marrow, also called the niche. A large portion of HSCs are quiescent and can be rapidly activated by acute or chronic extrinsic stress signals (Boulais & Frenette, 2015; Schofield, 1978; Takizawa & Manz, 2017; A. Wilson et al., 2008), like injury, inflammation, cancer and during aging (Gnani et al., 2019; Morrison & Spradling, 2008). Not only HSCs, but also the niche responds to these stress factors and it has been reported that the niche stress response is required for a normal regeneration, and may also contribute to malignant transformation (Batsivari et al., 2020; Bhagat et al., 2017; Takubo, Morikawa, & Kobayashi, 2017).

Prior to this thesis, SFRP1, secreted by the microenvironment, was identified as a niche factor regulating the cycling activity and maintenance of HSCs (Renström et al., 2009). In this thesis, the function of SFRP1 was analyzed by specific deletion the *Sfrp1* gene in osteogenic lineage stromal cells. For this purpose, we crossed newly generated *Sfrp1*$^{lox/lox}$ mice with transgenic *OSX-GFP::CRE* mice (Osx-Cre), which express GFP and the CRE recombinase under the SP7 (Osterix1) promotor. To study the extrinsic role of *Sfrp1* and to unravel the signals elicited by niche cells, the cells of *Sfrp1* conditional mice were analyzed *in vitro* and *in vivo* under steady-state conditions as well as under different stress conditions, such as lipopolysaccharide (LPS) treatment, bone marrow transplantation, and the presence of BCR-ABL1^{+} leukemia.

4.1. Stromal cells support the maintenance of hematopoietic stem cells in non-contact setting

An important goal of experimental and clinical hematology is the identification of mechanisms of stem cell self-renewal and maintenance, and to identify conditions that support the expansion of transplantable hematopoietic stem cells.

A problem for stem cell maintenance is that stem cells exhaust after repeated stress and over time. Entry of stem cells into cell cycle is by default associated with increased DNA damage (and mitochondrial/metabolic activation) (Walter et al., 2015). *In vivo*, different niche cell populations interact with stem cells to limit their activation and prevent the stem cells from becoming exhausted during stress responses (Ruf et al., 2016). Knowledge about the niche factors involved in limiting stem cell exhaustion, is, however, limited.

To self-renew, HSCs must divide and retain their LTR ability. We previously identified the murine stromal cell line UG26-1B6 which maintains HSCs in non-contact setting (Buckley et al., 2011; Oostendorp et al., 2005). We further showed that secreted factors produced by UG26-1B6 cells in combination with cytokines KITL (also known as Stem Cell Factor, or SCF) plus IL-11 (2GF) produce a significant expansion of serially transplantable HSCs *in vitro* and identified nerve growth factor (NGF) and collagen 1 (Col1) to be the most effective substitute for UG26-1B6 conditioned medium (CM) (Wohrer et al., 2014).

Since the UG26-1B6 stromal clone transforms over time, and only low passage cells can be used (Oostendorp et al., 2002a; 2002b), we sought to establish a culture system with similar characteristics using stromal cells from a primary cell source. For this purpose, we studied mouse embryonic fibroblasts (MEFs) to act as a robust and versatile alternative source of CM from midgestation stromal cells to maintain and expand mouse HSCs (Figure 13).

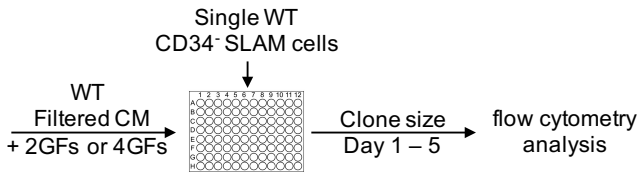

Figure 13. Experimental design of the single cell cultures in SFM and MEF conditioned medium. Single $CD34^{-}CD150^{+}$ LSK cells were sorted into 96-round-bottomed plate prefilled with SFM or WT MEF-CM. WT MEF-CM was either supplemented with mSCF (100 ng/ml) and IL-11 (20 ng/ml) (2GFs) or additionally with NGF (10 ng/ml) and Col1 (100 ng/ml) (4GFs). SFM was supplemented with 4GFs. Cells were microscopically inspected and counted every 24 h for five days.

Our experiments showed that CM from WT MEFs (MEF-CM) supports survival (Figure 14A) and phenotypical identity of HSCs, as well as cell cycle entry (Figure 14B) in single cell cultures of $CD34^{-}$ $CD48^{-}$ $CD150^{+}$ $Lineage^{-}$ $SCA\text{-}1^{+}$ KIT^{+} ($CD34^{-}$ SLAM) cells supplemented with SCF and IL-11 (2GFs) in single cell cultures. Strikingly, in comparison with cultures in serum-free medium with four growth factors (4GFs: SCF, IL-11, NGF, and Col1), WT MEF-CM increases the numbers of proliferating clones (Figure 14D) and the number of LSKs (Figure 14E), both with two and four growth factors. It does not improve time to first division (Figure 14C) (Marquez Romero et al., 2020).

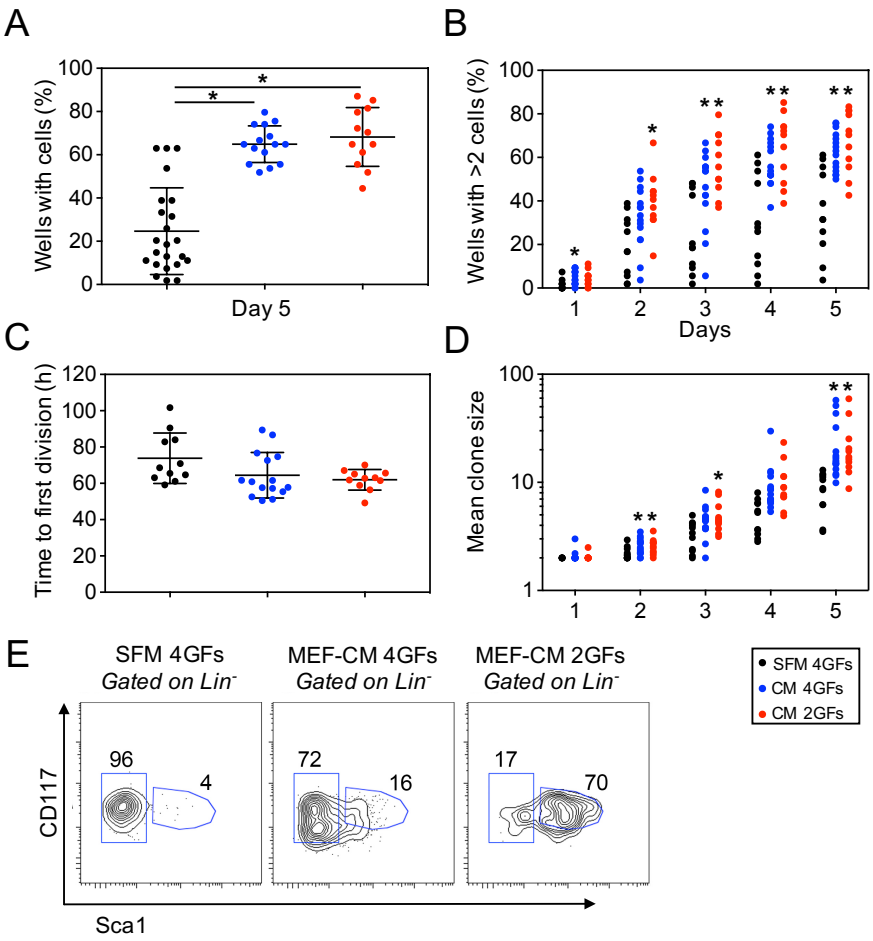

Figure 14. Single cell cultures in SFM and MEF conditioned medium. (A) Percentage of wells with cells (survival) at day 5 for each plate cultured in SFM 2GFs (n = 23) or WT MEF-CM 2 GFs (n = 12) and 4GFs (n = 15). **(B)** Percentage of wells with divided cells per day at each plate cultured in SFM 2GFs (n = 10) or WT MEF-CM 2 GFs (n = 10) and 4GFs (n = 11). **(C)** Mean hours of time to first division of cells cultured in SFM 2GFs (n = 11) or WT MEF-CM 2 GFs (n = 11) and 4GFs (n = 15). **(D)** Mean of clone size per day at each plate cultured in SFM 2GFs (n = 10) or WT MEF-CM 2 GFs (n = 10) and 4GFs (n = 11). **(E)** Representative flow cytometry plots of LSKs (Lineage$^-$SCA-1$^+$KIT$^+$), 5 days after culture in certain conditions. Black dots represent SFM 4GFs; Blue dots represent MEF-CM 4GFs; Red dots represent MEF-CM 2GFs. Each dot represents one plate. Figure A and C: Represented values are illustrated as Mean ± SD; Figure B and D: Represented values are illustrated as Mean. * p-value ≤0.05 show significant differences in the comparison between SFM 4GFs and either MEF-CM 4GFs or MEF-CM 2GFs determined by ANOVA, Tukey`s post hoc test (scheme adapted from (Marquez Romero et al., 2020)). [Data were generated in cooperation with S. Romero Marquez (Stem Cell Physiology Lab, Munich)].

Most importantly, WT MEF-CM supports division of HSCs in culture with retention of both short- and long-term hematopoiesis-repopulating ability *in vivo* (Figure 15) (Marquez Romero et al., 2020).

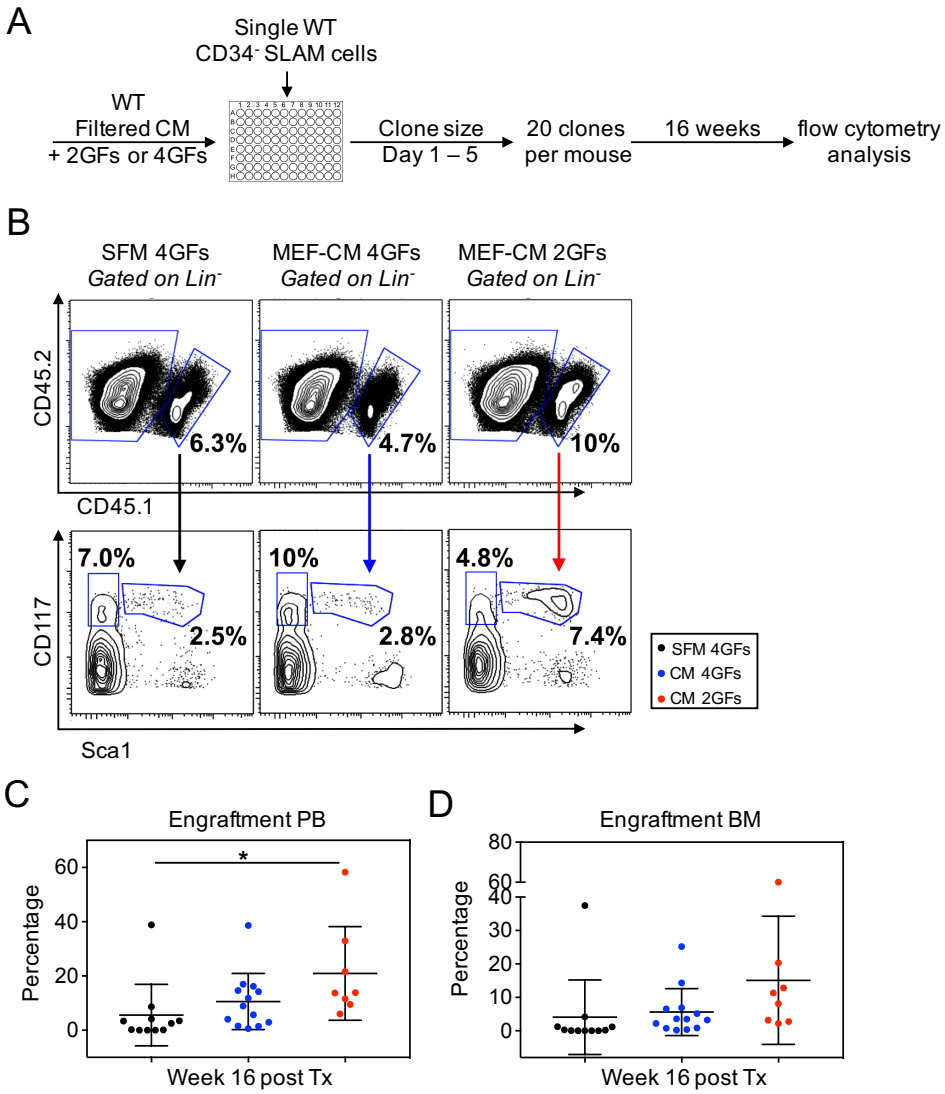

Figure 15. Self-renewal of repopulating HSCs in single cell cultures. (A) Experimental design: single CD34$^-$CD150$^+$ LSK cells were sorted into 96-round-bottomed plate prefilled with SFM and WT MEF-CM. WT MEF-CM was either supplemented with mSCF (100 ng/ml) and IL-11 (20 ng/ml) (2GFs) or additionally with NGF (10 ng/ml) and Col1 (100 ng/ml) (4GFs). SFM was supplemented with 4GFs. After 5 days of culture, 20 wells with at least one cell division were harvested and transplanted into lethally irradiated primary recipients (CD45.2) together with competitor cells (CD45.2) as described in the section: *3.1.8 In* vivo repopulation assay. **(B)** Above: Representative flow cytometry plots of donor and recipient cells from the BM, 16 weeks after transplantation (Tx). Below: Representative flow cytometry plots of donor-derived lineage$^-$ fraction, showing myeloid progenitors (MPs; SCA-1$^-$ KIT$^+$) cells and LSKs (Lineage$^-$SCA-1$^+$KIT$^+$), 16 weeks after Tx. **(C)** Percentage of donor cell engraftment in PB of cells cultured in SFM 2GFs (n = 11) or WT MEF-CM 2 GFs (n = 8) and 4GFs (n = 13), 16 weeks after Tx. **(D)** Percentage of donor cell engraftment in BM, of cells cultured in SFM 2GFs (n = 11) or WT MEF-CM 2 GFs (n = 8) and 4GFs (n = 13), 16 weeks after Tx. Black dots represent SFM 4GFs; Blue dots represent MEF-CM 4GFs; Red dots represent MEF-CM 2GFs. Each dot represents one animal. Represented values are illustrated as Mean ± SD. * p-value ≤0.05 show significant differences in the comparison between SFM 4GFs and either MEF-CM 4GFs or MEF-CM 2GFs determined by ANOVA, Tukey`s post hoc test (scheme adapted from (Marquez Romero et al., 2020)). [Data were generated in cooperation with S. Romero Marquez (Stem Cell Physiology Lab, Munich)].

Since previous studied had shown that the *Sfrp1* deficient microenvironment do not efficiently maintain HSCs (Renström et al., 2009). We further wondered whether CM collected from MEFs grown from embryos at day E13.5 of Sfrp1$^{-/-}$ mice supports proliferation and maintenance of murine WT HSCs (Marquez Romero et al., 2020).

In our previous paper (Renström et al., 2009), we were unable to determine whether deletion of *Sfrp1* in the microenvironment influenced HSC behavior through direct contact, or through secreted factors. Thus, we used the single cell technology, mentioned in the previous paragraphs, and performed single-cell cultures by using WT MEF-CM with either 2GFs or 4GFs and compared this CM with the CM prepared from *Sfrp1*$^{-/-}$ MEFs with 2GFs. As in the above experiments, we counted the presence and number of cells per well (Figure 16). The results with WT MEF-CM were reported as part of a larger study, which was published separately (Marquez Romero et al., 2020) (Figures 14, 15), but only the results of parallel experiments with *Sfrp1*$^{-/-}$ MEF-CM are shown below.

Generally, the percentage of wells with cells were significantly decreased on all five days when using *Sfrp1*$^{-/-}$-CM 2GFs compared to WT MEF-CM 4GFs and on the first three days when using *Sfrp1*$^{-/-}$-CM 2GFs compared to WT MEF-CM 2GFs. In addition, the survival on day five was significant decreased when using *Sfrp1*$^{-/-}$-CM 2GFs compared to WT MEF-CM 4GFs (Figure 16A, B), suggesting that *Sfrp1* regulates secreted factors important for HSC survival. When evaluating proliferation, it was found that wells with dividing cells were significantly decreased on day two, four and five when using *Sfrp1*$^{-/-}$-CM 2GFs compared to WT MEF-CM 4GFs (Figure 16C). Overall, *Sfrp1*$^{-/-}$-CM 2GFs stimulated cell cycle almost in the same way compared to WT MEF-CM 2GFs or 4GFs (Figure 16C). We found that the time to first division of murine CD34^{-} SLAM cells cultured in *Sfrp1*$^{-/-}$-CM 2GFs was similar compared to the WT MEF-CM with 2GFs or 4GFs (Figure 16D). Interestingly, the cultures with *Sfrp1*$^{-/-}$-CM 2GF showed similar clone sizes at day one to five of culture compared to WT MEF-CM 2GFs and 4GFs (Figure 16A, E), suggesting *Sfrp1*-regulated secreted factors do not affect proliferation.

In summary, our results show that cultures of murine WT HSCs in WT MEF-CM 2GFs or 4GFs support induction and propagation of cell division, as well as survival. More importantly, our results show that *Sfrp1* expression in MEFs is required to promote early stem cell survival as well as recruitment into cell cycle. However, since clone sizes in cultures with *Sfrp1*$^{-/-}$-CM do not differ from those with WT MEF-CM, *Sfrp1* expression is not necessary for HSC proliferation.

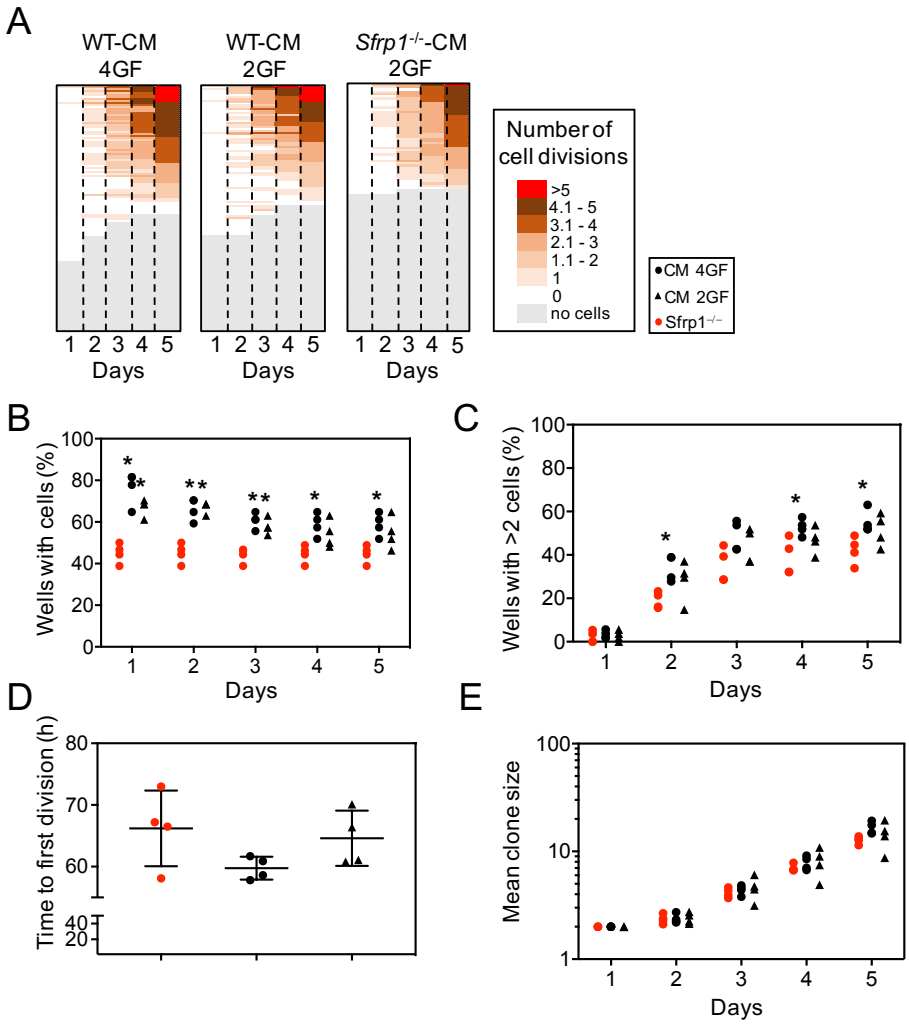

Figure 16. Single cell cultures in *Sfrp1*$^{-/-}$-MEF and WT-MEF conditioned medium. (A) Heat maps of the clone size per well for each CD34^{-}CD150^{+} LSK cell at each day of culture (left heat map culture in WT MEF-CM with 4GFs, middle heat map culture in WT MEF-CM with 2GFs, right heat map culture in *Sfrp1*$^{-/-}$ with 2GFs). **(B)** Percentage of wells with cells (survival) at each plate cultured in WT MEF-CM 2 GFs (n = 4) and 4GFs (n = 4) or *Sfrp1*$^{-/-}$ 2GFs (n = 4), 16 weeks after Tx. **(C)** Percentage of wells with divided cells at each plate cultured in WT MEF-CM 2 GFs (n = 4) and 4GFs (n = 4) or *Sfrp1*$^{-/-}$ 2GFs (n = 4). **(D)** Mean hours of time to first division of cells and wells with cells cultured in WT MEF-CM 2 GFs (n = 4) and 4GFs (n = 4) or *Sfrp1*$^{-/-}$ 2GFs (n = 4). **(E)** Mean of clone size per day at each plate cultured in WT MEF-CM 2 GFs (n = 4) and 4GFs (n = 4) or *Sfrp1*$^{-/-}$ 2GFs (n = 4). In A, a representative example is shown. Black dots represent WT MEF-CM 4GFs; Black triangle represent WT MEF-CM 2GFs; Red dots represent *Sfrp1*$^{-/-}$ 2GFs. Each dot represents one plate. Figure B, C, E: Represented values are illustrated as Mean; Figure D: Represented values are illustrated as Mean ± SD. * p-value ≤0.05 show significant differences in the comparison of *Sfrp1*$^{-/-}$ and WT MEF-CM with 2GFs or 4GFs determined by ANOVA, Tukey`s post hoc test.

4.2. Human *SFRP1* gene expression in bone marrow cells from leukemic and healthy donors

To assess whether *SFRP1* expression is of relevance in human clinical conditions, we then made a brief exploration in human samples. It has been reported that in cells from patients, with various malignant conditions, an increased promoter methylation of the *SFRP1* gene and expression of *SFRP1*-targeting miRNAs can be observed in tumor samples, which both decrease expression of SFRP1 (Baharudin et al., 2020). Similarly, in peripheral blood (PB) and bone marrow (BM), *SFRP1* promotor methylation is associated with malignant hematological diseases, such as acute myeloid leukemia (AML) (Jost et al., 2008), chronic myeloid leukemia (CML) (Seeliger et al., 2009) and myelodysplastic syndromes (MDS) (Reins et al., 2010).

Since SFRP1 promotor methylation associates with mRNA downregulation, we determined *SFRP1* gene expression in cryopreserved cell suspensions of whole bone marrow (BM) samples of healthy donors and leukemic donors (AML and CML) between 24 and 55 years. For this, we thawed and prepared the cells for the analyzation of the RNA expression profile of *SFRP1*. The gene expression was analyzed by calculating the ΔΔCt value relative to the housekeeping gene eukaryotic initiation factor-3 (*EIF-3*) and a human universal cDNA.

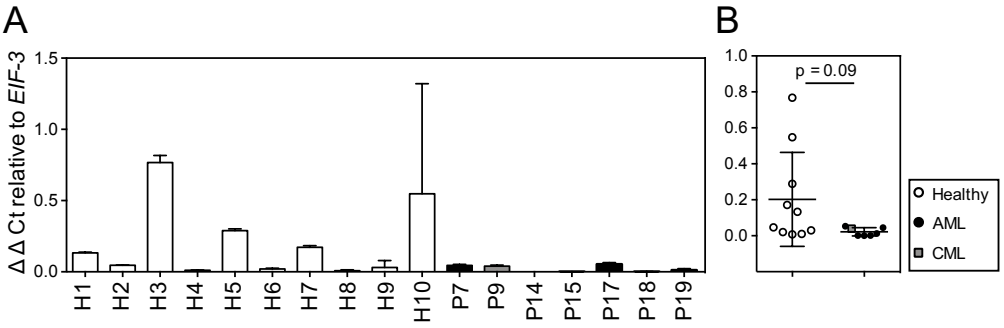

Figure 17. *SFRP1* expression profiles in whole BM samples of healthy and leukemic donors between 24 and 55 years. (A) *SFRP1* expression of individual healthy (H1 – H10) donors, AML (P7, P14, P15, P17, P18, P19) and CML (P9) patients. **(B)** Grouped *SFRP1* content of healthy and leukemic (AML and CML) patients (determined by unpaired t test p = 0.09). The data represent the relative ΔΔCt value to the housekeeping gene *EIF-3* and a human universal cDNA. Figure A and B show healthy donors (n = 10) in white, AML donors (n = 6) in black and CML donor (n = 1) in grey. Represented values are illustrated as Mean ± SD. [Data were generated in cooperation with S. Romero Marquez (Stem Cell Physiology Lab, Munich)].

These experiments showed that RNA expression levels of human *SFRP1* is lower in the leukemic patient samples when compared to the healthy samples (Figure 17A, B), confirming observations also made by other groups (Vincent & Postovit, 2017).

4.3. *Sfrp1* expression in stromal cells and hematopoietic cells from wild-type mice

The above and previously published experiments show expression of *SFRP1* expression in whole BM samples, but do not distinguish expression in different BM subpopulations. For the analysis of the SFRP1 protein content and further study of the relevance of *Sfrp1* gene expression in different cell compartments we decided to switch back to the mouse system.

To determine *Sfrp1* and SFRP1 expression in cells of the BM, we sorted the stromal cells of the niche ($CD45^-Ter119^-CD31^-CD166^-SCA\text{-}1^+$ mesenchymal stromal cells (MSCs), $CD45^-Ter119^-CD31^-CD166^+SCA\text{-}1^-$ osteoblastic lineage cells (OBCs) and $CD45^-Ter119^-CD31^+$ $SCA\text{-}1^+$ endothelial cells (ECs), Figure 18) and of mature hematopoietic cells ($GR1^+CD11b^+$ granulocytes, $GR1^{med}CD11b^+$ monocytes and $B220^+$ B cells; Figure 19) of wild-type (*Sfrp1*$^{+/+}$, WT) mice. For antibody verification of the SFRP1 antibody (2.8.2 Primary antibodies immunofluorescence and western blot), we used cultured mouse embryonic fibroblasts (MEFs) from WT and *Sfrp1*$^{-/-}$ mice (Satoh et al., 2006) (Figure 18B).

The immunofluorescence staining of sorted cell populations indicated that SFRP1 protein is expressed in stromal cells and there were no significant differences detectable between the MSCs, OBCs and ECs; (Figure 18A, D). However, the highest mRNA expression level of *Sfrp1* was found in $SCA\text{-}1^+$ mesenchymal stromal cells (MSCs) and both OBCs and ECs showed a significant lower expression level of *Sfrp1* compared to the MSCs (Figure 18C). Considering similar detection of SFRP1 protein, we hypothesize that SFRP1 produced by MSCs may be taken up by OBCs and ECs. To test this hypothesis, we attempted uptake experiments using biotinylated recombinant murine SFRP1. Unfortunately, these experiments were not successful and the question remains to be answered.

Dolgalev and Tikhonova, performed an integrated analysis of the niche heterogeneity incorporating several published single BM niche cell datasets (Dolgalev & Tikhonova, 2021). A searchable website can be found under the Single Cell Portal https://singlecell.broadinstitute.org/single_cell/study/SCP1248 from the Broad Institute. In their analysis, it can be found, that *Sfrp1* is mainly expressed in CXCL12-abundant mesenchymal stem/progenitor cells (MSPCs), at the interface of the two MSPC populations defined as MSPC-Adipo and -Osteo (Figure 18E). Based on their analysis, these two MSPC populations correspond best to the $ALCAM^{-/med}$ $SCA\text{-}1^+$ MSCs used in this thesis.

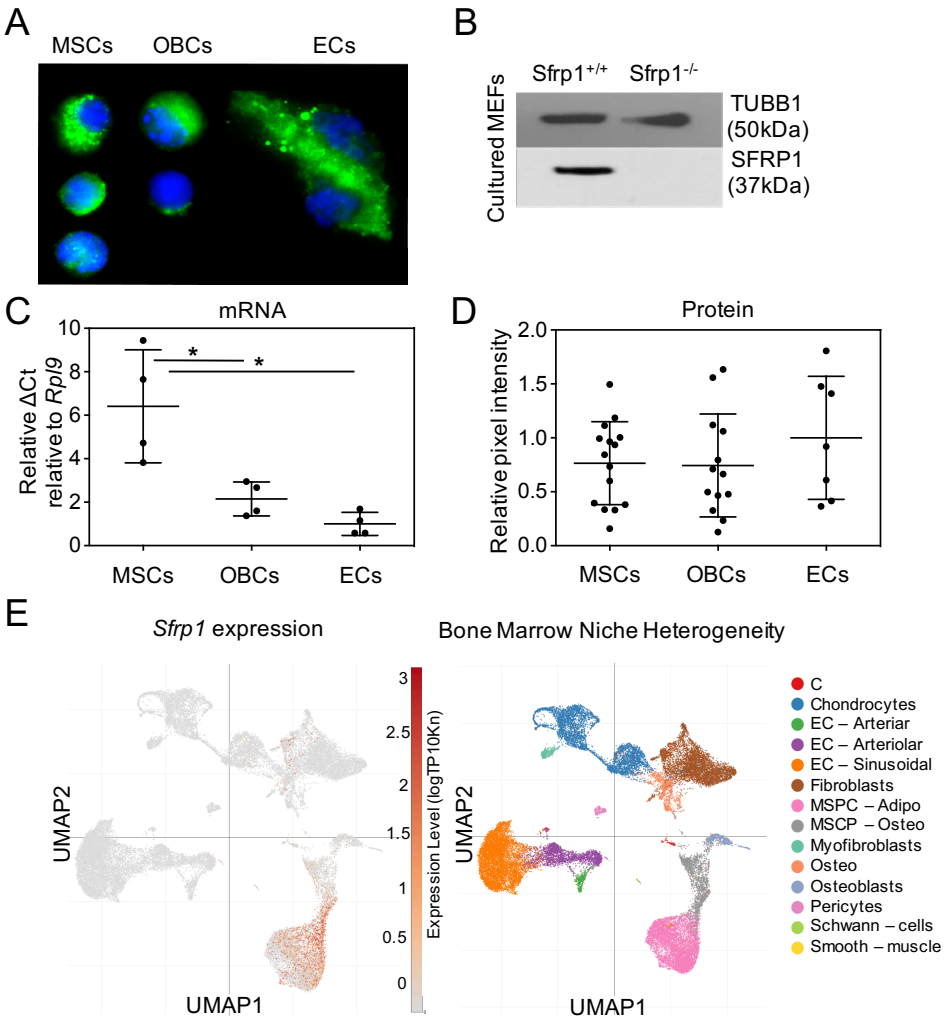

Figure 18. Sfrp1 expression in stromal cells from wild-type mice. (A) Representative pictures of single-cell stains showing the expression of SFRP1 protein in stromal cell compartments. **(B)** Representative pictures of the antibody verification using cultured MEFs from the WT and SFRP1$^{-/-}$ mice. Tubulin Beta 1 Class VI (TUBB1) was used as housekeeping gene. **(C)** *Sfrp1* mRNA content of sorted MSCs (n = 4), OBCs (n = 4) and ECs (n = 4). The data represent the relative ΔCt value to the housekeeping gene *Rpl9*. **(D)** Relative fluorescence pixel intensity measurements to the ECs of SFRP1 in sorted MSCs (n = 15), OBCs (n = 13) and ECs (n = 7). **(E)** Overview of the published single cell sequencing datasets of *Sfrp1* expression in the bone marrow niche (https://singlecell.broadinstitute.org/single_cell/study/SCP1248). Figure A show staining for the SFRP1 protein in green, the nuclei staining with DAPI in blue. For quantification of the proteins, cells were snapped on Leica fluorescent microscope, 100-fold enlarged. For Figure C, each dot represents one animal. Figure D the total pixels were quantified by ImageJ; each dot represents one cell. Represented values are illustrated as Mean ± SD; * p-value ≤0.05 show significant differences in the comparison of the different cell compartments determined by ANOVA, Tukey`s post hoc test.

We further analyzed hematopoietic cell compartments of the BM, including GR1^{+}CD11b^{+} granulocytes, GR1^{med}CD11b^{+} monocytes, and B220^{+} B cells. These experiments showed a significantly higher protein levels of SFRP1 in mature GR1^{hi}CD11b^{+} granulocytes (Figure 19A, C) compared to GR1^{med} CD11b^{+} monocytes and CD45R^{+} B cells. Similarly, these latter two populations showed a significantly lower mRNA expression of *Sfrp1* compared to the granulocytes (Figure 19B).

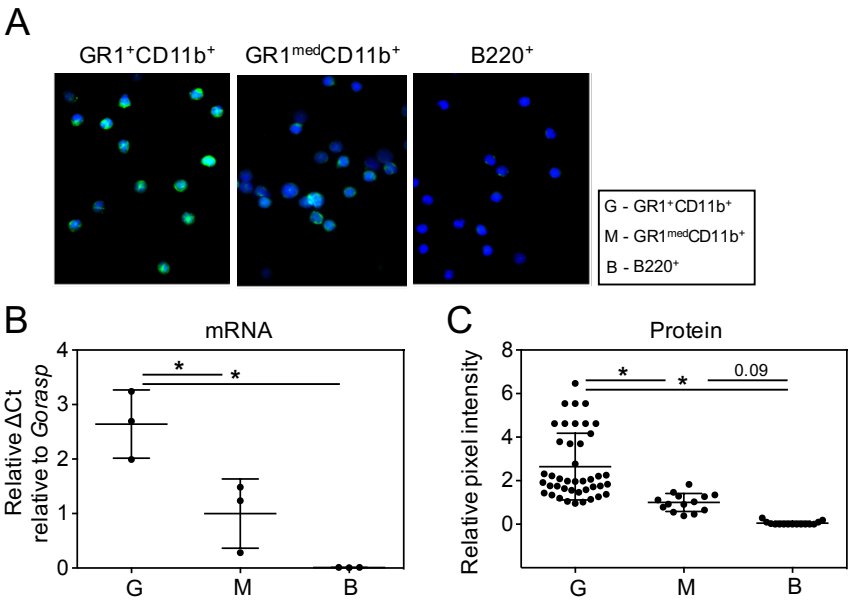

Figure 19. Sfrp1 expression in hematopoietic cells from wild-type mice. (A) Representative pictures of single-cell stains showing the expression of SFRP1 protein in hematopoietic cell compartments. **(B)** Relative *Sfrp1* mRNA content of sorted $GR1^{+}CD11b^{+}$ (n = 3), $GR1^{med}CD11b^{+}$ (n = 3) and $B220^{+}$ (n = 3) to the $GR1^{med}CD11b^{+}$ monocytes. The data represent the relative ΔCt value to the housekeeping gene *Gorasp*. **(C)** Relative fluorescence pixel intensity measurements to the $GR1^{med}CD11b^{+}$ monocytes of SFRP1 in sorted $GR1^{+}CD11b^{+}$ (n = 42 cells), $GR1^{med}CD11b^{+}$ (n = 14 cells) and $B220^{+}$ (n = 15 cells). Figure A show staining for the SFRP1 protein in green, the nuclei staining with DAPI in blue. For quantification of the proteins, cells were snapped on Leica fluorescent microscope, 100-fold enlarged. For Figure B, each dot represents one animal. Figure C the total pixels were quantified by ImageJ; each dot represents one cell. Represented values are illustrated as Mean ± SD; * p-value ≤0.05 show significant differences in the comparison of the different cell compartments determined by ANOVA, Tukey`s post hoc test.

Taken together, we identified *Sfrp1* expression in MSCs and mature granulocytes. In addition, we also found SFRP1 protein in OBCs and ECs with low levels of mRNA, suggesting uptake of extrinsic SFRP1.

4.4. Generation and analysis of *Sfrp1* conditional mice

In order to study the function of *Sfrp1* and SFRP1 in stromal MSPCs, we deleted the *Sfrp1* gene in stromal cells, by crossing newly generated *Sfrp1* conditional mice ($SFRP1^{tm1a}$ mouse line KO first, see 3.1.1 Generation of *Sfrp1* conditional knockout strain) with transgenic mice expressing CRE recombinase under the *Sp7* (=Osterix, or Osx) promotor (Figure 20A).

The *loxP* sites are on either side of the critical exon 2 of the *Sfrp1* gene. The activity of the CRE recombinase deletes the critical exon 2 and induced a frame shift mutation (Figure 20A). The promotor activity of Osx is limited to bone marrow osteolineage cells, like pre-osteoblasts, osteocytes, and hypertrophic chondrocytes (Rodda & McMahon, 2006).

In addition, progeny of Osx-GFP cells is found in perivascular cells and adipocytes in the bone marrow (Chen et al., 2014; Mizoguchi et al., 2014). Consequently, the deletion of *Sfrp1* in the Osx-Cre conditional mice is limited to the mesenchymal stromal cell compartments of the bone marrow, and does not affect gene expression in ECs and hematopoietic cells.

After crossing *Sfrp1*$^{lox/lox}$ mice with *OSX1-GFP::Cre* (Osx-Cre; *B6.Cg-Tg(Sp7-tTA,tetO-EGFP/cre)1Amc/J*; Jackson Labs Stock Nr.: 006361) transgenic mice, which express CRE and eGFP under the control of a tetO responsive Osx1 promotor (Rodda & McMahon, 2006). Without Doxycyclin to regulate the tetO-responsive element, Cre is constitutively active in Osx^{+} cells, allowing expression of the CRE recombinase, which cuts the “floxed” critical exon 2 (CE) of the *Sfrp1* target gene, resulting in deletion of the expression of *Sfrp1* gene in stromal cells.

The one Frt site is located on the 5`end of the exon from previFlp recombinase. Further crossing with Cre recombinase transgenic mice results into deleted allele. CRE gene insertion in the offspring was validated by CRE PCR (Figure 20B).

To validate deletion of the *Sfrp1* gene, we performed a *Sfrp1*-del PCR, as well as a HA5L-CCE3R PCR. The PCRs were performed to guarantee succeeded deletion of exon 2. The sizes of the resulting fragments after the specific PCRs are shown in Figure 20B. It is important to note, that the *Sfrp1* del PCR shows all expected genotypes. For the genotyping of *Sfrp1* conditional mouse model, the HA5L-CCE3R PCR, *Sfrp1* del PCR and CRE PCR are used.

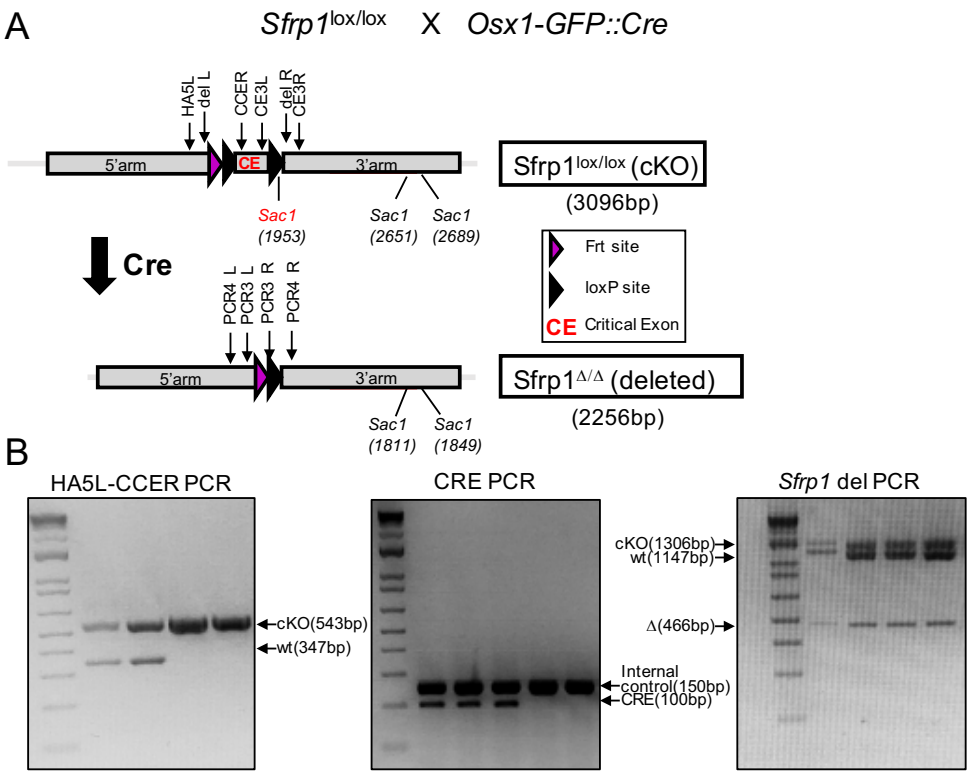

Figure 20. Genotyping of the *Sfrp1* conditional mice. (A) Generation and analyzation of *Sfrp1* conditional mice. In order to study Sfrp1 function we knock out *Sfrp1* gene in stromal compartment by using newly generated *Sfrp1* conditional mouse crossed with mice expressing CRE recombinase under Osx1 promoter. The used primer of the PCRs indicated in the scheme. **(B)** left: The expected PCR results (cKO 543bp; wt 347bp) are shown for the HA5L-CCE3R PCR; middle: The expected PCR results (internal control 150bp; CRE 100bp) are shown for the CRE PCR; right: The expected PCR results (cKO 1306bp; wt 1147bp; Δ 466bp) are shown for the *Sfrp1* del PCR.

After successful deletion of the *Sfrp1* gene in Osx-Cre stromal cells (*Sfrp1* conditional deletion (Δ) mutants (*Sfrp1*$^{+/\Delta}$ and *Sfrp1*$^{\Delta/\Delta}$ mice)), the resulting phenotypic alterations were analyzed. When observing the offspring, we found that the loss of *Sfrp1* does not lead to gross external abnormalities: the *Sfrp1* conditional mice reveal a normal embryonic, prenatal development and both males and females are fertile. However, the *Sfrp1*$^{+/\Delta}$ and *Sfrp1*$^{\Delta/\Delta}$ mice showed decreased weight and size compared to their Cre^{-} littermates independently of their gender (Figure 21A). The *Sfrp1* conditional mice have a significant additional reduction in body weight at the age of 8 weeks compared to the controls, as measured by weighing at weekly intervals (Figure 21B, C).

In general, males are heavier than females, except for the age range between 3 and 5 weeks. The weight difference between males and females is approx. 5 - 6 g. The *Sfrp1* deletion mutants have a significant decreased body weight. The weight difference between *Sfrp1*$^{lox/lox}$ and Osx-Cre controls, as well as for the *Sfrp1* conditional mice is approx. 4 g for both males and females.

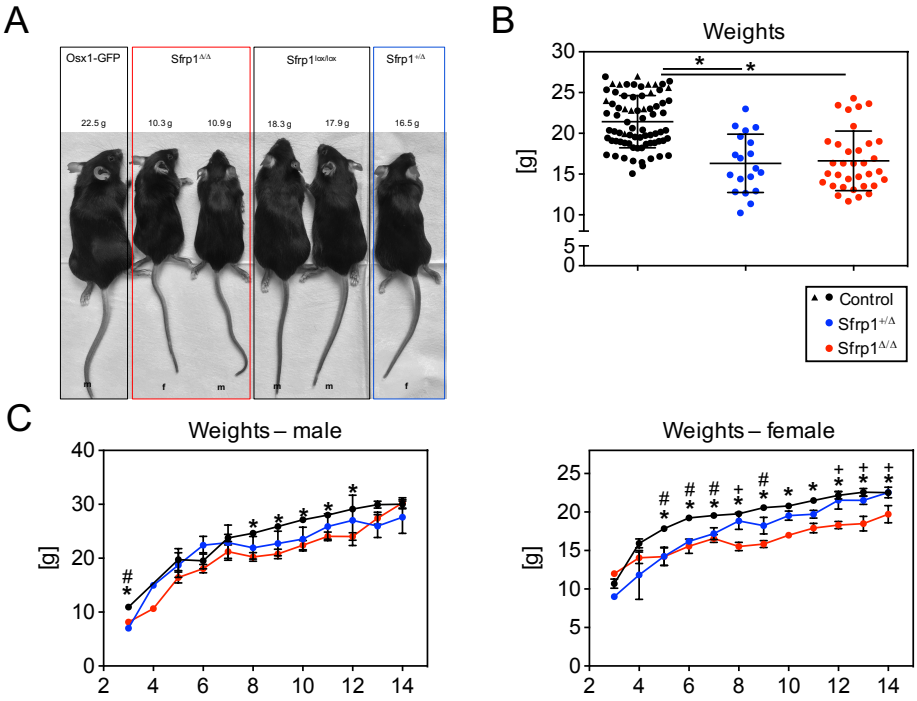

Figure 21. Alterations in the body weight of the *Sfrp1* conditional mice. (A) Representative pictures of *Sfrp1* conditional mice (*Sfrp1*$^{+/\Delta}$: n = 1; *Sfrp1*$^{\Delta/\Delta}$: n = 2) and the controls (*Sfrp1*$^{lox/lox}$: n = 2, Osx-Cre: n = 1). **(B)** Decreased body weight of *Sfrp1* conditional mice (*Sfrp1*$^{+/\Delta}$: n = 19; *Sfrp1*$^{\Delta/\Delta}$: n = 34) compared to the controls (n = 75) in week 8. * p-value ≤0.05 show significant differences in the comparison of *Sfrp1* conditional mice (*Sfrp1*$^{+/\Delta}$; *Sfrp1*$^{\Delta/\Delta}$) to each other or to controls (*Sfrp1*$^{lox/lox}$; Osx-Cre) determined by ANOVA, Tukey`s post hoc test. **(C)** left: Growth curve of the male mice; right: Growth curve of the female mice. Black dots represent controls (*Sfrp1*$^{lox/lox}$); Black triangles represent controls (Osx-Cre); Blue dots represent *Sfrp1*$^{+/\Delta}$; Red dots represent *Sfrp1*$^{\Delta/\Delta}$. Each dot represents one animal. Represented values are illustrated as Mean ± SD; * p-value ≤0.05 show significant differences in the comparison of *Sfrp1*$^{\Delta/\Delta}$ to *Sfrp1*$^{lox/lox}$; $^{\#}$ p-value ≤0.05 show significant differences in the comparison of *Sfrp1*$^{+/\Delta}$ to *Sfrp1*$^{lox/lox}$; $^{+}$ p-value ≤0.05 show significant differences in the comparison of *Sfrp1*$^{\Delta/\Delta}$ to *Sfrp1*$^{+/\Delta}$; determined by ANOVA, Tukey`s post hoc test.

4.4.1 Characterization of the bone homeostasis in *Sfrp1* conditional mice

SFRP1 is expressed by osteoblasts and inhibits osteoclast- and bone formation (Häusler et al., 2004; Yao et al., 2010), and *Sfrp1* is strongly expressed in multipotent MSCs and single MSPCs (Figure 18). Since these cells are also responsible for maintaining skeletal integrity (de Girolamo et al., 2013; Hayashi et al., 2008; Li et al., 2007; Otsuru et al., 2007; Pitchford et al., 2009), we analyzed the bone homeostasis in the *Sfrp1* conditional mice (*Sfrp1*$^{+/\Delta}$; *Sfrp1*$^{\Delta/\Delta}$) and control mice (*Sfrp1*$^{lox/lox}$, Osx-Cre) at the age of 8 weeks from male and female mice. As described before, there are gender-specific differences in the bone volume (BV) of the femur and vertebra (Sode et al., 2010). We described the gender-related differences where appropriate.

4.4.1.1 Gender specific alterations in bone volume of femur

The mean BV of the control male mice was 7.12%, whereas the mean BV of the control females was 1.95%. The mean BV of the *Sfrp1*$^{+/\Delta}$ male animals was 4.47% (a reduction of 37%), whereas the mean BV of the females was 1.31% (a reduction of 33%). The mean BV of the *Sfrp1*$^{\Delta/\Delta}$ male mice was 5.30% (a reduction of 25%), whereas the mean BV of the females was 1.53% (a reduction of 22%). Thus, the bone volume of the *Sfrp1*$^{+/\Delta}$ male animals was significantly decreased compared to the control mice (Figure 22A). In studying bone homeostasis, bone volume was the only parameter showing significant gender-specific differences with the control animals (combined results of *Sfrp1*$^{lox/lox}$ and Osx-Cre animals, both WT for *Sfrp1*).

4.4.1.2 Alterations in bone homeostasis parameters (not specific for gender) of femur

When studying the femur lengths, we found a significant reduction in *Sfrp1* conditional mice (*Sfrp1*$^{+/\Delta}$ mean: 14.08 [1/mm] (a reduction of 4.7%); *Sfrp1*$^{\Delta/\Delta}$ 14.29 [1/mm] (a reduction of 3.3%)) compared to controls (14.78 [1/mm], Figure 22B). But, the trabecular number (Figure 22C), trabecular thickness (Figure 22D) and trabecular separation (Figure 22E) in the *Sfrp1*$^{\Delta/\Delta}$ compared to the *Sfrp1*$^{+/\Delta}$ and the control mice was unchanged in the femora. Furthermore, the cortical thickness was reduced in *Sfrp1* conditional mice (*Sfrp1*$^{+/\Delta}$ mean: 0.14 [1/mm] (a reduction of 12.5%); *Sfrp1*$^{\Delta/\Delta}$ 0.13 [1/mm] (a reduction of 18.8%)) compared to controls (0.16 [1/mm], Figure 22F).

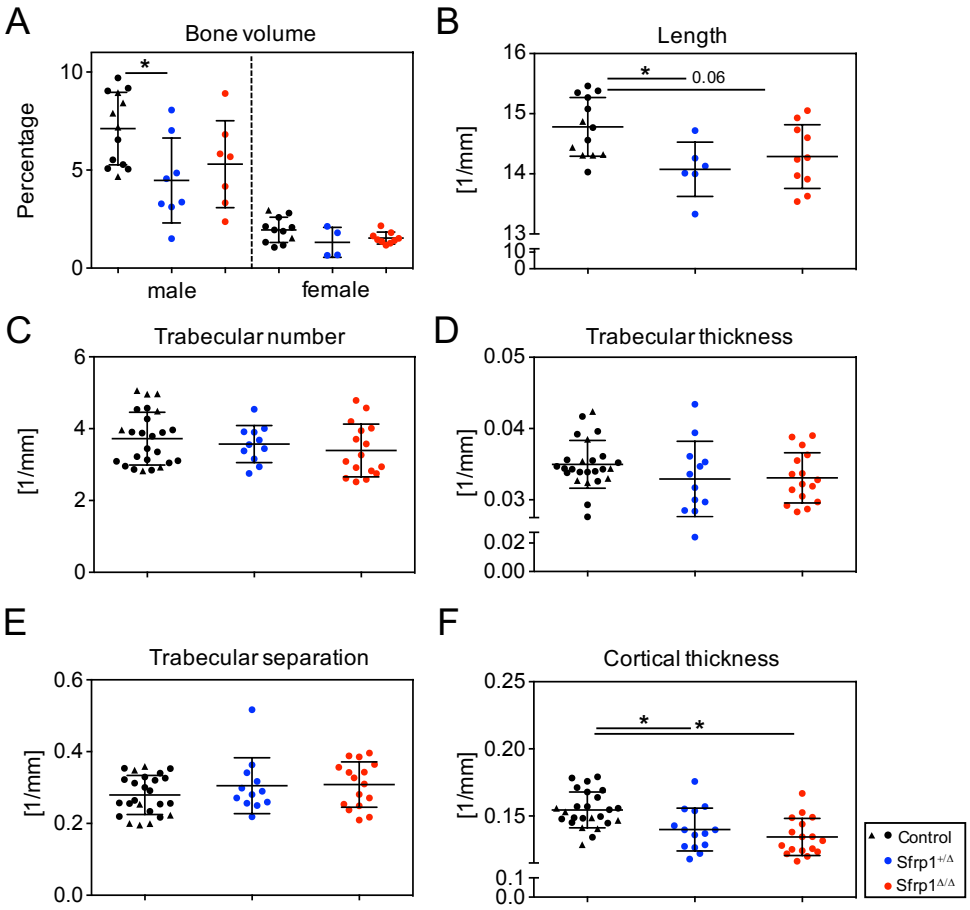

Figure 22. Trabecular bone phenotype of femur in *Sfrp1* conditional mice. Micro-computed tomography was used for the analysis of the trabecular bone from the femora of *Sfrp1* conditional mice and controls. **(A)** Percentage of bone volume of the femur in $Sfrp1^{+/\Delta}$ (male n = 8; female n = 4), $Sfrp1^{\Delta/\Delta}$ (male n = 7; female n = 9) compared to the controls (male n = 13; female n = 11). **(B)** Femur length in $Sfrp1^{+/\Delta}$ (n = 6), $Sfrp1^{\Delta/\Delta}$ (n = 10) compared to the controls (n = 13). **(C)** Trabecular number in $Sfrp1^{+/\Delta}$ (n = 11), $Sfrp1^{\Delta/\Delta}$ (n = 16) compared to the controls (n = 25). **(D)** Trabecular thickness and **(E)** separation in $Sfrp1^{+/\Delta}$ (n = 12), $Sfrp1^{\Delta/\Delta}$ (n = 16) compared to the controls (n = 25). **(F)** Cortical thickness in $Sfrp1^{+/\Delta}$ (n = 14), $Sfrp1^{\Delta/\Delta}$ (n = 17) compared to the controls (n = 25). Black dots represent controls ($Sfrp1^{lox/lox}$); Black triangles represent controls (Osx-Cre); Blue dots represent $Sfrp1^{+/\Delta}$; Red dots represent $Sfrp1^{\Delta/\Delta}$. Each dot represents one animal. Represented values are illustrated as Mean ± SD; * p-value ≤0.05 show significant differences in the comparison of *Sfrp1* conditional mice ($Sfrp1^{+/\Delta}$; $Sfrp1^{\Delta/\Delta}$) to each other or to controls ($Sfrp1^{lox/lox}$; Osx-Cre) determined by ANOVA, Tukey`s post hoc test. [Data were generated in cooperation with H. Weidner (Bone Lab, Dresden)].

4.4.1.3 Gender specific alterations in bone volume of vertebra

The mean BV of the control male mice was 12.58%, whereas the mean BV of the control females was 8.75%. The mean BV of the $Sfrp1^{+/\Delta}$ male animals was 10.10% (a reduction of 19.7%), whereas the mean BV of the females was 5.90% (a reduction of 32.6%). The mean BV of the $Sfrp1^{\Delta/\Delta}$ male mice was 9.88% (a reduction of 21.5%), whereas the mean BV of the females was 6.91% (a reduction of 21%). The bone volume of the $Sfrp1^{+/\Delta}$ of both genders were significantly decreased compared to the control mice (Figure 23A). Also, the bone volume of the $Sfrp1^{\Delta/\Delta}$ of both genders also show a trend to decrease (Figure 23A), indicating the importance of *Sfrp1* expression for bone volume.

There were no significantly gender-specific differences in the other bone parameters. The trabecular number (Figure 23B), trabecular thickness (Figure 23C) and trabecular separation (Figure 23D) in the *Sfrp1*$^{+/\Delta}$ and *Sfrp1*$^{\Delta/\Delta}$ mice were unchanged in the vertebra compared to the control animals.

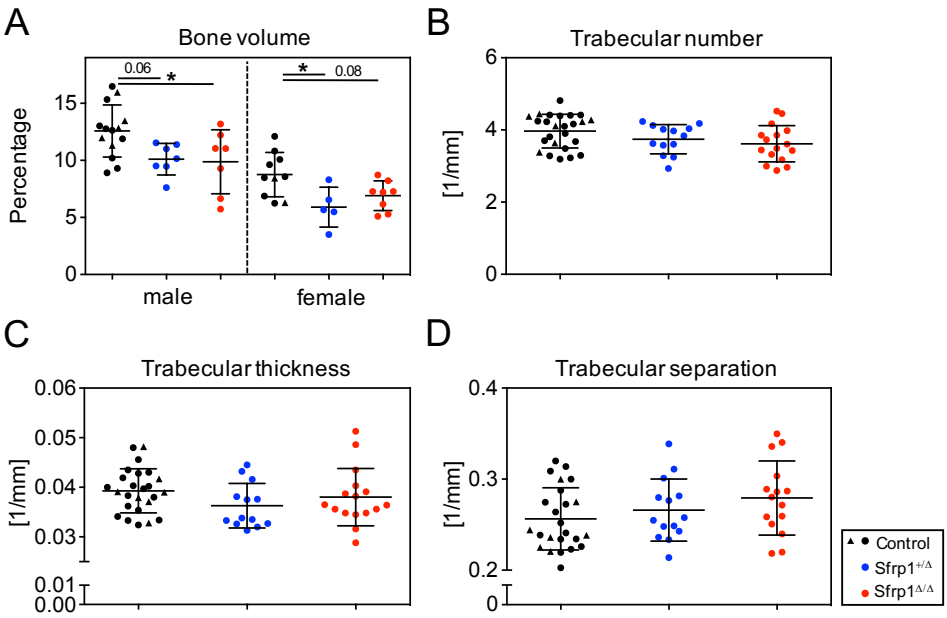

Figure 23. Trabecular bone phenotype of vertebra in *Sfrp1* conditional mice. Micro-computed tomography was used for the analysis of the trabecular bone from the vertebra of *Sfrp1* conditional mice and controls. **(A)** Percentage of bone volume of the vertebra in *Sfrp1*$^{+/\Delta}$ (male n = 7; female n = 5), *Sfrp1*$^{\Delta/\Delta}$ (male n = 7; female n = 8) compared to the controls (male n = 14; female n = 10). **(B)** Trabecular number and **(C)** thickness in *Sfrp1*$^{+/\Delta}$ (n = 13), *Sfrp1*$^{\Delta/\Delta}$ (n = 16) compared to the controls (n = 25). **(D)** Trabecular separation in *Sfrp1*$^{+/\Delta}$ (n = 14), *Sfrp1*$^{\Delta/\Delta}$ (n = 15) compared to the controls (n = 24). Black dots represent controls (*Sfrp1*$^{lox/lox}$); Black triangles represent controls (Osx-Cre); Blue dots represent *Sfrp1*$^{+/\Delta}$; Red dots represent *Sfrp1*$^{\Delta/\Delta}$. Each dot represents one animal. Represented values are illustrated as Mean ± SD; * p-value ≤0.05 show significant differences in the comparison of *Sfrp1*$^{+/\Delta}$ and *Sfrp1*$^{\Delta/\Delta}$ to each other or to controls (*Sfrp1*$^{lox/lox}$; Osx-Cre) determined by ANOVA, Tukey`s post hoc test. [Data were generated in cooperation with H. Weidner (Bone Lab, Dresden)].

To assess bone turnover, we analyzed sera for C-terminal telopeptide of type I collagen (CTX-I) and procollagen type I propeptide (P1NP) by ELISA (Szulc et al., 2018). We found that the bone formation marker P1NP was increased in the serum by 15.02% in *Sfrp1*$^{\Delta/\Delta}$ compared to *Sfrp1*$^{+/\Delta}$ mice. Similar to the µCT bone volume parameter, there are gender-specific differences in the P1NP serum levels in the control group. The control male mice had an average of 36.67 ng/mL, whereas the control females had a higher average of 50.9 ng/mL (increase of 28%, Figure 24A). The bone resorption marker CTX-I was decreased by 26,79 % (Figure 24B) in the male *Sfrp1*$^{\Delta/\Delta}$ compared to the male controls.

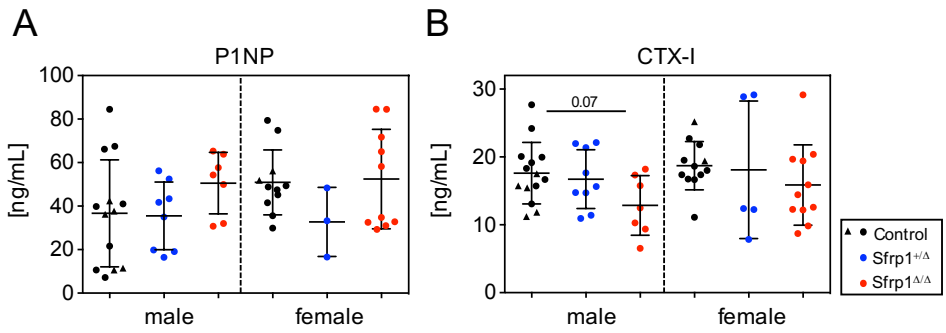

Figure 24. *Sfrp1* conditional mice show an altered bone turnover. (A) The functionality of osteoblasts (control: male n = 13, female n = 11; *Sfrp1*$^{+/\Delta}$: male n = 8, female n = 3; *Sfrp1*$^{\Delta/\Delta}$: male n = 7, female n = 10) and **(B)** osteoclasts (control: male n = 14, female n = 12; *Sfrp1*$^{+/\Delta}$: male n = 9, female n = 5; *Sfrp1*$^{\Delta/\Delta}$: male n = 7, female n = 11) were measured in serum by ELISA. Black dots represent controls (*Sfrp1*$^{lox/lox}$); Black triangles represent controls (Osx-Cre); Blue dots represent *Sfrp1*$^{+/\Delta}$; Red dots represent *Sfrp1*$^{\Delta/\Delta}$. Each dot represents one animal. Represented values are illustrated as Mean ± SD; * p-value ≤0.05 show significant differences in the comparison of *Sfrp1*$^{+/\Delta}$ and *Sfrp1*$^{\Delta/\Delta}$ to each other or to controls (*Sfrp1*$^{lox/lox}$; Osx- Cre) determined by ANOVA, Tukey`s post hoc test. [Data were generated in cooperation with H. Weidner (Bone Lab, Dresden)].

Since expression of CTX-I suggested a possibly lower bone resorption, we determined the osteoclast number per bone perimeter, we measured staining for the osteoclast-specific enzyme tartrate-resistant acid phosphatase (TRAP; Figure 25A). In addition, this staining also allowed for assessment of the number of osteoblasts. Here, we only used the male animals for this histological analysis because the *Sfrp1* knockout showed a stronger effect in the bone phenotype in male mice. These experiments showed, that both numbers of TRAP-positive osteoclasts and osteoblasts were very similar in *Sfrp1*$^{+/\Delta}$ and *Sfrp1*$^{\Delta/\Delta}$ mice compared to the controls in femora (Figure 25B) and vertebra (Figure 25C).

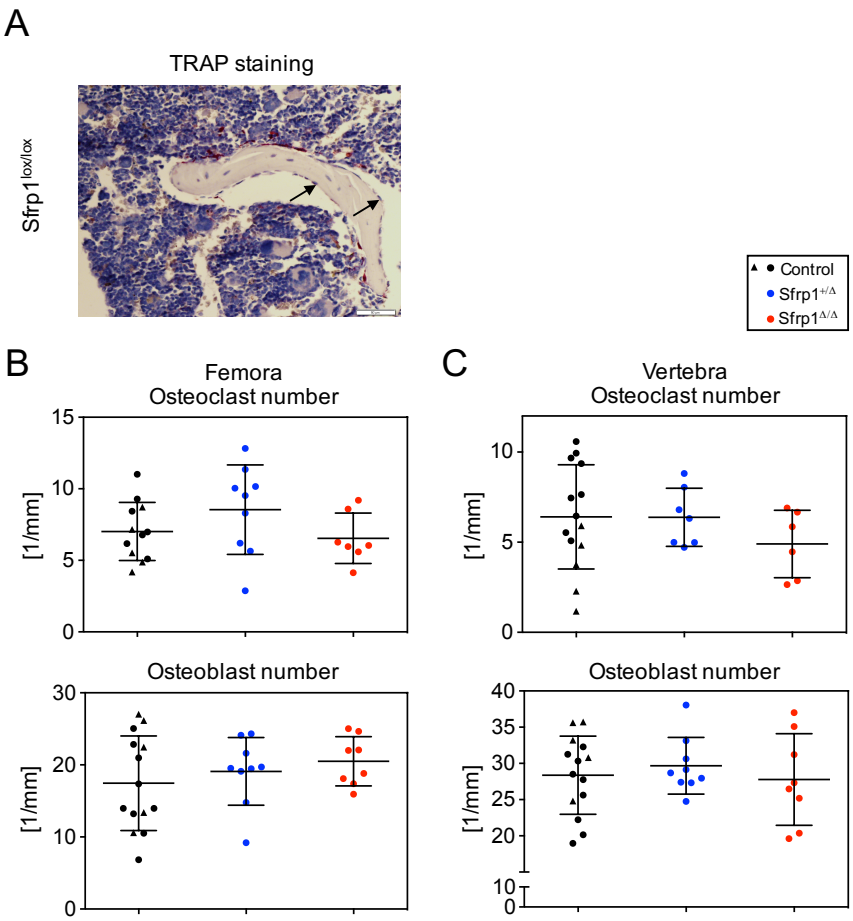

Figure 25. *Sfrp1* conditional mice show normal osteoclast and osteoblast number. (A) Representative images of tartrate-resistant acid phosphatase–stained (TRAP-stained) vertebra of 8-week-old control are depicted using the CellSens program and Microscope Axio Imager M1 (Carl Zeiss). In the TRAP-staining, osteoclasts are stained in red, while arrows indicate osteoblasts. Magnification: zoom of trabeculae 20× (scale bars: 50 µm). **(B)** top: osteoclasts number in *Sfrp1*$^{+/\Delta}$ (n = 9), *Sfrp1*$^{\Delta/\Delta}$ (n = 7) compared to the controls (n = 12); bottom: osteoblasts number in *Sfrp1*$^{+/\Delta}$ (n = 9), *Sfrp1*$^{\Delta/\Delta}$ (n = 8) compared to the controls (n = 14) per bone perimeter in femora. **(C)** top: osteoclasts number in *Sfrp1*$^{+/\Delta}$ (n = 7), *Sfrp1*$^{\Delta/\Delta}$ (n = 6) compared to the controls (n = 14); bottom: osteoblasts number in *Sfrp1*$^{+/\Delta}$ (n = 9), *Sfrp1*$^{\Delta/\Delta}$ (n = 8) compared to the controls (n = 14) per bone perimeter in vertebra. Black dots represent controls (*Sfrp1*$^{lox/lox}$); Black triangles represent controls (Osx-Cre); Blue dots represent *Sfrp1*$^{+/\Delta}$; Red dots represent *Sfrp1*$^{\Delta/\Delta}$. Each dot represents one animal. Represented values are illustrated as Mean ± SD; * p-value ≤0.05 show significant differences in the comparison of *Sfrp1*$^{+/\Delta}$ and *Sfrp1*$^{\Delta/\Delta}$ to each other or to controls (*Sfrp1*$^{lox/lox}$; Osx-Cre) determined by ANOVA, Tukey`s post hoc test. [Data were generated in cooperation with H. Weidner (Bone Lab, Dresden)].

To determine the degree of bone mineralization, we injected mice with calcein (a calcium-binding fluorescent dye) five and two days before sacrifice. Calcein "is incorporated into the mineralization fronts, and the distance between the labeling lines (mineral apposition rate, MAR) multiplied by the mineral surface per bone surface (MS/BS) provides the bone formation rate per bone surface (BFR/BS)" (Weidner et al., 2020) (Figure 26A). Our measurements show that the MAR and BFR/BS in the femur (Figure 26C, D) were similar in the *Sfrp1*$^{+/\Delta}$, *Sfrp1*$^{\Delta/\Delta}$ compared to the control mice. Interestingly, the MS/BS showed a slightly increased trend in the *Sfrp1*$^{\Delta/\Delta}$ compared to the *Sfrp1*$^{+/\Delta}$ (increase of 19.7%) and control animals (increase of 20.7%, Figure 26B).

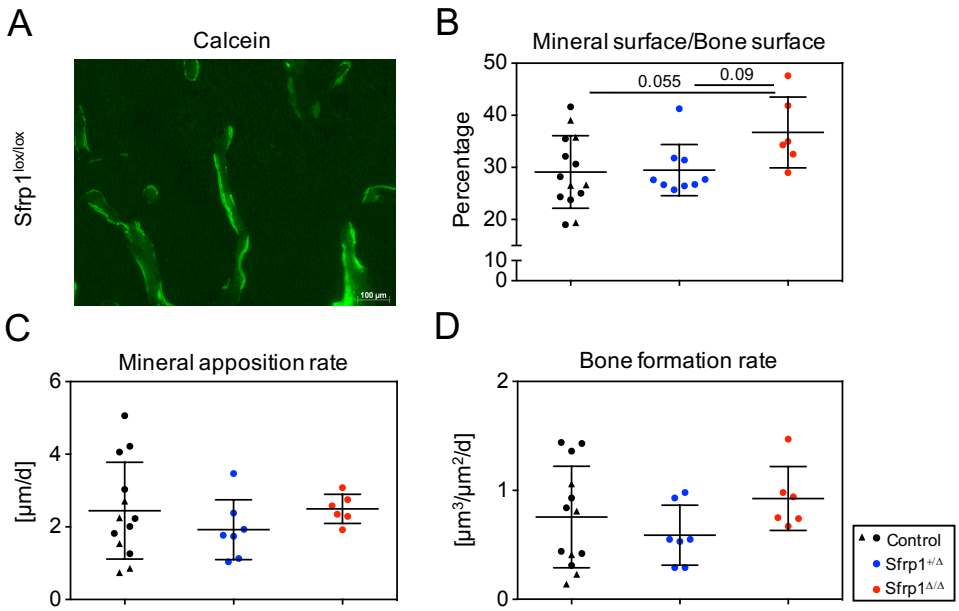

Figure 26. *Sfrp1* conditional mice show unchanged bone formation. (A) Representative images of calcein double labelling of trabecular bone (bar, 100 µm) of 8-week-old control. **(B)** Mineral surface/Bone surface in *Sfrp1*$^{+/\Delta}$ (n = 9), *Sfrp1*$^{\Delta/\Delta}$ (n = 6) compared to the controls (n = 14). **(C)** Mineral apposition rate in *Sfrp1*$^{+/\Delta}$ (n = 7), *Sfrp1*$^{\Delta/\Delta}$ (n = 6) compared to the controls (n = 13). **(D)** Bone formation rate in *Sfrp1*$^{+/\Delta}$ (n = 7), *Sfrp1*$^{\Delta/\Delta}$ (n = 6) compared to the controls (n = 13). Black dots represent controls (*Sfrp1*$^{lox/lox}$); Black triangles represent controls (Osx-Cre); Blue dots represent *Sfrp1*$^{+/\Delta}$; Red dots represent *Sfrp1*$^{\Delta/\Delta}$. Each dot represents one animal. Represented values are illustrated as Mean ± SD; * p-value ≤0.05 show significant differences in the comparison of *Sfrp1*$^{+/\Delta}$ and *Sfrp1*$^{\Delta/\Delta}$ to each other or to controls (*Sfrp1*$^{lox/lox}$; Osx-Cre) determined by ANOVA, Tukey`s post hoc test. [Data were generated in cooperation with H. Weidner (Bone Lab, Dresden)].

In summary, *Sfrp1*$^{\Delta/\Delta}$ mice show a loss of 22-35% of the bone volume in the cortical bone compared to control mice, and the male *Sfrp1*$^{\Delta/\Delta}$ mice additionally show reduction of about 20% of CTX-I serum levels. However, *Sfrp1*$^{+/\Delta}$ mice have an altered bone phenotype in the trabecular and cortical bone. Since we found that trabecular parameters, as well as the numbers of both osteoclasts and osteoblasts as well as the serum marker P1NP were normal in *Sfrp1*$^{\Delta/\Delta}$, these do not serve to explain the differences found in bone volume and serum CTX-I. Bodine et al. showed that in adult mice with a knock-out of *Sfrp1*, WNT signaling in osteoblasts is activated, which leads to increased trabecular bone formation (Bodine et al., 2004). Our results show there are changes in the cortical bone in both heterogeneous and homogenous conditional knockout mice and higher bone mineralized surface in *Sfrp1*$^{\Delta/\Delta}$ mice, suggesting this part of the bone may have an altered quality of bone stiffness. Thus, our results confirm earlier results with *Sfrp1*$^{-/-}$ mice, which suggests that these changes are at least partly dependent on *Osterix-GFP::Cre* expressing cells.

4.5. Characterization of *Sfrp1* loss in bone marrow niche cells

The reciprocal interaction between the bone marrow niche and HSCs is essential for proper homeostasis (Morrison & Scadden, 2014; Morrison & Spradling, 2008). Since molecular events involved in these interactions still have to be elucidated, we further studied the deletion of *Sfrp1* specifically in osteolineage cells in *Sfrp1* conditional deletion mutants to determine whether these cells are responsible for the loss of HSC self-renewal previously noted in *Sfrp1*$^{-/-}$ mice (Renström et al., 2009).

4.5.1 SFRP1 expression in the MSCs of the *Sfrp1* conditional mice

Analysis of SFRP1 protein expression in different cell types (paragraph 4.3) shows that the main expression was found in SCA-1^{+} mesenchymal stromal cells (MSCs) and GR1^{high} hematopoietic cells (granulocytes). Since the complete knock out of *Sfrp1* in mice changes HSCs behavior in a cell non-autonomous manner (Renström et al., 2009), an extrinsic regulation of stromal cells onto HSCs is assumed (Nakajima et al., 2009). This statement is supported by the fact that extrinsic SFRP1 regulates the behavior of hematopoietic cells (Oostendorp et al., 2002; Oostendorp et al., 2005; Renström et al., 2009). Since expression in MSCs is the highest, we specifically knocked out the expression of the gene in MSCs and OBCs to study the bone marrow stromal cells and their hematopoietic niche function of *Sfrp1* conditional mice. First, we validated deletion of SFRP1 in stromal cells. Consequently, the bone marrow stromal cells were isolated from collagenase-treated bones and separated by sorting based on the expression of specific surface markers.

The cell populations (ECs, OBCs and MSCs) were gated as CD45^{-}Ter119^{-} cells out of the live cell (PI^{-}) population. The ECs were gated as CD45^{-}Ter119^{-}CD31^{+}Sca1^{+} cells. Afterwards, OBCs were sorted as CD45^{-}Ter119^{-}CD31^{-}CD166^{+}SCA-1^{+} cells and the MSCs were gated as CD45^{-}Ter119^{-}CD31^{-}CD166^{-}SCA-1^{+} cells (Figure 27A) (Nakamura et al., 2010) and immediately used for immunofluorescent staining or cultured for western blot. We verified SFRP1 deletion by immunofluorescent staining of sorted MSCs with the reporter IRES GFP as a selectable marker (Figure 27B) and a western blot of cultured MSCs (Figure 27C) from control animals and *Sfrp1*$^{\Delta/\Delta}$ mice.

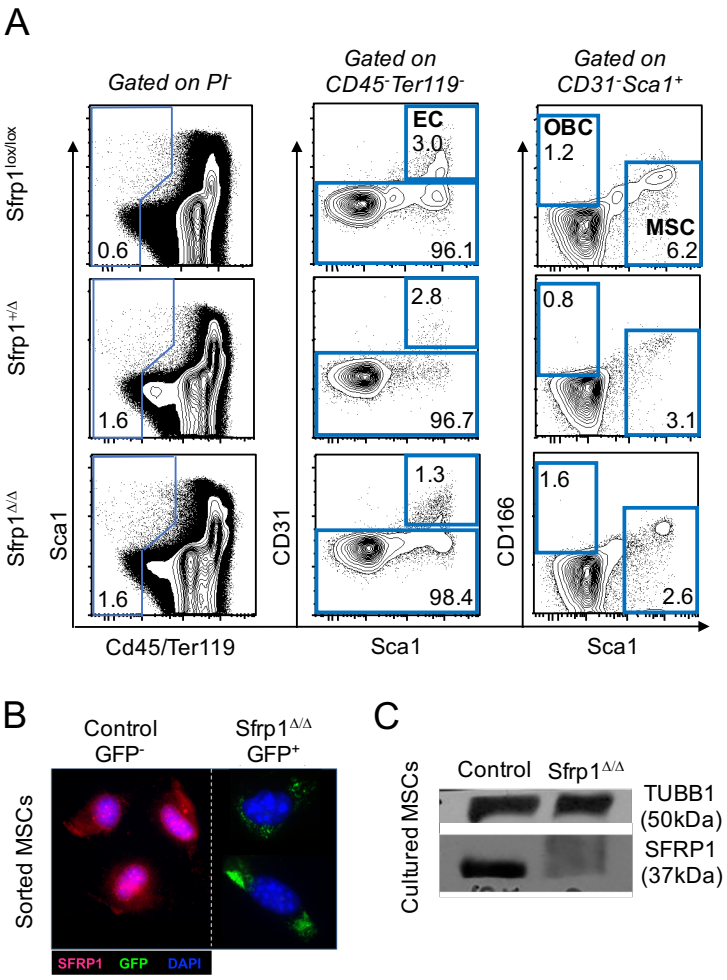

Figure 27. *SFRP1* expression in MSCs from control (GFP$^-$) mice and *Sfrp1*$^{\Delta/\Delta}$ (GFP$^+$) mice. (A) Gating strategy for cell sorting of bone marrow mesenchymal stem cell population. The mesenchymal stromal cells were gated as CD45$^-$Ter119$^-$CD31$^-$CD166$^-$SCA$^-$1$^+$ cells. **(B)** Representative fluorescence microscopy images of sorted MSCs with the reporter IRES GFP as a selectable marker from control (GFP$^-$) mice and *Sfrp1*$^{\Delta/\Delta}$ (GFP$^+$) mice. **(C)** Western blot analysis of SFRP1 (37kDa) of control (GFP$^-$) mice and *Sfrp1*$^{\Delta/\Delta}$ (GFP$^+$) mice. TUBB1 (50kDa) was used as housekeeping gene.

4.5.2 Functional analysis of the MSCs in *Sfrp1* conditional mice

For the functional analysis of the MSCs in *Sfrp1* conditional mice, at first the ability to form colony-forming unit fibroblasts (CFU-Fs) was analyzed. Therefore, sorted MSCs of *Sfrp1* conditional mice and controls were cultured in stroma medium and counted after 10 days. The analysis of *Sfrp1* deficient MSCs showed a decrease in total numbers of sorted MSCs (Figure 28A), but an increased proportion of colony forming units (CFU-F) after culture (Figure 28B). Furthermore, the MSCs from *Sfrp1*$^{\Delta/\Delta}$ mice compared to their controls and *Sfrp1*$^{+/\Delta}$ showed a significant increased number of small CFU-Fs while the number of large CFU-Fs is not significantly changed. In general, these results point out a remodeling of the BM, suggesting that the loss of *Sfrp1* in the microenvironment could have an impact on the function of the MSCs.

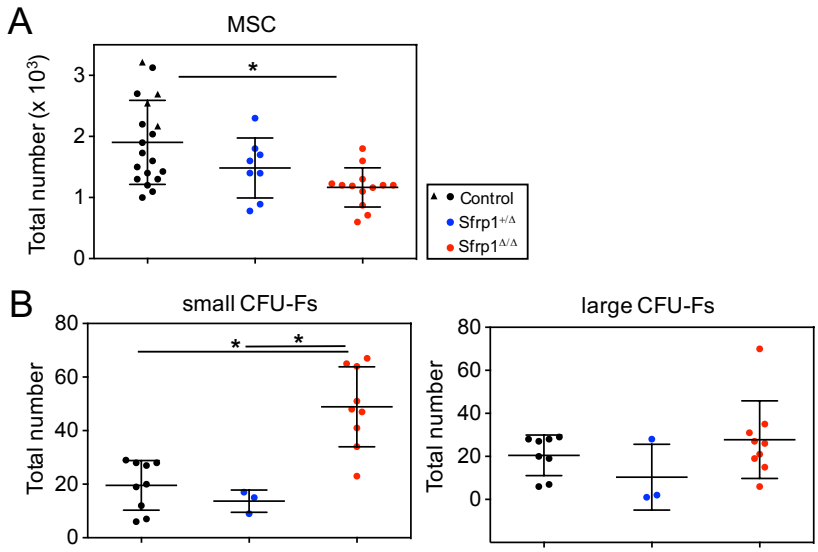

Figure 28. Ability to form CFU-Fs of the MSCs from *Sfrp1* conditional mice. **(A)** Total cell number of sorted MSCs from *Sfrp1*$^{+/\Delta}$ (n = 8), *Sfrp1*$^{\Delta/\Delta}$ (n = 13) compared to the controls (n = 19). **(B)** Total number of CFU-Fs of sorted MSCs. Left: Total number of small CFU-Fs (*Sfrp1*$^{+/\Delta}$: n = 3; *Sfrp1*$^{\Delta/\Delta}$: n = 9; controls: n = 9); Right: Total number of large CFU-Fs (*Sfrp1*$^{+/\Delta}$: n = 3; *Sfrp1*$^{\Delta/\Delta}$: n = 8; controls: n = 8). Black dots represent controls (*Sfrp1*$^{lox/lox}$); Black triangles represent controls (Osx-Cre); Blue dots represent *Sfrp1*$^{+/\Delta}$; Red dots represent *Sfrp1*$^{\Delta/\Delta}$. Each dot represents one animal. Represented values are illustrated as Mean ± SD; * p-value ≤0.05 show significant differences in the comparison of *Sfrp*1$^{+/\Delta}$ and *Sfrp1*$^{\Delta/\Delta}$ to each other or to controls (*Sfrp1*$^{lox/lox}$; Osx-Cre) determined by ANOVA, Tukey`s post hoc test. [Data were generated in cooperation with S. Romero Marquez (Stem Cell Physiology Lab, Munich)].

MSCs have the ability to differentiate into adipogenic, osteogenic and chondrogenic lineages (Kfoury & Scadden, 2015; Méndez-Ferrer et al., 2010; Robert et al., 2020; Visweswaran et al., 2015). To study the hypothesis that the loss of *Sfrp1* in niche of *Sfrp1* conditional mice has an effect on the cellular function of the MSCs in more detail, we performed differentiation assays *in vitro*. Therefore, the functional analysis of induced differentiation into adipogenic and osteogenic lineages was performed from sorted MSCs (passage 2 or p2) of *Sfrp1* conditional mice and their controls. The induced differentiation of MSCs from *Sfrp1* conditional mice showed that the MSCs from *Sfrp1*$^{+/\Delta}$ and *Sfrp1*$^{\Delta/\Delta}$ mice differentiated faster into adipogenic lineages (Figure 29B, Oil red stain). The osteogenic differentiation of *Sfrp1*$^{\Delta/\Delta}$ mice showed an enhanced mineralized matrix (red stain) and therefore an enhanced differentiation too, whereas *Sfrp1*$^{+/\Delta}$ cells were similar to the controls (Figure 29A, Alizarin red stain). In addition, the CFU-F-derived stromal cells from *Sfrp1*$^{\Delta/\Delta}$ mice differentiated spontaneously into adipocytes at passage 2 (data not shown).

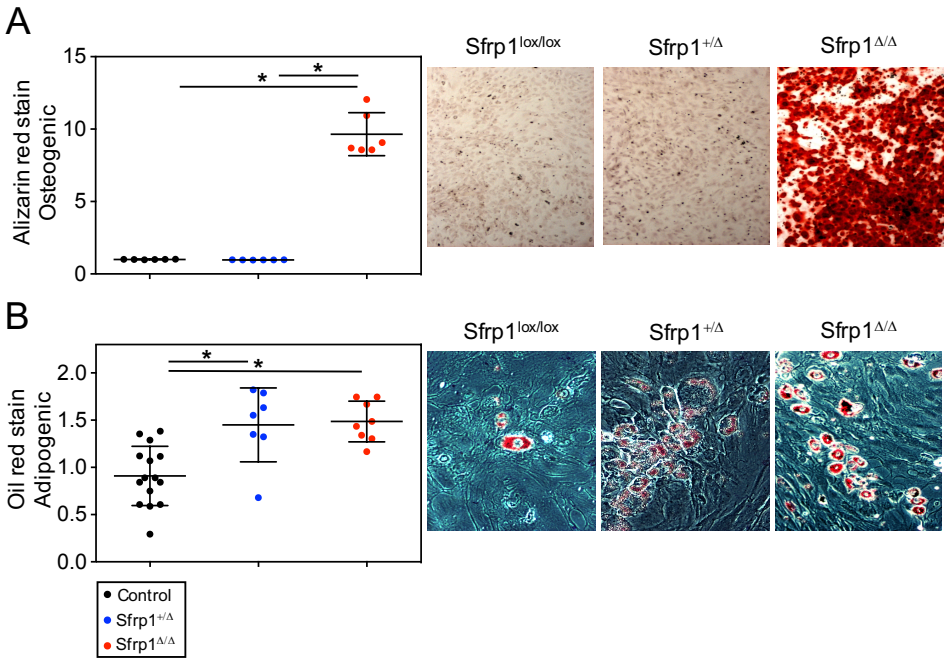

Figure 29. Differentiation potential of the MSCs from *Sfrp1* conditional mice. (A) Left: Quantification of Alizarin red content at OD 562 nm of *Sfrp1*$^{+/\Delta}$ (n = 6), *Sfrp1*$^{\Delta/\Delta}$ (n = 6) compared to the controls (n = 6) from osteogenic differentiated MSCs. Right: Microscopy of Alizarin red stained osteogenic differentiation of *Sfrp1* conditional mice compared to the controls. **(B)** Left: Quantification of Oil red content at OD 520 nm of *Sfrp1*$^{+/\Delta}$ (n = 7), *Sfrp1*$^{\Delta/\Delta}$ (n = 8) compared to the controls (n = 15) from adipogenic differentiated MSCs. Right: Microscopy of Oil red stained adipogenic differentiation *Sfrp1* conditional mice compared to the controls. Black dots represent controls (*Sfrp1*$^{lox/lox}$); Blue dots represent *Sfrp1*$^{+/\Delta}$; Red dots represent *Sfrp1*$^{\Delta/\Delta}$. Each dot represents one animal. Represented values are illustrated as Mean ± SD; * p-value ≤0.05 show significant differences in the comparison of *Sfrp1*$^{+/\Delta}$ and *Sfrp1*$^{\Delta/\Delta}$ to each other or to controls (*Sfrp1*$^{lox/lox}$) determined by ANOVA, Tukey`s post hoc test. [Data were generated in cooperation with S. Romero Marquez (Stem Cell Physiology Lab, Munich)].

To analyze the increased proliferation of the *Sfrp1* conditional cells, the functional analysis of cell cycle status of the MSCs was performed by PI/Ki-67 staining and analyzed by flow cytometry. The Ki-67 protein is a specific marker for cellular proliferation. The marker is present during proliferative phases of the cell cycle (G1, S, G2 and M phases), but is absent in quiescent cells (G0) (Gerdes et al., 1984; Gerdes, Schwab, Lemke, & Stein, 1983; Schwarting et al., 1986). PI was included in the staining to allow further analysis between G1-phase and S-phase, because cells in the S-phase have a higher level of PI. Therefore, endosteal cells (from collagenase treated bones) from controls and *Sfrp1* conditional mice were stained for surface marker and analyzed in bulk. The analysis of the cell cycle showed a decrease of MSCs from *Sfrp1*$^{\Delta/\Delta}$ mice in G0 phase compared to the controls. Furthermore, the MSCs of *Sfrp1*$^{\Delta/\Delta}$ mice are increased in the G1 and S phase of the cell cycle compared to the controls (Figure 30A). An increase of cells in the S-phase is associated with G2/M phase entrance in senescence, a state in which cells are metabolically active but do not divide.

To find out whether indeed, the number of senescent cells increases in MSCs of *Sfrp1* conditional mice and their controls, we sorted and cultured MSCs up to p1 to confluence. It was previously shown that senescent cells enhance their SA β-Galactosidase activity due to increased lysosome content (Dimri et al., 1995). The stromal cells (p1) of *Sfrp1* conditional cells grown *ex vivo* show increased senescence-associated β-galactosidase staining supporting the idea of increased senescence in *Sfrp1*$^{+/\Delta}$ and *Sfrp1*$^{\Delta/\Delta}$ mice compared to the controls (Figure 30B).

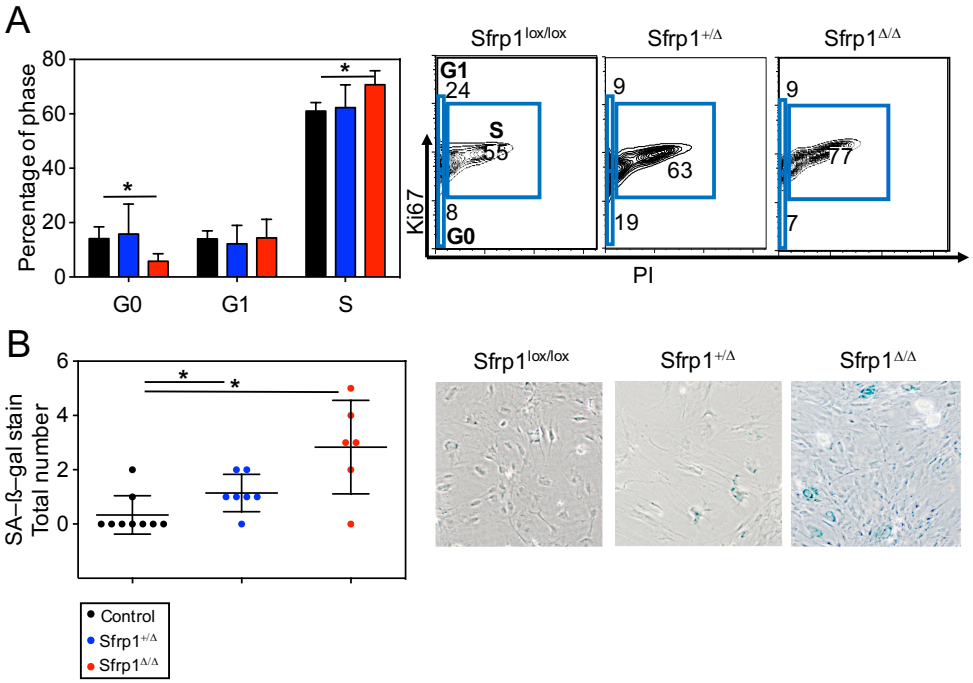

Figure 30. Functional analysis of the MSCs in *Sfrp1* conditional mice. (A) Left: Bar graph of cell cycle analysis of *Sfrp1*$^{+/\Delta}$ (n = 5), *Sfrp1*$^{\Delta/\Delta}$ (n = 5) compared to the controls (n = 5) in percentage. Right: Percentage of control and *Sfrp1* conditional MSCs lacking Ki67 and PI (in G0 of the cell cycle), positive for Ki67 and lacking PI (in G1 of the cell cycle), positive for Ki67 and PI (in S-phase of cell cycle). **(B)** Left: Total number of SA-β-gal (blue stained) positive colonies of *Sfrp1*$^{+/\Delta}$ (n = 7), *Sfrp1*$^{\Delta/\Delta}$ (n = 6) compared to the controls (n = 9). Right: Microscopy of SA-β-gal staining in *Sfrp1* conditional MSCs compared to the controls. Black dots represent controls (*Sfrp1*$^{lox/lox}$); Blue dots represent *Sfrp1*$^{+/\Delta}$; Red dots represent *Sfrp1*$^{\Delta/\Delta}$. Each dot represents one animal. Represented values are illustrated as Mean ± SD; * p-value ≤0.05 show significant differences in the comparison of *Sfrp1*$^{+/\Delta}$ and *Sfrp1*$^{\Delta/\Delta}$ to each other or to controls (*Sfrp1*$^{lox/lox}$) determined by ANOVA, Tukey`s post hoc test. [Data were generated in cooperation with S. Romero Marquez (Stem Cell Physiology Lab, Munich)].

In summary, *Sfrp1* deficient mice show a loss in total number of MSCs, increased generation of small CFU-Fs, strong differentiation into adipogenic and osteogenic lineages of MSCs, increased proliferative activity in endosteal cells and cellular senescence of MSCs, which indicates an altered functionality of stromal cells from *Sfrp1*$^{+/\Delta}$ and *Sfrp1*$^{\Delta/\Delta}$ mice.

4.6. Characterization of hematopoietic compartments by *Sfrp1* loss in bone marrow niche cells

We previously showed that *Sfrp1* expressed by the microenvironment is required to regulate the cycling activity and maintain functional HSCs (Renström et al., 2009). For the analysis of the influence on the hematopoietic system by loss of extrinsic SFRP1, BM cells of *Sfrp1* conditional mice (*Sfrp1*$^{+/\Delta}$, *Sfrp1*$^{\Delta/\Delta}$) and control mice were isolated and analyzed by flow cytometry.

4.6.1 Deletion of *Sfrp1* in osteoprogenitors does not affect hematopoiesis under steady-state conditions, except for a decrease in BM progenitors

After analyzing the effect of the *Sfrp1* deletion in niche stromal cells, we wondered how the loss of *Sfrp1* influence the hematopoietic compartment. To study this, we analyzed the mature and primary cell subpopulations in the peripheral blood (PB) and bone marrow (BM) of the *Sfrp1* conditional mice (*Sfrp1*$^{+/\Delta}$, *Sfrp1*$^{\Delta/\Delta}$) and control animals.

In Figure 31A, representative flow cytometry plots of mature cell populations in PB, isolated from the *Sfrp1*$^{+/\Delta}$, *Sfrp1*$^{\Delta/\Delta}$ mice and control animals, are shown. Out of the live cells and Ter119^{-} gate, the lymphoid cell populations (B220^{+} B cells and CD4^{+}CD8a^{+} T cells) and the myeloid cell populations (GR1^{+}CD11b^{+} granulocytes and GR1^{med}CD11b^{+} monocytes) were gated (Figure 31A).

The white blood cells (WBC) are unchanged in cell number in 10^3/µl (Figure 31B), as well as the lymphoid cell populations (B220^{+} B cells and CD4^{+}CD8a^{+} T cells) and myeloid cell populations (GR1^{med}CD11b^{+} monocytes and GR1^{+}CD11b^{+} granulocytes) in percentage of the *Sfrp1*$^{+/\Delta}$, *Sfrp1*$^{\Delta/\Delta}$ mice and control animals (Figure 31C-F). Thus, the loss of *Sfrp1* in the microenvironment has no strong effects on the number of mature cell subpopulations in the PB.

In Figure 32A, representative flow cytometry plots of mature cell populations in BM, isolated from the *Sfrp1*$^{+/\Delta}$, *Sfrp1*$^{\Delta/\Delta}$ mice and control animals, are shown. When comparing *Sfrp1*$^{+/\Delta}$, *Sfrp1*$^{\Delta/\Delta}$ and control mice (*Sfrp1*$^{lox/lox}$ or Osx-Cre), we found an unchanged total cell number of BM hematopoietic cells in the tibia and femur (Figure 32B), as well as the lymphoid cell populations (B220^{+} B cells and CD4^{+}CD8a^{+} T cells) and myeloid cell populations (GR1^{med}CD11b^{+} monocytes and GR1^{+}CD11b^{+} granulocytes) in absolute numbers of the *Sfrp1*$^{+/\Delta}$; *Sfrp1*$^{\Delta/\Delta}$ mice compared with control animals (Figure 32C-F). This shows that, as already found in the periphery, the loss of *Sfrp1* in the niche does not affect the number of mature hematopoietic cell subpopulations in the BM.

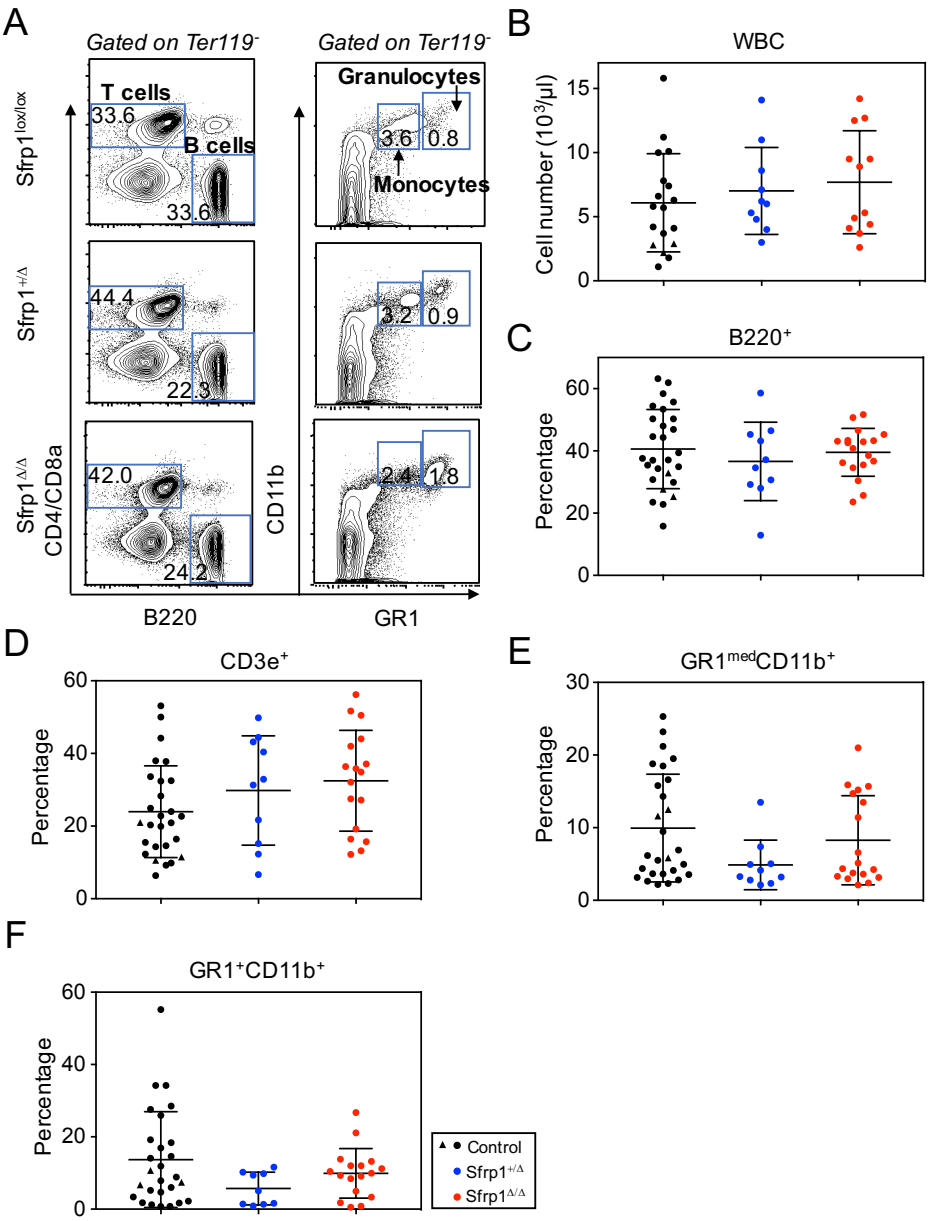

Figure 31. The influence on the mature hematopoietic compartment in the PB by *Sfrp1* loss in bone marrow niche cells. (A) Representative flow cytometry plots of the gating strategy for mature cell populations in PB. **(B)** Cell number of WBC in 10^3/µl of *Sfrp1*$^{+/\Delta}$ (n = 10), *Sfrp1*$^{\Delta/\Delta}$ (n = 12) compared to the controls (n = 18). **(C)** Percentage of the B220$^+$ B cells of *Sfrp1*$^{+/\Delta}$ (n = 10), *Sfrp1*$^{\Delta/\Delta}$ (n = 18) compared to the controls (n = 27). **(D)** Percentage of CD3e$^+$ T cells of *Sfrp1*$^{+/\Delta}$ (n = 10), *Sfrp1*$^{\Delta/\Delta}$ (n = 17) compared to the controls (n = 27). **(E)** Percentage of GR1^{med}CD11b$^+$ monocytes of *Sfrp1*$^{+/\Delta}$ (n = 10), *Sfrp1*$^{\Delta/\Delta}$ (n = 18) compared to the controls (n = 27). **(F)** Percentage of GR1$^+$CD11b$^+$ granulocytes of *Sfrp1*$^{+/\Delta}$ (n = 9), *Sfrp1*$^{\Delta/\Delta}$ (n = 17) compared to the controls (n = 27). Black dots represent controls (*Sfrp1*$^{lox/lox}$); Black triangles represent controls (Osx-Cre); Blue dots represent *Sfrp1*$^{+/\Delta}$; Red dots represent *Sfrp1*$^{\Delta/\Delta}$. Each dot represents one animal. Represented values are illustrated as Mean ± SD.

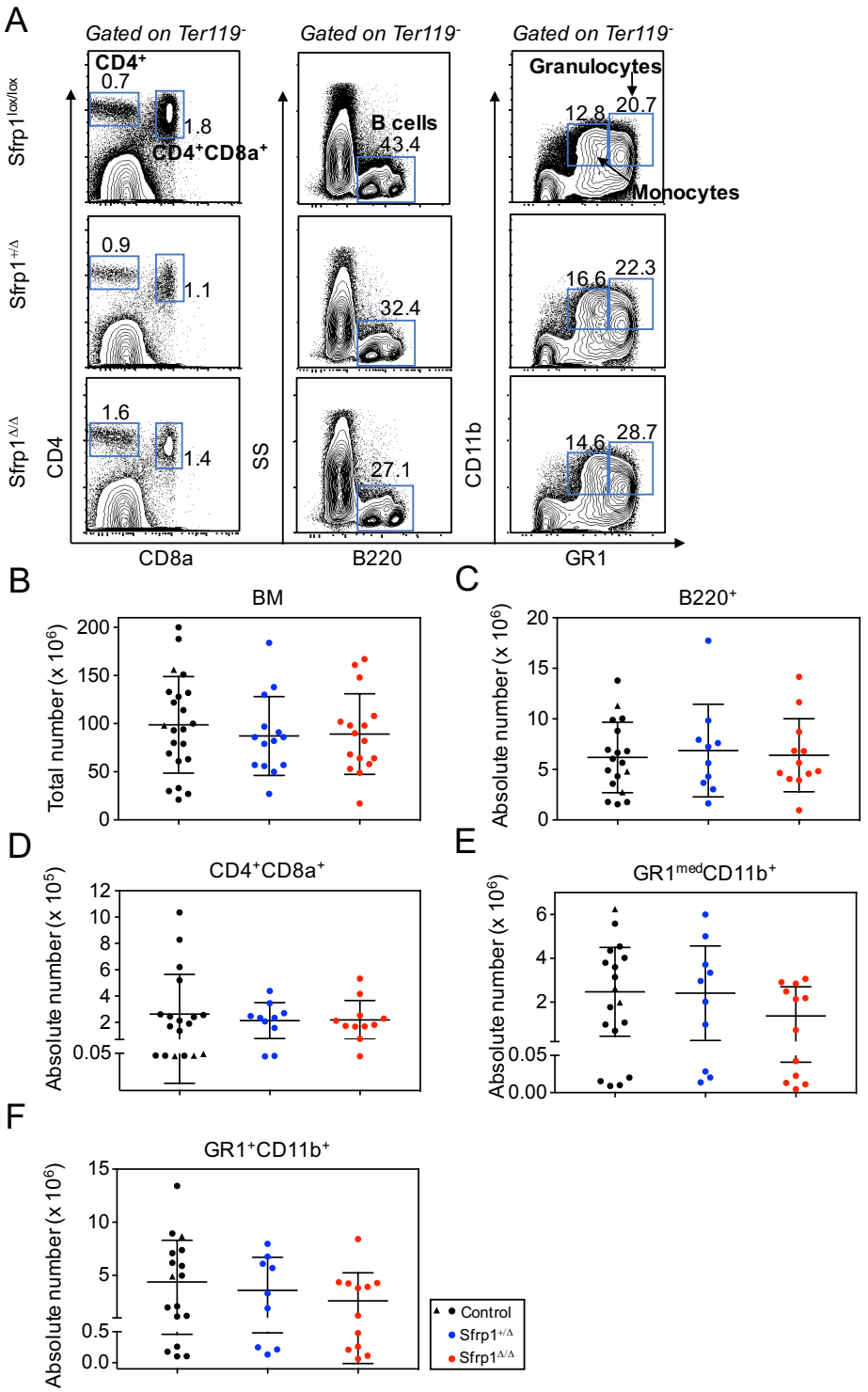

Figure 32. The influence on the mature hematopoietic compartment in the BM by *Sfrp1* loss in bone marrow niche cells. (A) Representative flow cytometry plots of the gating strategy for mature cell populations in BM. **(B)** Total number of BM of *Sfrp1*$^{+/\Delta}$ (n = 14), *Sfrp1*$^{\Delta/\Delta}$ (n = 16) compared to the controls (n = 22). **(C)** Absolute number of the B220^{+} B cells of *Sfrp1*$^{+/\Delta}$ (n = 10), *Sfrp1*$^{\Delta/\Delta}$ (n = 12) compared to the controls (n = 18). **(D)** Absolute number of CD4^{+}CD8a^{+} T cells of *Sfrp1*$^{+/\Delta}$ (n = 10), *Sfrp1*$^{\Delta/\Delta}$ (n = 11) compared to the controls (n = 18). **(E)** Absolute number of GR1^{med}CD11b^{+} monocytes of *Sfrp1*$^{+/\Delta}$ (n = 10), *Sfrp1*$^{\Delta/\Delta}$ (n = 12) compared to the controls (n = 18). **(F)** Absolute number of GR1^{+}CD11b^{+} granulocytes of *Sfrp1*$^{+/\Delta}$ (n = 9), *Sfrp1*$^{\Delta/\Delta}$ (n = 12) compared to the controls (n = 17). Black dots represent controls (*Sfrp1*$^{lox/lox}$); Black triangles represent controls (Osx-Cre); Blue dots represent *Sfrp1*$^{+/\Delta}$; Red dots represent *Sfrp1*$^{\Delta/\Delta}$. Each dot represents one animal. Represented values are illustrated as Mean ± SD.

To determine changes in the number of HSC-enriched CD34$^-$ SLAM (Long-Term HSCs (LT-HSCs)) in *Sfrp1*$^{\Delta/\Delta}$ mice, we performed flow cytometry on freshly isolated BM cells using a combination of surface markers described in the literature (Kiel et al., 2005; Osawa et al., 1996) and as our group described previously (Marquez Romero et al., 2020; Schreck et al., 2017). For assessment of live CD34$^-$ SLAM cells, we first gated out doublets, cell debris and possible cell clumps setting a gate in the dotplot of forward scatter (FS) against pulse width (PW). More cell debris was then gated out using a gate in the sideward scatter (SS) against FW dotplot. This was followed by gating on living cells using staining with the cell-impermeable DNA dye PI^{low} against FS^{high}. Out of the live cells (PI$^-$), the cells devoid of lineage markers (lineage$^-$) were chosen out by excluding CD45$^+$, Ter119$^+$ and CD48$^+$ cells (Figure 33A, first gate (left)).

In several experiments, we enriched for these lineage$^-$ cells using lineage cell separation before staining, as described in the Methods section (3.4.1 Lineage depletion), to more easily discern different subpopulations within the lineage$^-$ cells. To zoom into the HSC-enriched fractions of cells, Lin$^-$Sca-1$^+$Kit$^+$ cells (LSKs) were gated as KIT$^+$ and SCA-1$^+$ cells (Figure 33A, second gate (middle)). Within this LSK cell fraction, cells were further subdivided into CD34$^-$ SLAM cells (LT-HSCs) and CD34$^+$ cells (short-term HSCs (ST-HSCs), using the markers CD34 and CD150^{high} cells (Figure 33A, third gate (right)).

As we notice before, there was an unchanged total cell number of BM hematopoietic cells in the tibia and femur of the *Sfrp1*$^{+/\Delta}$, *Sfrp1*$^{\Delta/\Delta}$ mice compared with control animals (Figure 32B). However, we observed that the LSK compartment was similar in both *Sfrp1*$^{+/\Delta}$ and *Sfrp1*$^{\Delta/\Delta}$ mice compared to control animals (Figure 33B). We found an unchanged absolute number of the LT-HSCs subpopulation, as well as in the ST-HSCs in the *Sfrp1*$^{+/\Delta}$ and *Sfrp1*$^{\Delta/\Delta}$ mice compared to control animals (Figure 33C, D). However, there was a significant decreased in absolute cell number of myeloid progenitor cells (MPs, Figure 33E).

In conclusion, in the hematopoietic compartment, LT-HSCs (Lin$^-$CD48$^-$Sca-1$^+$CD117$^+$CD34$^-$CD150$^+$) were unchanged, while MPs (Lin$^-$CD48$^-$Sca-1$^-$CD117$^+$) were significantly decreased. This suggests that under steady-state conditions the LT-HSC produce less MPs, which could be caused by reduced differentiation, proliferation or increased MP cell death.

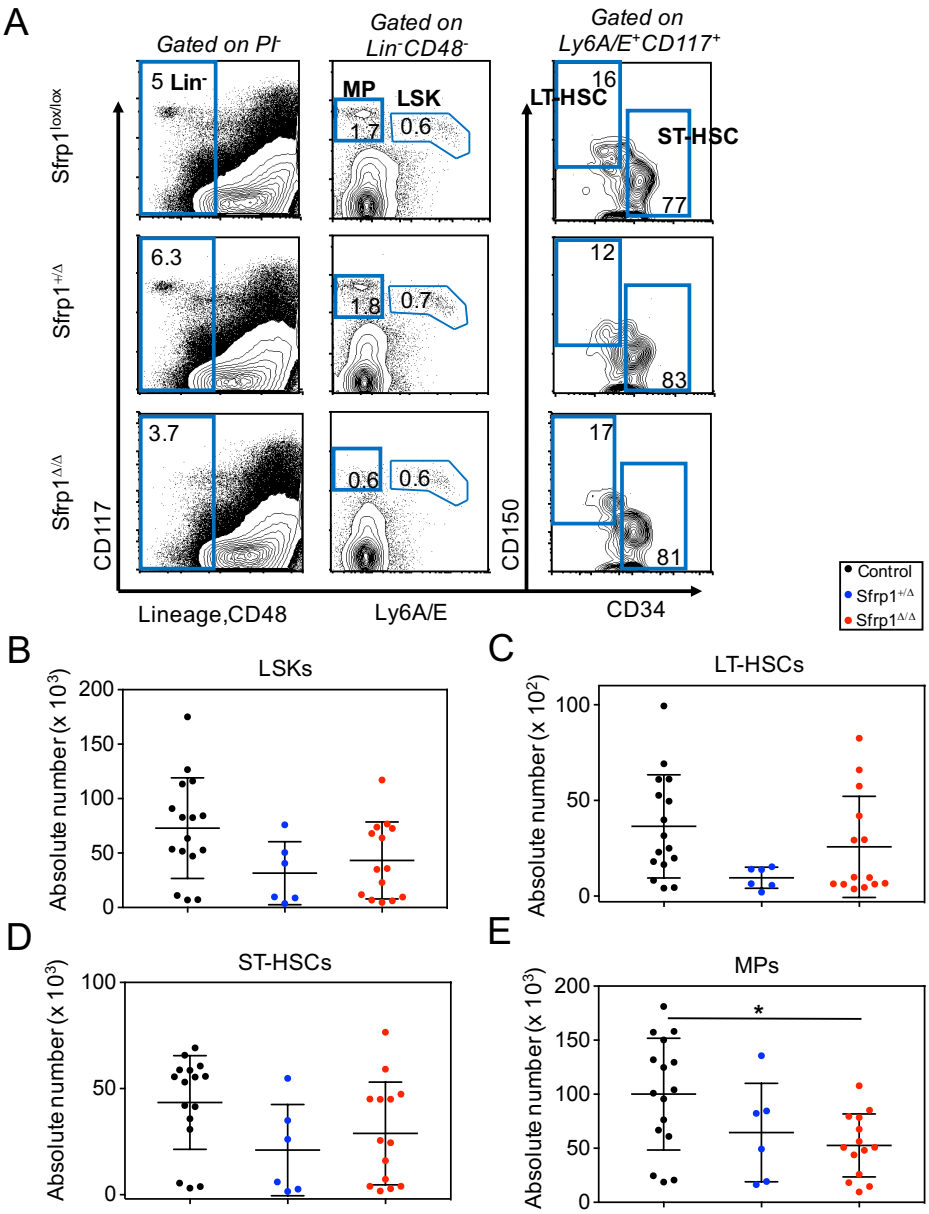

Figure 33. The influence on the primitive hematopoietic compartment by *Sfrp1* loss in bone marrow niche cells. (A) Representative flow cytometry plots of lineage depleted BM cells of the gating strategy for the primitive hematopoietic compartment. **(B)** Absolute number of LSKs isolated from tibia and femur of *Sfrp1*$^{+/\Delta}$ (n = 6), *Sfrp1*$^{\Delta/\Delta}$ (n = 14) compared to the controls (n = 16). **(C)** Absolute number of LT-HSCs of *Sfrp1*$^{+/\Delta}$ (n = 6), *Sfrp1*$^{\Delta/\Delta}$ (n = 14) compared to the controls (n = 16). **(D)** Absolute number of ST-HSCs of *Sfrp1*$^{+/\Delta}$ (n = 6), *Sfrp1*$^{\Delta/\Delta}$ (n = 14) compared to the controls (n = 16). **(E)** Absolute number of MPs of *Sfrp1*$^{+/\Delta}$ (n = 6), *Sfrp1*$^{\Delta/\Delta}$ (n = 14) compared to the controls (n = 16). Black dots represent controls (*Sfrp1*$^{lox/lox}$); Blue dots represent *Sfrp1*$^{+/\Delta}$; Red dots represent *Sfrp1*$^{\Delta/\Delta}$. Each dot represents one animal. Represented values are illustrated as Mean ± SD. * p-value ≤0.05 show significant differences in the comparison of *Sfrp1*$^{\Delta/\Delta}$ to controls *Sfrp1*$^{lox/lox}$ determined by ANOVA, Tukey`s post hoc test.

4.6.2 Limiting number of LT-HSCs from *Sfrp1* deficient mice failed to repopulated in WT recipients

To test whether the function of LT-HSCs generated in *Sfrp1*$^{\Delta/\Delta}$ mice is disturbed, we transplanted limiting number (100 cells) of sorted LT-HSCs from our *Sfrp1*$^{+/\Delta}$, *Sfrp1*$^{\Delta/\Delta}$ mice and controls (*Sfrp1*$^{lox/lox}$) into lethally irradiate WT recipients (Figure 34A).

Since the activity of the transcription factor *Osx-Cre* is limited to osteoblast lineage cells, bone marrow stromal cells, osteocytes, hypertrophic chondrocytes, perivascular cells and adipocytes in the bone marrow (Chen et al., 2014; Rodda & McMahon, 2006) the LT-HSCs should still normally express the *Sfrp1* gene, they are therefore considered wild-type. Any change in behavior of these cells is caused by the *Sfrp1* deficient osterix^{+} stromal compartment and their progeny.

These experiments showed that peripheral engraftment is severely impaired over the entire observation period of 24 weeks (Figure 34B, C). To find out whether this is due to an impairment of the regeneration of the stem cell compartment, we also analyzed the BM 24 weeks after transplantation (Figure 34B, D-G). The engraftment in the BM was significantly decreased in the *Sfrp1*$^{\Delta/\Delta}$ mice compared to the controls (Figure 34D), as well as a significantly decreased of donor CD34^{+} LSKs of *Sfrp1*$^{+/\Delta}$ and *Sfrp1*$^{\Delta/\Delta}$ compared to the controls (Figure 34G). The donor LSKs and donor CD34^{-} LSKs were unchanged of *Sfrp1*$^{+/\Delta}$ and *Sfrp1*$^{\Delta/\Delta}$ mice compared to the controls, whereby it is noticeable that 6 (donor LSKs) or 7 (donor CD34^{-} LSKs) out of 10 *Sfrp1*$^{\Delta/\Delta}$ mice showed a complete lack of donor cells (Figure 34E, F).

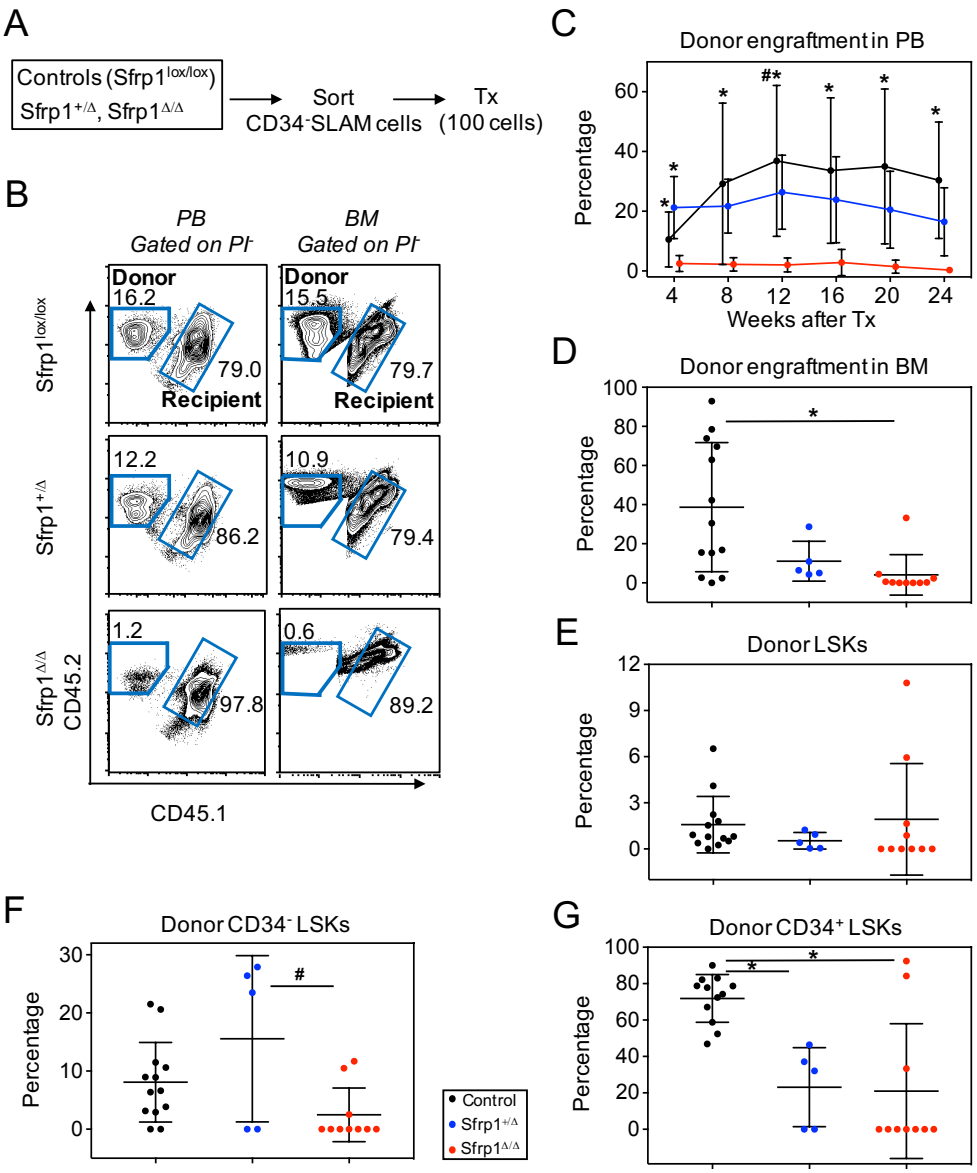

Figure 34. Limiting number of LT-HSCs from *Sfrp1* deficient mice failed to repopulated in WT recipients. **(A)** Experimental design: CD34$^-$ SLAM cells (LT-HSCs) of eight- to ten-week old *Sfrp1*$^{+/\Delta}$, *Sfrp1*$^{\Delta/\Delta}$ mice and control animals were sorted and transplanted into lethally irradiate WT recipients. **(B)** Representative flow cytometry plots of the gating strategy of Ly5.2$^+$ donor cells or Ly5.1$^+$Ly5.2$^+$ recipient cells in PB (left) and BM (right). **(C)** Donor cell engraftment in percentage in the PB four, eight, twelve, sixteen, twenty and twentyfour weeks after transplantation of *Sfrp1*$^{+/\Delta}$ (n = 5), *Sfrp1*$^{\Delta/\Delta}$ (n = 11) compared to the controls (n = 13). **(D)** Percentage of the donor engraftment in BM (week 24 after transplantation) of *Sfrp1*$^{+/\Delta}$ (n = 5), *Sfrp1*$^{\Delta/\Delta}$ (n = 10) compared to the controls (n = 13). **(E)** Percentage of the donor LSKs of *Sfrp1*$^{+/\Delta}$ (n = 5), *Sfrp1*$^{\Delta/\Delta}$ (n = 10) compared to the controls (n = 13). **(F)** Percentage of the donor CD34$^-$ LSKs of *Sfrp1*$^{+/\Delta}$ (n = 5), *Sfrp1*$^{\Delta/\Delta}$ (n = 10) compared to the controls (n = 13). **(G)** Percentage of the donor CD34$^+$ LSKs of *Sfrp1*$^{+/\Delta}$ (n = 5), *Sfrp1*$^{\Delta/\Delta}$ (n = 10) compared to the controls (n = 12). Black dots represent controls (*Sfrp1*$^{lox/lox}$); Blue dots represent *Sfrp1*$^{+/\Delta}$; Red dots represent *Sfrp1*$^{\Delta/\Delta}$. Each dot represents one animal. Represented values are illustrated as Mean ± SD. * p-value ≤0.05 show significant differences in the comparison of *Sfrp1*$^{+/\Delta}$, *Sfrp1*$^{\Delta/\Delta}$ to controls, whereas $^{\#}$ p-value ≤0.05 show significant differences in the comparison of *Sfrp1*$^{+/\Delta}$ to *Sfrp1*$^{\Delta/\Delta}$ determined by ANOVA, Tukey`s post hoc test.

We then studied whether the stem cells we transplanted were perhaps already damaged before we isolated them from the *Sfrp1*$^{\Delta/\Delta}$ mice. Because damaged LT-HSCs often present with accumulated DNA damage. It was published that DNA damage in LT-HSCs influences their repopulating activity during transplantation (Flach et al., 2014; Walter et al., 2015).

Indeed, in the sorted LT-HSCs from *Sfrp1*$^{\Delta/\Delta}$ mice we found an accumulation of DNA-double-strand breaks as identified with the comet assay (Figure 35A). Similarly, staining for γH2A.X foci is an indication of double-strand break repair, and we found an increase of such foci, indicating an increased number of DNA double-strand breaks in LT-HSC from *Sfrp1*$^{\Delta/\Delta}$ mice (Figure 35B). These results strongly suggest an accumulation of DNA damage in CD34^{-} SLAM cells from *Sfrp1*$^{\Delta/\Delta}$ mice.

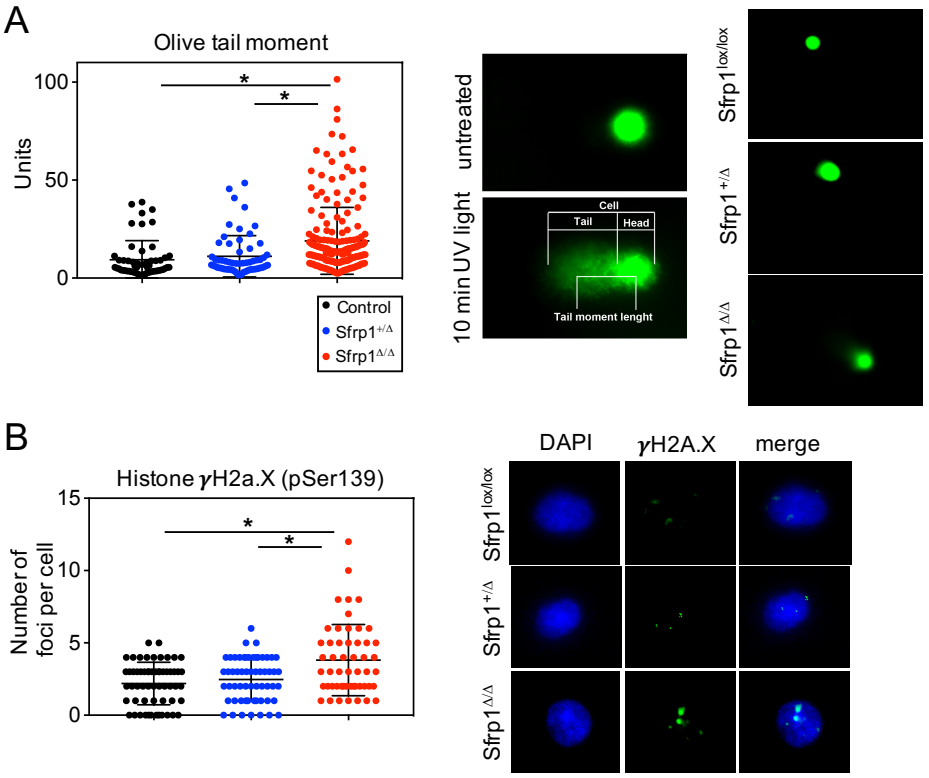

Figure 35. DNA double-strand breaks accumulation in CD34^{-} SLAM cells from *Sfrp1* deficient mice. **(A)** Left: Olive tail moment (Tail DNA/Cell DNA * TML) of LT-HSCs of *Sfrp1*$^{+/\Delta}$ (n = 61), *Sfrp1*$^{\Delta/\Delta}$ (n = 200) compared to the controls (n = 55) calculated after a comet assay; Middle: Immunofluorescence staining of a negative and positive control (cells treated for 10 min with UV light); Right: Representative immunofluorescence staining of *Sfrp1*$^{+/\Delta}$, *Sfrp1*$^{\Delta/\Delta}$ compared to the controls. **(B)** Number of Histone γH2A.X foci content of CD34^{-} SLAM cells of *Sfrp1*$^{+/\Delta}$ (n = 59), *Sfrp1*$^{\Delta/\Delta}$ (n = 52) compared to the controls (n = 59); Right: Representative immunofluorescence staining for the nuclei staining with DAPI in blue (left), histone γH2A.X foci content in green (middle), and the merged picture (right) of CD34^{-} SLAM cells of *Sfrp1*$^{+/\Delta}$, *Sfrp1*$^{\Delta/\Delta}$ mice compared to the controls. Black dots represent controls (*Sfrp1*$^{lox/lox}$); Blue dots represent *Sfrp1*$^{+/\Delta}$; Red dots represent *Sfrp1*$^{\Delta/\Delta}$. Each dot represents one animal. Represented values are illustrated as Mean ± SD. * p-value ≤0.05 show significant differences in the comparison of *Sfrp1*$^{+/\Delta}$ and *Sfrp1*$^{\Delta/\Delta}$ to each other or to controls determined by ANOVA, Tukey`s post hoc test.

We then studied whether the damaged CD34$^-$ SLAM cells, which harbor accumulation of DNA damage, present dysfunctional behavior *in vitro*. For this, we performed single cell cultures (Figure 36A), since this assay allows the separate assessment of survival, proliferation, and self-renewal (Marquez Romero et al., 2020; Wohrer et al., 2014). Here, we found that LT-HSCs from *Sfrp1*$^{\Delta/\Delta}$ mice show decreased clone size after four and five days of culture of single CD34$^-$ SLAM cells compared to the controls (Figure 36B). Interestingly, when the formed clones were pooled at the end of the culture at day 5 and assessed for differentiation, we found significantly increased differentiation of the clones grown from *Sfrp1*$^{\Delta/\Delta}$ CD34$^-$ SLAM cells into GR1$^+$CD11b$^+$ mature myeloid lineages (Figure 36C).

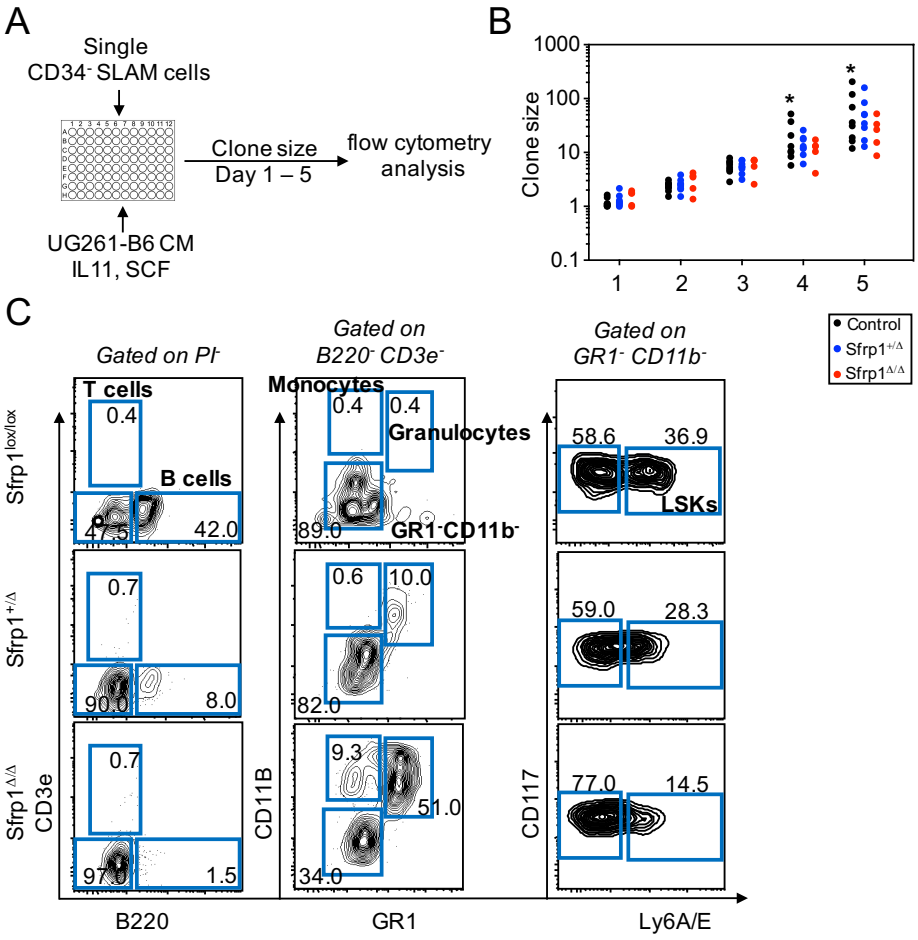

Figure 36. CD34$^-$ SLAM cells from *Sfrp1* deficient mice are slow-proliferating. (A) Experimental design: 96-round-bottomed plates were prefilled with UG26-1B6 CM, containing mSCF and IL-11. Single CD34$^-$ SLAM cells of *Sfrp1*$^{+/\Delta}$, *Sfrp1*$^{\Delta/\Delta}$ and the controls were sorted into each well. For five days, the clone size was counted every 24 hours. After five days, the clones (> 2 cells/well) were harvested and analyzed per flow cytometry. **(B)** Counted mean clone size over five days of *Sfrp1*$^{+/\Delta}$ (n = 8), *Sfrp1*$^{\Delta/\Delta}$ (n = 5) and the controls (n = 8). **(C)** Representative flow cytometry plots of the gating strategy for lymphoid lineages (left), myeloid lineages (middle) and the LSK populations (right) after 5 days of culture. Black dots represent controls (*Sfrp1*$^{lox/lox}$); Blue dots represent *Sfrp1*$^{+/\Delta}$; Red dots represent *Sfrp1*$^{\Delta/\Delta}$. Each dot represents one animal. Figure B: Represented values are illustrated as Mean. * p-value ≤0.05 show significant differences in the comparison of *Sfrp1*$^{\Delta/\Delta}$ to controls determined by Bartlett's test.

So, our results support the view that CD34$^-$ SLAM cells from *Sfrp1*$^{\Delta/\Delta}$ mice show decreased engraftment, accumulations of DNA damage and show unbalanced proliferation and differentiation.

4.6.3 LT-HSCs from *Sfrp1* deficient mice show unbalanced proliferation and differentiation

To understand our findings that CD34$^-$ SLAM cells from *Sfrp1*$^{\Delta/\Delta}$ mice proliferate less and show more myeloid differentiation, we decided to investigate the balance complex formation between β-catenin (CTNNB1) and either CREBBP (CBP) or EP300 (p300).

In embryonic cells (ES) these two complexes regulate the balance between differentiation and proliferation (Miyabayashi et al., 2007), where the β-catenin/CBP complex drives ES self-renewal, and the β-catenin/p300 complex promotes differentiation. Thus, we were interested whether a disbalance in the activity of β-catenin/CBP or β-catenin/p300 would explain the increased myeloid differentiation, found in cultures from CD34$^-$ SLAM cells from *Sfrp1*$^{\Delta/\Delta}$ mice (Figure 37A).

To test this hypothesis, we first assessed the expression of these three proteins in sorted CD34$^-$ SLAM cells using immunofluorescence staining (IF) experiments. We found that all three proteins are expressed. Furthermore, in CD34$^-$ SLAM cells from *Sfrp1*$^{\Delta/\Delta}$ mice, the protein content of β-catenin and p300 was increased, while the CBP content was unchanged (Figure 37B-D).

This could mean that perhaps due to the increased availability of p300, more of the β-catenin/p300 complex might be formed. In line with the hypothesis, increased presence of the β-catenin/p300 complex would promote differentiation of CD34$^-$ SLAM cells.

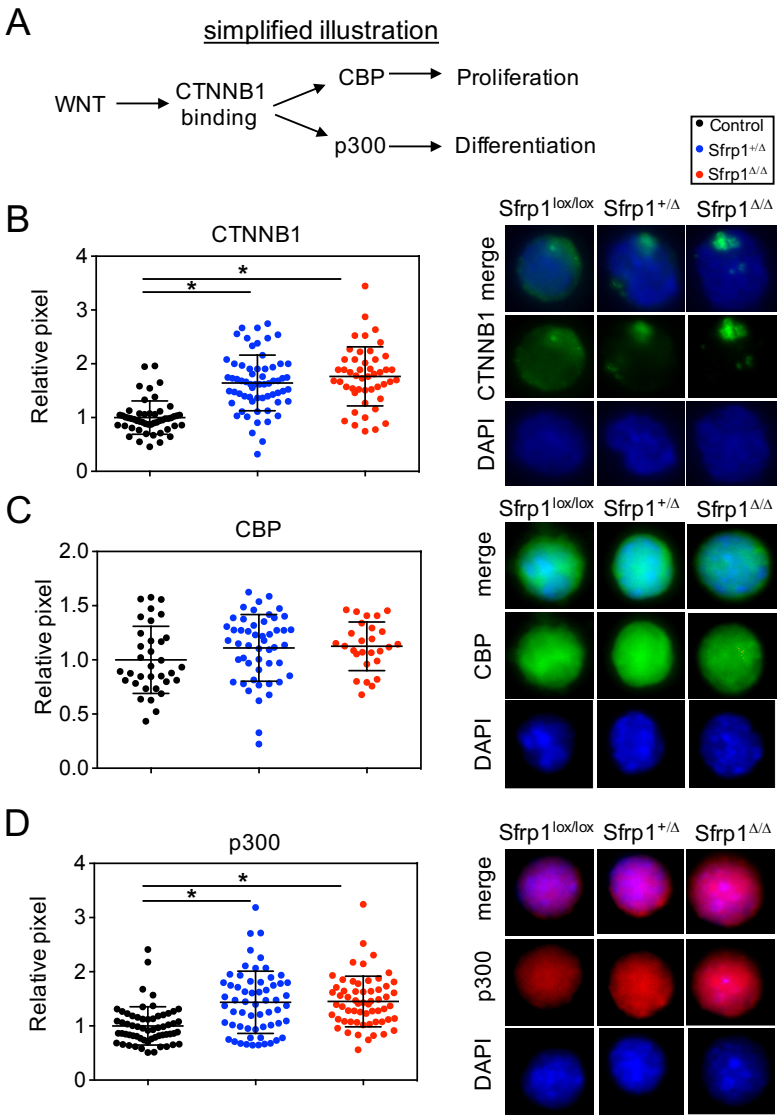

Figure 37. Protein content of CTNNB1, CBP and p300 in CD34$^-$ SLAM cells of *Sfrp1* conditional mice and the controls. (A) Schema of complex formation between CTNNB1 and either CBP or p300 leads to differentiation or proliferation. **(B)** Left: CTNNB1 protein content as pixel number of LT-HSCs of *Sfrp1*$^{+/\Delta}$ (n =63), *Sfrp1*$^{\Delta/\Delta}$ (n = 48) and the controls (n = 51); Right: Representative immunofluorescence staining for the nuclei staining with DAPI in blue (below), CTNNB1 protein in green (middle), and the merged picture (top) of LT-HSCs of *Sfrp1*$^{+/\Delta}$, *Sfrp1*$^{\Delta/\Delta}$ and the controls. **(C)** Left: CBP protein content as pixel number of LT-HSCs of *Sfrp1*$^{+/\Delta}$ (n = 50), *Sfrp1*$^{\Delta/\Delta}$ (n = 27) and the controls (n = 34); Right: Representative immunofluorescence staining for the nuclei staining with DAPI in blue (below), CBP protein in green (middle), and the merged picture (top) of LT-HSCs of *Sfrp1*$^{+/\Delta}$, *Sfrp1*$^{\Delta/\Delta}$ and the controls. **(D)** Left: p300 protein content as pixel number of LT-HSCs of *Sfrp1*$^{+/\Delta}$ (n = 60), *Sfrp1*$^{\Delta/\Delta}$ (n = 60) and the controls (n = 60); Right: Representative immunofluorescence staining for the nuclei staining with DAPI in blue (below), p300 protein in green (middle), and the merged picture (top) of LT-HSCs of *Sfrp1*$^{+/\Delta}$, *Sfrp1*$^{\Delta/\Delta}$ and the controls. Black dots represent controls (*Sfrp1*$^{lox/lox}$); Blue dots represent *Sfrp1*$^{+/\Delta}$; Red dots represent *Sfrp1*$^{\Delta/\Delta}$. Each dot represents a cell. Represented values are illustrated as Mean ± SD. * p-value ≤0.05 show significant differences in the comparison of *Sfrp1*$^{+/\Delta}$ and *Sfrp1*$^{\Delta/\Delta}$ to each other or to controls determined by ANOVA, Tukey`s post hoc test.

4.6.3.1 Impact of the IQ-1 treatment *in vitro*

To determine the impact of the β-catenin/p300 complex in CD34$^-$ SLAM cells, we treated these cells with a specific inhibitor of the formation of this complex, IQ-1. Miyabayashi et al. have demonstrated that IQ-1 specifically prevents the interaction of β-catenin with p300, by targeting PR72/130 (PPP2R3A), a subunit of the serine/threonine phosphatase PP2A complex (Miyabayashi et al., 2007). Thus, IQ-1 reduces the interaction between β-catenin and p300, thus favoring formation of the proliferation-promoting β-catenin/CBP complex (Figure 38A). We therefore hypothesized that reducing the formation of the CTNNB1/p300 complex by IQ-1 treatment could, rescue the aberrant balance between differentiation and proliferation of CD34$^-$ SLAM cells from *Sfrp1*$^{\Delta/\Delta}$ mice.

To test this hypothesis, we set up a single CD34$^-$ SLAM cell culture with and without addition of 10 µM IQ-1, a concentration previously used to inhibit formation of the CTNNB1/p300 complex (Miyabayashi et al., 2007). We then determined proliferation and survival and at the end of culture (day 5) we assessed changes in CFUs and flow cytometry assays (Figure 38B).

In cultures of untreated CD34$^-$ SLAM cells of *Sfrp1*$^{\Delta/\Delta}$ mice, we again note decreased clone size formation at day 4 and 5 of culture compared to the untreated *Sfrp1*$^{+/\Delta}$ and the controls (*Sfrp1*$^{lox/lox}$), reproducing the reduced proliferation noted before (Figure 36B, Figure 38C). Interestingly, IQ-1 treatment did not increase, but rather decreased proliferation rates (Figure 38D). At the same time, the number of colony-forming cells (CFCs) was not significantly changed, suggesting that less cells, produce more colonies per cell. Since CFC are enriched in LSK cells, we then assessed LSK cell numbers with and without IQ-1 treatment. Intriguingly, treatment of the cultures with IQ-1 (inhibitor is present during the culture) maintained the LSK surface phenotype at higher levels compared to the untreated cells in all cultures, regardless of the genotype of the CD34$^-$ SLAM cells (Figure 38E, F).

Thus, IQ-1 does not promote proliferation per sé, in fact, IQ-1 treatment reduces the total number of cells in culture, but it improves retention of early cell types, such as LSK cells and improve their colony-forming ability, not only in CD34$^-$ SLAM cells from *Sfrp1*$^{\Delta/\Delta}$, but also in control cells. The increased numbers of LSK cells and the increased potential to form more colonies/LSK after IQ-1 treatment, strongly suggests that with IQ-1, CD34$^-$ SLAM cells from *Sfrp1*$^{\Delta/\Delta}$ show less differentiation and more self-renewal activity in the absence of increased proliferation.

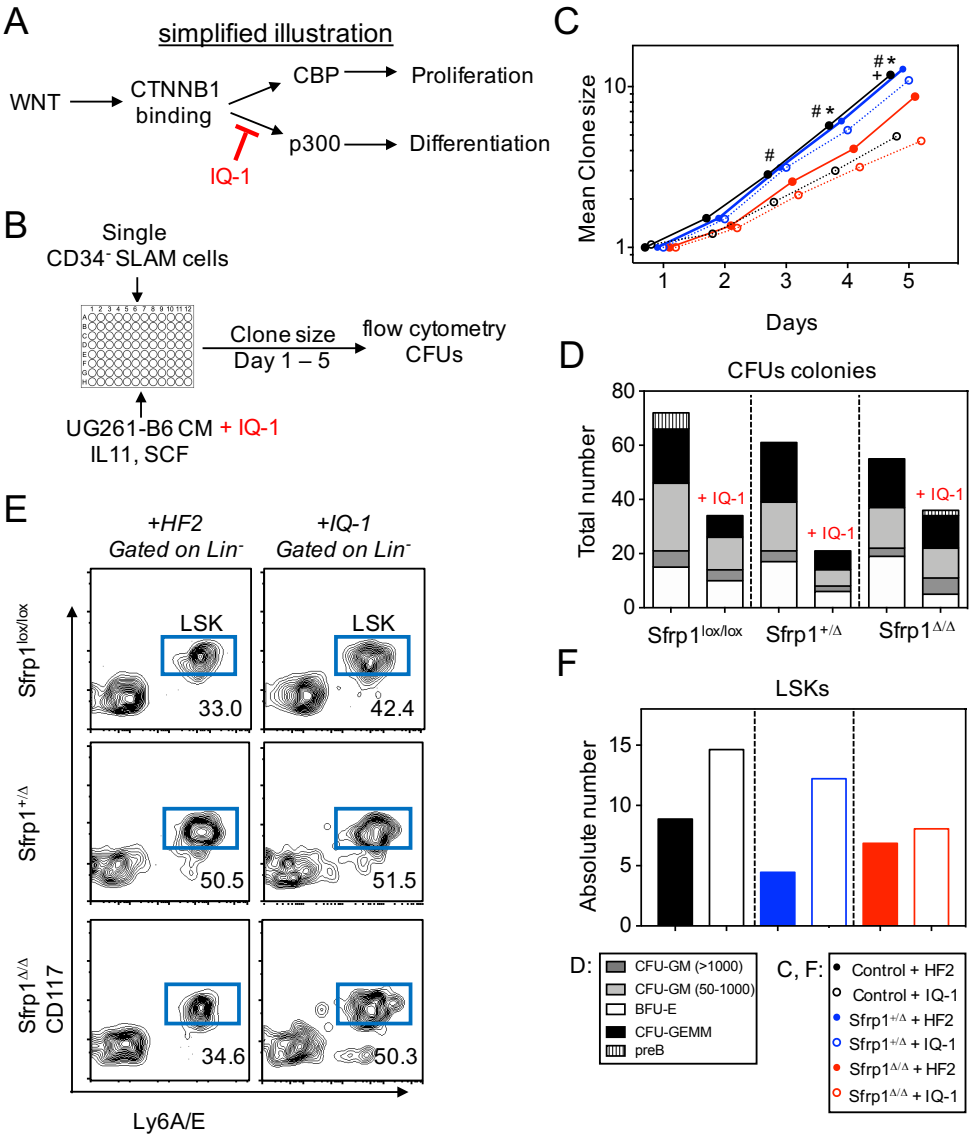

Figure 38. Single cell culture of LT-HSCs with inhibitor IQ-1. (A) Regulation of proliferation versus differentiation in ES cells and inhibited CTNNB1-p300 binding with specific inhibitor IQ-1 *in vitro*. **(B)** Experimental design: 96-round-bottomed plates were prefilled with UG26-1B6 CM, containing mSCF, IL-11 and HF2+ or 10 µM IQ-1. Single CD34$^-$ SLAM cells of *Sfrp1*$^{+/\Delta}$, *Sfrp1*$^{\Delta/\Delta}$ and the controls were sorted into each well. For five days, the clone size was counted every 24 h. After five days, the clones (> 2 cells/well) were harvested and either analyzed per flow cytometry or further cultured in M3434. **(C)** Counted mean clone size over five days of *Sfrp1*$^{+/\Delta}$, *Sfrp1*$^{\Delta/\Delta}$ and the controls with and without IQ-1. **(D)** Counted total numbers of CFUs from single-cell cultured cells after five days. **(E)** Representative plots of the gating strategy for LSK populations after five days of culture. **(F)** Bar plots in absolute number of LSK cells after five days of culture of *Sfrp1*$^{+/\Delta}$, *Sfrp1*$^{\Delta/\Delta}$ and the controls with and without IQ-1. Black dots represent controls (*Sfrp1*$^{lox/lox}$); white dots surrounded by black represents IQ-1 treated controls (*Sfrp1*$^{lox/lox}$). Blue dots represent *Sfrp1*$^{+/\Delta}$; white dots surrounded by blue represents IQ-1 treated *Sfrp1*$^{+/\Delta}$. Red dots represent *Sfrp1*$^{\Delta/\Delta}$; white dots surrounded by red represents IQ-1 treated *Sfrp1*$^{\Delta/\Delta}$ mice. Each dot represents the mean of a plate. Represented values are illustrated as Mean. * p-value ≤0.05 show significant differences in the comparison of IQ-1 treated *Sfrp1*$^{\Delta/\Delta}$ to untreated controls and *Sfrp1*$^{+/\Delta}$; whereas $^{\#}$ p-value ≤0.05 show significant differences in the comparison of untreated controls to IQ-1 treated controls and *Sfrp1*$^{+/\Delta}$, as well as IQ-1 treated *Sfrp1*$^{+/\Delta}$ to the untreated *Sfrp1*$^{+/\Delta}$ and *Sfrp1*$^{\Delta/\Delta}$; whereas $^{+}$ p-value ≤0.05 show significant differences in the comparison of untreated *Sfrp1*$^{+/\Delta}$ to controls, as well as untreated *Sfrp1*$^{\Delta/\Delta}$ to IQ-1 treated *Sfrp1*$^{\Delta/\Delta}$ determined by ANOVA, Tukey`s post hoc test.

4.6.3.2 Impact of the IQ-1 treatment *in vivo*

To study whether IQ-1 treatment would similarly antagonize differentiation of LT-HSC *in vivo*, we treated control (*Sfrp1*$^{lox/lox}$), *Sfrp1*$^{+/\Delta}$ and *Sfrp1*$^{\Delta/\Delta}$ for five days with 14 µg IQ-1 inhibitor via daily i.p. injections (Sasaki & Kahn, 2014). After the treatment, we analysed several parameters possibly contributing to differentiation, as well as repopulating activity of LT-HSCs. The parameters of contributing factors included the measurement of inflammatory cytokines in peripheral blood (PB) using cytokine beads assay, analysis of cell populations from PB by flow cytometry as well as with an animal blood counter Scil Vet Abc^{TM}. Also, we studied differentiation of BM-derived MSCs and their migratory behaviour. Finally, we assessed LT-HSCs for the self-renewal, proliferation and differentiation (Figure 39).

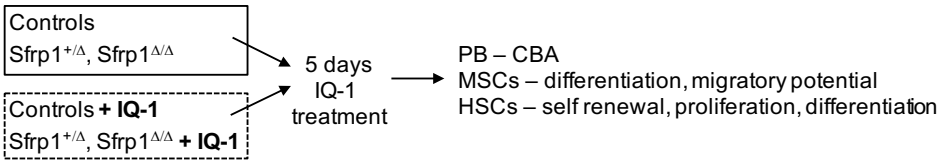

Figure 39. Experimental design of the IQ-1 treatment *in vivo*. Eight- to ten-week old *Sfrp1*$^{+/\Delta}$ and *Sfrp1*$^{\Delta/\Delta}$ mice and control animals were i.p injected with the IQ-1 inhibitor (14 µg) for 5 days. 24 hours later the PB, BM and MSC cell compositions were analyzed.

4.6.3.2.1 Impact of the IQ-1 treatment *in vivo* in the peripheral blood

We wondered how the five-day *in vivo* IQ-1 treatment impacts the mature hematopoietic compartment in the PB of the *Sfrp1*$^{+/\Delta}$, *Sfrp1*$^{\Delta/\Delta}$ mice and controls. To study this, we analyzed the mature cell compartments of the PB by flow cytometry (Figure 40A, C-F) and with an animal blood counter (Figure 40B), as well as with an inflammatory cytokines assay (Figure 41).

In Figure 40A, representative flow cytometry plots for the gating (explained under 4.6.1) of mature cell populations in PB, isolated from *Sfrp1*$^{+/\Delta}$, *Sfrp1*$^{\Delta/\Delta}$ mice and control animals, are shown.

The analysis of the PB with the animal blood counter, as well as flow cytometric analyses showed an unchanged white blood cell number in 10^3/µl (Figure 40B), an unchanged percentage of B220$^+$ B cells (Figure 40C), as well as for the CD3e$^+$ T cells (Figure 40D), GR1^{med}CD11b$^+$ monocytes (Figure 40E) and GR1$^+$CD11b$^+$ granulocytes (Figure 40F).

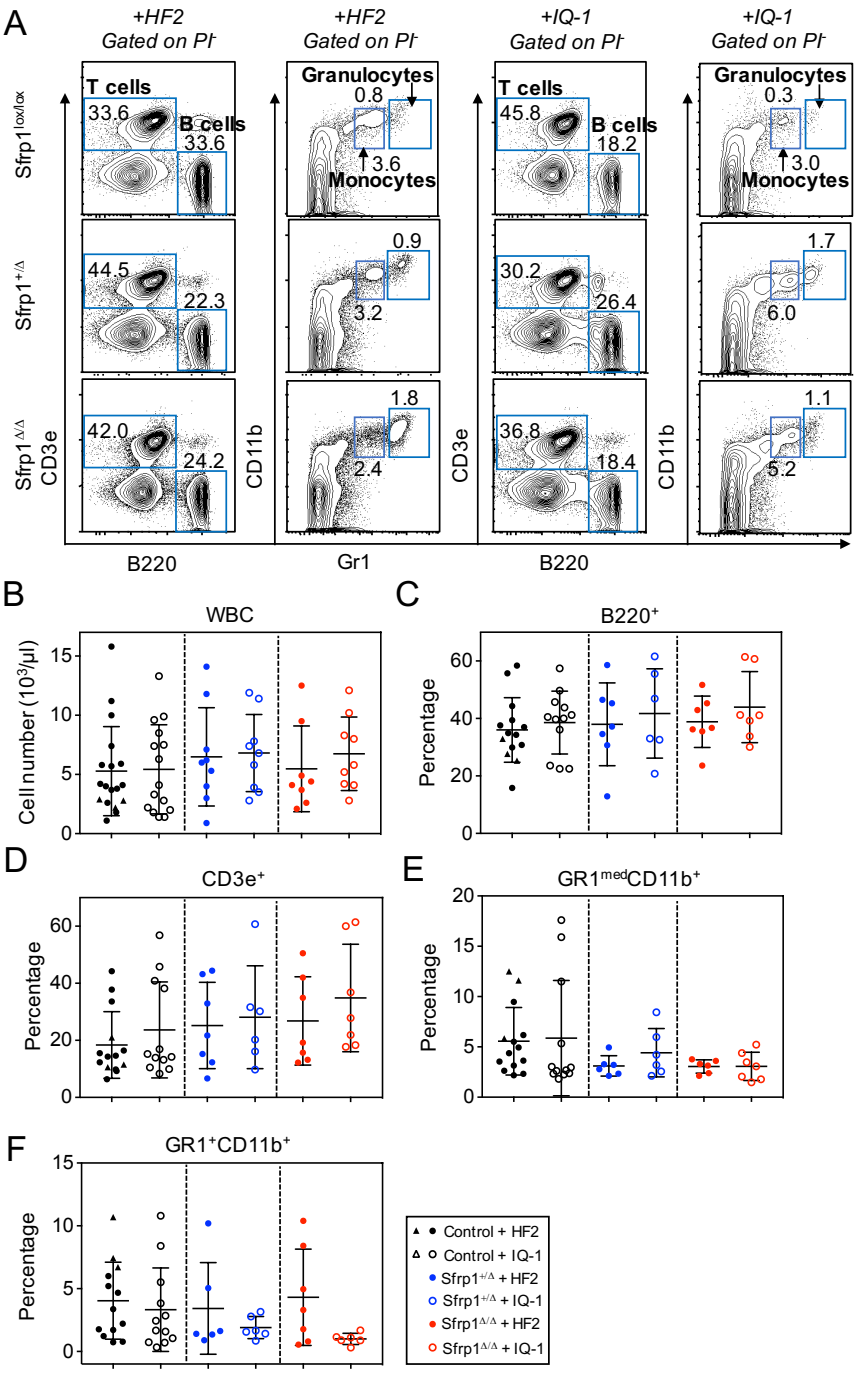

Figure 40. The impact of *in vivo* IQ-1 treatment in PB. (A) Representative flow cytometry plots of the gating strategy for mature cell populations in PB. **(B)** Cell number of WBC in 10^3/µl of *Sfrp1* conditional mice (with HF2+: *Sfrp1*$^{+/\Delta}$: n = 9; *Sfrp1*$^{\Delta/\Delta}$: n = 8; with IQ-1: *Sfrp1*$^{+/\Delta}$: n = 9; *Sfrp1*$^{\Delta/\Delta}$: n = 9) compared to the controls (with HF2+: n = 18; with IQ-1: n = 15). **(C)** Percentage of the B220$^+$ B cells, **(D)** Percentage of CD3e$^+$ T cells of *Sfrp1* conditional mice (with HF2+: *Sfrp1*$^{+/\Delta}$: n = 7; *Sfrp1*$^{\Delta/\Delta}$: n = 7; with IQ-1: *Sfrp1*$^{+/\Delta}$: n = 6; *Sfrp1*$^{\Delta/\Delta}$: n = 7) compared to the controls (with HF2+: n = 14; with IQ-1: *Sfrp1*$^{lox/lox}$: n = 12). **(E)** Percentage of GR1^{med}CD11B$^+$ monocytes of *Sfrp1* conditional mice (with HF2+: *Sfrp1*$^{+/\Delta}$: n =6; *Sfrp1*$^{\Delta/\Delta}$: n = 6; with IQ-1: *Sfrp1*$^{+/\Delta}$: n = 6; *Sfrp1*$^{\Delta/\Delta}$: n = 7) compared to the controls (with HF2+: n = 14; with IQ-1: n = 12). **(F)** Percentage of GR1$^+$CD11b$^+$ granulocytes of *Sfrp1* conditional mice (with HF2+: *Sfrp1*$^{+/\Delta}$: n = 6; *Sfrp1*$^{\Delta/\Delta}$: n = 7; with IQ-1: *Sfrp1*$^{+/\Delta}$: n = 6; *Sfrp1*$^{\Delta/\Delta}$: n = 6) compared to the controls (with HF2+: n = 13; with IQ-1: n = 12). Black dots represent controls (*Sfrp1*$^{lox/lox}$); white dots surrounded by black represents IQ-1 treated controls (*Sfrp1*$^{lox/lox}$). Black triangles represent controls (Osx-Cre); white triangles surrounded by black represents IQ-1 treated controls (Osx-Cre). Blue dots represent *Sfrp1*$^{+/\Delta}$; white dots surrounded by blue represents IQ-1 treated *Sfrp1*$^{+/\Delta}$. Red dots represent *Sfrp1*$^{\Delta/\Delta}$; white dots surrounded by red represents IQ-1 treated *Sfrp1*$^{\Delta/\Delta}$ mice. Each dot represents an animal. Represented values are illustrated as Mean ± SD.

To find out whether the loss of SFRP1 in the niche has an impact on the inflammatory response, we analyzed the inflammatory cytokines IL-6, IL-10, MCP-1, IFNγ, TNF, and IL-12p70 in the serum of *Sfrp1*$^{+/\Delta}$, *Sfrp1*$^{\Delta/\Delta}$ mice and control animals (Figure 41A, B). The analyzed inflammatory cytokines were unchanged in the serum of *Sfrp1*$^{+/\Delta}$, *Sfrp1*$^{\Delta/\Delta}$ mice compared to the control animals before and after *in vivo* IQ-1 treatment (Figure 41B).

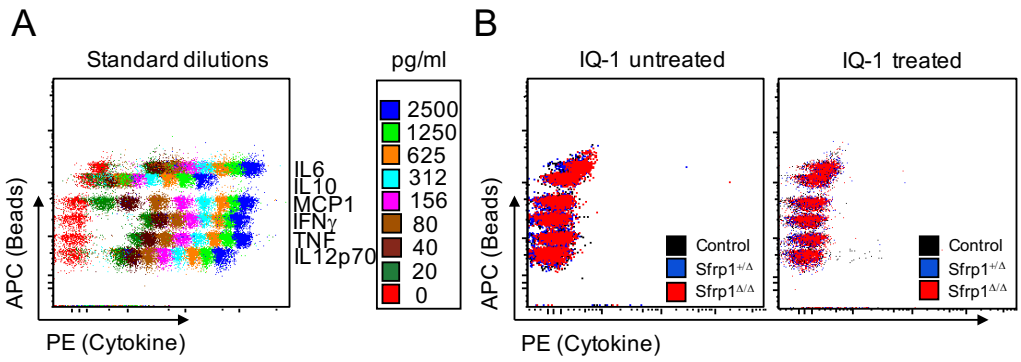

Figure 41. The inflammatory response after five days of IQ-1 treatment in serum. (A) Standard dilutions for the inflammatory cytokines (IL-6, IL-10, MCP-1, INFγ, TNF, IL-12p70). **(B)** Representative flow cytometry plot for the analyzation of the cytokines in the serum, 24 h after the IQ-1 treatment. Left: untreated animals; Right: IQ-1 treated animals. In Figure B: Black dots represent controls (*Sfrp1*$^{lox/lox}$); Blue dots represent *Sfrp1*$^{+/\Delta}$; Red dots represent *Sfrp1*$^{\Delta/\Delta}$. A representative example for each genotype is shown.

4.6.3.2.2 Impact of the IQ-1 treatment *in vivo* in the stromal compartment and functional analysis of the MSCs

Considering that the primary defect in the *Sfrp1*$^{+/\Delta}$, *Sfrp1*$^{\Delta/\Delta}$ mice is the lack of *Sfrp1* expression in Osx^{+} mesenchymal cells, we then investigated how the stromal cell compartmnent was affected by *in vivo* IQ-1 treatment. These experiments did not reveal significant changes in the total number of endosteal cells (from collagenase treated bones) from the IQ-1 treated *Sfrp1*$^{+/\Delta}$ and *Sfrp1*$^{\Delta/\Delta}$ mice compared to the IQ-1 treated control animals. Also, both IQ-1 and untreated *Sfrp1*$^{+/\Delta}$ and *Sfrp1*$^{\Delta/\Delta}$ mice showed similar numbers of endosteal cells (from collagenase treated bones) in their BM (Figure 42A).

Despite the lack of effects of IQ-1 on numbers of endosteal cells, we found that the slightly higher CFU-F colony formation from cultured compact bone-derived MSCs isolated from untreated *Sfrp1*$^{\Delta/\Delta}$ animals is reduced in IQ-1 treated animals (Figure 42B).

However, although the slightly increased CFU-F frequency in untreated animals, IQ-1 treatment unexpectedly decreases CFU-F frequencies even below control levels, suggesting that high CFU-F frequencies do not necessarily correlate with MSC health in *Sfrp1*$^{\Delta/\Delta}$ mice.

In order to analyze whether the differentiation behavior of cultured compact bone-derived MSCs from *Sfrp1*$^{+/\Delta}$ and *Sfrp1*$^{\Delta/\Delta}$ mice is affected after IQ-1 treatment compared to controls, we characterized the cultured compact bone-derived MSCs grown from the bones for the differentiation, senescence and migratory behavior in cultures of untreated or IQ-1-treated animals.

These experiments show that adipogenic and osteogenic induction in cultures of cultured compact bone-derived MSCs from *Sfrp1*$^{+/\Delta}$, *Sfrp1*$^{\Delta/\Delta}$ and controls showed no significant differences in adipogenesis or osteogenesis between the untreated and IQ-1-treated mice (Figure 42C).

In addition, we also do not find that the percentage of senescence-associated (SA)-β-gal (blue stained) in cultured compact bone-derived MSCs was affected by *in vivo* IQ-1 treatment in *Sfrp1*$^{\Delta/\Delta}$ animals compared to untreated controls. The mean of 23 % SA-β-gal-expressing cells of treated *Sfrp1*$^{\Delta/\Delta}$ MSCs is comparable to that in cultures with MSCs from untreated controls. However, we found again that the percentage of SA-β-gal (blue stained) in cultured compact bone-derived MSCs from untreated *Sfrp1*$^{\Delta/\Delta}$ animals was increased compared to the untreated controls (Figure 42D).

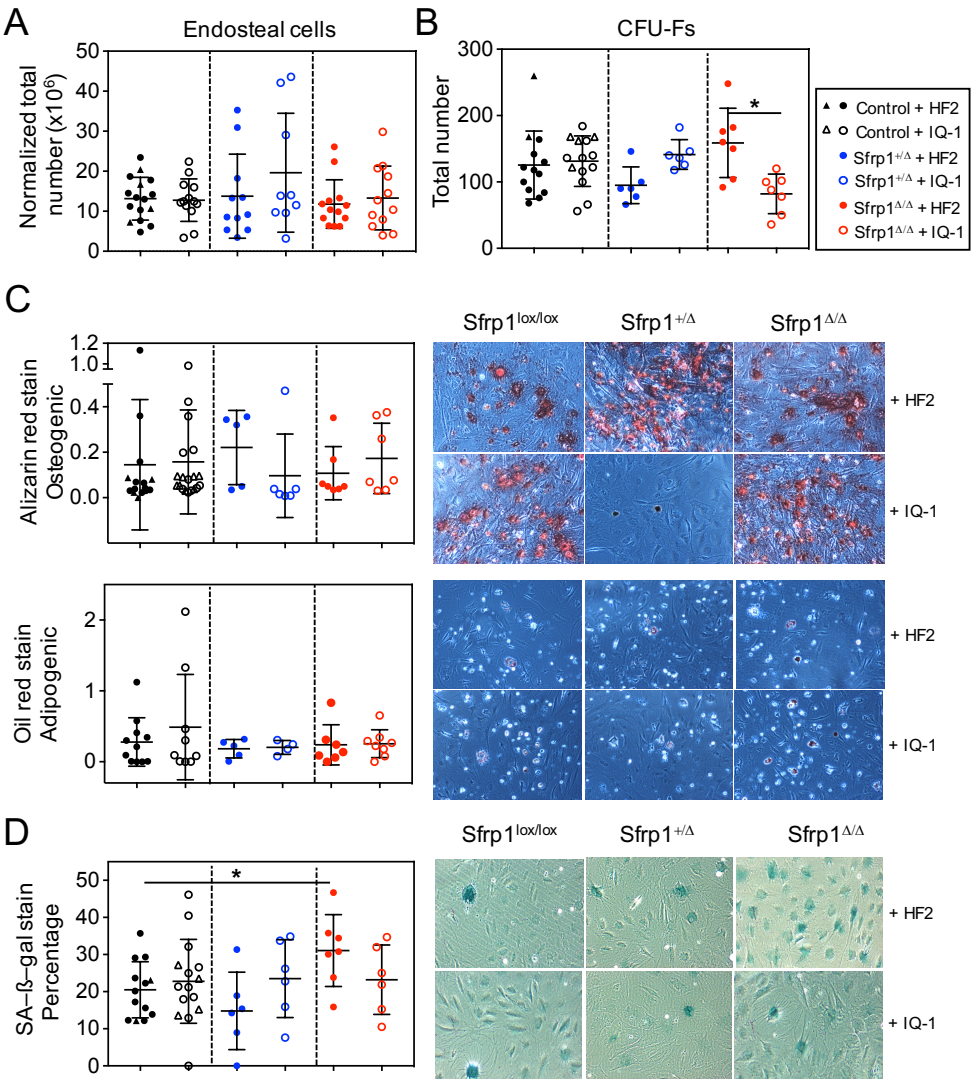

Figure 42. Functional analysis of cultured compact bone-derived MSCs in *Sfrp1* conditional mice after IQ-1 treatment. (A) Normalized total cell number of endosteal cells (from collagenase treated bones) of *Sfrp1* conditional mice (with HF2+: *Sfrp1*$^{+/\Delta}$: n = 11; *Sfrp1*$^{\Delta/\Delta}$: n = 13; with IQ-1: *Sfrp1*$^{+/\Delta}$: n = 9; *Sfrp1*$^{\Delta/\Delta}$: n = 12) compared to the controls (with HF2+: n = 16; with IQ-1: n = 13). **(B)** Total number of CFU-Fs of cultured compact bone-derived MSCs of *Sfrp1* conditional mice (with HF2+: *Sfrp1*$^{+/\Delta}$: n = 6; *Sfrp1*$^{\Delta/\Delta}$: n = 7; with IQ-1: *Sfrp1*$^{+/\Delta}$: n = 6; *Sfrp1*$^{\Delta/\Delta}$: n = 7) compared to the controls (with HF2+: n = 13; with IQ-1: n = 14). **(C)** Above, left: Quantification of Alizarin red content at OD 562 nm of *Sfrp1* conditional mice (with HF2+: *Sfrp1*$^{+/\Delta}$: n = 5; *Sfrp1*$^{\Delta/\Delta}$: n = 7; with IQ-1: *Sfrp1*$^{+/\Delta}$: n = 6; *Sfrp1*$^{\Delta/\Delta}$: n = 7) compared to the controls (with HF2+: n = 15; with IQ-1: n = 19) of osteogenic differentiated cultured compact bone-derived MSCs. Above, right: Microscopy of Alizarin red stained osteogenic differentiation of *Sfrp1* conditional mice compared to the controls. Below, left: Quantification of Oil red content at OD 520 nm of *Sfrp1* conditional mice (with HF2+: *Sfrp1*$^{+/\Delta}$: n = 5; *Sfrp1*$^{\Delta/\Delta}$: n = 7; with IQ-1: *Sfrp1*$^{+/\Delta}$: n = 4; *Sfrp1*$^{\Delta/\Delta}$: n = 8) compared to the controls (with HF2+: n = 11; with IQ-1: n = 9) from adipogenic differentiated cultured compact bone-derived MSCs. Below, right: Microscopy of Oil red stained adipogenic differentiation *Sfrp1* conditional mice compared to the controls. **(D)** Left: Percentage of SA-β-gal (blue stained) positive cells *Sfrp1* conditional cultured compact bone-derived MSCs (with HF2+: *Sfrp1*$^{+/\Delta}$: n = 6; *Sfrp1*$^{\Delta/\Delta}$: n = 7; with IQ-1: *Sfrp1*$^{+/\Delta}$: n = 6; *Sfrp1*$^{\Delta/\Delta}$: n = 6) compared to the controls (with HF2+: n = 13; with IQ-1: n = 15). Right: Microscopy of SA-β-gal staining in *Sfrp1* conditional cultured compact bone-derived MSCs compared to the controls. Black dots represent controls (*Sfrp1*$^{lox/lox}$); white dots surrounded by black represents IQ-1 treated controls (*Sfrp1*$^{lox/lox}$). Black triangles represent controls (Osx-Cre); white triangles surrounded by black represents IQ-1 treated controls (Osx-Cre). Blue dots represent *Sfrp1*$^{+/\Delta}$; white dots surrounded by blue represents IQ-1 treated *Sfrp1*$^{+/\Delta}$. Red dots represent *Sfrp1*$^{\Delta/\Delta}$; white dots surrounded by red represents IQ-1 treated *Sfrp1*$^{\Delta/\Delta}$ mice. Each dot represents an animal. Represented values are illustrated as Mean ± SD. * p-value ≤0.05 show significant differences in the comparison of IQ-1 treated *Sfrp1*$^{+/\Delta}$, *Sfrp1*$^{\Delta/\Delta}$ and controls to each other or to the untreated controls determined by ANOVA, Tukey`s post hoc test.

Furthermore, the population doubling potential of cultured compact bone-derived MSCs from the IQ-1 treated *Sfrp1*$^{+/\Delta}$, *Sfrp1*$^{\Delta/\Delta}$ mice and controls (*Sfrp1*$^{lox/lox}$, Osx-Cre) were analyzed by long-term culture. For this, cultured compact bone-derived MSCs were continuously counted and reseeded at a fixed density.

Until passage 12, growth potentials of cultured compact bone-derived MSCs from all genotypes were in the same range (Figure 43). Although, the untreated control animals show a high variance of data set and reaching a cumulative growth rate at around 11 at passage 12, followed by the untreated *Sfrp1*$^{+/\Delta}$ and *Sfrp1*$^{\Delta/\Delta}$ cultured compact bone-derived MSCs that achieved a value of 10 on average at the passage 12. The growth potential of the IQ-1 treated cultured compact bone-derived MSCs was weaker compared to the untreated once. The IQ-1 treated control animals and *Sfrp1*$^{\Delta/\Delta}$ reaching a cumulative growth rate at around 10 at passage 12, followed by the IQ-1 treated *Sfrp1*$^{+/\Delta}$ cultured compact bone-derived MSCs that achieved a value of 9. Nevertheless, it was reported that MSCs cultured from compact bones *in vitro* lose their capacity for multilineage differentiation after 10 passages (Guo et al., 2006; Zhu et al., 2010). The regular growth exhaustion of the cultured compact bone-derived MSCs became clear at passage 12.

Furthermore, cultured compact bone-derived MSCs from a IQ-1-treated and untreated *Sfrp1*$^{+/\Delta}$, *Sfrp1*$^{\Delta/\Delta}$ mice and control animals were analyzed for migratory potential. For this purpose, we used the "scratch assay" (Liang et al., 2007). The assay shows the potential of MSCs to fill a scratched surface, which is oftentimes also used to predict wound healing potential (Liang et al., 2007).

The cultured compact bone-derived MSCs from untreated controls show slightly higher migration rates of 4 % captured at 12 hours compared to the cultured compact bone-derived MSCs from IQ-1 treated control mice (Figure 44A). Interestingly, the cultured compact bone-derived MSCs from untreated *Sfrp1*$^{+/\Delta}$ mice show almost the same, but reduced migration rates of 13% captured at 12 hours compared to the treated once (Figure 44B). In the comparison of cultured compact bone-derived MSCs of untreated and IQ-1-treated *Sfrp1*$^{\Delta/\Delta}$ mice, there was no measurable difference in migration rate (Figure 44C). All in all, no noticeable alterations in migratory potential were observed between MSCs from either genotypes or the IQ-1 treatment.

Taken together, we found that IQ-1 treatment did not change the functional characteristics of these cultured compact bone-derived MSCs overall. The ability to form CFU-Fs is not changed, as well as the induced multi-lineage differentiation behavior or the number of SA-β-gal-expressing cells. However, in our dataset, no functional changes in the long-term culture or wound healing potential could be observed after IQ-1 treatment.

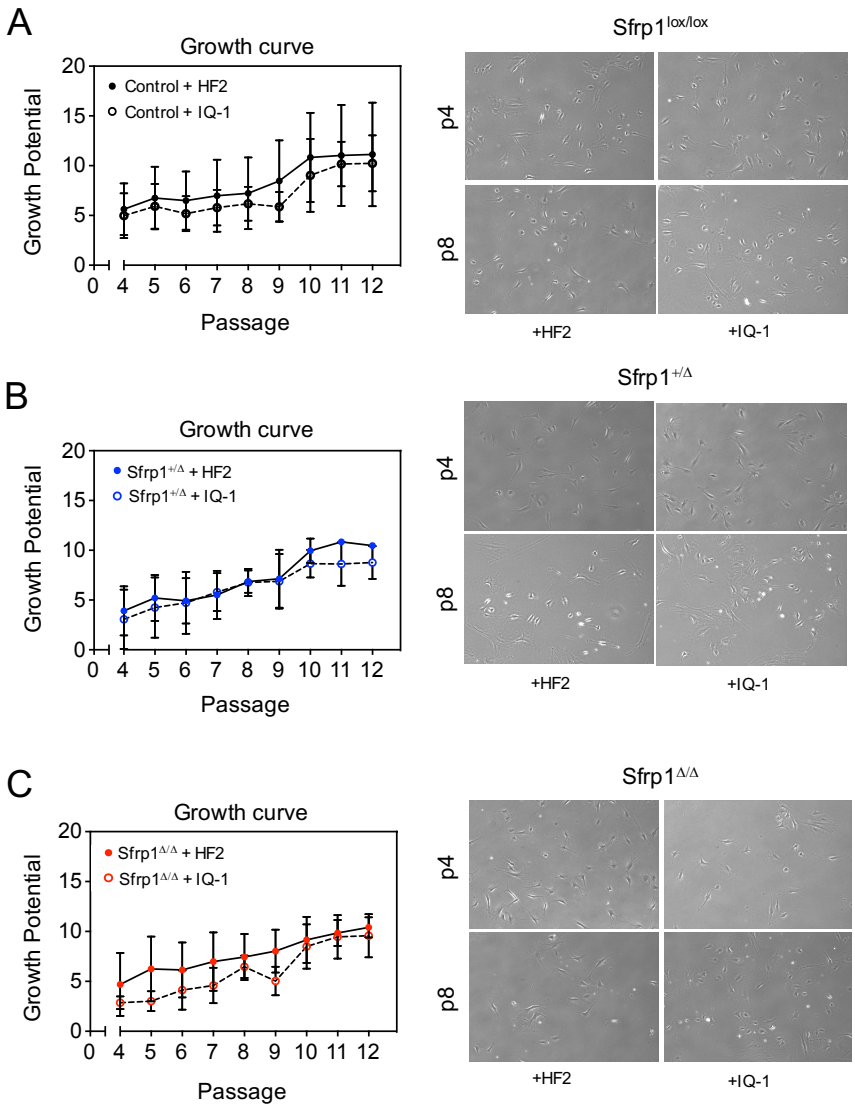

Figure 43. Growth potential of cultured compact bone-derived MSCs from a IQ-1 treated *Sfrp1* conditional mice and controls. (A) Left: Long-term culture of control (with HF2+: *Sfrp1*$^{lox/lox}$: n = 7, Osx-Cre: n = 2; with IQ-1: *Sfrp1*$^{lox/lox}$: n = 5, *OSX1-GFP::Cre*: n = 4) cultured compact bone-derived MSCs over 12 passages; Right: Representative images of cell morphology of cultured control MSCs at passage 4 and 8. **(B)** Left: Long-term culture of *Sfrp1*$^{+/\Delta}$ (with HF2+: *Sfrp1*$^{+/\Delta}$: n = 5; with IQ-1: *Sfrp1*$^{+/\Delta}$: n = 4) cultured compact bone-derived MSCs over 12 passages; Right: Representative images of cell morphology of cultured *Sfrp1*$^{+/\Delta}$ MSCs at passage 4 and 8. **(C)** Left: Long-term culture of *Sfrp1*$^{\Delta/\Delta}$ (with HF2+: *Sfrp1*$^{\Delta/\Delta}$: n = 4; with IQ-1: *Sfrp1*$^{\Delta/\Delta}$: n = 4) cultured compact bone-derived MSCs over 12 passages; Right: Representative images of cell morphology of cultured *Sfrp1*$^{\Delta/\Delta}$ MSCs at passage 4 and 8. Black dots represent controls (*Sfrp1*$^{lox/lox}$, Osx-Cre); white dots surrounded by black represents IQ-1 treated controls (*Sfrp1*$^{lox/lox}$, Osx-Cre*)*. Blue dots represent *Sfrp1*$^{+/\Delta}$; white dots surrounded by blue represents IQ-1 treated *Sfrp1*$^{+/\Delta}$. Red dots represent *Sfrp1*$^{\Delta/\Delta}$; white dots surrounded by red represents IQ-1 treated *Sfrp1*$^{\Delta/\Delta}$ mice. Represented values are illustrated as Mean ± SD.

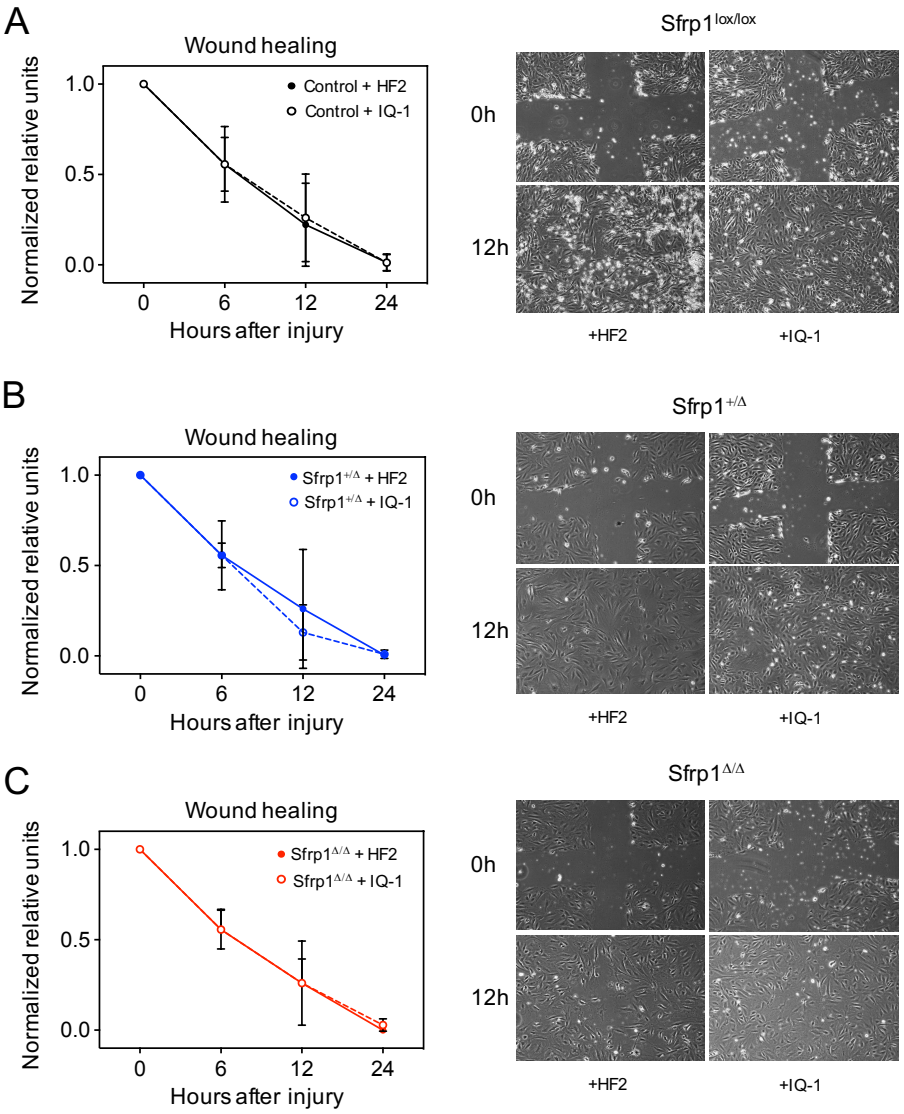

Figure 44. Wound healing potential of cultured compact bone-derived MSCs from *Sfrp1* conditional mice and controls. (A) Left: Wound healing potential of control (with HF2+: *Sfrp1*$^{lox/lox}$: n = 11, Osx-Cre: n = 2; with IQ-1: *Sfrp1*$^{lox/lox}$: n = 10, Osx-Cre: n = 4) cultured compact bone-derived MSCs in passage 4; Right: Representative images of cell morphology of control cultured compact bone-derived MSCs in the scratch assay at 0 h and 12 h in passage 4. **(B)** Left: Long-term culture of *Sfrp1*$^{+/\Delta}$ (with HF2+: *Sfrp1*$^{+/\Delta}$: n = 6; with IQ-1: *Sfrp1*$^{+/\Delta}$: n = 6) cultured compact bone-derived MSCs in passage 4; Right: Representative images of cell morphology of *Sfrp1*$^{+/\Delta}$ cultured compact bone-derived MSCs in the scratch assay at 0 h and 12 h in passage 4. **(C)** Left: Long-term culture of *Sfrp1*$^{\Delta/\Delta}$ (with HF2+: *Sfrp1*$^{\Delta/\Delta}$: n = 8; with IQ-1: *Sfrp1*$^{\Delta/\Delta}$: n = 6) cultured compact bone-derived MSCs in passage 4; Right: Representative images of cell morphology of *Sfrp1*$^{\Delta/\Delta}$ cultured compact bone-derived MSCs in the scratch assay at 0 h and 12 h in passage 4. Black dots represent controls (*Sfrp1*$^{lox/lox}$, Osx-Cre); white dots surrounded by black represents IQ-1 treated controls (*Sfrp1*$^{lox/lox}$, Osx-Cre). Blue dots represent *Sfrp1*$^{+/\Delta}$; white dots surrounded by blue represents IQ-1 treated *Sfrp1*$^{+/\Delta}$. Red dots represent *Sfrp1*$^{\Delta/\Delta}$; white dots surrounded by red represents IQ-1 treated *Sfrp1*$^{\Delta/\Delta}$ mice. Represented values are illustrated as Mean ± SD.

4.6.3.3 Rescue of LT-HSCs proliferation with IQ-1 treatment *in vivo*

Miyabayashi et al. have demonstrated that the specific IQ-1 inhibitor prevents the interaction of β-catenin with p300, by targeting the PR72/130 a subunit of the serine/threonine phosphatase PP2A. They showed that IQ-1 reduces the β-catenin/p300 complex and increases the β-catenin/CBP complex (Miyabayashi et al., 2007).

As showed before, in LT-HSCs from *Sfrp1*$^{\Delta/\Delta}$, protein content of β-catenin and p300 was increased, while CBP content was unchanged (Figure 37). This could mean that perhaps due to the increased expression of p300, more of its complex with β-catenin is formed and differentiation is the dominant behavior of LT-HSC. Reducing the p300 complex by IQ-1 treatment could, therefore, rescue the aberrant behavior of LT-HSC of the *Sfrp1*$^{\Delta/\Delta}$ mice.

In the first step, we analyzed the influence of the IQ-1 treatment on the mature hematopoietic compartment in the BM. In our first assessment of the mature hematopoietic compartment, we found no changes in the total cell number of the BM (Figure 45B) nor of the absolute number of B220^{+} B cells (Figure 45A, C), CD8a^{+}CD4^{+} T cells (Figure 45A, D), GR1^{med}CD11b^{+} monocytes (Figure 45A, E) and GR1^{+}CD11b^{+} granulocytes (Figure 45A, F) in comparisons to IQ-1-treated *Sfrp1*$^{+/\Delta}$, *Sfrp1*$^{\Delta/\Delta}$ mice compared to the controls with untreated animals. These results show that IQ-1 treatment does not directly affect mature hematopoietic cell compartments in the BM.

In mouse embryonic stem cells (ESC), IQ-1 supports WNT/β-catenin-driven expansion and inhibits spontaneous differentiation and maintains ESC pluripotency (Miyabayashi et al., 2007). To find whether IQ-1 had comparable effects on LT-HSC from *Sfrp1*$^{\Delta/\Delta}$ mice, we analyzed also the hematopoietic stem cell compartment of treated mice.

There, the absolute number of LSKs, the ST-HSCs as well as the LT-HSCs from the IQ-1-treated controls and *Sfrp1*$^{+/\Delta}$, as well as *Sfrp1*$^{\Delta/\Delta}$ were unchanged (Figure 46A-D). In contrast, similar to untreated steady-state animals, the absolute number of the hematopoietic myeloid progenitors (MPs) was significantly decreased before and after IQ-1 treatment in *Sfrp1*$^{\Delta/\Delta}$ mice compared to their untreated controls (Figure 46A, E). This suggests that the decrease in MPs did not depend on PP2A/PR27 or β-catenin/p300 complex activity.

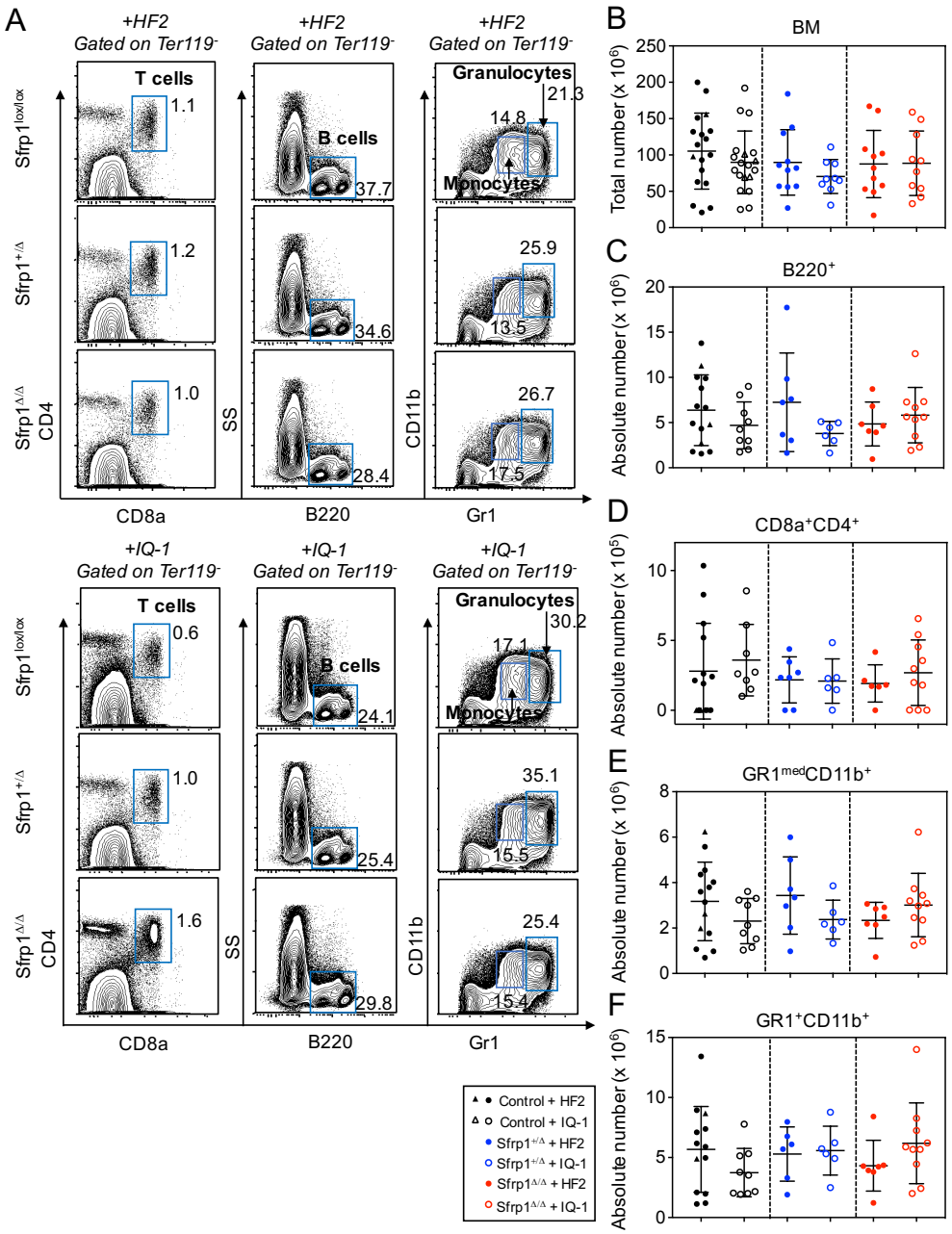

Figure 45. The impact of the IQ-1 treatment on the mature hematopoietic compartment of the BM. **(A)** Representative flow cytometry plots of BM cells of the gating strategy for mature hematopoietic compartment with (below) and without (above) IQ-1 treatment. **(B)** Total number of BM from *Sfrp1* conditional mice (with HF2+: *Sfrp1*$^{+/\Delta}$: n = 11; *Sfrp1*$^{\Delta/\Delta}$: n = 11; with IQ-1: *Sfrp1*$^{+/\Delta}$: n = 9; *Sfrp1*$^{\Delta/\Delta}$: n = 10) compared to the controls (with HF2+: n = 18; with IQ-1: n = 19). **(C)** Absolute number of B220^{+} B cells from *Sfrp1* conditional mice (with HF2+: *Sfrp1*$^{+/\Delta}$: n = 7; *Sfrp1*$^{\Delta/\Delta}$: n = 7; with IQ-1: *Sfrp1*$^{+/\Delta}$: n = 6; *Sfrp1*$^{\Delta/\Delta}$: n = 10) compared to the controls (with HF2+: n = 14; with IQ-1: n = 9). **(D)** Absolute number of CD8a^{+}CD4^{+} T cells from *Sfrp1* conditional mice (with HF2+: *Sfrp1*$^{+/\Delta}$: n = 7; *Sfrp1*$^{\Delta/\Delta}$: n = 6; with IQ-1: *Sfrp1*$^{+/\Delta}$: n = 6; *Sfrp1*$^{\Delta/\Delta}$: n = 10) compared to the controls (with HF2+: n = 14; with IQ-1: n = 8). **(E)** Absolute number of GR1^{med}CD11b^{+} monocytes from *Sfrp1* conditional mice (with HF2+: *Sfrp1*$^{+/\Delta}$: n = 7; *Sfrp1*$^{\Delta/\Delta}$: n = 7; with IQ-1: *Sfrp1*$^{+/\Delta}$: n = 6; *Sfrp1*$^{\Delta/\Delta}$: n = 10) compared to the controls (with HF2+: n = 14; with IQ-1: n = 9). **(F)** Absolute number of GR1^{+}CD11b^{+} granulocytes from *Sfrp1* conditional mice (with HF2+: *Sfrp1*$^{+/\Delta}$: n = 6; *Sfrp1*$^{\Delta/\Delta}$: n = 7; with IQ-1: *Sfrp1*$^{+/\Delta}$: n = 6; *Sfrp1*$^{\Delta/\Delta}$: n = 10) compared to the controls (with HF2+: n = 13; with IQ-1: n = 9). Black dots represent controls (*Sfrp1*$^{lox/lox}$); white dots surrounded by black represents IQ-1 treated controls (*Sfrp1*$^{lox/lox}$). Black triangles represent controls (Osx-Cre); white triangles surrounded by black represents IQ-1 treated controls (Osx-Cre). Blue dots represent *Sfrp1*$^{+/\Delta}$; white dots surrounded by blue represents IQ-1 treated *Sfrp1*$^{+/\Delta}$. Red dots represent *Sfrp1*$^{\Delta/\Delta}$; white dots surrounded by red represents IQ-1 treated *Sfrp1*$^{\Delta/\Delta}$ mice. Each dot represents an animal. Represented values are illustrated as Mean ± SD.

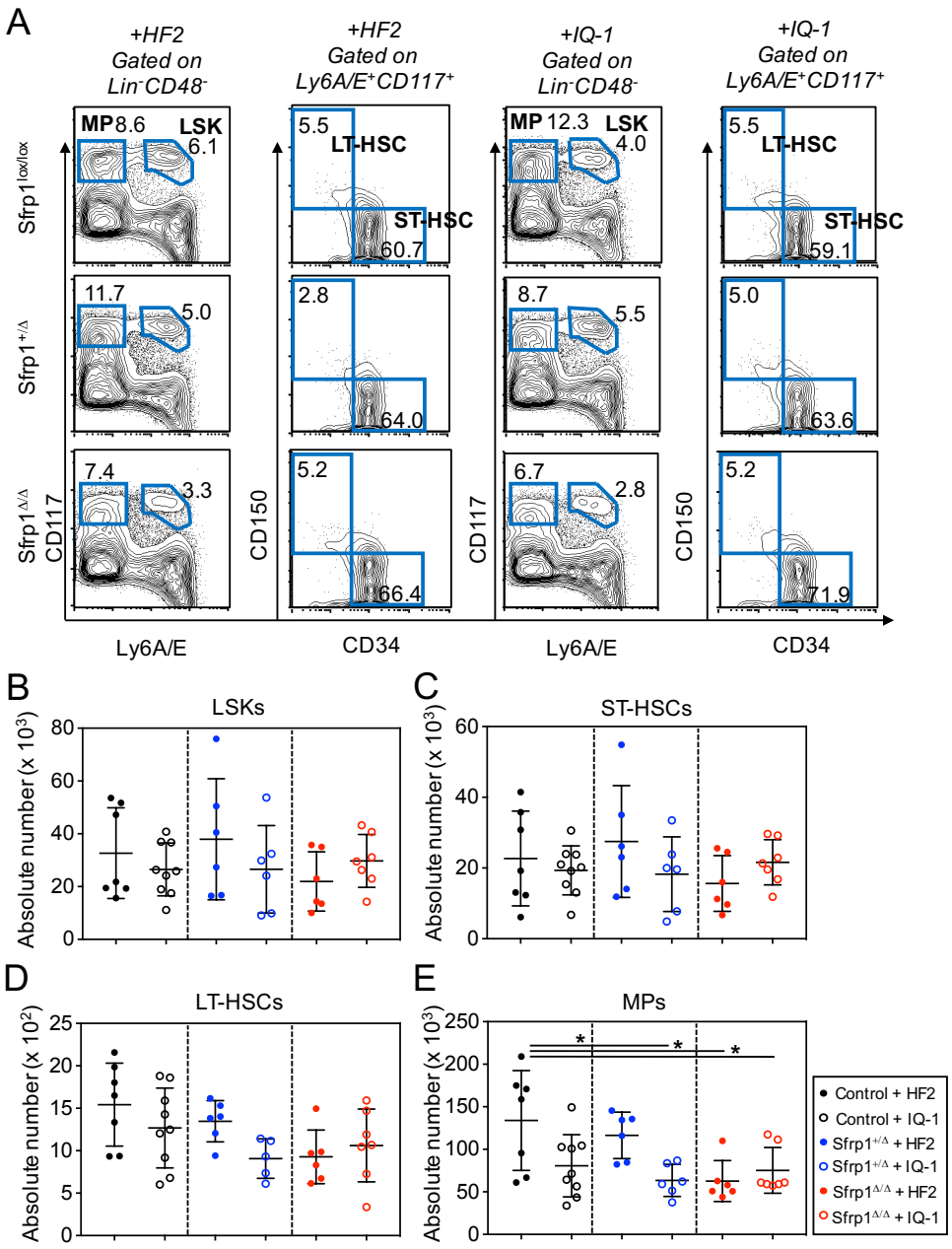

Figure 46. The impact of the IQ-1 treatment on the primitive hematopoietic compartment of the BM. **(A)** Representative flow cytometry plots of the gating strategy for primitive hematopoietic compartment. **(B)** Absolute number of LSKs from *Sfrp1* conditional mice (with HF2+: $Sfrp1^{+/\Delta}$: n = 6; $Sfrp1^{\Delta/\Delta}$: n =6; with IQ-1: $Sfrp1^{+/\Delta}$: n = 6; $Sfrp1^{\Delta/\Delta}$: n = 7) compared to the controls (with HF2+: $Sfrp1^{lox/lox}$: n = 7; with IQ-1: $Sfrp1^{lox/lox}$: n = 9). **(C)** Absolute number of ST-HSCs from *Sfrp1* conditional mice (with HF2+: $Sfrp1^{+/\Delta}$: n = 6; $Sfrp1^{\Delta/\Delta}$: n =6; with IQ-1: $Sfrp1^{+/\Delta}$: n = 6; $Sfrp1^{\Delta/\Delta}$: n = 7) compared to the controls (with HF2+: $Sfrp1^{lox/lox}$: n =7; with IQ-1: $Sfrp1^{lox/lox}$: n = 9). **(D)** Absolute number of LT-HSCs from *Sfrp1* conditional mice (with HF2+: $Sfrp1^{+/\Delta}$: n = 6; $Sfrp1^{\Delta/\Delta}$: n =6; with IQ-1: $Sfrp1^{+/\Delta}$: n = 5; $Sfrp1^{\Delta/\Delta}$: n = 7) compared to the controls (with HF2+: $Sfrp1^{lox/lox}$: n = 7; with IQ-1: $Sfrp1^{lox/lox}$: n = 9). **(E)** Absolute number of MPs from *Sfrp1* conditional mice (with HF2+: $Sfrp1^{+/\Delta}$: n = 6; $Sfrp1^{\Delta/\Delta}$: n =6; with IQ-1: $Sfrp1^{+/\Delta}$: n = 6; $Sfrp1^{\Delta/\Delta}$: n = 7) compared to the controls (with HF2+: $Sfrp1^{lox/lox}$: n = 7; with IQ-1: $Sfrp1^{lox/lox}$: n = 9). Black dots represent controls ($Sfrp1^{lox/lox}$); white dots surrounded by black represents IQ-1 treated controls ($Sfrp1^{lox/lox}$). Blue dots represent $Sfrp1^{+/\Delta}$; white dots surrounded by blue represents IQ-1 treated $Sfrp1^{+/\Delta}$. Red dots represent $Sfrp1^{\Delta/\Delta}$; white dots surrounded by red represents IQ-1 treated $Sfrp1^{\Delta/\Delta}$ mice. Each dot represents the mean of a cell. Represented values are illustrated as Mean ± SD. * p-value ≤0.05 show significant differences in the comparison of IQ-1 treated $Sfrp1^{+/\Delta}$, $Sfrp1^{\Delta/\Delta}$ and controls to each other or to the untreated controls determined by ANOVA, Tukey`s post hoc test.

To study the possible normalization of functional LT-HSC numbers in *Sfrp1*$^{\Delta/\Delta}$ mice, we again performed *in vivo* treatments for 5 days with IQ-1 inhibitor via daily i.p. injections. After the treatment, we sorted LT-HSCs and analyzed their cellular functions.

Since phosphorylation of p300 at Serine 89 is required for its association with β-catenin (Miyabayashi et al., 2007), we first assessed whether pSer89-p300 expressed by LT-HSC is affected by *in vivo* IQ-1 treatment. We found that in LT-HSCs from untreated *Sfrp1*$^{\Delta/\Delta}$ mice, protein content of pSer89-p300 was increased compared to the untreated controls. Interestingly, pSer89-p300 was decreased after IQ-1 treatment in the *Sfrp1*$^{\Delta/\Delta}$ mice (Figure 47A).

To determine whether IQ-1 treatment modulated the functional activity of LT-HSCs, we sorted LT-HSCs from treated *Sfrp1*$^{\Delta/\Delta}$ mice, and found that these cells formed colonies, whereas LT-HSCs from untreated *Sfrp1*$^{\Delta/\Delta}$ mice did not form colonies. Indeed, LT-HSCs from IQ-1-treated *Sfrp1*$^{\Delta/\Delta}$ mice were now indistinguishable from cells from treated controls (Figure 47B, C). Importantly, where LT-HSCs from untreated *Sfrp1*$^{\Delta/\Delta}$ mice could not maintain the LSK phenotype after 14 days of culture, whereas LT-HSC from IQ-1 treated *Sfrp1*$^{\Delta/\Delta}$ mice and control animals showed a clear maintenance of LSK cells (Figure 47D). These *in vitro* colony cultures showed a change in the treated LT-HSCs of the *Sfrp1*$^{\Delta/\Delta}$ mice as well as in the controls (Figure 47D).

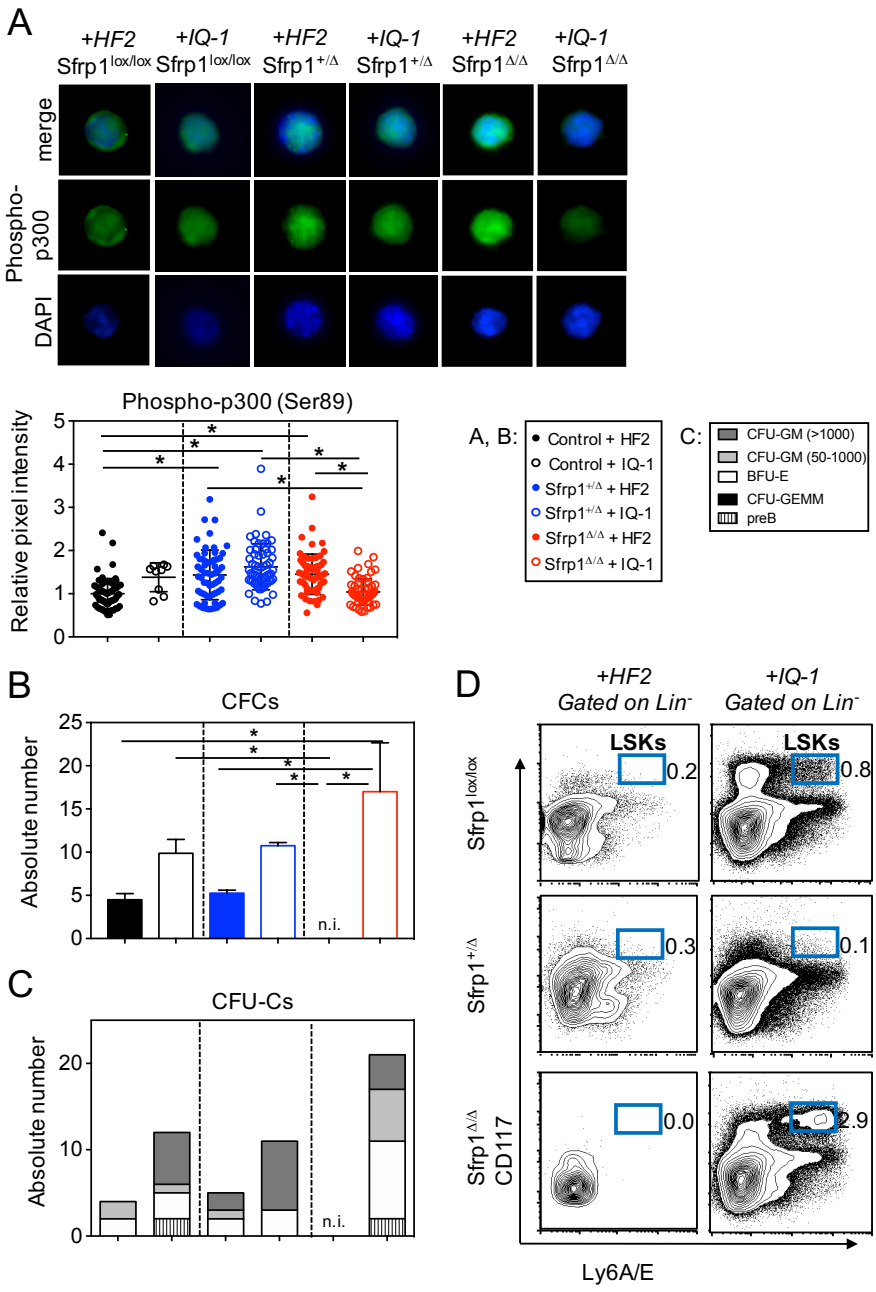

Figure 47. Cellular functions of LT-HSCs from IQ-1 treated and untreated *Sfrp1* conditional mice and controls. (A) Left: Phospho-p300 protein content as relative pixel number of LT-HSCs from IQ-1 treated and untreated *Sfrp1* conditional mice (with HF2+: *Sfrp1*$^{+/\Delta}$: n = 60; *Sfrp1*$^{\Delta/\Delta}$: n = 60; with IQ-1: *Sfrp1*$^{+/\Delta}$: n = 60; *Sfrp1*$^{\Delta/\Delta}$: n = 60) and controls (with HF2+: n = 60; with IQ-1: n = 9); Right: Representative immunofluorescence staining for the nuclei staining with DAPI in blue (below), phospho-p300 protein in green (middle), and the merged picture (top) of LT-HSCs from IQ-1 treated and untreated *Sfrp1*$^{+/\Delta}$, *Sfrp1*$^{\Delta/\Delta}$ mice and controls. **(B)** Counted total numbers of CFCs from IQ-1 treated and untreated *Sfrp1* conditional mice (with HF2+: *Sfrp1*$^{+/\Delta}$: n = 2; *Sfrp1*$^{\Delta/\Delta}$: n = 2; with IQ-1: *Sfrp1*$^{+/\Delta}$: n = 2; *Sfrp1*$^{\Delta/\Delta}$: n = 2) and controls (with HF2+: n = 2; with IQ-1: n = 2). **(C)** Representative colonies of CFCs from IQ-1 treated and untreated *Sfrp1* conditional mice (with HF2+: *Sfrp1*$^{+/\Delta}$: n = 1; *Sfrp1*$^{\Delta/\Delta}$: n = 1; with IQ-1: *Sfrp1*$^{+/\Delta}$: n = 1; *Sfrp1*$^{\Delta/\Delta}$: n = 1) and controls (with HF2+: n = 1; with IQ-1: n = 1). **(D)** Representative flow cytometry plots of LSK cells after methylcellulose from IQ-1 treated and untreated *Sfrp1*$^{+/\Delta}$, *Sfrp1*$^{\Delta/\Delta}$ and controls. Black dots represent controls (*Sfrp1*$^{lox/lox}$); white dots surrounded by black represents IQ-1 treated controls (*Sfrp1*$^{lox/lox}$). Blue dots represent *Sfrp1*$^{+/\Delta}$; white dots surrounded by blue represents IQ-1 treated *Sfrp1*$^{+/\Delta}$. Red dots represent *Sfrp1*$^{\Delta/\Delta}$; white dots surrounded by red represents IQ-1 treated *Sfrp1*$^{\Delta/\Delta}$ mice. Each dot represents a cell. Represented values are illustrated as Mean ± SD. * p-value ≤0.05 show significant differences in the comparison of IQ-1 treated *Sfrp1*$^{+/\Delta}$, *Sfrp1*$^{\Delta/\Delta}$ and controls to each other or to the untreated controls determined by ANOVA, Tukey`s post hoc test.

To determine whether IQ-1 treatment not only restores *in vitro* hematopoietic activity, but also repopulating activity *in vivo*, we isolated and transplanted LT-HSC from IQ-1 treated *Sfrp1*$^{\Delta/\Delta}$ mice (Figure 48).

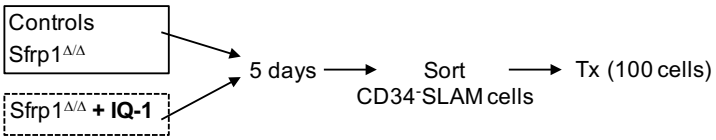

Figure 48. Experimental design of primary transplantation from IQ-1 treated LT-HSCs into lethally irradiate recipients. Eight- to ten-week old *Sfrp1*$^{\Delta/\Delta}$ mice were i.p treated for 5 days with IQ-1 (14 µg). 24 h after the last treatment the CD34$^-$ SLAM cells were sorted and transplanted into lethally irradiate recipients.

These experiments showed that LT-HSCs from IQ-1-treated *Sfrp1*$^{\Delta/\Delta}$ mice engraft to comparable levels as untreated control donors, whereas LT-HSCs from untreated *Sfrp1*$^{\Delta/\Delta}$ mice do not show donor engraftment (Figure 49A-C). Importantly, the LT-HSCs from IQ-1-treated mice now were also capable of efficiently regenerating the LT-HSC compartments (Figure 49D-G). Interestingly, the absolute number of donor-derived CD34$^-$ LSKs and donor-derived MPs from the transplanted LT-HSCs of IQ-1-treated *Sfrp1*$^{\Delta/\Delta}$ mice were increased compared to the donor-derived CD34$^-$ LSKs and donor-derived MPs from transplanted untreated controls (Figure 49E, G).

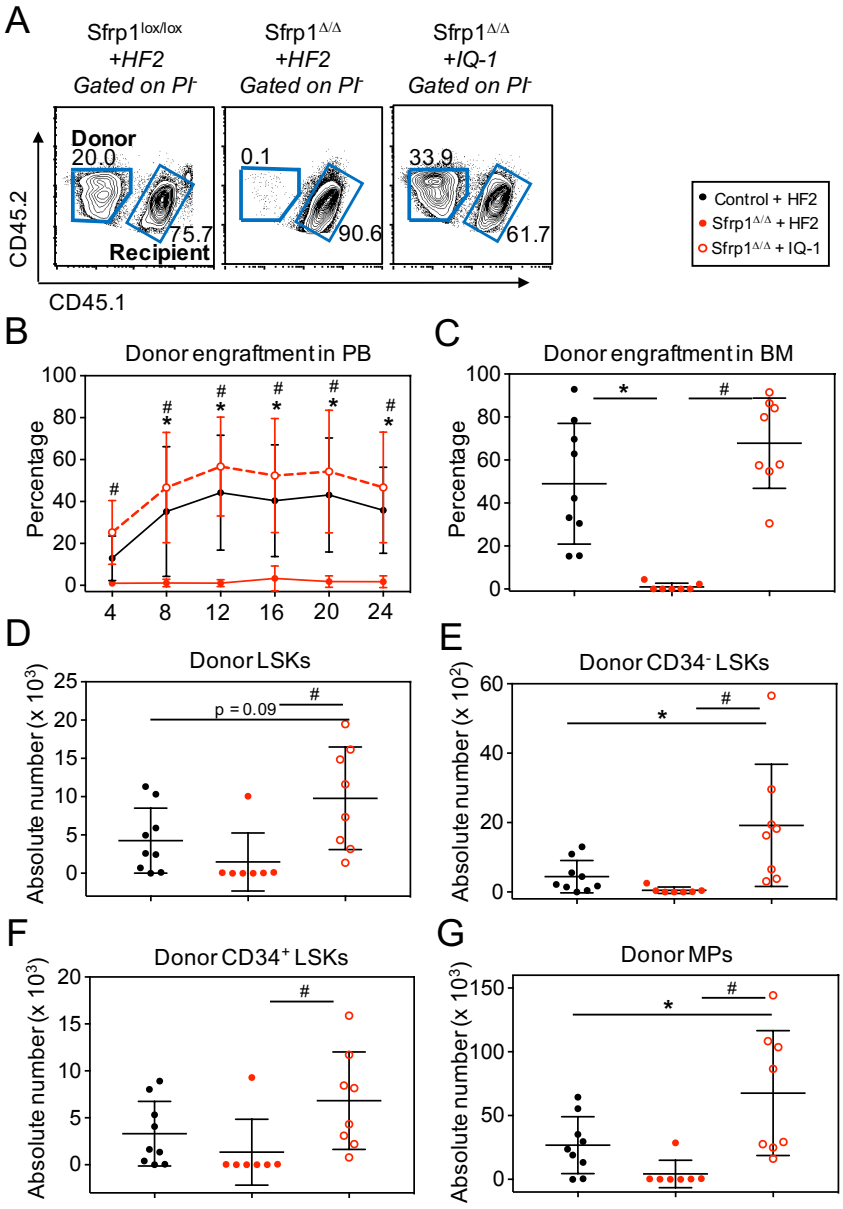

Figure 49. Functionality of LT-HSCs at steady state and after IQ-1 treatment. (A) Representative flow cytometry plots of the gating strategy of Ly5.2^{+} donor cells or Ly5.1^{+}Ly5.2^{+} recipient cells. **(B)** Donor cell engraftment in percentage in the PB four, eight, twelve, sixteen, twenty and twentyfour weeks after Tx of *Sfrp1*$^{\Delta/\Delta}$ mice (with HF2+: n = 7; with IQ-1: n = 8) compared to the controls (with HF2+: n = 9). **(C)** Percentage of the donor engraftment in BM, **(D)** Absolute number of the donor LSKs, **(E)** Absolute number of the donor CD34^{-} LSKs, **(F)** Absolute number of the donor CD34^{+} LSKs and **(G)** bsolute number of donor MPs of *Sfrp1*$^{\Delta/\Delta}$ mice (with HF2+: n = 7; with IQ-1: n = 8) compared to the controls (with HF2+: n = 9). Black dots represent controls (*Sfrp1*$^{lox/lox}$); Red dots represent *Sfrp1*$^{\Delta/\Delta}$; white dots surrounded by red represents IQ-1 treated *Sfrp1*$^{\Delta/\Delta}$ mice. Each dot represents an animal. Represented values are illustrated as Mean ± SD. * p-value ≤0.05 show significant differences in the comparison of IQ-1 treated *Sfrp1*$^{\Delta/\Delta}$ and untreated controls (*Sfrp1*$^{lox/lox}$), whereas $^{\#}$ p-value ≤0.05 show significant differences in the comparison of IQ-1 treated *Sfrp1*$^{\Delta/\Delta}$ and untreated once determined by ANOVA, Tukey`s post hoc test.

These results show that IQ-1 treatment restores LT-HSC repopulating activity from *Sfrp1*$^{\Delta/\Delta}$ mice. To assess whether *in vivo* self-renewal activity was similarly restored, we sorted donor LSK cells from treated and untreated *Sfrp1*$^{\Delta/\Delta}$ animals and control mice 24 weeks after primary transplantation and determined their secondary repopulation ability (Figure 50).

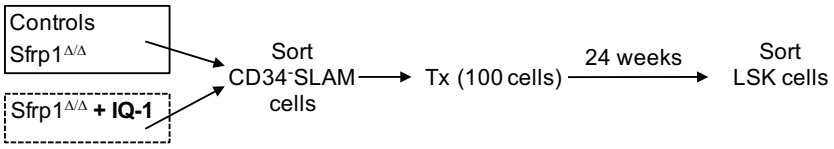

Figure 50. Experimental design of functionality analysis of IQ-1 treated LT-HSCs repopulated for 24 weeks in WT recipients. Eight- tol ten-week old *Sfrp1*$^{\Delta/\Delta}$ mice were i.p treated for 5 days with IQ-1 (14 µg). 24 h after the last treatment the CD34$^-$ SLAM cells were sorted and transplanted into lethally irradiate recipients. 24 weeks after the transplantation the donor LSK cells were sorted and analyzed for cellular functions.

Due to very low number of sorted donor LSKs from the untreated *Sfrp1*$^{\Delta/\Delta}$ group (only 80 donor cells in total from 5 recipient mice), we only studied their hematopoietic activity *in vitro* in semi-solid medium (M3434).

Here, the prior treatment of *Sfrp1*$^{\Delta/\Delta}$ donor mice with IQ-1 inhibitor rescued colony-forming ability of donor LSK cells recovered after 24 weeks from WT recipients (Figure 51A). On the molecular level, the donor LSK cells from control donors and IQ-1-treated *Sfrp1*$^{\Delta/\Delta}$ donors showed a similar protein content of phospho-p300 (Ser89), as well as similar numbers of γH2A.X foci, indicating a rescue of *Sfrp1*$^{\Delta/\Delta}$ donor LSK cell signaling by the IQ-1 treatment (Figure 51B, C).

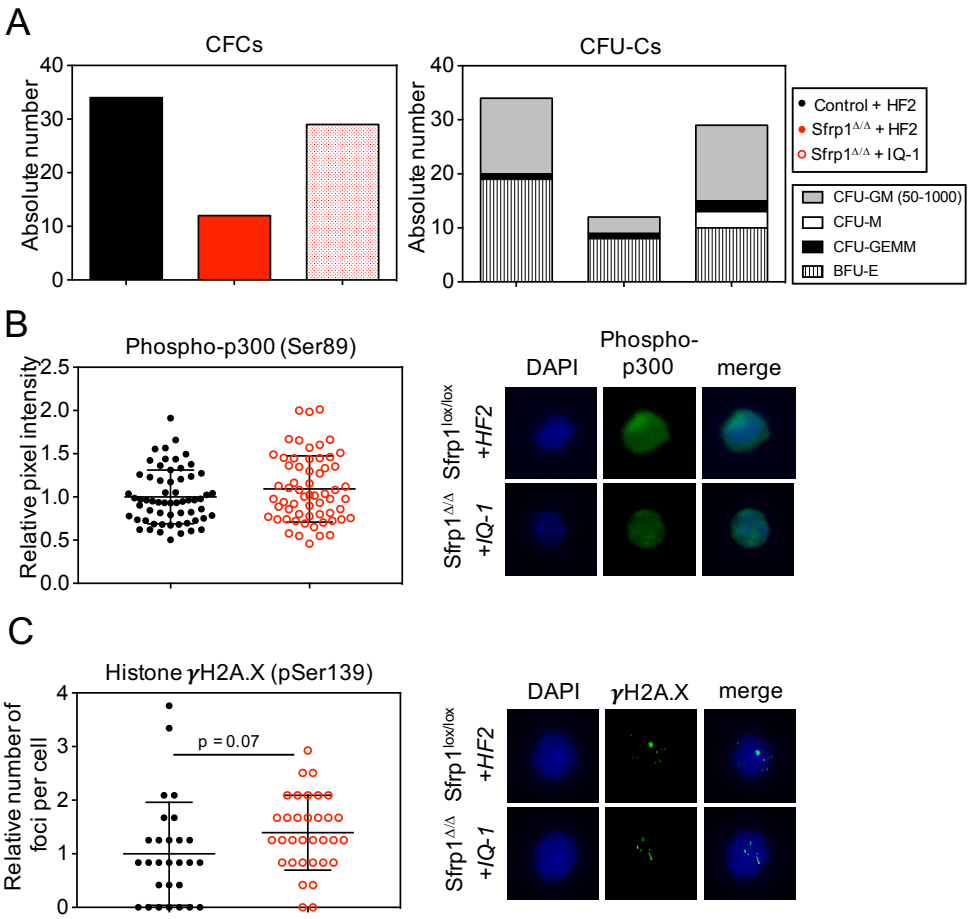

Figure 51. Cellular functions from primary transplantation of IQ-1 treated and untreated *Sfrp1* deficient mice and the controls. (A) Left: Counted total numbers of CFCs from primary transplantation of IQ-1 treated and untreated *Sfrp1*$^{\Delta/\Delta}$ mice and the controls. Right: Representative colonies of CFCs from IQ-1 treated and untreated *Sfrp1*$^{\Delta/\Delta}$ mice and the controls. **(B)** Left: Phospho-p300 protein content as relative pixel number of LSK cells from IQ-1 treated and untreated *Sfrp1*$^{\Delta/\Delta}$ mice (n = 61) and the controls (n = 61); Right: Representative immunofluorescence staining for the nuclei staining with DAPI in blue (left), phospho-p300 protein in green (middle), and the merged picture (right) of LSK cells from IQ-1 treated and untreated *Sfrp1*$^{\Delta/\Delta}$ mice and the controls. **(C)** Left: Relative histone γH2A.X foci content of LSK cells from IQ-1 treated and untreated *Sfrp1*$^{\Delta/\Delta}$ mice (n = 33) and the controls (n = 28); Right: Representative immunofluorescence staining for the nuclei staining with DAPI in blue (left), histone γH2A.X foci content in green (middle), and the merged picture (right) of LSK cells from IQ-1 treated and untreated *Sfrp1*$^{\Delta/\Delta}$ mice and the controls. Black bar/dots represent controls (*Sfrp1*$^{lox/lox}$); Red bar represent *Sfrp1*$^{\Delta/\Delta}$; White bar/dots surrounded by red represent IQ-1 treated *Sfrp1*$^{\Delta/\Delta}$ mice. Each dot represents a cell. Represented values are illustrated as Mean ± SD.

In a final experiment, we transplanted the sorted donor LT-HSCs in two different doses of 1000 and 2000 LSKs further in secondary WT recipients (Figure 52A).

Figure 52. Experimental design of secondary transplantation of IQ-1 treated LT-HSCs into lethally irradiate recipients. Eight- to ten-week old *Sfrp1*$^{\Delta/\Delta}$ mice were i.p treated for 5 days with IQ-1 (14 µg). 24 h after the last treatment the CD34^{-} SLAM cells were sorted and transplanted into lethally irradiate WT recipients. 24 weeks after the transplantation the donor LSK cells were sorted and transplanted into lethally irradiate WT recipients.

Here, we found successful engraftment of the donor cells (1000 and 2000 LSKs) derived from IQ-1-treated *Sfrp1*$^{\Delta/\Delta}$ donor mice in the PB of secondary recipients, indicating a rescue of long-term repopulating HSC activity (Figure 53).

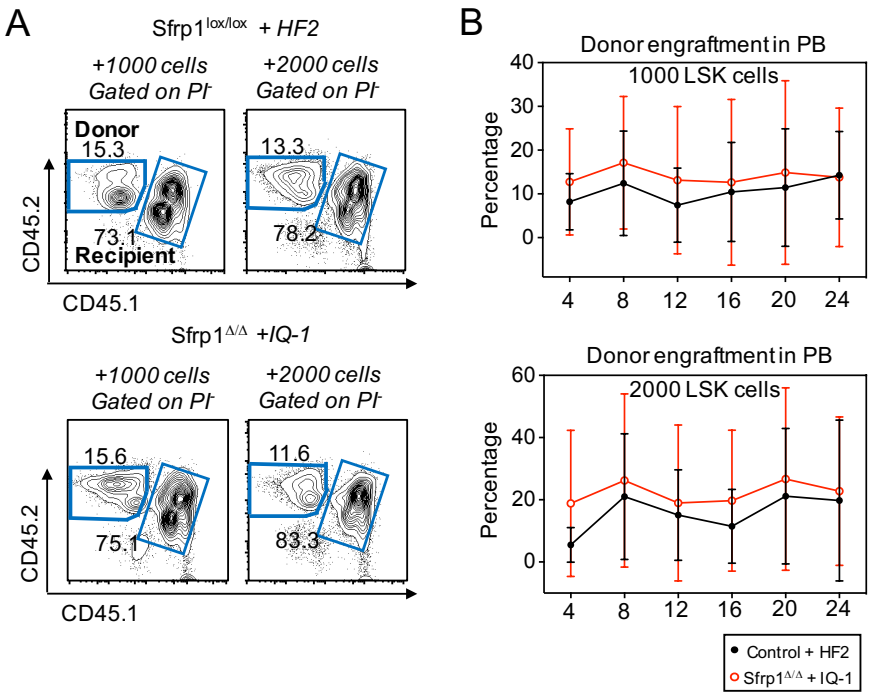

Figure 53. Engraftment of secondary transplanted IQ-1 treated LSKs. (A) Representative flow cytometry plots of the gating strategy of Ly5.2^{+} donor cells or Ly5.1^{+}Ly5.2^{+} recipient cells. **(B)** Donor cell engraftment in percentage in the PB four, eight, twelve, sixteen, twenty and twentyfour weeks after secondary Tx from *Sfrp1*$^{\Delta/\Delta}$ mice (with IQ-1: 1000 cells: n = 8, 2000 cells: n = 7) compared to the controls (with HF2+: 1000 cells: n = 4, 2000 cells: n = 6). Black dots represent controls (*Sfrp1*$^{lox/lox}$). White dots surrounded by red represent IQ-1 treated *Sfrp1*$^{\Delta/\Delta}$ mice. Each dot represents a cell. Represented values are illustrated as Mean ± SD.

We found that in the BMs of the secondary recipients, LT-HSCs from IQ-1-treated *Sfrp1*$^{\Delta/\Delta}$ donor mice repopulated in the same way as the untreated control LT-HSCs (Figure 54A-E).

In conclusion, based on our observation that LT-HSCs from *Sfrp1*$^{\Delta/\Delta}$ mice differentiate in culture, and the published observation that ES cell differentiation is determined by the β-catenin/p300 complex (Miyabayashi et al., 2007), we hypothesize that in *Sfrp1*$^{\Delta/\Delta}$ HSCs, β-catenin preferably forms a differentiation promoting complex with p300. The treatment with IQ-1 inhibits the binding of β-catenin with p300 and promotes the formation of the proliferation-stimulating β-catenin/CBP complex and in this manner, rescues the repopulating cell function of damaged HSCs from *Sfrp1*$^{\Delta/\Delta}$ mice.

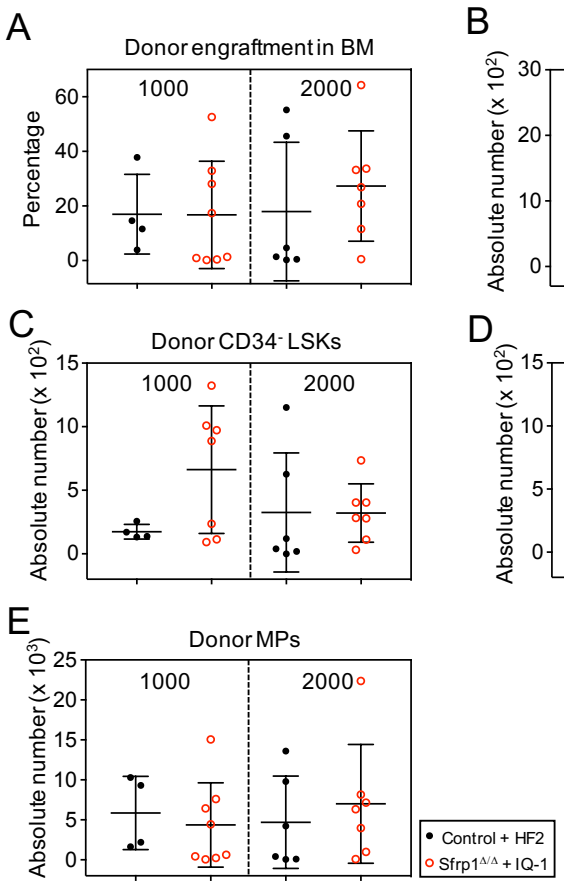

Figure 54. Secondary transplantation of LSKs at steady state and after IQ-1 treatment. (A) Percentage of the donor engraftment in BM from *Sfrp1*$^{\Delta/\Delta}$ mice (with IQ-1: 1000 cells: n = 8, 2000 cells: n = 7) compared to the controls (with HF2+: 1000 cells: n = 4, 2000 cells: n = 6). **(B)** Absolute number of the donor LSKs, **(C)** Absolute number of the donor CD34$^-$ LSKs from *Sfrp1*$^{\Delta/\Delta}$ mice (with IQ-1: 1000 cells: n = 7, 2000 cells: n = 7) compared to the controls (with HF2+: 1000 cells: n = 4, 2000 cells: n = 6). **(D)** Absolute number of the donor CD34$^+$ LSKs, **(E)** Absolute number of the donor MPs from *Sfrp1*$^{\Delta/\Delta}$ mice (with IQ-1: 1000 cells: n = 8, 2000 cells: n = 7) compared to the controls (with HF2+: 1000 cells: n = 4, 2000 cells: n = 6). Black dots represent controls (*Sfrp1*$^{lox/lox}$). White dots surrounded by red represents IQ-1 treated *Sfrp1*$^{\Delta/\Delta}$ mice. Each dot represents a cell. Represented values are illustrated as Mean ± SD.

4.7. Impact of *Sfrp1* loss in bone marrow niche cells during stress conditions

Above, we explored the steady-state niche and hematopoiesis of the *Sfrp1*$^{\Delta/\Delta}$ mice. In the next few paragraphs, we explored how *Sfrp1* in osteoprogenitors is involved in stress responses, such as inflammation. In relation to inflammation, two major niche functions have been proposed: forming a hematopoietic microenvironment for immune cell development (Szade et al., 2018) and modulating the activity of already formed immune cells (Bernardo & Fibbe, 2013). We here studied the effects of the loss of *Sfrp1* in osteoprogenitors by triggering immune response with a lipopolysaccharides (LPS) treatment of *Sfrp1*$^{+/\Delta}$, *Sfrp1*$^{\Delta/\Delta}$ mice and control animals.

Since inflammation also plays a critical role in the development of tumors, we additionally analyzed the impact of the *Sfrp1* deficient niche on development of malignant cells. As describe before, an altered promoter methylation of the human *SFRP1* gene contributes to the severity of several hematological diseases (Jost et al., 2008; Reins et al., 2010; Seeliger et al., 2009).

4.7.1 LPS treatment to stimulate the immune system of *Sfrp1* conditional mice

In order to analyze the impact of the microenvironmental loss of *Sfrp1* and the altered immune surveillance during a stress condition, we treated the *Sfrp1*$^{+/\Delta}$, *Sfrp1*$^{\Delta/\Delta}$ mice and control animals (*Sfrp1*$^{lox/lox}$; Osx-Cre) with LPS to simulate a bacterial infection. A single LPS treatment suffices to elicit "emergency hematopoiesis" characterized by a rapid increase of granulocytes and monocytes into the periphery (Boettcher et al., 2012). Thus, we analyzed the stromal and hematopoietic cell composition in PB and other hematopoietic tissues in reaction of a single LPS injection.

4.7.1.1 The impact on modulating the activity of immune cells during LPS treatment in PB

We treated *Sfrp1*$^{+/\Delta}$, *Sfrp1*$^{\Delta/\Delta}$ mice and control animals with 1000 ng of LPS and analyzed 24 hours later the inflammatory molecules in PBs with cytokine beads assay (CBA), the MSCs for the differentiation and migration property potential, as well as the LT-HSCs in the context of self-renewal, proliferation and differentiation (Figure 55).

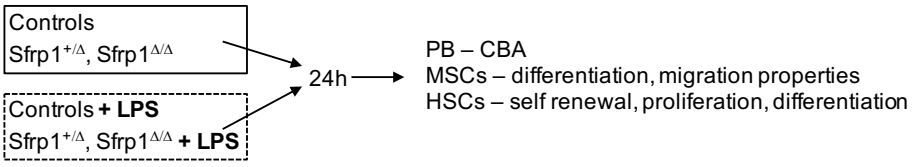

Figure 55. The analysis of the impact after LPS treatment *in vivo*. Experimental design: eight- to ten-week old *Sfrp1*$^{+/\Delta}$, *Sfrp1*$^{\Delta/\Delta}$ mice and control animals were i.p injected with 1000 ng LPS. 24 h later, the PB, BM and MSC cell compositions were analyzed.

First, we analyzed the cell populations from PB by flow cytometry and with an animal blood cell counter Scil Vet Abc^{TM}. (Figure 56A-F). The cell number of white blood cells (Figure 56B), the percentage of B220^{+} B cells (Figure 56C), the CD3e^{+} T cells (Figure 56D), as well as for GR1^{med}CD11b^{+} monocytes (Figure 56E) and GR1^{+}CD11b^{+} granulocytes (Figure 56F) in the PB were unchanged in *Sfrp1*$^{\Delta/\Delta}$ mice compared to control mice.

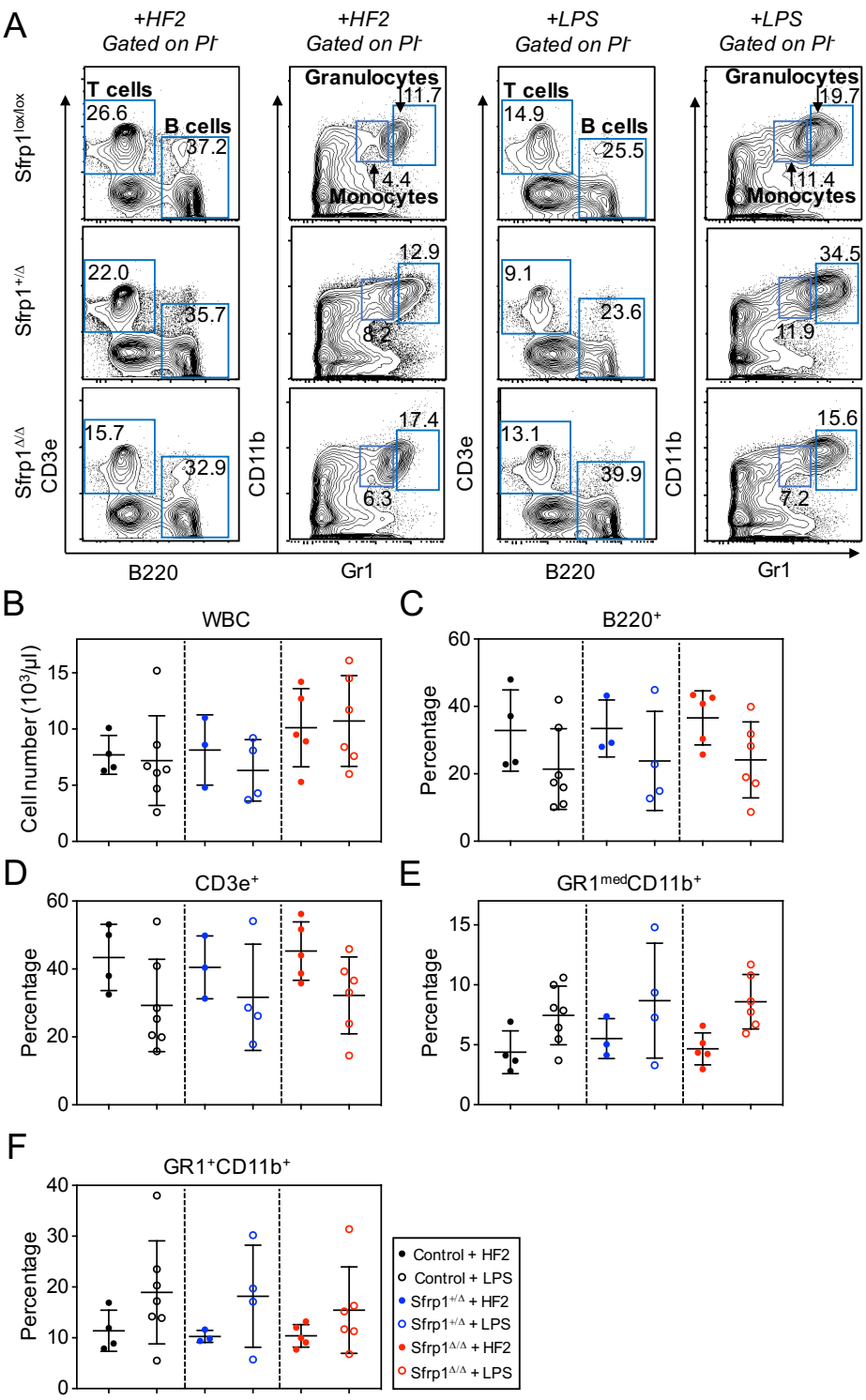

Figure 56. The impact on modulating the activity of immune cells during LPS treatment in PB. (A) Representative flow cytometry plots of the gating strategy for mature cell populations in PB. **(B)** Cell number of WBC in 10^3/µl, **(C)** Percentage of the B220$^+$ B cells, **(D)** Percentage of CD3e$^+$ T cells, **(E)** Percentage of GR1^{med}CD11b$^+$ monocytes, **(F)** Percentage of GR1$^+$CD11b$^+$ granulocytes from *Sfrp1* conditional mice (with HF2+: *Sfrp1*$^{+/\Delta}$: n = 3; *Sfrp1*$^{\Delta/\Delta}$: n = 5; with LPS: *Sfrp1*$^{+/\Delta}$: n = 4; *Sfrp1*$^{\Delta/\Delta}$: n = 6) compared to the controls (with HF2+: n = 4; with LPS: n = 7). Black dots represent controls (*Sfrp1*$^{lox/lox}$); white dots surrounded by black represents LPS treated controls (*Sfrp1*$^{lox/lox}$). Blue dots represent *Sfrp1*$^{+/\Delta}$; white dots surrounded by blue represents LPS treated *Sfrp1*$^{+/\Delta}$. Red dots represent *Sfrp1*$^{\Delta/\Delta}$; white dots surrounded by red represents LPS treated *Sfrp1*$^{\Delta/\Delta}$ mice. Each dot represents an animal. Represented values are illustrated as Mean ± SD.

To find out whether the loss of SFRP1 in the niche has an impact on modulating the activity of immune cells and the inflammatory response during acute inflammation, we analyzed the inflammatory cytokines IL-6, IL-10, MCP-1, IFNγ, TNF, and IL-12p70 in the serum of *Sfrp1* conditional mice (*Sfrp1*$^{+/\Delta}$, *Sfrp1*$^{\Delta/\Delta}$) and control animals (Figure 57A, B). After LPS treatment, the analyzed inflammatory cytokines, IL-10, IFNγ, TNF, IL-12p70 were unchanged in the serum of *Sfrp1*$^{+/\Delta}$, *Sfrp1*$^{\Delta/\Delta}$ mice compared to the control animals (data not shown, Figure 57B), as well as MCP-1 (Figure 57D). With regard to IL-6, we detected increased levels in the serum of LPS-treated *Sfrp1*$^{+/\Delta}$ compared to untreated *Sfrp1*$^{\Delta/\Delta}$ homozygous animals (Figure 57C), but not in treated *Sfrp1*$^{\Delta/\Delta}$ homozygous deletion mutants.

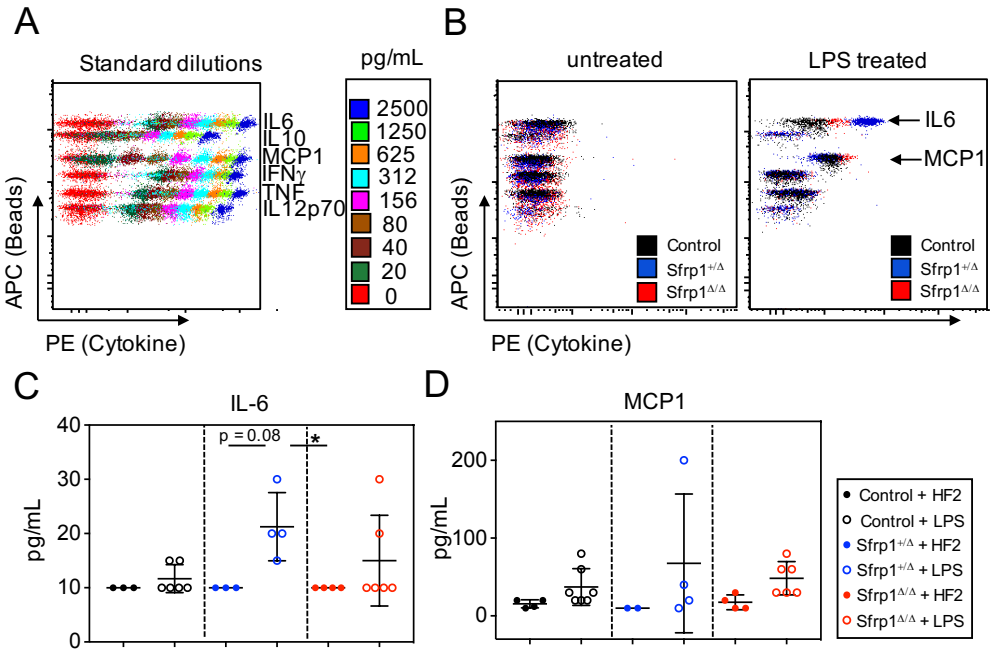

Figure 57. The inflammatory response during LPS treatment in PB. (A) Standard dilutions for the inflammatory cytokines (IL-6, IL-10, MCP-1, INFγ, TNF, IL12p70). **(B)** Representative flow cytometry plot for the analyzation of the cytokines in the serum, 24 h after LPS treatment. Left: untreated animals. Right: LPS treated animals. A representative example for each genotype is shown. **(C)** Analyzation of the IL-6 protein content in pg/mL from *Sfrp1* conditional mice (with HF2+: *Sfrp1*$^{+/\Delta}$: n = 3; *Sfrp1*$^{\Delta/\Delta}$: n = 4; with LPS: *Sfrp1*$^{+/\Delta}$: n = 4; *Sfrp1*$^{\Delta/\Delta}$: n = 6) compared to the controls (with HF2+: n = 3; with LPS: n = 6). **(D)** Analyzation of the MCP-1 protein content in pg/mL from *Sfrp1* conditional mice (with HF2+: *Sfrp1*$^{+/\Delta}$: n = 2; *Sfrp1*$^{\Delta/\Delta}$: n = 4; with LPS: *Sfrp1*$^{+/\Delta}$: n = 4; *Sfrp1*$^{\Delta/\Delta}$: n = 6) compared to the controls (with HF2+: n = 4; with LPS: n = 7). Black dots represent controls (*Sfrp1*$^{lox/lox}$); white dots surrounded by black represents LPS treated controls (*Sfrp1*$^{lox/lox}$). Blue dots represent *Sfrp1*$^{+/\Delta}$; white dots surrounded by blue represents LPS treated *Sfrp1*$^{+/\Delta}$. Red dots represent *Sfrp1*$^{\Delta/\Delta}$; white dots surrounded by red represents LPS treated *Sfrp1*$^{\Delta/\Delta}$ mice. Each dot represents an animal. Represented values are illustrated as Mean ± SD. * p-value ≤0.05 show significant differences in the comparison of LPS treated *Sfrp1*$^{+/\Delta}$, *Sfrp1*$^{\Delta/\Delta}$ and controls to each other or to the untreated controls determined by ANOVA, Tukey`s post hoc test.

4.7.1.2 The impact on modulating the activity of immune cells during LPS treatment in stromal compartment

Furthermore, we analysed the stromal compartment by flow cytometry and analysed their cellular functions. Altogether, the percentages of MSCs, and OBCs from the LPS-treated *Sfrp1*$^{+/\Delta}$ and *Sfrp1*$^{\Delta/\Delta}$ mice were unchanged compared to the cells from LPS-treated control animals. Also, when comparing MSCs and OBCs from LPS-treated and untreated *Sfrp1*$^{+/\Delta}$ and *Sfrp1*$^{\Delta/\Delta}$ mice there appeared to be no significant changes in these populations after one day of LPS treatment (Figure 58A-C). We detected decreased percentage in the ECs of LPS-treated *Sfrp1*$^{+/\Delta}$ and LPS-treated *Sfrp1*$^{\Delta/\Delta}$ compared to untreated *Sfrp1*$^{+/\Delta}$ animals, as well as to the untreated *Sfrp1*$^{\Delta/\Delta}$ animals (Figure 58D).

In order to analyze the functional changes of MSCs from the *Sfrp1*$^{+/\Delta}$ and *Sfrp1*$^{\Delta/\Delta}$ mice and control animals, we characterized the cultured compact bone-derived MSCs for their differentiation potential and migration properties in a scratch assay.

After LPS treatment, the induced adipogenic differentiation of cultured compact bone-derived MSCs from *Sfrp1*$^{+/\Delta}$, *Sfrp1*$^{\Delta/\Delta}$ and controls was unchanged. However, the cultured compact bone-derived MSCs from LPS-treated *Sfrp1*$^{+/\Delta}$, *Sfrp1*$^{\Delta/\Delta}$ and controls, as well as the untreated *Sfrp1*$^{\Delta/\Delta}$ were significantly decreased compared to the untreated *Sfrp1*$^{+/\Delta}$ cultured compact bone-derived MSCs (Figure 59A).

Similarly, although the cultured compact bone-derived MSCs from LPS treated and untreated *Sfrp1*$^{\Delta/\Delta}$ migrated slightly slower when evaluated 6 hours and at 12 hours after scratching, at the 24-hour time point, cultured compact bone-derived MSCs from *Sfrp1*$^{\Delta/\Delta}$ mice showed similar migration patterns compared to the cultured compact bone-derived MSCs from LPS-treated and untreated controls. Of interest, none of the cultured compact bone-derived MSCs from untreated or LPS-treated *Sfrp1*$^{\Delta/\Delta}$ or controls closed the scratch gap completely within 24 hours (Figure 59B).

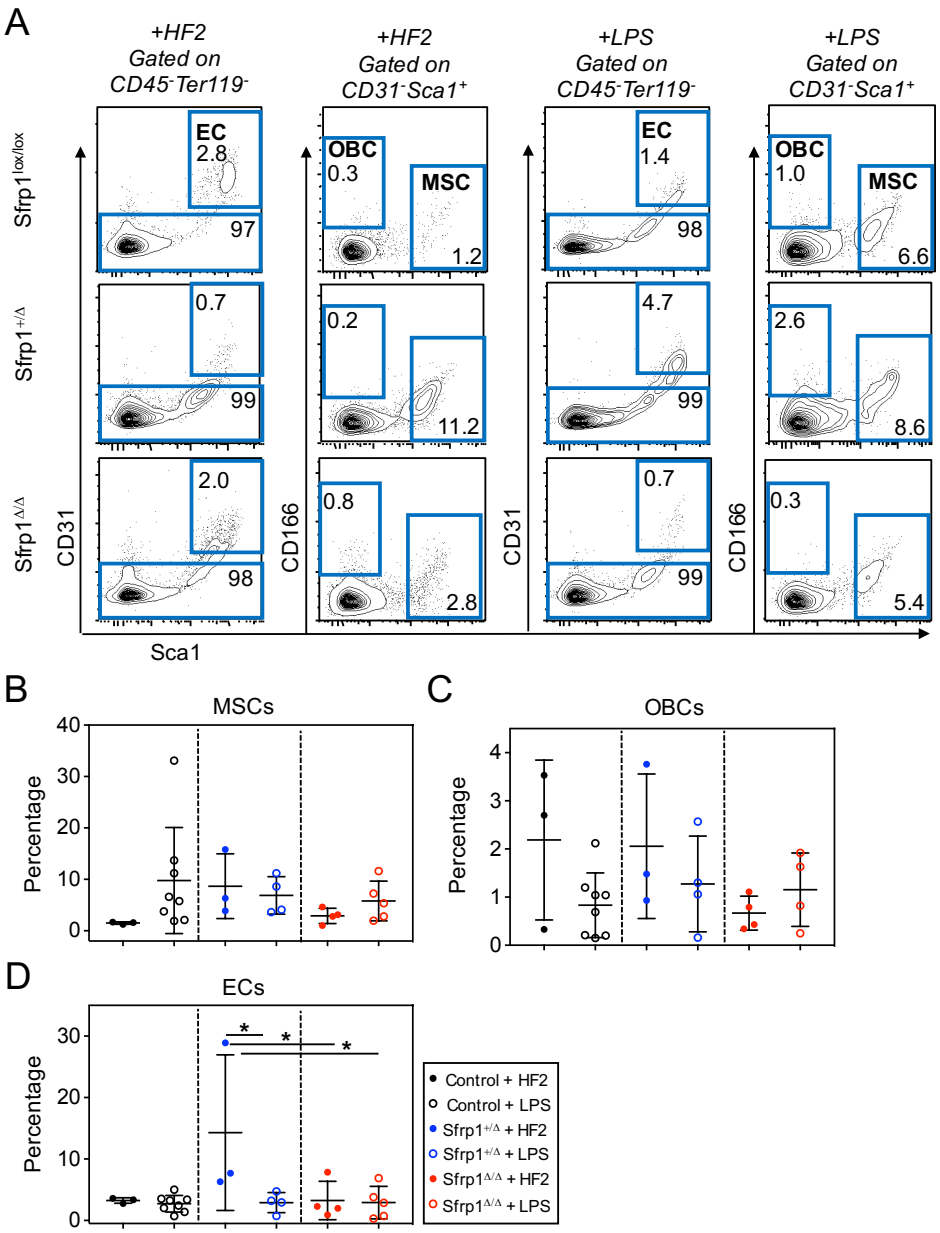

Figure 58. The impact from the LPS treatment of cultured compact bone-derived MSCs in *Sfrp1* conditional mice in the stromal compartment. (A) Representative flow cytometry plots of the gating strategy for the stroma populations. **(B)** Percentage of the MSCs from *Sfrp1* conditional mice (with HF2+: $Sfrp1^{+/\Delta}$: n = 3; $Sfrp1^{\Delta/\Delta}$: n = 4; with LPS: $Sfrp1^{+/\Delta}$: n = 4; $Sfrp1^{\Delta/\Delta}$: n = 5) compared to the controls (with HF2+: n = 3; with LPS: n = 8). **(C)** Percentage of the OBCs from *Sfrp1* conditional mice (with HF2+: $Sfrp1^{+/\Delta}$: n = 3; $Sfrp1^{\Delta/\Delta}$: n = 4; with LPS: $Sfrp1^{+/\Delta}$: n = 4; $Sfrp1^{\Delta/\Delta}$: n = 4) compared to the controls (with HF2+: n = 3; with LPS: n = 8). **(D)** Percentage of the ECs from *Sfrp1* conditional mice (with HF2+: $Sfrp1^{+/\Delta}$: n = 3; $Sfrp1^{\Delta/\Delta}$: n = 4; with LPS: $Sfrp1^{+/\Delta}$: n = 4; $Sfrp1^{\Delta/\Delta}$: n = 5) compared to the controls (with HF2+: n = 3; with LPS: n = 8). Black dots represent controls ($Sfrp1^{lox/lox}$); white dots surrounded by black represents LPS treated controls ($Sfrp1^{lox/lox}$). Blue dots represent $Sfrp1^{+/\Delta}$; white dots surrounded by blue represents LPS treated $Sfrp1^{+/\Delta}$. Red dots represent $Sfrp1^{\Delta/\Delta}$; white dots surrounded by red represents LPS treated $Sfrp1^{\Delta/\Delta}$ mice. Each dot represents an animal. Represented values are illustrated as Mean ± SD. * p-value ≤0.05 show significant differences in the comparison of LPS treated $Sfrp1^{+/\Delta}$, $Sfrp1^{\Delta/\Delta}$ and controls to each other or to the untreated controls determined by ANOVA, Tukey`s post hoc test.

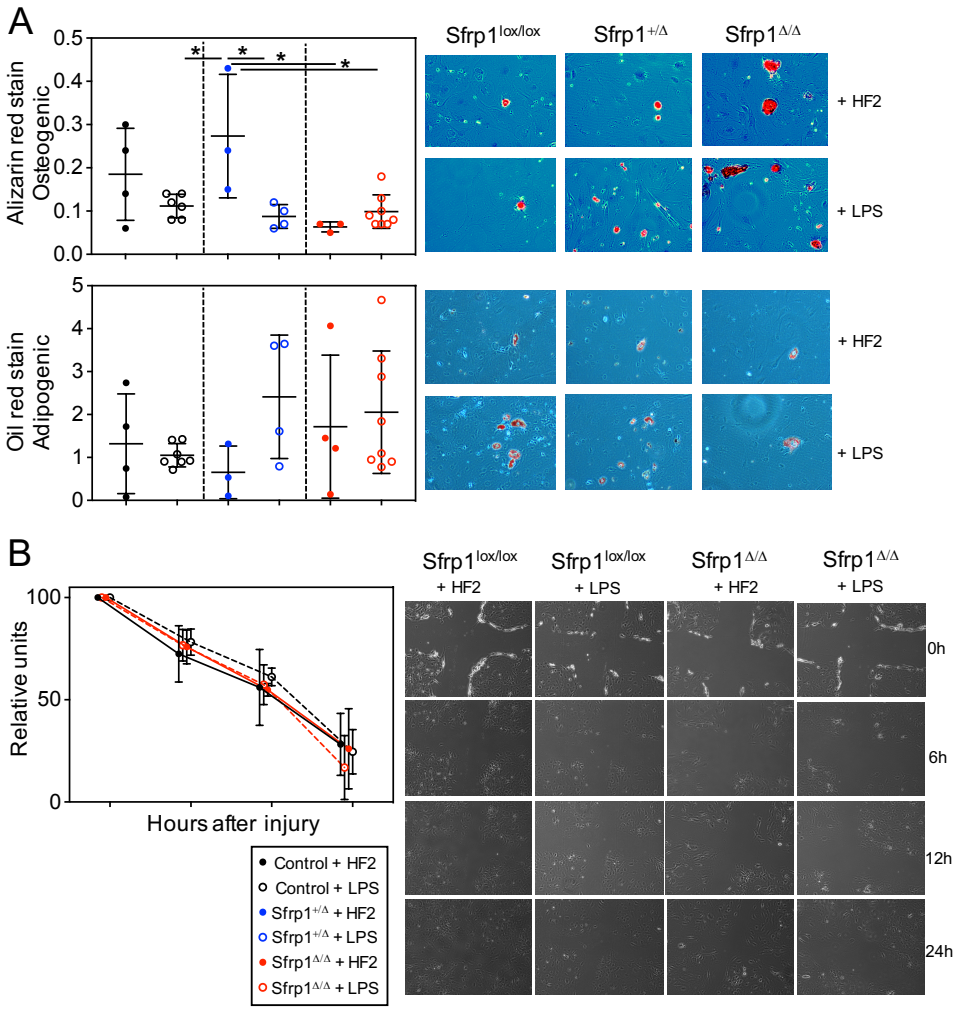

Figure 59. Differentiation- and migration potential of cultured compact bone-derived MSCs after LPS treatment. (A) Above, left: Quantification of Alizarin red content at OD 562 nm of *Sfrp1* conditional mice (with HF2+: *Sfrp1*$^{+/\Delta}$: n = 3; *Sfrp1*$^{\Delta/\Delta}$: n = 3; with LPS: *Sfrp1*$^{+/\Delta}$: n = 4; *Sfrp1*$^{\Delta/\Delta}$: n = 8) compared to the controls (with HF2+: n = 4; with LPS: n = 6) from osteogenic differentiated cultured compact bone-derived MSCs. Above, right: Microscopy of Alizarin red stained osteogenic differentiation of *Sfrp1* conditional mice compared to the controls. Below, left: Quantification of Oil red content at OD 520 nm of *Sfrp1* conditional mice (with HF2+: *Sfrp1*$^{+/\Delta}$: n = 3; *Sfrp1*$^{\Delta/\Delta}$: n = 4; with LPS: *Sfrp1*$^{+/\Delta}$: n = 4; *Sfrp1*$^{\Delta/\Delta}$: n = 8) compared to the controls (with HF2+: n = 4; with LPS: n = 7) from adipogenic differentiated cultured compact bone-derived MSCs. Below, right: Microscopy of Oil red stained adipogenic differentiation *Sfrp1* conditional mice compared to the controls. **(B)** Left: Migration rate over 24 h. Right: Representative pictures of the scratch assay at 0 h until 24 h of *Sfrp1*$^{lox/lox}$ control cultured compact bone-derived MSCs and *Sfrp1*$^{\Delta/\Delta}$ cultured compact bone-derived MSCs. Black dots represent controls (*Sfrp1*$^{lox/lox}$); white dots surrounded by black represents LPS treated controls (*Sfrp1*$^{lox/lox}$). Blue dots represent *Sfrp1*$^{+/\Delta}$; white dots surrounded by blue represents LPS treated *Sfrp1*$^{+/\Delta}$. Red dots represent *Sfrp1*$^{\Delta/\Delta}$; white dots surrounded by red represents LPS treated *Sfrp1*$^{\Delta/\Delta}$ mice. Each dot represents an animal. Represented values are illustrated as Mean ± SD. * p-value ≤0.05 show significant differences in the comparison of LPS treated *Sfrp1*$^{+/\Delta}$, *Sfrp1*$^{\Delta/\Delta}$ and controls to each other or to the untreated controls determined by ANOVA, Tukey`s post hoc test.

Our results show, that other than increased secretion of IL-6 in the serum from *Sfrp1*$^{+/\Delta}$ and *Sfrp1*$^{\Delta/\Delta}$ mice upon *in vivo* LPS treatment, none of the other niche cell properties were affected in a different manner than those of control niche cells.

4.7.1.3 The impact on modulating the activity of immune cells during LPS treatment in BM

To study whether the LPS treatment affected the regulation of mature hematopoietic cells, we went on to examine the mature hematopoietic compartment in LPS-treated mice.

These experiments showed, that the total cell number of the BM as well as the absolute number of $CD3e^+$ T cell, $GR1^{med}CD11b^+$ monocytes and $GR1^+CD11b^+$ granulocytes were unchanged in *Sfrp1*$^{+/\Delta}$, *Sfrp1*$^{\Delta/\Delta}$ mice and controls (Figure 60A, B, D-F). However, we observed a significant decrease of absolute $B220^+$ B cell numbers in the BM of LPS-treated *Sfrp1*$^{+/\Delta}$ mice (Figure 60C). But, when examining, *Sfrp1*$^{\Delta/\Delta}$ mice, no significant changes could be observed compared to the controls (Figure 60B-F).

We then investigated the earlier cells of the hematopoietic hierarchy and found that in the BM, the absolute number of LSK cells, as well as LT-HSCs and MPs were unchanged after LPS treatment (Figure 61A, B, D, E). Interestingly, the absolute number of the ST-HSCs were significantly decreased in the treated *Sfrp1*$^{+/\Delta}$ after LPS treatment compared to the BM of untreated *Sfrp1*$^{\Delta/\Delta}$ mice (Figure 61C).

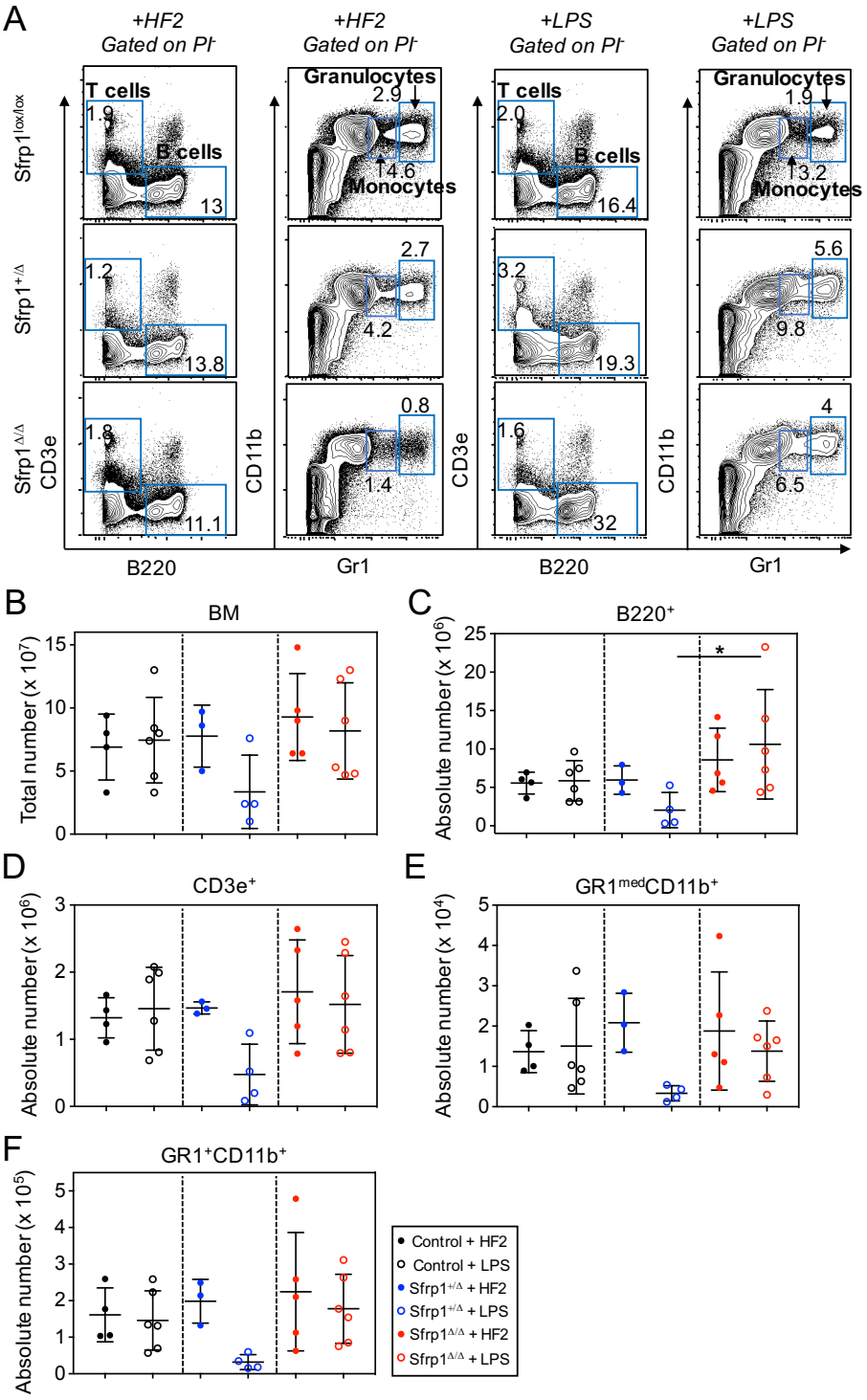

Figure 60. The impact of the LPS treatment on the mature hematopoietic compartment. **(A)** Representative flow cytometry plots of the gating strategy for mature hematopoietic compartment in BM. **(B)** Total number of BM, **(C)** Absolute number of $B220^+$ B cells, **(D)** Absolute number of $CD3e^+$ T cells, **(E)** Absolute number of $GR1^{med}CD11b^+$ monocytes, **(F)** Absolute number of $GR1^+CD11b^+$ granulocytes from *Sfrp1* conditional mice (with HF2+: $Sfrp1^{+/\Delta}$: n = 3; $Sfrp1^{\Delta/\Delta}$: n = 5; with LPS: $Sfrp1^{+/\Delta}$: n = 4; $Sfrp1^{\Delta/\Delta}$: n = 6) compared to the controls (with HF2+: n = 4; with LPS: n = 6). Black dots represent controls ($Sfrp1^{lox/lox}$); white dots surrounded by black represents LPS treated controls ($Sfrp1^{lox/lox}$). Blue dots represent $Sfrp1^{+/\Delta}$; white dots surrounded by blue represents LPS treated $Sfrp1^{+/\Delta}$. Red dots represent $Sfrp1^{\Delta/\Delta}$; white dots surrounded by red represents LPS treated $Sfrp1^{\Delta/\Delta}$ mice. Each dot represents an animal. Represented values are illustrated as Mean ± SD. * p-value ≤0.05 show significant differences in the comparison LPS treated $Sfrp1^{+/\Delta}$, $Sfrp1^{\Delta/\Delta}$ and controls to each other or to the untreated controls determined by ANOVA, Tukey`s post hoc test.

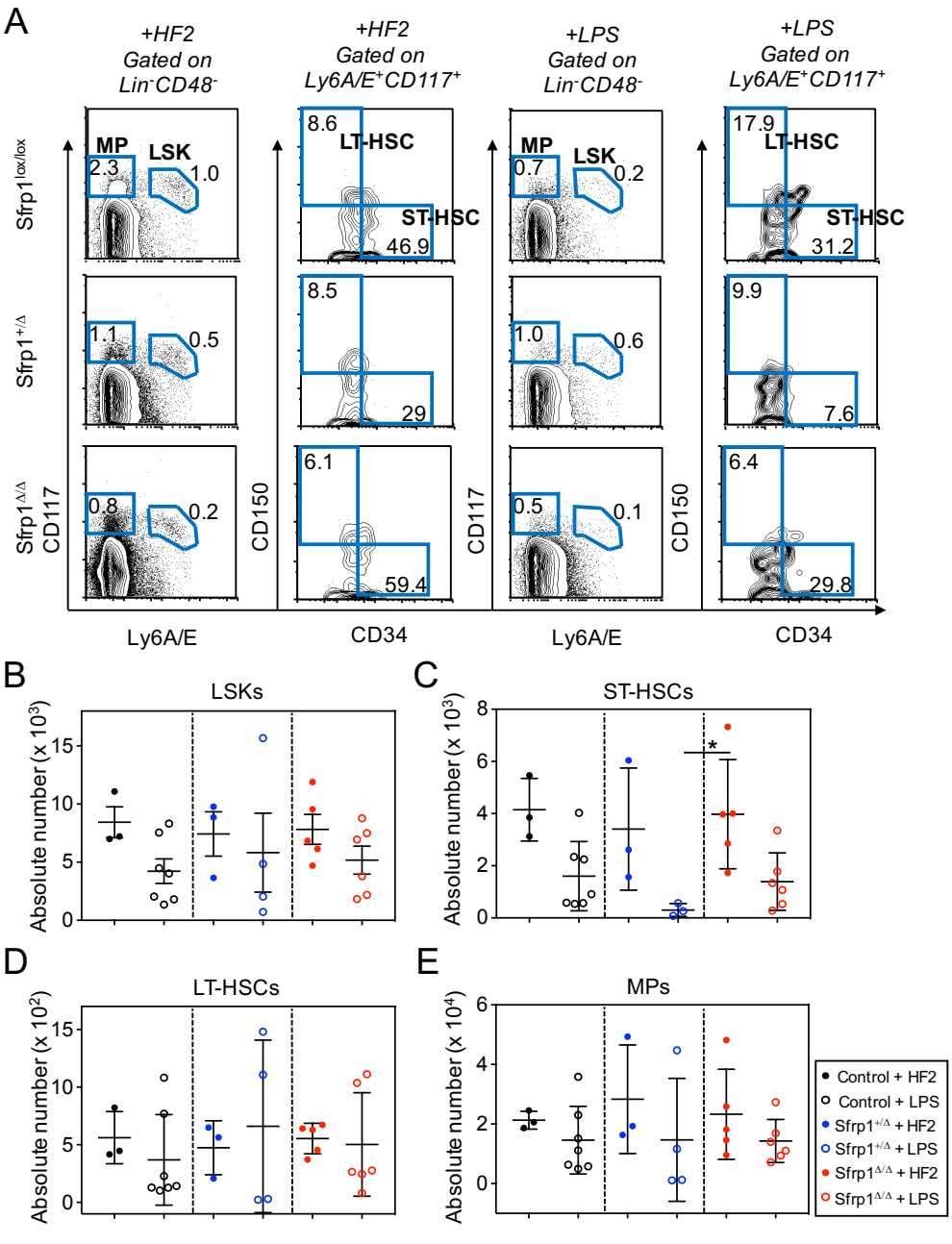

Figure 61. The impact of the LPS treatment on the primitive hematopoietic compartment. **(A)** Representative flow cytometry plots of the gating strategy for primitive hematopoietic compartment of lineage depleted BM cells. **(B)** Absolute number of LSKs from *Sfrp1* conditional mice (with HF2+: $Sfrp1^{+/\Delta}$: n = 3; $Sfrp1^{\Delta/\Delta}$: n = 5; with LPS: $Sfrp1^{+/\Delta}$: n = 4; $Sfrp1^{\Delta/\Delta}$: n = 6) compared to the controls (with HF2+: n = 3; with LPS: n = 7). **(C)** Absolute number of ST-HSCs from *Sfrp1* conditional mice (with HF2+: $Sfrp1^{+/\Delta}$: n = 3; $Sfrp1^{\Delta/\Delta}$: n = 5; with LPS: $Sfrp1^{+/\Delta}$: n = 3; $Sfrp1^{\Delta/\Delta}$: n = 6) compared to the controls (with HF2+: n = 3; with LPS: n = 7). **(D)** Absolute number of LT-HSCs from *Sfrp1* conditional mice (with HF2+: $Sfrp1^{+/\Delta}$: n = 3; $Sfrp1^{\Delta/\Delta}$: n = 5; with LPS: $Sfrp1^{+/\Delta}$: n = 4; $Sfrp1^{\Delta/\Delta}$: n = 6) compared to the controls (with HF2+: n = 3; with LPS: n = 7). **(E)** Absolute number of MPs from *Sfrp1* conditional mice (with HF2+: $Sfrp1^{+/\Delta}$: n = 3; $Sfrp1^{\Delta/\Delta}$: n = 5; with LPS: $Sfrp1^{+/\Delta}$: n = 4; $Sfrp1^{\Delta/\Delta}$: n = 6) compared to the controls (with HF2+: n = 3; with LPS: n = 7). Black dots represent controls ($Sfrp1^{lox/lox}$); white dots surrounded by black represents LPS treated controls ($Sfrp1^{lox/lox}$). Blue dots represent $Sfrp1^{+/\Delta}$; white dots surrounded by blue represents LPS treated $Sfrp1^{+/\Delta}$. Red dots represent $Sfrp1^{\Delta/\Delta}$; white dots surrounded by red represents LPS treated $Sfrp1^{\Delta/\Delta}$ mice. Each dot represents an animal. Represented values are illustrated as Mean ± SD. * p-value ≤0.05 show significant differences in the comparison of LPS treated $Sfrp1^{+/\Delta}$, $Sfrp1^{\Delta/\Delta}$ and controls to each other or to the untreated controls determined by ANOVA, Tukey`s post hoc test.

4.7.1.4 Functionality of LT-HSCs after LPS treatment

Our results so far suggest that the myeloid differentiation of LT-HSCs towards ST-HSCs and more mature myeloid lineages could be affected 24 hours after LPS treatment. In previous experiments, we also found that LT-HSCs from *Sfrp1*$^{\Delta/\Delta}$ mice showed reduced engraftment. To test whether LT-HSC from LPS-treated mice were similarly reduced in function, we transplanted limiting numbers (100 cells) of sorted LT-HSC from the LPS-treated and untreated mice of different *Sfrp1* genotypes (Figure 62).

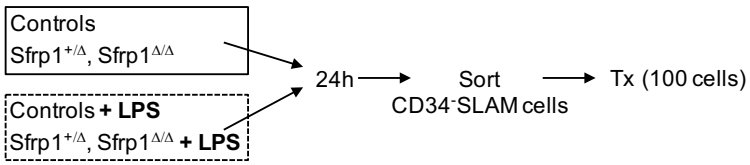

Figure 62. Impact of the LPS treatment on the functionality of LT-HSCs. Experimental design: eight- to ten-week old *Sfrp1*$^{+/\Delta}$, *Sfrp1*$^{\Delta/\Delta}$ mice and control animals were i.p injected with1000 ng LPS. 24 h later, the CD34^{-} SLAM cells were sorted and transplanted into lethally irradiate recipients.

Interestingly, LT-HSCs from *Sfrp1*$^{\Delta/\Delta}$ display decreased engraftment in PBs over the entire observation period of 24 weeks independently of LPS treatment (Figure 63A, B). Examination of the BM stem cell compartment after 24 weeks demonstrated a strongly decreased BM engraftment, as well as a failed repopulation of HSCs from the *Sfrp1*$^{\Delta/\Delta}$ donors, independently of LPS treatment (Figure 63C-F).

When examining the engraftment of LT-HSCs from control animals, we found that LT-HSCs from LPS-treated control donors engrafted significantly less than LT-HSCs from untreated controls (Figure 63A-C). Indeed, engraftment of the LT-HSCs from LPS-treated controls was very similar to that of LT-HSCs from treated or untreated *Sfrp1*$^{\Delta/\Delta}$ donors (Figure 63F).

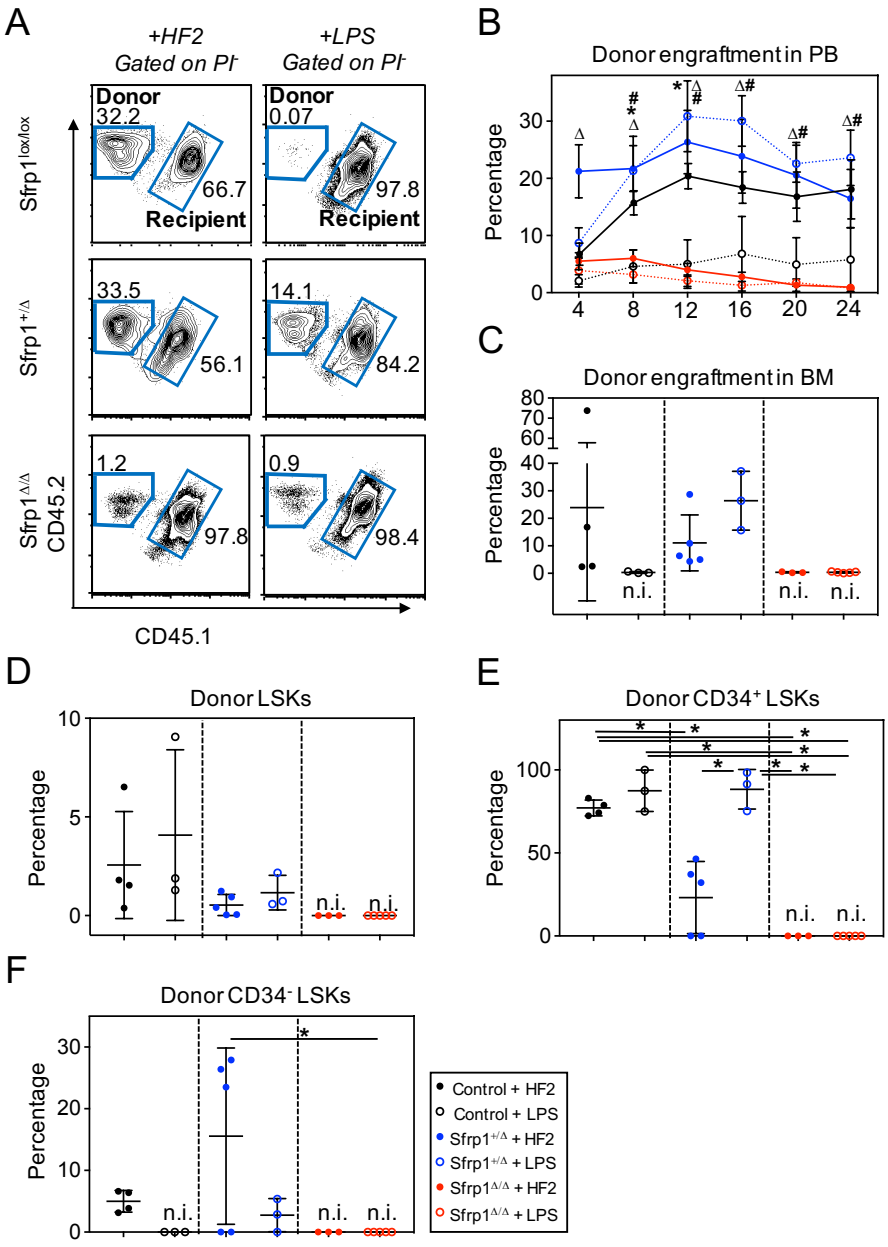

Figure 63. Repopulating activity of LT-HSCs after LPS treatment. (A) Representative flow cytometry plots of the gating strategy of Ly5.2^{+} donor cells or Ly5.1^{+}Ly5.2^{+} recipient cells. **(B)** Donor cell engraftment in percentage in the PB four, eight, twelve, sixteen, twenty and twentyfour weeks after Tx, **(C)** Percentage of the donor engraftment in BM, **(D)** Percentage of the donor LSKs, **(E)** Percentage of the donor CD34^{+} LSKs from *Sfrp1* conditional mice (with HF2+: *Sfrp1*$^{+/\Delta}$: n = 5; *Sfrp1*$^{\Delta/\Delta}$: n = 3; with LPS: *Sfrp1*$^{+/\Delta}$: n = 3; *Sfrp1*$^{\Delta/\Delta}$: n = 5) compared to the controls (with HF2+: n = 4; with LPS: n = 4). **(F)** Percentage of the donor CD34^{-} LSKs from *Sfrp1* conditional mice (with HF2+: *Sfrp1*$^{+/\Delta}$: n = 5; *Sfrp1*$^{\Delta/\Delta}$: n = 3; with LPS: *Sfrp1*$^{+/\Delta}$: n = 3; *Sfrp1*$^{\Delta/\Delta}$: n = 5) compared to the controls (with HF2+: n = 4; with LPS: n = 3). Black dots represent controls (*Sfrp1*$^{lox/lox}$); white dots surrounded by black represents LPS treated controls (*Sfrp1*$^{lox/lox}$). Blue dots represent *Sfrp1*$^{+/\Delta}$; white dots surrounded by blue represents LPS treated *Sfrp1*$^{+/\Delta}$. Red dots represent *Sfrp1*$^{\Delta/\Delta}$; white dots surrounded by red represents LPS treated *Sfrp1*$^{\Delta/\Delta}$ mice. Each dot represents an animal. Represented values are illustrated as Mean ± SD. Figure C: * p-value ≤0.05 show significant differences in the comparison of untreated *Sfrp1*$^{lox/lox}$ with every other untreated sample; $^{\Delta}$ p-value ≤0.05 show significant differences in the comparison of untreated *Sfrp1*$^{+/\Delta}$ with every other sample; $^{\#}$ p-value ≤0.05 show significant differences in the comparison of treated *Sfrp1*$^{+/\Delta}$ with every other sample; Figure D - G: * p-value ≤0.05 show significant differences in the comparison of each sample with every other sample determined by ANOVA, Tukey`s post hoc test.

In summary, *Sfrp1* deficiency in osteoprogenitors results in increased systemic secretion of the inflammatory cytokine IL-6 in the PB of *Sfrp1*$^{+/\Delta}$ mice, but not in the *Sfrp1*$^{\Delta/\Delta}$ mice. In the BM, *Sfrp1* deficient niche cells spontaneously differentiate into adipocytes, and show increased senescence after passaging. But, the LPS treatment does not further affect niche cells from *Sfrp1*$^{+/\Delta}$ and *Sfrp1*$^{\Delta/\Delta}$.

The primary *Sfrp1* deficiency in niche cells strongly affects hematopoiesis. Indeed, we found that HSCs from *Sfrp1*$^{\Delta/\Delta}$ mice are senescent with evidence of accumulation of DNA-damage. Furthermore, HSCs from *Sfrp1*-deficient mice fail to repopulate recipient mice and tend to differentiate more towards the myeloid lineage, which can be mitigated by treatment of the inhibitor IQ-1.

Moreover, the observed increase of IL-6 response after LPS treatment could be taken as evidence of a smoldering inflammation in *Sfrp1*$^{+/\Delta}$ animals. Because of the preferential myeloid differentiation in *Sfrp1*$^{\Delta/\Delta}$ mice and the increased expression of IL-6 in *Sfrp1*$^{+/\Delta}$ mice, we wondered whether leukemic-initiating cells would develop more easily in mice with an *Sfrp1* deficiency in osteolineage cells of the BM niche.

4.7.2 Transplantation of p185$^{BCR-ABL}$ expressing fetal liver cells into *Sfrp1* conditional microenvironment

Inflammation is a known driver of cancerogenesis (Hanahan & Weinberg, 2011). Specifically, in *Sfrp1*$^{\Delta/\Delta}$ mice, we noted spontaneous MSC differentiation into adipocytes (Figure 29), which are known supporters of tumorigenesis and producers of IL-6 and also MCP-1 (Zhao et al., 2020). We elevated IL-6 in these mice. In addition, promoter methylation of the human *SFRP1* gene in patients promote propagation of hematological diseases (Jost et al., 2008; Reins et al., 2010; Seeliger et al., 2009). Thus, we wondered whether in *Sfrp1*$^{\Delta/\Delta}$ mice, the niche would facilitate leukemogenesis, and we investigated development of leukemia propagating cells in mice with *Sfrp1* deficient niche.

In order to study the impact of the *Sfrp1* deficient inflammatory niche on development of malignant cells, leukemia was induced by injecting pMIGp185$^{BCR-ABL}$ expressing WT fetal liver (FL) cells (E13.5) into lethally irradiated *Sfrp1* conditional pups (*Sfrp1*$^{+/\Delta}$, *Sfrp1*$^{\Delta/\Delta}$) and control pups. Upon development of lethal leukemia, or after the designated observation period, the stromal- and hematopoietic cell compositions of the mice were analyzed.

4.7.2.1 Establishment of the mouse model with extended exposure of leukemic cells to the microenvironment

First of all, we established a mouse model were leukemic cells would be longer exposed to the niche in order to extend leukemia cell- niche interaction. For this purpose, we infected FL cells in medium containing cytokines (IL-3, IL-6 and mSCF) that supports HSCs in culture and monitored infection efficiency per flow cytometry. Furthermore, we transplanted GFP^+ FL cells into lethally irradiated newborn recipient mice at day 1 to 3 after birth (Figure 64).

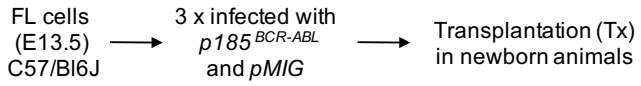

Figure 64. Transplantation of $p185^{BCR-ABL}$ expressing fetal liver cells into newborn animals. Experimental design: WT fetal liver cells (E 13.5) were infected three-times with $p185^{BCR-ABL}$ or pMIG. GFP^+ cells were measured by flow cytometry and cells were injected into lethally irradiated newborn animals (Tx).

From our previous findings, when we transplanted $p185^{BCR-ABL}$ positive cells into newborn and adult WT mice, we observed a prolonged survival of new born recipients as compared to adult recipient mice with a median survival of new born mice of 47 days as compared to 20 days in 8 weeks old mice transplanted with 400.000 leukemic cells (Figure 65C).

Therefore, we decided to use new born animals as recipients. As donor cells, we used FL cells from embryonic day 13.5 (E13.5) that are highly enriched for LT-HSCs (Figure 65A, B). Furthermore, these cells show high levels of engraftment in the newborn mice (Garcia-Ortega et al., 2010; Sands & Barker, 1999; West, Morris, & Wood, 1994; Yoder et al., 1996) and the cell number is sufficient to potently generate leukemia-inducing cells (LIC).

To determine the optimal cell dose for an extended latency of leukemia, we transplanted three different numbers of cells (50,000 cells, 200,000 cells and 400,000 cells) of the $p185^{BCR-ABL}$ transduced GFP^+ FL cells into sublethally irradiated WT new born recipient mice. It is important to note that transplantation of 200,000 or 400,000 $p185^{BCR-ABL}$-expressing FL cells induced disease in WT animals with almost same median survival (74 days or 72 days, respectively). New born recipients receiving 50,000 $p185^{BCR-ABL}$ cells succumb to leukemic disease significantly later (Figure 65D).

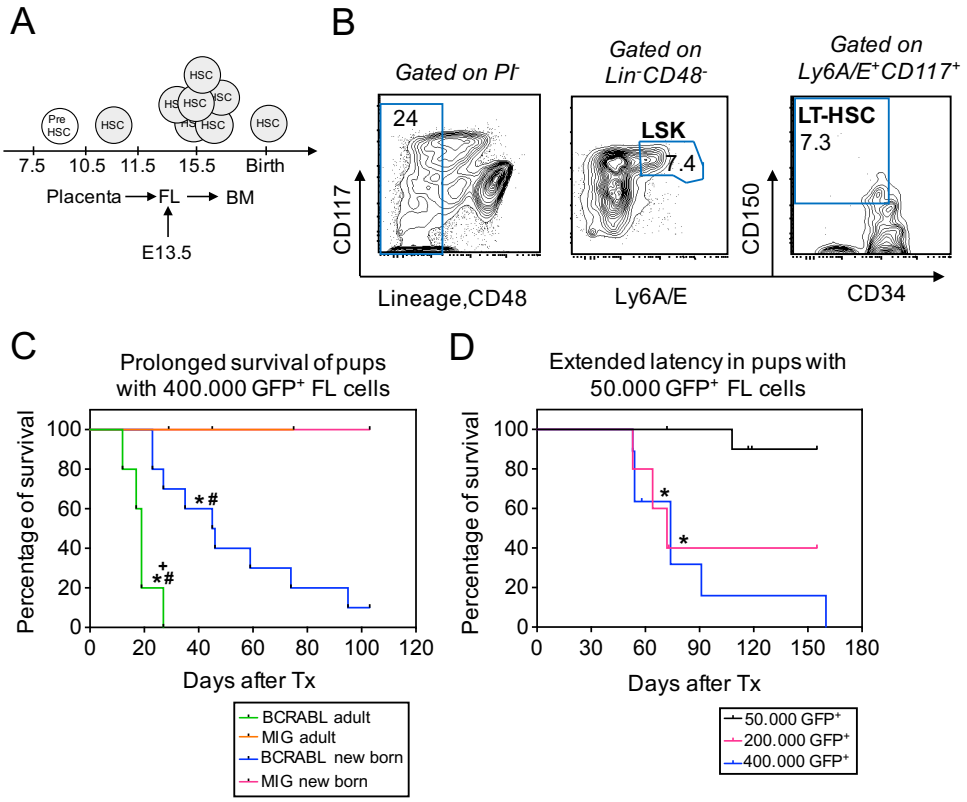

Figure 65. Establishment of the mouse model with extended exposure of leukemic cells to the niche. **(A)** FL cells from embryo day 13.5 are enriched for LT-HSCs. **(B)** Representative flow cytometry plots of $CD150^{+}CD34^{-}CD48^{-}$ LSKs from fetal liver cells (E13.5). **(C)** Kaplan-Meier survival plot visualizing the percentage of survival over time (days after transplantation) of $p185^{BCR\text{-}ABL}$ cells transplanted in WT new born mice (n = 10, blue), WT 8 weeks old mice (n = 7, green) and of pMIG cells transplanted in WT new born mice (n = 11, pink), WT 8 weeks old mice (n = 3, orange). **(D)** Kaplan-Meier survival plot visualizing the percentage of survival over time (days after transplantation) of $p185^{BCR\text{-}ABL}$ cells transplanted in WT new born mice to determine the dose, in three groups: 50,000 $p185^{BCR\text{-}ABL}$ cells (black, n= 11), 200,000 $p185^{BCR\text{-}ABL}$ cells (pink, n= 5), 400,000 $p185^{BCR\text{-}ABL}$ cells (blue, n = 9). Figure C: * p-value ≤0.05 show significant differences in the comparison of pMIG adult vs. $p185^{BCR\text{-}ABL}$ adult and $p185^{BCR\text{-}ABL}$ new born; # p-value ≤0.05 show significant differences in the comparison of pMIG new born vs. $p185^{BCR\text{-}ABL}$ adult and $p185^{BCR\text{-}ABL}$ new born; + p-value ≤0.05 show significant differences in the comparison of $p185^{BCR\text{-}ABL}$ adult vs. $p185^{BCR\text{-}ABL}$ new born determined by log-rank (Mantel-Cox) test. Figure D: * p-value ≤0.05 show significant differences in the comparison of 50,000 GFP^{+} FL cells vs. 200,000 GFP^{+} FL cells and 400,000 GFP^{+} FL cells determined by log-rank (Mantel-Cox) test. [Data from (C) provided/generated by S. Grziwok (Stem Cell Physiology Lab, Munich)].

4.7.2.2 BCR-ABL give interleukin-7 independence to pre-B cells

To characterize FL donor cells after IL-3, IL-6 and mSCF-facilitated infection, we analyzed some of their hematopoietic functions. First, we determined donor cell clonogenic capacity and differential potential. For this purpose, we sorted 1000 GFP^{+} FL cells and cultured the cells for 14 days in methylcellulose (M3434) supplemented with growth factors (3.3.2 Mouse colony-forming unit assay). In addition, we added IL-7 cytokine, that was shown to support formation of pro-B colonies and induces myelopoiesis and erythropoiesis (Figure 66A) (Aiello et al., 2007; Wei, Zeff, & Goldschneider, 2000). Williams et al. demonstrated that the fusion oncogene BCR-ABL can give “interleukin-7 (IL-7) independence to pre-B cells” (Williams & Sherr, 2007).

In contrast to control pMIG expressing FL cells, $p185^{BCR-ABL}$ cells generated more colonies without IL-7 cytokine (Figure 66B). Furthermore, we introduced cells differentiated in methylcellulose to flow cytometry. We found that $p185^{BCR-ABL}$ cells differentiated in all lineages independently of IL-7, excluding $GR1^{med}CD11b^{+}$ monocytes (Figure 66C-E), as described by other investigators (Raitano, Whang, & Sawyers, 1997; Williams & Sherr, 2007). In contrast pMIG expressing cells generated more $B220^{+}$ B cells and $CD3e^{+}$ T cells in the presence of IL-7, excluding $GR1^{med}CD11b^{+}$ monocytes (Figure 66E).

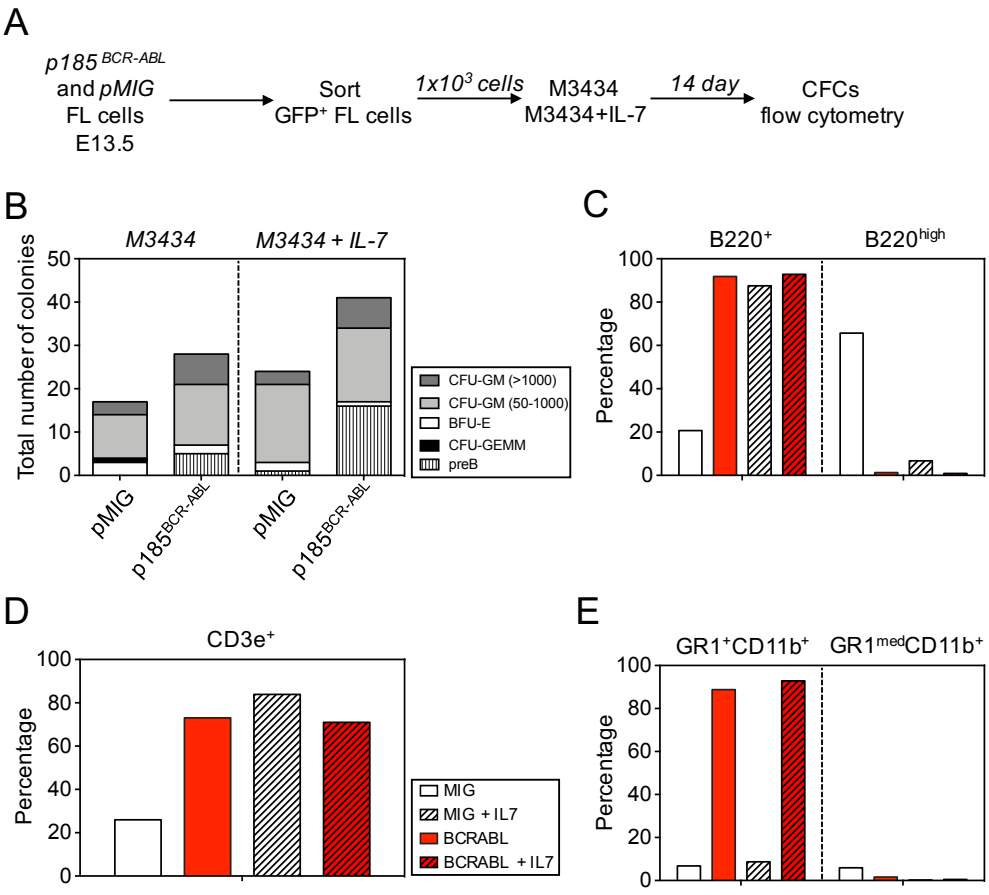

Figure 66. BCR-ABL expressing FL cells differentiated in all cell types independently of IL-7. **(A)** Experimental design: WT fetal liver cells (E 13.5) were infected three-times with $p185^{BCR-ABL}$ or pMIG. GFP^{+} cells were sorted by FACS and 1000 GFP^{+} FL cells cultured in M3434 with or without IL-7. After 14 days, we analyzed the cells. **(B)** Total number of CFCs of sorted GFP^{+} cells from WT FL cells in M3434 with or without IL-7. **(C)** Percentage of the $B220^{+}$ and $B220^{high}$ B cells of cultured GFP^{+} FL cells in M3434 with or without IL-7. **(D)** Percentage of the $CD3e^{+}$ T cells of cultured GFP^{+} fetal liver cells in M3434 with or without IL-7. **(E)** Percentage of the $GR1^{+}CD11b^{+}$ granulocytes and $GR1^{med}CD11b^{+}$ monocytes of cultured GFP^{+} FL cells in M3434 with or without IL-7. Figure B show CFU-GM (>1000) in dark grey, CFU-GM (50-1000) in grey, BFU-E in white and pre-B cells in black. Figure C, D and E show FL cells infected with $p185^{BCR-ABL}$ (red, n = 1) or pMIG (white, n = 1) and afterwards cultured in M3434 with (with strips, n = 1) or without IL-7 (without strips, n = 1).

4.7.2.3 *Sfrp1* deletion in the niche resulted into accelerated propagation of leukemic cells

Considering the long leukemia latency time when 50,000 GFP$^+$ FL cells were transplanted, and our hypothesis that deletion of *Sfrp1* in osteoprogenitors would facilitate leukemogenesis, we transplanted 50,000 GFP$^+$ p185$^{BCR\text{-}ABL}$ FL cells and pMIG FL cells into *Sfrp1*$^{+/\Delta}$, *Sfrp1*$^{\Delta/\Delta}$ control pups (*Sfrp1*$^{lox/lox}$). Since BCR-ABL expressing cells differentiate in all cell lineages independently of IL-7, we decided to infect the FL cells only with IL-3, IL-6 and mSCF (Figure 67).

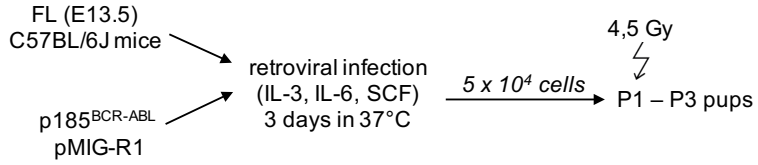

Figure 67. Transplantation of 50,000 p185$^{BCR\text{-}ABL}$ expressing FL cells into newborn pubs. Experimental design: WT fetal liver cells were infected three times with p185$^{BCR\text{-}ABL}$ or pMIG and 50,000 GFP$^+$ cells were injected intra-hepatically into sublethally irradiated newborn pubs (1° Tx). After severe disease symptoms, mice were sacrificed and analyzed by flow cytometry for hematopoietic stem cells, their progenitor cells and mature cells.

We observed a clear difference in survival of the mice. None of the animals transplanted with 5 x 10^4 pMIG-GFP$^+$ cells became diseased within the observation period of 342 days post-transplantation, as well as the *Sfrp1*$^{lox/lox}$ animals transplanted with 5 x 10^4 p185$^{BCR\text{-}ABL}$. However, 3 out of 8 *Sfrp1*$^{+/\Delta}$ animals transplanted with 5 x 10^4 p185$^{BCR\text{-}ABL}$ FL cells showed lethal leukemia (median survival: 321 days) and 2 animals additionally developed a tumor. Importantly, all *Sfrp1*$^{\Delta/\Delta}$ mice transplanted with 5 x 10^4 p185$^{BCR\text{-}ABL}$ FL cells died of leukemia (median survival: 65 days) and 6 out of 11 animals developed additional tumors (Figure 68A, B).

Interestingly, we found that the frequency of leukemic stem cells (LSCs) was 10-fold lower in the controls (*Sfrp1*$^{lox/lox}$, 1/224000), and 3-fold less frequent in the *Sfrp1*$^{+/\Delta}$ (1/72000) compared to the *Sfrp1*$^{\Delta/\Delta}$ mice (1/21000), which we analyzed with the limiting dilution analysis (Figure 68C) (Hu & Smyth, 2009), clearly showing that the lack of *Sfrp1* in osteoprogenitors increases the chance of leukemia development.

To study the effects of p185$^{BCR\text{-}ABL}$ activation in the *Sfrp1*$^{\Delta/\Delta}$ mice on normal and leukemic hematopoiesis, PB cell counts were determined. These showed that the white blood cell (WBC) numbers were significantly increased in the *Sfrp1*$^{\Delta/\Delta}$ mice compared to the *Sfrp1*$^{+/\Delta}$ mice and control animals (Figure 68D). The peripheral blood smear showed an abundance of damaged cells which indicate the presence of a disease (Figure 68E).

A

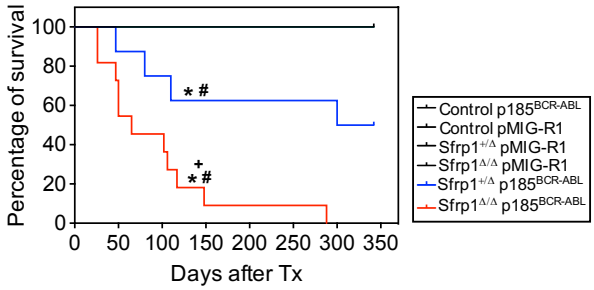

B

	1° Tx with p185$^{BCR-ABL}$			1° Tx with pMIG-R1		
Genotype	Total	Diseased	Tumor	Total	Diseased	Tumor
Sfrp1$^{lox/lox}$	12	0	0	5	0	0
Sfrp1$^{+/\Delta}$	8	3	2	4	0	0
Sfrp1$^{\Delta/\Delta}$	11	11	6	4	0	0

C

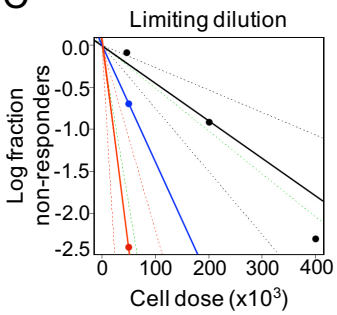

D

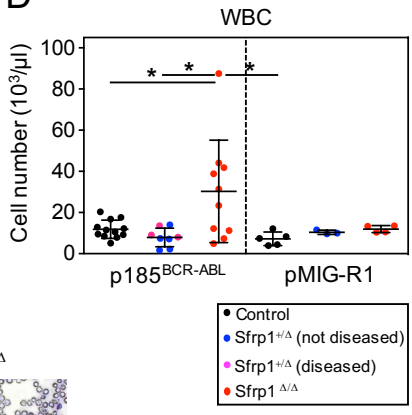

E

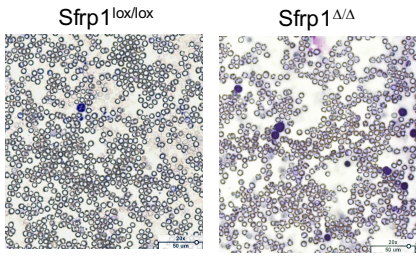

Figure 68. BCR-ABL expressing FL cells in *Sfrp1* deficient microenvironment. (A) Kaplan-Meier survival plot visualizing the percentage of survival over time (days after transplantation) of p185$^{BCR-ABL}$ cells transplanted in *Sfrp1* conditional pups (*Sfrp1*$^{+/\Delta}$: n = 8 (blue); *Sfrp1*$^{\Delta/\Delta}$: n = 11 (red)) and control animals (*Sfrp1*$^{lox/lox}$: n = 12 (black)), as well as pMIG cells transplanted in *Sfrp1* conditional pups (*Sfrp1*$^{+/\Delta}$: n = 4 (black); *Sfrp1*$^{\Delta/\Delta}$: n = 4 (black)) and control animals (*Sfrp1*$^{lox/lox}$: n = 5 (black)). **(B)** Table of mice transplanted with p185$^{BCR-ABL}$ positive cells (left) and with pMIG positive cells (right). **(C)** Limiting dilution analysis of p185$^{BCR-ABL}$ cells transplanted in *Sfrp1*$^{+/\Delta}$ (blue), *Sfrp1*$^{\Delta/\Delta}$ (red) and control animals (*Sfrp1*$^{lox/lox}$, black). **(D)** Cell number of WBC in 10^3/µl of the PB. **(E)** Blood smear of a diseased *Sfrp1*$^{\Delta/\Delta}$ mice transplanted with 50,000 BCR-ABL cells compared to a control. Represented values are illustrated as Mean ± SD. Figure A: * p-value ≤0.05 show significant differences in the comparison of p185$^{BCR-ABL}$ *Sfrp1*$^{lox/lox}$ vs. p185$^{BCR-ABL}$ *Sfrp1*$^{+/\Delta}$ and p185$^{BCR-ABL}$ *Sfrp1*$^{\Delta/\Delta}$; # p-value ≤0.05 show significant differences in the comparison of pMIG *Sfrp1*$^{lox/lox}$, *Sfrp1*$^{+/\Delta}$, *Sfrp1*$^{\Delta/\Delta}$ vs. p185$^{BCR-ABL}$ *Sfrp1*$^{+/\Delta}$ and p185$^{BCR-ABL}$ *Sfrp1*$^{\Delta/\Delta}$; + p-value ≤0.05 show significant differences in the comparison of p185$^{BCR-ABL}$ *Sfrp1*$^{+/\Delta}$ vs. p185$^{BCR-ABL}$ *Sfrp1*$^{\Delta/\Delta}$ determined by log-rank (Mantel-Cox) test. Figure D: Each dot represents an animal. * p-value ≤0.05 show significant differences in the comparison of each sample with every other sample determined by ANOVA, Tukey`s post hoc test. [Data from (A-D) generated with F. Koller (Stem Cell Physiology Lab, Munich)]. [Data from (E) generated by K. Steiger (Comparative experimental Pathology (CeP), Munich)].

Moreover, *Sfrp1* deletion in the niche resulted in increased numbers of GFP$^+$ leukemic cells (Figure 69), which invaded all hematological organs, like PB, BM and SP, as well as the LN.

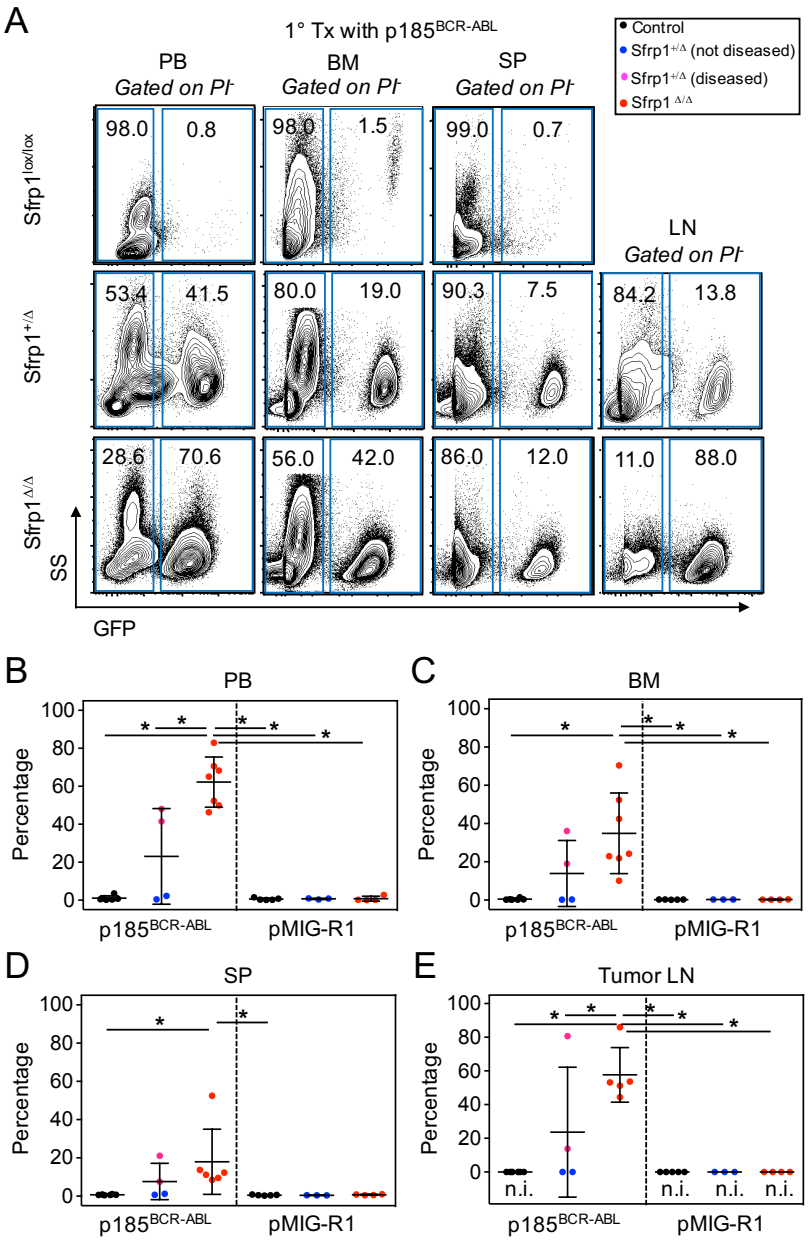

Figure 69. GFP$^+$ leukemic cells invaded all hematological organs of *Sfrp1* conditional mice. **(A)** Representative flow cytometry plots of GFP$^+$ leukemic cells in PB, BM, SP and LN from *Sfrp1*$^{+/\Delta}$, *Sfrp1*$^{\Delta/\Delta}$ and controls, gated on PI$^-$ cells. **(B)** Percentage of GFP$^+$ leukemic cells gated on live cells of PB, **(C)** BM, **(D)** SP from *Sfrp1* conditional animals transplanted with p185$^{BCR-ABL}$ positive cells (*Sfrp1*$^{+/\Delta}$: n = 4; *Sfrp1*$^{\Delta/\Delta}$: n = 7) and control animals (n = 6) and transplanted with pMIG positive cells (*Sfrp1*$^{+/\Delta}$: n = 3; *Sfrp1*$^{\Delta/\Delta}$: n = 4) and control animals (n = 5). **(E)** Percentage of GFP$^+$ leukemic cells gated on live cells of Tumor LN from *Sfrp1* conditional animals transplanted with p185$^{BCR-ABL}$ positive cells (*Sfrp1*$^{+/\Delta}$: n = 4; *Sfrp1*$^{\Delta/\Delta}$: n = 5) and control animals (n = 6) and transplanted with pMIG positive cells (*Sfrp1*$^{+/\Delta}$: n = 3; *Sfrp1*$^{\Delta/\Delta}$: n = 4) and control animals (n = 5). Black dots represent controls (*Sfrp1*$^{lox/lox}$); Blue dots represent not diseased *Sfrp1*$^{+/\Delta}$; Pink dots represent diseased *Sfrp1*$^{+/\Delta}$; Red dots represent *Sfrp1*$^{\Delta/\Delta}$. Each dot represents an animal. Represented values are illustrated as Mean ± SD. * p-value ≤0.05 show significant differences in the comparison of each sample with every other sample determined by ANOVA, Tukey`s post hoc test. [Data generated with F. Koller (Stem Cell Physiology Lab, Munich)].

Furthermore, we analyzed expression of lineage markers and found that GFP$^+$ p185$^{BCR-ABL}$ cells differentiated into B220$^+$ B cells in all animals and all analyzed tissues (PB, BM, SP and LN; Figure 70).

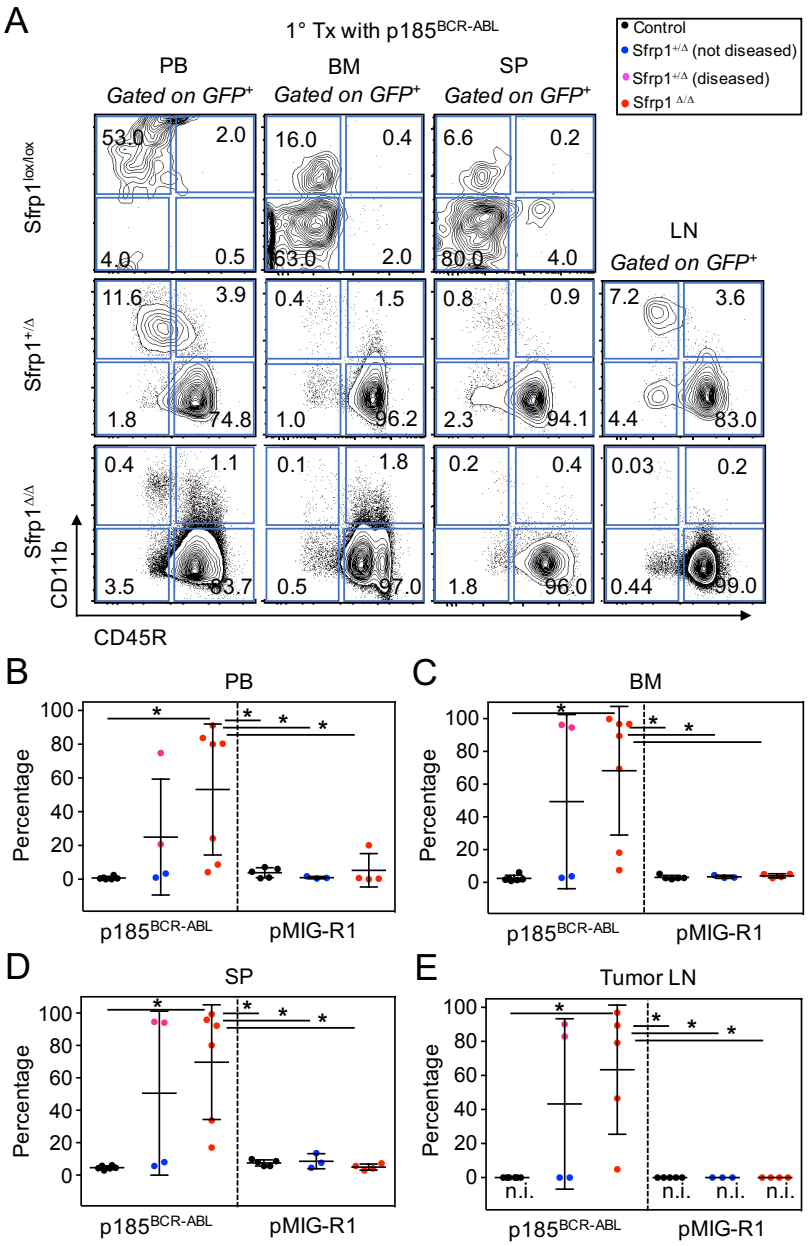

Figure 70. GFP$^+$ p185$^{BCR-ABL}$ cells differentiated into B220$^+$ B cells in *Sfrp1* conditional mice. **(A)** Representative flow cytometry plots of B220$^+$ GFP$^+$ leukemic cells in PB, BM, SP and LN from *Sfrp1*$^{+/\Delta}$, *Sfrp1*$^{\Delta/\Delta}$ and control animals, gated on GFP$^+$ cells. **(B)** Percentage of B220$^+$ GFP$^+$ leukemic cells of PB, **(C)** BM, **(D)** SP from *Sfrp1* conditional animals transplanted with p185$^{BCR-ABL}$ positive cells (*Sfrp1*$^{+/\Delta}$: n = 4; *Sfrp1*$^{\Delta/\Delta}$: n = 7) and control animals (n = 6) and transplanted with pMIG positive cells (*Sfrp1*$^{+/\Delta}$: n = 3; *Sfrp1*$^{\Delta/\Delta}$: n = 4) and control animals (n = 5). **(E)** Percentage of B220$^+$ GFP$^+$ leukemic cells gated of tumor LN from *Sfrp1* conditional animals transplanted with p185$^{BCR-ABL}$ positive cells (*Sfrp1*$^{+/\Delta}$: n = 4; *Sfrp1*$^{\Delta/\Delta}$: n = 5) and control animals (n = 6) and transplanted with pMIG positive cells (*Sfrp1*$^{+/\Delta}$: n = 3; *Sfrp1*$^{\Delta/\Delta}$: n = 4) and control animals (n = 5). Black dots represent controls (*Sfrp1*$^{lox/lox}$); Blue dots represent not diseased *Sfrp1*$^{+/\Delta}$; Pink dots represent diseased *Sfrp1*$^{+/\Delta}$; Red dots represent *Sfrp1*$^{\Delta/\Delta}$. Each dot represents an animal. Represented values are illustrated as Mean ± SD. * p-value ≤0.05 show significant differences in the comparison of each sample with every other sample determined by ANOVA, Tukey`s post hoc test. [Data generated with F. Koller (Stem Cell Physiology Lab, Munich)].

Consistent with murine leukemia data, all leukemic animals developed splenomegaly with increase in weight and cell number compared to the non-diseased controls (Figure 71A-C) (Schreck et al., 2017).

Also, the spleen anatomy in diseased *Sfrp1*$^{\Delta/\Delta}$ mice was completely modified due to infiltrations of leukemic cells compared to not sick control animals (Figure 71E). We found infiltration of leukemic cells in the liver and thymus (Figure 71D, F). In 6 out of 11 *Sfrp1*$^{\Delta/\Delta}$ mice we found a tumor-like infiltration of the lymph nodes and neighboring organs like the kidney (Figure 71G, H).

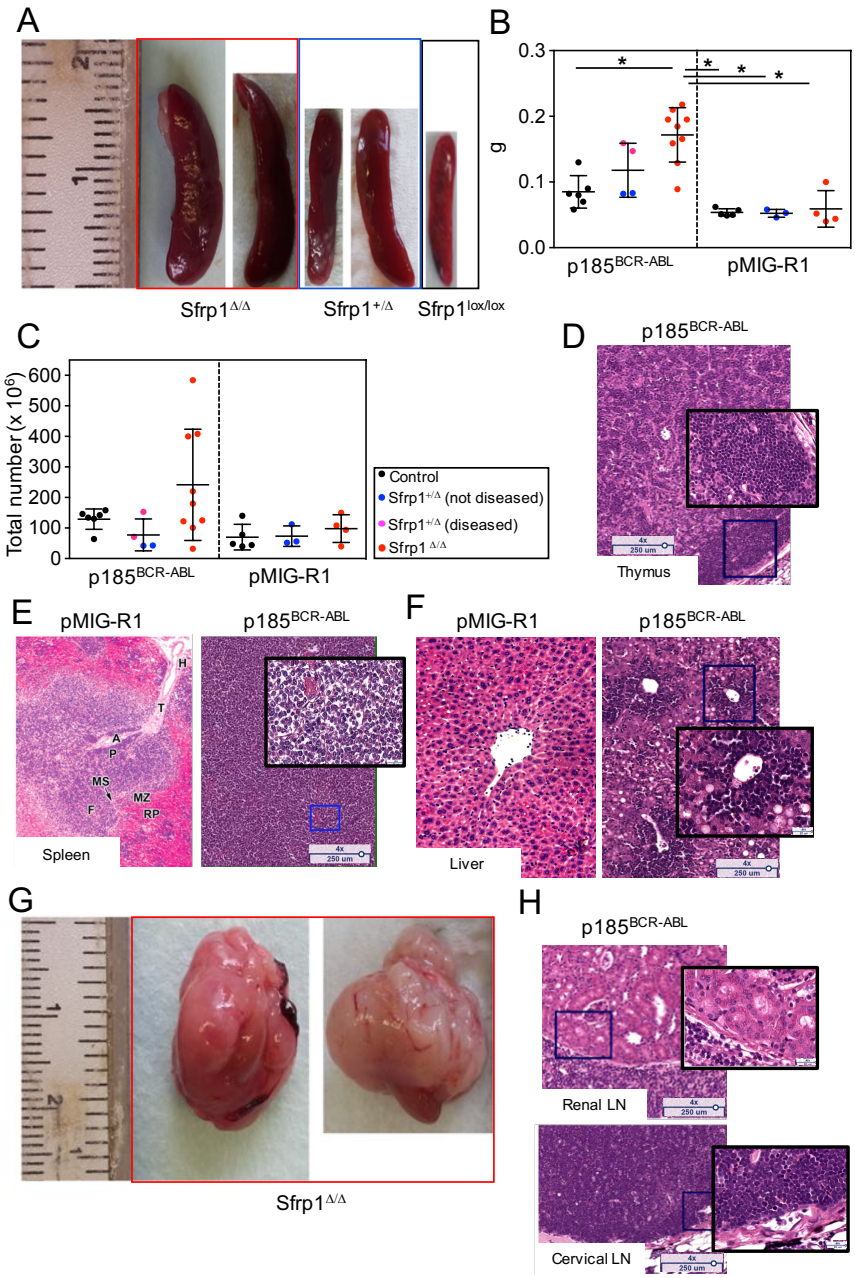

Figure 71. Altered spleen, liver, thymus and lymph node anatomy in diseased animals. (A) Representative pictures of spleens of *Sfrp1*$^{+/\Delta}$, *Sfrp1*$^{\Delta/\Delta}$ and control animals (*Sfrp1*$^{lox/lox}$) transplanted with p185$^{BCR-ABL}$ positive cells. **(B)** Weight of the spleens in g from *Sfrp1* conditional animals and control animals with p185$^{BCR-ABL}$ positive cells (*Sfrp1*$^{lox/lox}$: n = 6, *Sfrp1*$^{+/\Delta}$: n = 4; *Sfrp1*$^{\Delta/\Delta}$: n = 9) and pMIG positive cells (*Sfrp1*$^{lox/lox}$: n = 5, *Sfrp1*$^{+/\Delta}$: n = 4; *Sfrp1*$^{\Delta/\Delta}$: n = 3). **(C)** Total cell number of the spleen cells from *Sfrp1* conditional animals and control animals with p185$^{BCR-ABL}$ positive cells (*Sfrp1*$^{lox/lox}$: n = 6, *Sfrp1*$^{+/\Delta}$: n = 4; *Sfrp1*$^{\Delta/\Delta}$: n = 9) and pMIG positive cells (*Sfrp1*$^{lox/lox}$: n = 5, *Sfrp1*$^{+/\Delta}$: n = 4; *Sfrp1*$^{\Delta/\Delta}$: n = 3). **(D)** Altered thymus anatomy in diseased animals. **(E)** Altered spleen anatomy in diseased animals (right) compared to the control (left). Marginal zone (MZ), marginal sinus region (MS), follicle (F), PALS (P), red pulp (RP), central artery (A), trabeculus (T) and hilus (H) are shown. **(F)** Altered liver anatomy in diseased animals (right) compared to the control (left). **(G)** Representative pictures of tumors of mouse transplanted with p185$^{BCR-ABL}$ positive cells. **(H)** Altered lymph node anatomy in diseased animals. Figure B and C: Black dots represent controls (*Sfrp1*$^{lox/lox}$); Blue dots represent not diseased *Sfrp1*$^{+/\Delta}$; Pink dots represent diseased *Sfrp1*$^{+/\Delta}$; Red dots represent *Sfrp1*$^{\Delta/\Delta}$. Each dot represents an animal. Figure D, E, F and H: on the left side, a 4-fold magnification (white bar = 250 µm) and on the right side, a 40-fold magnification (white bar = 25 µm). Represented values are illustrated as Mean ± SD. * p-value ≤0.05 show significant differences in the comparison of each sample with every other sample determined by ANOVA, Tukey`s post hoc test. [Data (A –C, G) generated with F. Koller (Stem Cell Physiology Lab, Munich)]. [Data (D –F, H) generated with K. Steiger (Comparative experimental Pathology (CeP), Munich)].

In summary, we can say that BCR-ABL expressing cells propagated disease only in animals with *Sfrp1* deletion in the niche compartment. First analysis characterizes the disease as a precursor B cell lymphoblastic disease.

In order to analyze the contribution of inflammatory cytokines in the PB serum, we determined IL-6, IL-10, MCP-1, IFNγ, TNF, and IL-12p70 in the PB serum using a cytokine bead assay (Figure 72A). The secretion of IL-6 was increased in *Sfrp1*$^{\Delta/\Delta}$ mice (Figure 72B, C), as we could also see in previous experiments after LPS exposure (Figure 57). Interestingly, in p185$^{BCR-ABL}$ leukemic *Sfrp1*$^{\Delta/\Delta}$ mice, we additionally found an increase in MCP-1 and TNF in the serum compared to the non-leukemic control recipients (Figure 72B, D, E).

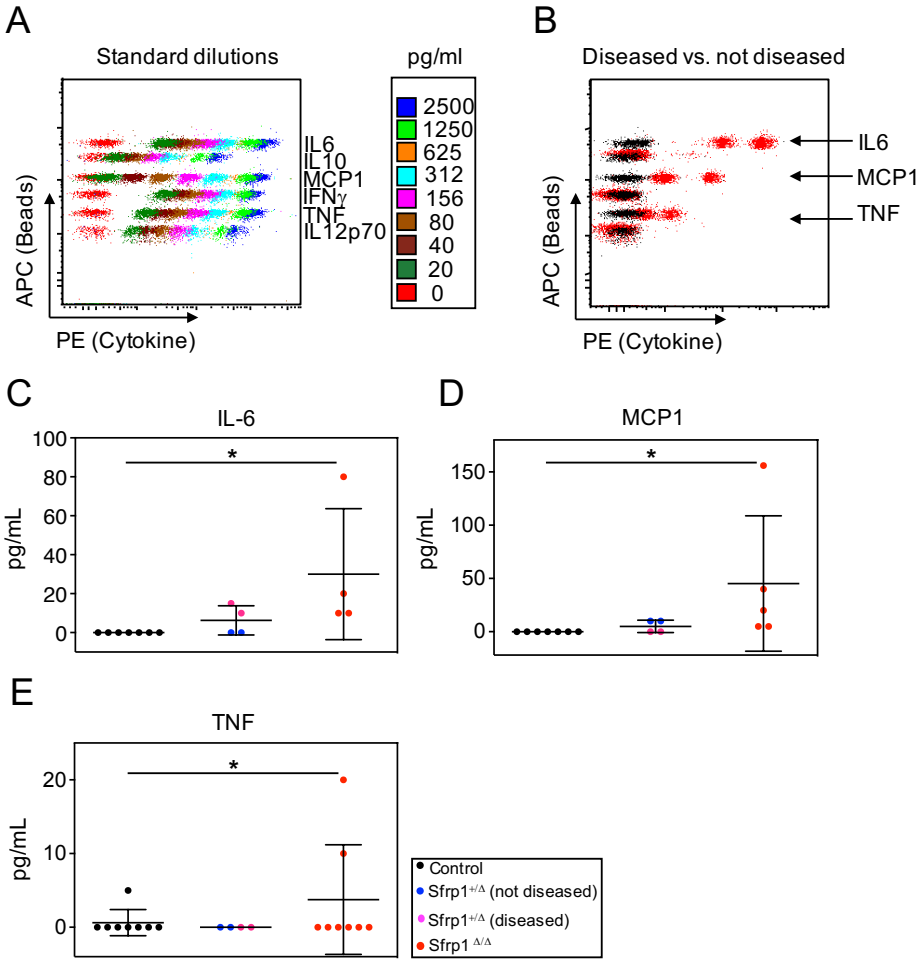

Figure 72. The inflammatory response after transplantation of 50,000 p185$^{BCR-ABL}$ leukemic FL cells. **(A)** Standard dilutions for the analyzed cytokines (IL-6, IL-10, MCP-1, INFγ, TNF, IL-12p70) in pg/mL. **(B)** Representative flow cytometry plot for the analyzation of the cytokines in the serum of the PB from *Sfrp1*$^{\Delta/\Delta}$ mice (red, diseased, n = 2) and control mice (black, not diseased, n = 2) transplanted with 50,000 p185$^{BCR-ABL}$ leukemic FL cells. **(C)** Analyzation of the protein content in pg/mL from IL-6, **(D)** MCP-1 and **(E)** TNF. Black dots represent controls (*Sfrp1*$^{lox/lox}$); Blue dots represent not diseased *Sfrp1*$^{+/\Delta}$; Pink dots represent diseased *Sfrp1*$^{+/\Delta}$; Red dots represent *Sfrp1*$^{\Delta/\Delta}$. Each dot represents an animal. Represented values are illustrated as Mean ± SD. * p-value ≤0.05 show significant differences in the comparison of each sample with every other sample determined by Bartlett's test.

In summary, *Sfrp1* deficiency in the niche accelerates leukemia formed from 50,000 BCR-ABL-expressing cells, whereas control animals do not develop disease. The control animals do also develop leukemia if at least 4-times more cells are being transplanted. The median survival of diseased animals transplanted with different cell number (WT: 200,000 cells; *Sfrp1*$^{\Delta/\Delta}$ mice: 50,000 cells) was almost identical (WT: 72 days; *Sfrp1*$^{\Delta/\Delta}$ mice: 65 days). In *Sfrp1*$^{\Delta/\Delta}$ mice, the secretion of inflammatory cytokines, like IL-6, MCP-1 and TNF, is increased compared to the control animals. These findings indicate that leukemia in mice with a *Sfrp1-deficient* osteogenic niche is associated with systemic inflammation. Since one of these cytokines (IL-6) is already elevated without leukemia, our results suggest that in general, *Sfrp1*$^{\Delta/\Delta}$ mice show a tendency towards systemic inflammation. These findings hint to the possibility that the function of mature inflammatory cells is altered in *Sfrp1*$^{\Delta/\Delta}$ mice. Early in tumorigenesis, tumor cells may persist because of reduced immune surveillance of immune cells in the *Sfrp1*$^{\Delta/\Delta}$ mice.

Immune surveillance includes the process of phagocytosis (Moxey-Mims et al., 1991). Neutrophils specialize in phagocytizing invading microorganisms, but are also able to take up other particles, such as *E.coli* - FITC particles. A reduced or defective function of the neutrophil granulocytes can be the cause of excessive inflammation and thus tissue damage.

To test this hypothesis that cancer cells evade the immune system by disrupting the effect of phagocytosis on induction of antitumor immune responses in the *Sfrp1*$^{\Delta/\Delta}$ mice, we analyzed phagocytosis of mature granulocytes.

In these experiments, we used sorted GR1^{+}CD11b^{+} cells from adult control mice and their littermates with *Sfrp1* deletion in the niche and cultured these cells with and without *E.coli* membrane particles coupled with FITC. After 3 hours of culture at 37 °C we analyzed cells by flow cytometry (Figure 73A). The histograms show that the granulocytes from the *Sfrp1* deficient animals (red line) as well as the controls (black line, Figure 73B) are able to phagocyte the *E.coli* particles (green line). The experiment performed with FL cells transfected with GFP and the BCR-ABL oncogene did not reveal major differences in the phagocytic activity of the GR1^{+}CD11b^{+} cells between the groups (Figure 73C).

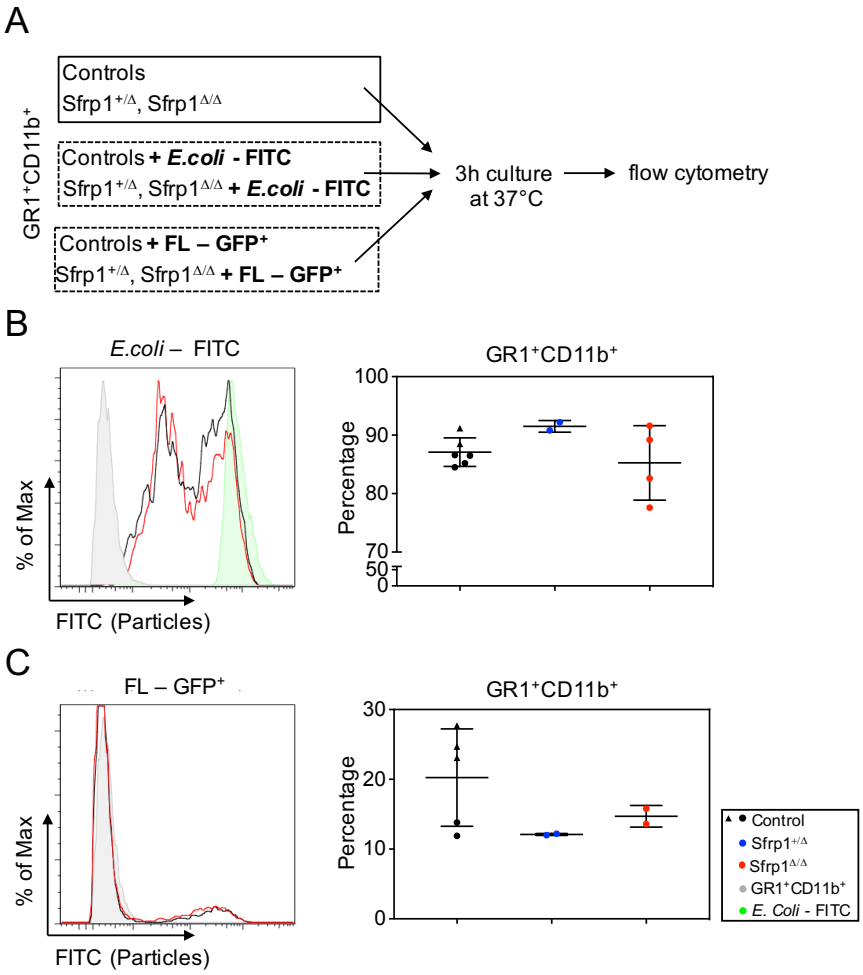

Figure 73. Unchanged phagocytosis activity of GR1$^+$CD11b$^+$ cells from *Sfrp1* deficient animals. **(A)** Experimental design: Sorted GR1$^+$CD11b$^+$ cells from control mice, *Sfrp1*$^{+/\Delta}$ and *Sfrp1*$^{\Delta/\Delta}$ were cultured for 3 h with and without *E.coli* membrane particles coupled with FITC or FL GFP$^+$ cells and analyzed by flow cytometry. **(B)** Left: Representative histogram plot for the analyzation of the phagocytosis activity from *Sfrp1* deficient mice (red) and control mice (black) with and without *E.coli* membrane particles (green). Right: Percentage of *E.coli* - FITC positive GR1$^+$CD11b$^+$ cells. **(C)** Left: Representative histogram plot for the analyzation of the phagocytosis activity from *Sfrp1*$^{\Delta/\Delta}$ mice (red) and control mice (black) with and without FL - GFP$^+$ cells. Right: Percentage of FL - GFP$^+$ positive GR1$^+$CD11b$^+$ cells. Black dots or lines represent controls (*Sfrp1*$^{lox/lox}$); Black triangles represent controls (Osx-Cre); Blue dots represent *Sfrp1*$^{+/\Delta}$; Red dots or lines represent *Sfrp1*$^{\Delta/\Delta}$; Grey lines represent untreated GR1$^+$CD11b$^+$; Green line represent *E.coli* - FITC particle only. Each dot represents an animal. Represented values are illustrated as Mean ± SD.

4.8. Changes in gene expression in MSCs of *Sfrp1* conditional mice

The above results indicate that deletion of *Sfrp1* in osteoprogenitors reduces the functional quality of LT-HSCs, increases systemic IL-6, and promotes formation of LSCs from BCR-ABL$^+$ cells. Since in all of these studies, deletion of *Sfrp1* in osteoprogenitors was the primary event, we analyzed and compared the whole transcriptome of MSC populations isolated from mice bones of *Sfrp1*$^{+/\Delta}$ and *Sfrp1*$^{\Delta/\Delta}$ to controls (*Sfrp1*$^{lox/lox}$; Osx-Cre) to determine the impact of primary *Sfrp1* loss in the niche cells on secondary effects in hematopoiesis. The goal of the gene expression analysis is to connect the two.

Furthermore, by studying the transcriptomes of niche cells from *Sfrp1*$^{\Delta/\Delta}$ and control animals, we hope to gain a deeper understanding of the molecular mechanisms underlying the observed changes in biology (3.10.1 RNA sequencing analysis).

After sequencing of sorted primary (CD45/Ter119)$^{-}$ CD31^{-} ALCAM$^{-/med}$ SCA-1^{+} MSCs and normalization of the transcriptomes, the samples were clustered according to the genotype in the principle component analysis (PCA). It is noticeable, that only the global transcriptional profiles of Osx-Cre revealed clear cluster, but the *Sfrp1*$^{+/\Delta}$ and *Sfrp1*$^{\Delta/\Delta}$ samples were not clearly separated (Figure 74A, B).

Nevertheless, pairwise comparison of *Sfrp1*$^{+/\Delta}$ and *Sfrp1*$^{\Delta/\Delta}$ to controls (*Sfrp1*$^{lox/lox}$; Osx-Cre) and between each other led to the identification of 535 differently expressed genes (DEGs) with an adjusted p-value ≤ 0.05 and logFoldChange (logFC) > 1 (327 genes), as well as logFC < -1 (208 genes, Figure 74C).

It is important to note, that the aberrant functional behaviors of the *Sfrp1*$^{\Delta/\Delta}$ MSCs, like increased generation of small CFU-Fs, strong differentiation into adipogenic and osteogenic lineages, increased proliferative activity in endosteal cells and cellular senescence occur in culture. Therefore, it is possible that the primary sorted MSCs are not activated after sorting and show no aberrant phenotype.

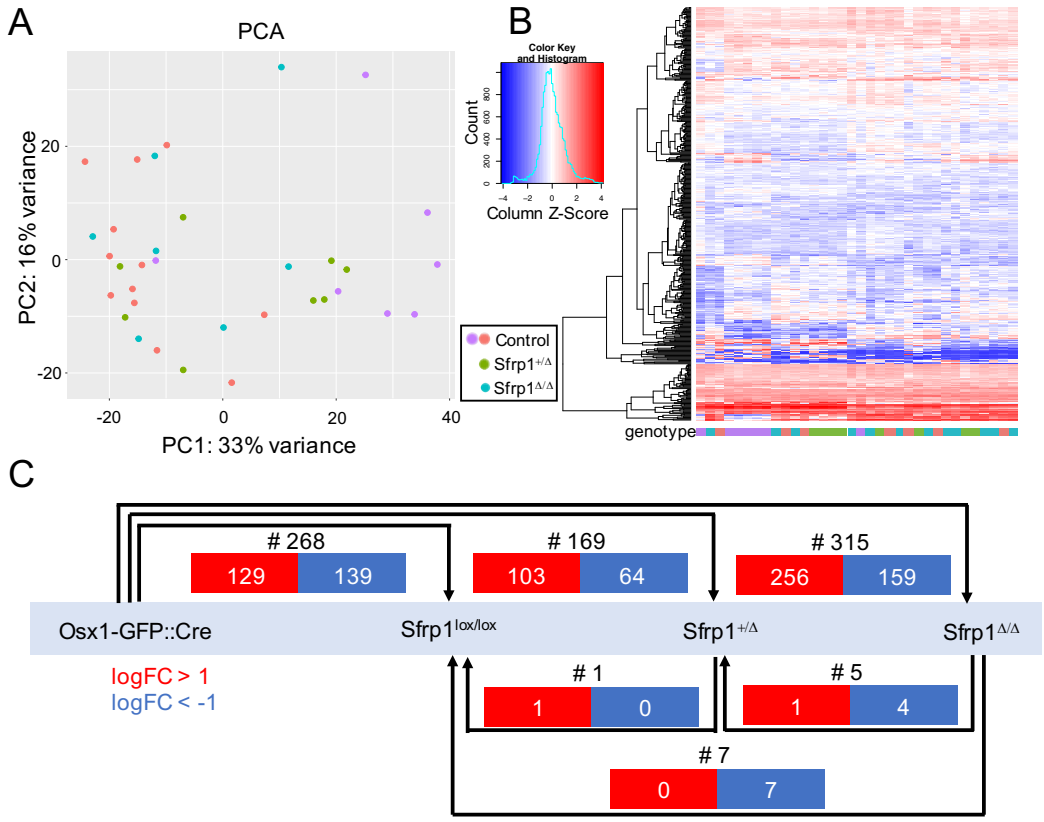

Figure 74. Global gene expression analysis. (A) PCA of gene expression of *Sfrp1*$^{+/\Delta}$ and *Sfrp1*$^{\Delta/\Delta}$ compared to controls (*Sfrp1*$^{lox/lox}$; Osx-Cre). **(B)** Heatmap of the top 500 DEGs in *Sfrp1*$^{+/\Delta}$ and *Sfrp1*$^{\Delta/\Delta}$ compared to controls (*Sfrp1*$^{lox/lox}$; Osx-Cre). Orange dots represent controls (*Sfrp1*$^{lox/lox}$); Purple dots represent controls (Osx-Cre); Green dots represent *Sfrp1*$^{+/\Delta}$; Blue dots represent *Sfrp1*$^{\Delta/\Delta}$. Each dot represents one animal. **(C)** Number of DEGs of *Sfrp1*$^{+/\Delta}$ and *Sfrp1*$^{\Delta/\Delta}$ compared to controls (*Sfrp1*$^{lox/lox}$; Osx-Cre) and between each other. Numbers in blue rectangles indicate down-regulated genes (logFC < -1); numbers in red rectangles indicate up-regulated genes (logFC > 1).

In order to gain a better understand whether the DEGs represented specifically deregulated molecular functions or pathways, GO enrichment analysis (enrichGO, clusterProfiler) (Yu et al., 2012) of the DEGs between *Sfrp1*$^{\Delta/\Delta}$ compared to controls (Osx-Cre) was performed. We found that DEGs were enriched in 20 GO categories including `endoplasmic reticulum (ER) to cytosol transport´, `retrograde protein transport - ER to cytosol´, and `response to endoplasmic reticulum stress´ (Figure 75A). In addition, PANTHER was used to perform functional analyses of the gene set. There, the DEGs were dysregulated in the `ERAD pathway´, `response to endoplasmic reticulum stress´, `with endoplasmic reticulum to cytosol transport´, `regulation of retrograde protein transport – ER to cytosol´ and the `ubiquitin-dependent ERAD pathway´ (GeneMANIA, Figure 75B) (Warde-Farley et al., 2010). Interestingly, a combination of these DEGs which were expressed in 2 out of 5 biological functions revealed 14 genes down-regulated in *Sfrp1*$^{\Delta/\Delta}$ MSCs compared to the controls (Figure 75B, C). We decided to take a closer look to four key DEGs categorized as essential in the ER and the ERAD pathway (*Sel1l, Ubxn4, Syvn1, Derl1*).

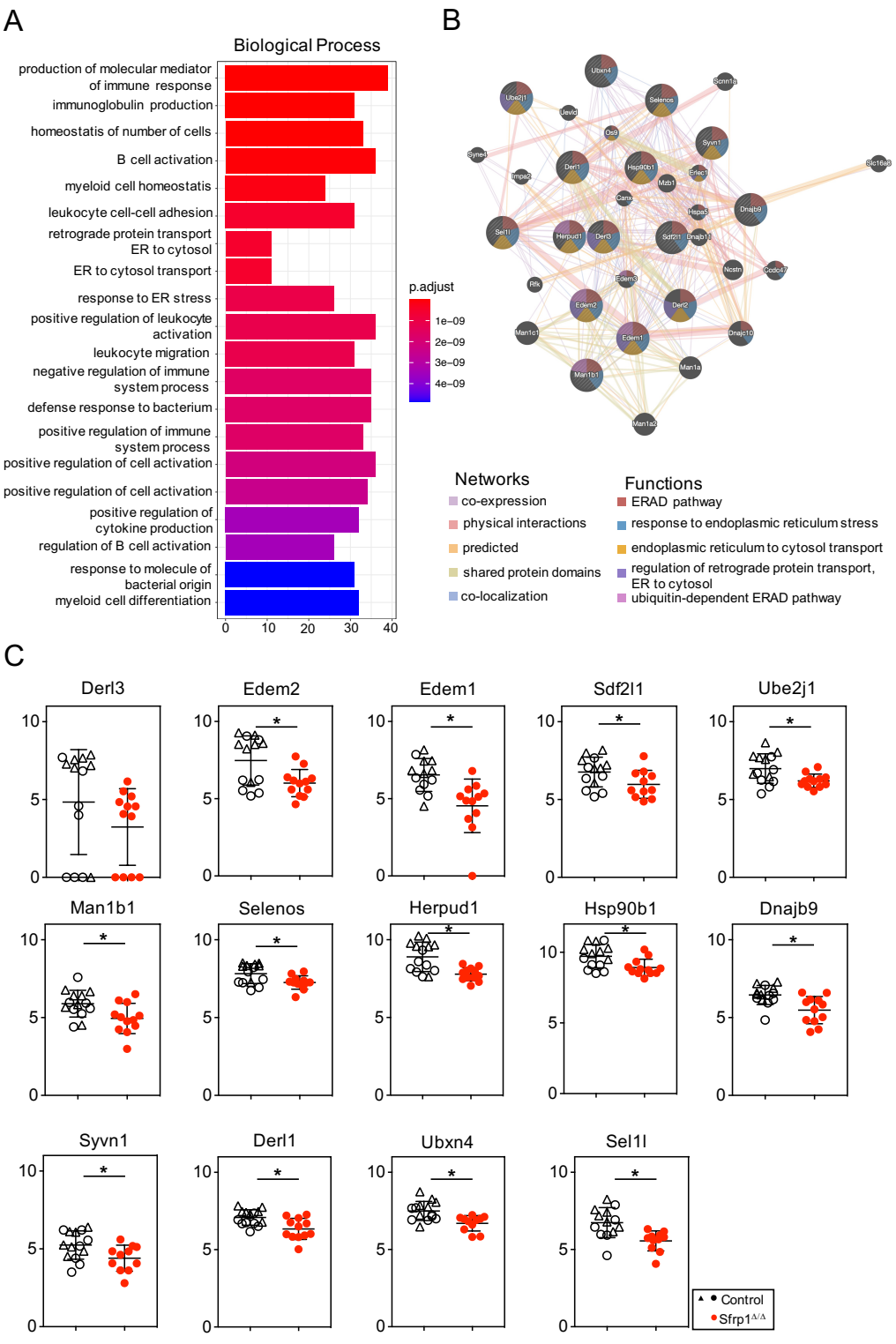

Figure 75. The endoplasmic reticulum pathway is dysregulated in *Sfrp1*$^{\Delta/\Delta}$ MSCs. (A) The 20 enriched terms of the DEGs between *Sfrp1*$^{\Delta/\Delta}$ compared to controls (Osx-Cre). The barplot shows the enrichment scores and ratio as bar height and color. **(B)** Gene connections of DEGs that are down-regulated in the biological functions between *Sfrp1*$^{\Delta/\Delta}$ compared to controls. **(C)** The normalized raw count data using the TMM (Robinson et al., 2010) normalization method of the 14 differentially down-regulated genes of *Sfrp1*$^{\Delta/\Delta}$ compared to controls (*Sfrp1*$^{lox/lox}$; Osx-Cre). Black dots represent controls (*Sfrp1*$^{lox/lox}$); black triangles represent controls (Osx-Cre); Red dots represent *Sfrp1*$^{\Delta/\Delta}$. Each dot represents one animal. Represented values are illustrated as Mean ± SD. * p-value ≤0.05 show significant differences in the comparison of *Sfrp1*$^{\Delta/\Delta}$ to controls (*Sfrp1*$^{lox/lox}$; Osx-Cre) determined by unpaired t test.

Therefore, we cultured MSCs (p3) and performed IF experiments to analyze the protein expression for SEL1L, UBXN4, SYVN1 and DERL1.

We found that all four proteins are expressed. Importantly, in line with the transcriptome results, MSCs from *Sfrp1*$^{\Delta/\Delta}$ mice showed decreased protein content of SEL1L, UBXN4 and SYVN1, while protein content of DERL1 was unchanged. IF also allows assessment of the protein localization within the cells. However, while DERL1 and UBXN4 proteins were mainly expressed in the cytoplasm and SEL1L and SYVN1 proteins could be observed in both cytoplasm and ER (Figure 76A-D), there were no obvious differences between protein localization within the cells from different genotypes.

In conclusion, since the protein content of SEL1L, UBXN4 and SYVN1 was down-regulated in the SFRP1-deficient MSCs, it is likely that SFRP1 regulates the ERAD pathway and proteostasis.

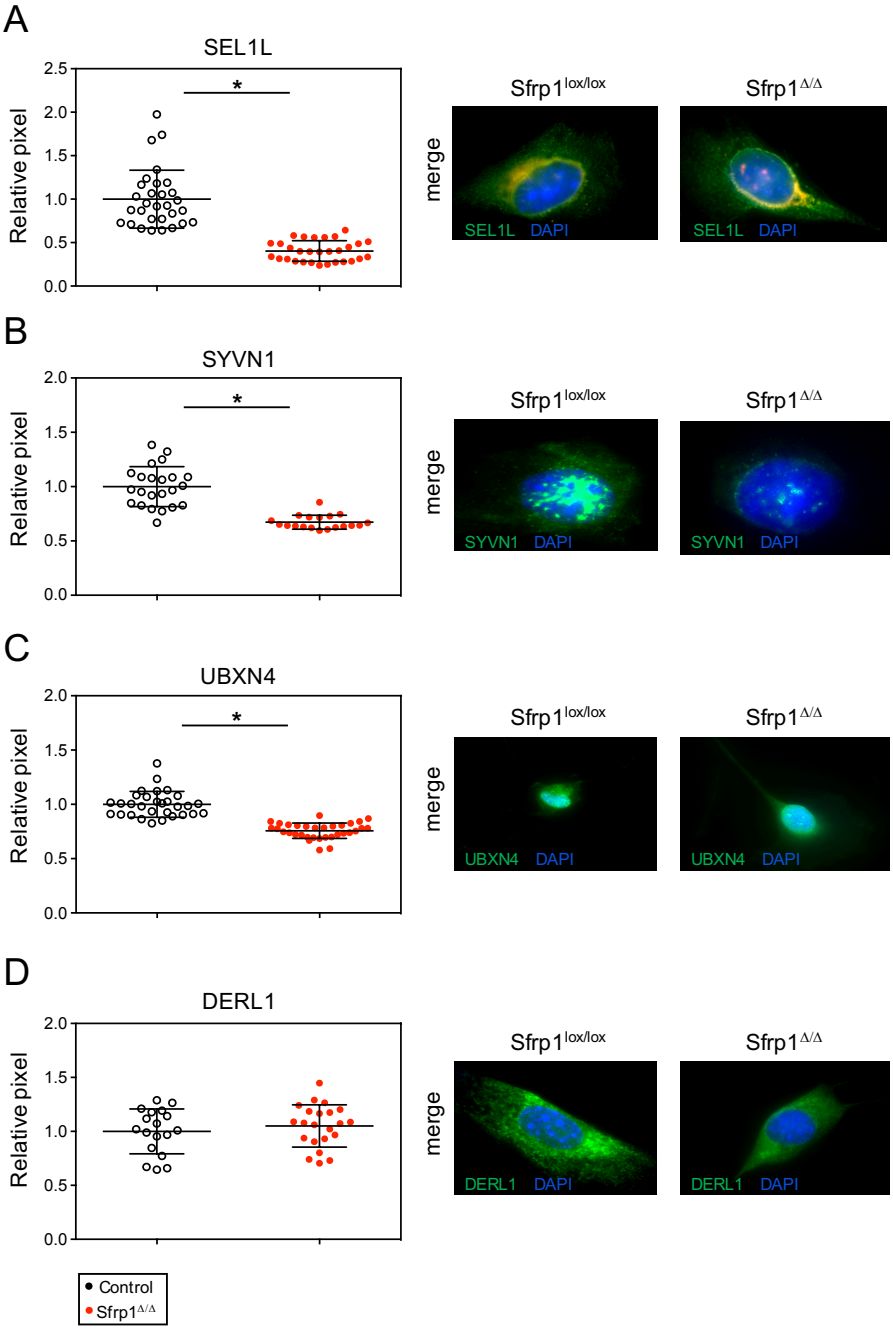

Figure 76. Protein content of SEL1L, UBXN4, SYVN1 and DERL1 in MSCs of *Sfrp1*$^{\Delta/\Delta}$ mice and the controls. (A) Left: SEL1L protein content as relative pixel number of MSCs from *Sfrp1*$^{\Delta/\Delta}$ (n = 30) and the controls (n = 30); Right: Representative immunofluorescence staining for the nuclei staining with DAPI in blue and SEL1L protein in green of MSCs from *Sfrp1*$^{\Delta/\Delta}$ and the controls. **(B)** Left: SYVN1 protein content as relative pixel number of MSCs from *Sfrp1*$^{\Delta/\Delta}$ (n = 20) and the controls (n = 23); Right: Representative immunofluorescence staining for the nuclei staining with DAPI in blue and SYVN1 protein in green of MSCs from *Sfrp1*$^{\Delta/\Delta}$ and the controls. **(C)** Left: UBXN4 protein content as relative pixel number of MSCs from *Sfrp1*$^{\Delta/\Delta}$ (n = 33) and the controls (n = 30); Right: Representative immunofluorescence staining for the nuclei staining with DAPI in blue and UBXN4 protein in green of MSCs from *Sfrp1*$^{\Delta/\Delta}$ and the controls. **(D)** Left: DERL1 protein content as relative pixel number of MSCs from *Sfrp1*$^{\Delta/\Delta}$ (n = 22) and the controls (n = 18); Right: Representative immunofluorescence staining for the nuclei staining with DAPI in blue and DERL1 protein in green of MSCs from *Sfrp1*$^{\Delta/\Delta}$ and the controls. Black dots represent controls (*Sfrp1*$^{lox/lox}$); Red dots represent *Sfrp1*$^{\Delta/\Delta}$. Each dot represents a cell. Represented values are illustrated as Mean ± SD. * p-value ≤0.05 show significant differences in the comparison of *Sfrp1* deficient mice (*Sfrp1*$^{\Delta/\Delta}$) to controls (*Sfrp1*$^{lox/lox}$) determined by unpaired t test.

5. Discussion

In this thesis, I show that deletion of *Sfrp1* in *Sp7*-expressing osteolineage cells has profound effects on HSC numbers and function during steady-state maintenance as well as under stress conditions. The effects of *Sfrp1* are found in all major cellular behaviors: proliferation, differentiation, and survival. I found that *Sfrp1* expressed by the microenvironment is required for the repopulating activity and optimal proliferation of single LT-HSCs, and that without *Sfrp1*, HSCs are prone to p300-dependent differentiation. Most importantly, HSC behavior can be rescued by short *in vivo* treatment with the PP2A/PR72 inhibitor IQ-1, showing deregulation of PP2A/PR72-mediated regulation of the CTNNB1/p300 WNT enhanceosome. In addition, I could show that SFRP1 deficiency induced alterations in the bone marrow niche which enable development of BCR-ABL^{+} lymphoblastic leukemia in juvenile animals. In gene expression studies aimed at delineating possible underlying mechanisms of altered hematopoietic support from niche cells, it was found that osteolineage *Sfrp1* expression is required to maintain endoplasmic reticulum (ER)-associated processes, immune processes, and cytokine production.

5.1. Establishment of a method for studying HSC maintenance and expansion *ex vivo*

To study behavior of single HSCs, a first aim of this thesis was to establish single cell cultures and to identify additional stromal cell sources maintaining HSC number and activity in culture. Such an experimental model would facilitate the study of mechanisms and conditions that support the expansion of transplantable HSCs as well as enable targeting of defective HSCs in therapeutic settings.

In previous work, we found that the UG26-1B6 cell line was able to maintain HSCs under non-contact conditions (Buckley et al., 2011; Oostendorp et al., 2005; Wohrer et al., 2014). However, UG26-1B6 bears the tsA58 temperature-sensitive large T antigen and is transformed in long-term culture. Thus, the cell line is usually not used past passage twelve (Oostendorp et al., 2002; Oostendorp et al., 2002a). In this thesis, I demonstrated that WT E13.5 MEF-CM with 2GFs (SCF and IL-11) and WT E13.5 MEF-CM with 4GFs (additionally NGF and Col1) support induction and propagation of cell division, as well as survival of WT HSCs (Marquez Romero et al., 2020). Interestingly, CM from *Sfrp1*$^{-/-}$ MEFs show decreased survival compared to WT-CM 2GFs or 4GFs, which indicates an effect of *Sfrp1*-regulated secreted factors on the survival of cells.

5.2. *Sfrp1* loss in osteoprogenitors and bone structure

In this thesis, I find that the loss of *Sfrp1* in the osteolineage cells in mice (*Sfrp1*$^{\Delta/\Delta}$) does not lead to external abnormalities, but *Sfrp1* mutant animals tended to show decreased body weight and size compared to their WT littermates (*Sfrp1*$^{lox/lox}$) independently of their gender. Davey et al. showed that Osx-Cre mice had a decreased body weight at 6 weeks of age, compared to wild type controls. At 12 weeks of age the weight loss is adjusted (Davey et al., 2012). However, a comparison of the WT littermates at the age of 8 weeks showed no reduced body weight of the Osx-Cre mice compared to the *Sfrp1*$^{lox/lox}$. The characterization of the bone homeostasis of the *Sfrp1* deficient mice demonstrated a loss of 22-35 % of the bone volume in the cortical bone compared to control mice. Furthermore, the male *Sfrp1*$^{\Delta/\Delta}$ mice show reduction of about 20 % of CTX-I serum levels. The trabecular parameters and the numbers of both osteoclasts and osteoblasts as well as the serum marker P1NP were unchanged in *Sfrp1*$^{\Delta/\Delta}$ mice. All in all, the results show changes in the cortical bone in the *Sfrp1*$^{\Delta/\Delta}$ mice, proposing this part of the bone may show alterations of bone stiffness.

The loss of the expression of SFRP1, as a WNT/ β-catenin signaling inhibitor results into an increase of the β-catenin level in the cytoplasm (Kawano & Kypta, 2003). β-catenin supports the self-renewal of embryonic stem cells causing decreased absolute numbers of progenitor cells (Reya et al., 2003). Therefore, a loss of SFRP1 could result in an increasing level of β-catenin, which leads to decreased numbers of progenitor cells and thereby has a negative influence on the bone homeostasis (Bodine et al., 2004; Satoh et al., 2006). The decreased differentiation of progenitor cells could lead to altered bone quality, which leads to a deceased body size and weight.

5.3. *Sfrp1* loss in osteoprogenitors alters the behavior of MSCs

MSCs are characterized as adherent, fibroblastic cells with the ability of multilineage differentiation in adipogenic, osteogenic and chondrogenic cells (Friedenstein, Chailakhyan, & Gerasimov, 1987; Friedenstein, Piatetzky, & Petrakova, 1966; Pittenger et al., 1999). We found that in *Sfrp1*$^{\Delta/\Delta}$ mice, the number of MSCs is decreased, but these cells show an increased fraction of cells in the S-phase of cell cycle and a higher potential to form colony forming units (CFU-Fs) in culture, which, however, tend to be smaller than in control MSCs. Furthermore, stromal cells grown *ex-vivo* show an increased senescence-associated β-galactosidase staining. Importantly, the CFU-F-derived stromal cells seem to be primed for adipogenic and osteogenic lineages, since both lineages are more easily formed than in control MSCs. Furthermore, the MSCs show an increased proliferative activity.

The smaller size of the CFU-F-derived colonies and the increased differentiation are both in line with the increased senescence we observed. Since SFRP1 is known as a WNT inhibitor, its deletion should promote WNT activation. This would be in line with the observation of increased numbers of MSCs in the S-phase, which could promote replicative senescence due to DNA damage during genomic replication in the S-phase of cell cycle (in analogy to HSCs) (Walter et al., 2015). Senescent cells are metabolically active cells but do not divide (Krizhanovsky et al., 2008). Our finding that *Sfrp1*-deficient MSCs tend to form more small CFU-Fs might be explained by *Sfrp1* deficient MSCs becoming more easily senescent. Indeed, our finding that these MSC express more senescence-associated β-galactosidase activity (Dimri et al., 1995), is in line with this hypothesis.

With regard to differentiation, *Sfrp1*$^{\Delta/\Delta}$ MSCs show reduced osteogenesis and increased adipogenic potential under non-induced conditions, which is similar to observations of MSCs from aged animals or human individuals (Moerman et al., 2004; Muraglia, Cancedda, & Quarto, 2000; Ross et al., 2000; Wilson et al., 2010; Zheng et al., 2007). This observation suggests a curious uncoupling of osteo- and adipogenesis under non-induced and growth factor-induced differentiation in *Sfrp1*$^{\Delta/\Delta}$ MSCs. Thus, we hypothesize that *Sfrp1*$^{\Delta/\Delta}$ MSCs adopt an aging phenotype under non-induced conditions. The observation that under induction, both adipo- and osteogenic differentiation suggests that induction conditions may override aging-related changes in MSCs. This hypothesis should be tested in the future.

5.4. *Sfrp1* loss in MSCs reduces endoplasmic proteostasis

The *Sfrp1*$^{\Delta/\Delta}$ MSCs show alterations in their transcriptome compared to the *Osx1-GFP::Cre* controls that leads to the identification of 535 differently expressed genes (DEGs) comparing the two groups. The dysregulated expressions of these genes were involved in the `ERAD pathway´, `response to endoplasmic reticulum stress´, `with endoplasmic reticulum to cytosol transport´, `regulation of retrograde protein transport - ER to cytosol´, as well as the `ubiquitin-dependent and endoplasmic reticulum associated protein degradation (ERAD) pathway´. The endoplasmic reticulum (ER) is a cellular maintenance system regulating protein synthesis, protein transport, protein folding, protein quality, as well as other essential cellular events, like calcium (Ca^{2+}) storage and release, in eukaryotic cells. ER can be found as smooth (SER) and rough (RER) organelles, in which the RER is mostly involved in proteostasis and the communication with the Golgi apparatus (Meusser et al., 2005; Phillips & Voeltz, 2016; Rogers, 2020). Once misfolded proteins are detected in the ER lumen, these proteins are glycosylated and then recognized by the transmembrane ERAD complex, which eliminates these selected proteins by a translocation process and targeting by the cytoplasmic ubiquitin-VCP complex and the 26S proteasome (Ubiquitin-Proteasome System; UPS).

This process maintains cellular integrity by reducing ER stress (Lemus & Goder, 2014; Neal, Duttke, & Hampton, 2019). Reduced ERAD has been associated with aging of the brain (Sekiya et al., 2017), and our observations of *Sfrp1*$^{\Delta/\Delta}$ MSCs also suggest a connection between reduced ERAD and the observed aging-like phenotype.

The effect of *Sfrp1*-deletion on ERAD pathway opens the intriguing possibility that *Sfrp1* regulates ER-dependent cellular processes, such as vesicle transport, endocytosis and autophagy. The ERAD pathway is part of the unfolded protein response (UPR). Intriguingly, genes that we validated (*Sel1l*, *Syvn1*) are known targets of the UPR (Kaneko et al., 2007).

ERAD pathway consists of four different sub-processes: recognition, retro-translocation, ubiquitination and degradation (Figure 77). The differentially downregulated ER Degradation Enhancing α-Mannosidase-like protein (EDEM) removes a mannose from misfolded glycoproteins, which promotes the binding of membrane associated receptors, such as OS9 and Derlin (DERL1) (Groisman et al., 2011). The 26S proteasome is located in the cytosol. Therefore, to be degraded, the misfolded proteins need to be retro-transported into the cytoplasm. For this purpose, ERAD includes a retro-transport complex, consisting of the adaptor protein Suppressor/Enhancer of Lin-12-like (SEL1L) and the E3 ligase hydroxymethylglutaryl reductase degradation protein 1 (HRD1 or SYVN1) (Meusser et al., 2005; Sun et al., 2014). SEL1L is involved in several cellular processes, such as tumorigenesis of various cancer types (Biunno et al., 2006), stem cell differentiation (Cardano et al., 2011) and lipid metabolism (Sha et al., 2014). In HSCs, deletion of *Sel1l* led to their displacement from the niche and a complete loss of HSC identity, due to aggregation of the critical HSC receptor MPL in the ER (Xu et al., 2020). In MSCs, the adipogenic protein lipoprotein lipase (LPL) is retained in the ER and forms protein aggregates in the absence of SEL1L, which leads to hypertriglyceridemia (Péterfy et al., 2007; Sha et al., 2014). Several ERAD genes, including *Derl2* and *Syvn1*, are also involved in regulating bone homeostasis and bone diseases such as arthritis, due to faulty collagen matrix secretion (Dougan et al., 2011; Gao et al., 2008). Next, the misfolded proteins are ubiquitinated and the ubiquitin-binding factors valosin-containing protein (VCP/p97) is recruited to the misfolded protein by UBXN4 and ensure degradation by the 26S proteasome in the cytosol (Neuber et al., 2005; Schuberth & Buchberger, 2005).

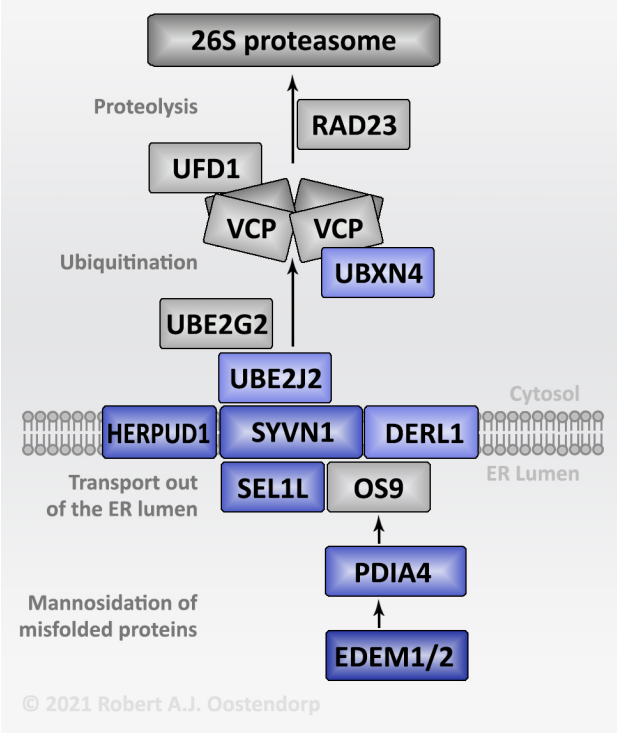

Figure 77. Endoplasmic reticulum associated protein degradation pathway. Misfolded proteins are marked by EDEM and recruited to the ERAD complex. The ERAD complex is formed by proteins like HERPUD1, SYVN1, DERL1, and SEL1L, which inserted the misfolded proteins across the ER membrane. During translocation, the misfolded proteins are poly-ubiquitylated. Afterwards, the ubiquitylated misfolded proteins are transported by the VCP-UBXN4 complex to the 26S proteasome for degradation.

Alternatively, Lee et al. demonstrated that misfolded proteins in the cytoplasm can also be secreted into the extracellular milieu via the misfolding-associated protein secretion (MAPS) pathway (Lee et al., 2016). Together, reported findings and findings reported in this thesis support a role for ERAD downregulation in aging-like skeletal deregulation, possibly by deregulating proteostasis of critical receptors, secreted WNT factors, and extracellular matrix proteins.

To further confirm the aberrant ERAD pathway, I would suggest to stain announced downregulated proteins on bone slices. Furthermore, to further study the involvement of *Sfrp1*-deletion and ERAD down-modulation in MSCs in secretory pathways, analysis of misfolded proteins in the extracellular milieu by secretome protein enrichment would be helpful. For instance, secretome delineation with click sugars (SPECS) method (Kuhn et al., 2012) would be a possible confirmatory strategy in this respect.

The RNAseq did not give clues to the mechanism of the transcriptional down-regulation of *Edem1*, *Sel1l*, *Syvn1*, or *Ubxn4* by the loss of *Sfrp1*. So far, there is no specific knowledge about the interaction of SFRP1 and ER and/or the ERAD pathway.

We could speculate, though, since secreted SFRP1 is an inhibitor of the WNT/ β-catenin signaling pathway and β-catenin levels are controlled through ubiquitination and the proteasome, that β-catenin might be cross-regulated by ERAD components, particularly through the cytosolic ubiquitination machinery, including UBE2J1/2 and UBXN4, which are both modulated by *Sfrp1* deletion in MSCs. Indeed, it was reported that GSK3β, and both α- and β-catenin were regulated through ERAD upon ER stress (thapsigargin and tunicamycin treatment) in HeLa cells (Fabre et al., 2019). Thus, a potential additional layer of SFRP1-mediated regulation could be the modulation of canonical WNT signaling in osteolineage niche cells through ERAD machinery.

It has been reported that ERAD is an important part of the secretory pathway (Meusser et al., 2005). In the WNT pathway, WNT factors are transported to the plasma membrane by the WNT receptor EVI (WLS/GPR177) after a posttranslational modification, such as N-glycosylation and lipidation/acylation at the ER (Azbazdar et al., 2021; Glaeser et al., 2018; Gradilla et al., 2018). It was further shown that ERAD ubiquitinates EVI through UBE2J2 in the absence of WNT ligands in a VCP-dependent manner and that EVI is stabilized in the presence of WNT ligands (Glaeser et al., 2018). Additionally, Wolf et al. identified the interaction of the VCP-binding proteins FAF2 and UBXN4 with EVI, as well as the ubiquitination of EVI through ERAD is linked to ERLIN2. They further showed that SEL1L had a variable or weak effects in the degradation of EVI, but, the knock-down of ERLIN2, FAF2, UBXN4 increased EVI protein levels, again stressing the importance of the VCP complex (Wolf et al., 2021).

Therefore, the data presented in this thesis support the hypothesis that when SFRP1 is present, EVI (WLS) is ubiquitinated and degraded through ERAD. Whereas, in the absence of SFRP1, UBXN4 is down-modulated, and, as a consequence, EVI is stabilized, possibly enabling increased transport and secretion of WNT factors. Therefore, the influence of the SFRP1 loss in the secretome of stromal cells, and on possible protein levels of EVI should be studied further.

5.5. *Sfrp1* loss in stromal cells influence the hematopoietic cell behavior

In our *Sfrp1*$^{\Delta/\Delta}$ model, we analyzed whether and how the deletion of *Sfrp1* in osteoprogenitors affected hematopoiesis and the HSCs. Since the gene is only deleted in the stromal cell compartment, any change in behavior of these cells is a secondary effect to the primary deletion of *Sfrp1* in osterix^{+} stromal cells and their progeny. The BM microenvironment controls the functional behavior of HSCs, including self-renewal (S), maturation (M, differentiation), apoptosis (A), resting (R, quiescence), and trafficking (T, migration), which is also known as “SMART” properties (Cheng, 2008).

In *Sfrp1*$^{\Delta/\Delta}$ mice, we identified no strong effects on the number of mature cell subpopulations in either PB or BM. This result differs from analyses of the *Sfrp1*$^{-/-}$ mice, where both CD45R/B220 and GR1^{+} populations were significantly affected (Renström et al., 2009). The difference in findings between *Sfrp1*$^{\Delta/\Delta}$ and *Sfrp1*$^{-/-}$ mice could be caused by the different backgrounds in the two mouse models (*Sfrp1*$^{-/-}$: 129S2xC57BL/6.J; *Sfrp1*$^{\Delta/\Delta}$: C57BL/6.J). Alternatively, in the *Sfrp1*$^{\Delta/\Delta}$ mice, the loss of SFRP1 and its deleterious effects on B-cell and myeloid maturation could be compensated by other *Sfrp1*-expressing populations.

In the most immature SCA-1^{+} ST-HSCs and LT-HSCs, we found no significant changes in the BM of *Sfrp1*$^{\Delta/\Delta}$ mice, which was similar to findings in *Sfrp1*$^{-/-}$ animals. But, SCA-1^{-} myeloid progenitors (MP) were decreased in *Sfrp1*$^{\Delta/\Delta}$ and *Sfrp1*$^{-/-}$ mice (Renström et al., 2009). This result suggests that the deficient transition of LT-HSC to MPs in *Sfrp1*$^{-/-}$ mice, might depend on loss of *Sfrp1* expression in osteolineage cells. This idea is strengthened by the finding, that LT-HSCs from *Sfrp1*$^{\Delta/\Delta}$ mice fail to repopulate WT recipients with complete loss of the regeneration of the stem cell compartment. Thus, our experiments suggest that LT-HSCs from *Sfrp1* deficient mice are already damaged prior to their transplantation, which is confirmed by the observation of increased DNA damage, and slow-proliferation with increased differentiation in the single cell culture assay.

We were intrigued by the latter observation that the LT-HSC from *Sfrp1*$^{\Delta/\Delta}$ mice proliferate less and show more differentiation *in vitro*. It has previously been reported that the balance between differentiation and proliferation is governed by the WNT/β-catenin enhanceosome pairing with either CBP (proliferation) or p300 (differentiation) (Rebel et al., 2002; Teo & Kahn, 2010; Teo et al., 2005). Interestingly, in LT-HSCs from *Sfrp1*$^{\Delta/\Delta}$ mice, the protein content of both CTNNB1 and p300 was increased, while CBP content was not affected, suggesting the formation of a p300-containing enhanceosome would be facilitated simply because more p300 was present. Miyabayashi et al. have demonstrated that specific IQ-1 inhibitor prevents the interaction of β-catenin with p300, by targeting the PR72/130. Since PR72/130 is a subunit of the serine/threonine phosphatase PP2A, this phosphatase is an additional important regulator of the WNT enhanceosome. They further showed that the PKC-dependent phosphorylation of p300 Ser-89 is important to increase the β-catenin/p300 interaction, which then increases differentiation not only in ES cells (Miyabayashi et al., 2007), but also in teratocarcinoma cells (Ugai et al., 1999), alveolar progenitors (Rieger et al., 2016), and HSCs (Rebel et al., 2002).

We showed that IQ-1 increased the numbers of LSK cells and the increased potential to form more colonies *in vitro*. This leads us to the suggestion that with IQ-1 treatment, LT-HSCs from *Sfrp1*$^{\Delta/\Delta}$ mice show less production of mature cell types and more retention of more immature colony-forming activity in the absence of increased proliferation.

This could mean that perhaps in LT-HSC from *Sfrp1*$^{\Delta/\Delta}$ mice the subunit (PR72/130) reduces the serine/threonine phosphatase activity of PP2A towards p300. Thus, we propose that the PR72 subunit is a negative regulator of PP2A. Due to the increased expression of p300 and β-catenin, and in line with the observation that high levels of β-catenin induce differentiation of HSCs (Famili et al., 2016), we believe that more of its complex with β-catenin is formed and differentiation is the dominant behavior of LT-HSCs (Figure 78A). To confirm our hypothesis that p300 and β-catenin form more of its complex *in vivo,* further analyses are required. Therefore, an immunoprecipitation would be identifying β-catenin and differential CBP or p300 coactivator usage in the *Sfrp1*$^{\Delta/\Delta}$ mice.

IQ-1 inhibitor was shown to prevent the interaction of β-catenin with p300, by binding to the PR72/130 subunit of the PP2A. Thus, IQ-1 treatment modulates the activity of the PP2A/PR72 complex to decrease the content of phospho-p300 Ser-89 in the *Sfrp1* deficient mice. Subsequently, this would then reduce the p300 complex-mediated differentiation, by means of which the aberrant behavior of LT-HSC might be improved or even rescued completely (Figure 78B).

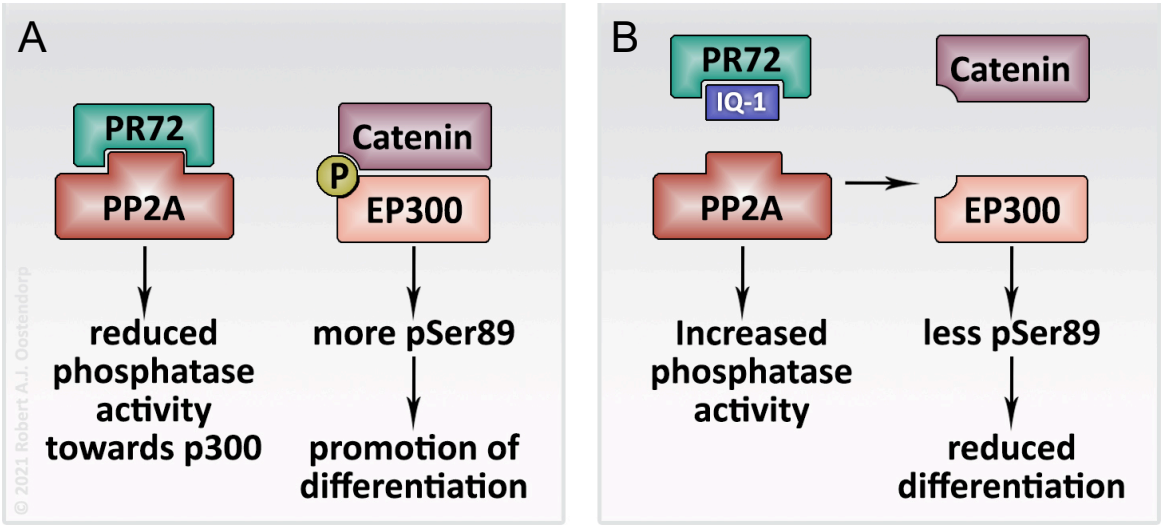

Figure 78. Hypothesis: IQ-1 treatment reduces the p300 complex-mediated differentiation. **(A)** PR72 down-modulates PP2A phosphatase activity towards p300, thereby promoting increasing the level of pSer89-p300 and its complex formation with β-catenin. The result of this would be increased differentiation. **(B)** Treatment with IQ1 inhibits binding of PR72 to PP2A, thereby increasing dephosphorylation of pSer-p300 and decreasing its binding to β-catenin with p300 restoring the balance between proliferation and differentiation in LT-HSC from the *Sfrp1* deficient mice.

We found that the LT-HSCs from *Sfrp1*$^{\Delta/\Delta}$ mice, the content of pSer89-p300 was increased compared to the controls. In line with our hypothesis shown in Figure 78B, pSer-p300 was decreased after *in vivo* IQ1 treatment. Importantly, IQ-1 treatment restored the long-term repopulating ability of LT-HSCs from *Sfrp1*$^{\Delta/\Delta}$ mice in primary, as well as secondary WT recipients, which indicates that IQ-1 restores the function of LT-HSCs.

To understand how IQ-1 restores long-term repopulating of the LT-HSCs and how p300 regulation is involved in this process further investigation need to be performed. A first step, would be assessing the gene expression levels of the *Sfrp1*$^{\Delta/\Delta}$ animals compared to the controls with and without IQ-1 treatment, as well as the additional study of differences in marrow homing capacity of the transplanted HSCs and localization of the LT-HSCs.

In conclusion, our results support the hypothesis that *Sfrp1* deficiency in osterix-positive stromal cells, indirectly cause HSC dysfunction with increased differentiation. Our results further support the view that differentiation is controlled at least in part by the phosphorylation status of p300 at Serine 89. We propose that treatment with IQ-1 inhibits preferred binding of β-catenin with p300 to re-establish the balanced proliferation and differentiation of LT-HSCs. In this manner, IQ-1 treatment rescues repopulating cell function of impaired HSCs from mice showing deletion of *Sfrp1* in osterix-positive cells.

5.6. Loss of *Sfrp1* in the stromal cells in response to LPS stimulation

As described above, in *Sfrp1*$^{\Delta/\Delta}$ mice, a reduction in MSCs was observed. However, these MSCs show increased S-phase and CFU-F formation, as well as cellular senescence. These changes in the MSCs could have an impact on two major hematopoietic niche functions: forming hematopoietic microenvironment for immune cell development (Szade et al., 2018) and modulating the activity of already formed immune cells (Bernardo & Fibbe, 2013).

In this thesis, the response to bacterial infections was simulated using lipopolysaccharide (LPS) treatment of *Sfrp1*$^{\Delta/\Delta}$ mice and control animals. LPS, a main component of gram-negative bacteria, can cause septic shock and dysfunctions of the heart (Kawai & Akira, 2010; Yücel et al., 2017) though activation of the Toll-like receptor 4 (TLR4) in innate immune cells (Farhana & Khan, 2021; Kawai & Akira, 2010). In early hematopoiesis, prolonged exposure to low doses of LPS, strongly reduces LT-HSC function (Esplin et al., 2011).

In our experiments, a single LPS treatment did not alter cell populations in the PB and BM in the *Sfrp1*$^{\Delta/\Delta}$ mice and control animals after 24 h. Tak et al. described a decreased number of monocytes after 1 - 1.5 h of LPS treatment, but an increased after 6 - 8 h of LPS treatment (Tak et al., 2017). In addition, pro-inflammatory IL-6 and MCP-1 in the peripheral blood of *Sfrp1*$^{\Delta/\Delta}$ mice and controls were unchanged 24 h after LPS, indicating no early deviations in the immune system reaction to the LPS treatment. These results suggest that deletion of *Sfrp1* from Osterix^{+} cells of the BM does not alter the early systemic response in cytokines or mature hematopoietic cells to LPS treatment.

In contrast in the BM, we found a decreasing trend in the numbers of all immature populations (LSKs, ST-HSCs, LT-HSCs, as well as in the MPs), showing reduced initiation of emergency hematopoiesis. On a functional level, LT-HSCs isolated 24 h from the BM of *Sfrp1*$^{\Delta/\Delta}$ animals after LPS treatment showed a significant additional reduction in PB engraftment over the entire observation period of 24 weeks. Our results agree with the results in a sepsis murine mouse model, where the function of the stem cells show also a change behavior by decreased repopulating activity and decrease in cell cycle activity (Rodriguez et al., 2009), suggesting reduced self-renewal capacity. However, the reduction of engraftment activity after LPS treatment was similar in both control and *Sfrp1*$^{\Delta/\Delta}$ animals, indicating the additional reduction by LPS did not depend on *Sfrp1* expression.

To sum up our results so far, although the loss of *Sfrp1* in the microenvironment strongly affects hematopoiesis and LT-HSCs from *Sfrp1*$^{\Delta/\Delta}$ mice show decreased engraftment *in vivo*, our results do not favor the view that the early response to LPS depends on *Sfrp1* expression in the BM niche.

5.7. Loss of *Sfrp1* in the stromal cells enable development of malignant cells

Several investigators have shown that SFRP1 acts as a tumor suppressor (Finch et al., 1997; Huang et al., 2007). In addition, *SFRP1* expression was found to be inactivated by epigenetic silencing or chromosome deletions in different kinds of leukemic disease, such as AML, ALL, CLL and MDS (Jost et al., 2008; Liu et al., 2006; Reins et al., 2010; Román-Gómez et al., 2007). In previously unpublished studies from our laboratory, we found that *Sfrp1*$^{-/-}$ recipients suffer from a noticeably more severe leukemia phenotype with lymphoma characteristics as the WT controls. Additionally, secondary transplantation of malign cells from diseased primary animals showed a transformation of the leukemic phenotype (Kehr, 2016).

In experiments designed to discern whether *Sfrp1* expression in osterix^{+} cells were responsible for the more severe leukemia/lymphoma phenotype, we found that *Sfrp1* deficiency in the recipient niche accelerated the development of leukemia from a low dose of BCR-ABL-expressing cells, with an almost ten-fold increase in LSC compared to control recipients as determined by limiting-dilution (Figure 68). A contributing factor in this respect, could be that diseased *Sfrp1*$^{\Delta/\Delta}$ recipients show an increased systemic level of the inflammatory cytokines IL-6, MCP-1, and TNF. These findings indicate that hematopoietic malignancy in mice with a *Sfrp1*-deficient microenvironment is associated with systemic inflammation. This observation agrees well with literature reports that inflammation affects the functions of MSCs (Leimkühler & Schneider, 2019).

It has been shown, that inflammatory cytokines secreted by MSCs have an effect on the differentiation of HSCs and more differentiated cells, like macrophages (Leimkühler & Schneider, 2019). Macrophages indirectly support HSCs through the regulation of MSCs (Ehninger & Trumpp, 2011; Winkler et al., 2010). The loss of macrophages in the bone marrow causes HSCs to egress their microenvironment (Winkler et al., 2010). Therefore, studying how BCR-ABL$^+$ cells induce systemic inflammation, and how the innate immune cells, such as macrophages are affected in steady-state conditions and after LPS stimulation of the *Sfrp1*$^{\Delta/\Delta}$ animals, could provide further insights into how to prevent HSC exhaustion and development of malignancies.

Interestingly, similar to the *Sfrp1*$^{-/-}$ animals previously studied by our laboratory, the majority of the diseased *Sfrp1*$^{\Delta/\Delta}$ animals not only develop the characteristic leukemic splenomegaly, but also lymph node tumors, suggestive of lymphoma (Frederiksen et al., 2013; Ward, 2006), which was only rarely observed in control recipients. Although Groffen et al. assumed that the BCR-ABL fusion oncogene is restricted to the hematopoietic leukemia (Groffen et al., 1993), Pathak et al. demonstrated that by mechanisms ascribed to BCR-ABL, cyclin D1 can be upregulated to drive B-cell lymphomagenesis (Mitani et al., 1990; Pathak et al., 2017). The observation that *Sfrp1*-deficiency drives a more lymphoma-type disease from BCR-ABL positive cells is intriguing and suggests that the BM microenvironment has a role in determining the type of disease developing from already transformed cells. In the case of SFRP1, it may be of significance that SFRP1 is known to inhibit lymphopoiesis through the WNT/ β-catenin pathway (Yokota et al., 2008). Furthermore, the total loss of *Sfrp1* in *Sfrp1*$^{-/-}$ mice resulted in an increase in CD45R/ B220 positive cells in the peripheral blood and BM *in vivo* (Renström et al., 2009). In contrast, an overexpression of SFRP1 decrease CD45R/ B220 positive cells *in vivo* (Yokota et al., 2015). Therefore, the loss of SFRP1 in the microenvironment could promote B cell lymphopoiesis and leukemia. It remains to be studied, whether an increase of B-lymphopoiesis favors the formation of BCR-ABL$^+$ B lymphoma in *Sfrp1*$^{\Delta/\Delta}$ animals, or whether increased trafficking of BCR-ABL$^+$ B progenitors into lymph nodes is a possibility. The classification of the immunophenotype of B cell leukemia and lymphoma is challenging (Loghavi, Kutok, & Jorgensen, 2015; Morse et al., 2002). Therefore, the extended analysis of lymph nodes, as well as a peripheral blood (PB) smear is required.

All in all, this thesis describes an intriguing switch of leukemia to lymphoma in B-ALL in *Sfrp1*$^{\Delta/\Delta}$ animals. However, to interrogate mechanisms involved, further classification of the phenotype from the diseased *Sfrp1* deficient mice, further analyses of all samples from the *Sfrp1*-deficient mice compared to the control groups (pMIG, *Sfrp1*$^{lox/lox}$) is required. Nevertheless, our results confirm the function of a tumor suppressor of SFRP1 as described before (Finch et al., 1997; Huang et al., 2007).

Our results further suggest an additional contribution of increased proinflammatory cytokines IL-6, MCP-1 and TNF in serum from $p185^{BCR-ABL}$ leukemic *Sfrp1*$^{\Delta/\Delta}$ mice compared to the non-leukemic control recipients. TNF-α and IL-6 are proinflammatory cytokines that occur in the first phase of an inflammation. TNF-α is an important attractant for neutrophils and can increase their phagocytic activity and cytotoxicity (Moxey-Mims et al., 1991). TNFα modulates the expression of many other proteins, including IL-6 (Bonavida, 1991; Brouckaert et al., 1993). IL-6 can extend the lifespan of neutrophils (Biffl et al., 1995; Lesur et al., 2000). In other experiments, we observed that neutrophils from *Sfrp1*$^{\Delta/\Delta}$ animals phagocytize *E. coli* - FITC particles at a much-reduced efficiency than controls. It remains to be established how the reduced phagocytic activity of *Sfrp1*$^{\Delta/\Delta}$ neutrophils connects to the increased severity of leukemia and the formation of the lymphoma subtype in these animals.

All in all, the dysfunction of the BM niche is detected in BCR-ABL$^+$ malignancies in a malignancy-dependent manner (Schepers et al., 2015). Our results strongly support a role for *Sfrp1* expression in osteolineage niche cells by not only increasing disease severity, but also through a switch to a lymphoma phenotype associated with increased expression of IL-6, MCP-1, and TNF with an associated decrease in phagocytic function of neutrophils. The mechanisms tying these observations together still need to be deciphered and will be studied in future projects. What will be an interesting issue to study in these future studies is the involvement of the WNT enhanceosome in development of hematopoietic malignancy. Although He et al. showed that the IQ-1 treatment supports the development of cancer cells into a cancer cell subpopulation with a drug resistance and highly tumorigenicity (He et al., 2014), it may be possible to slow the malignant transformation of HSCs to leukemic stem cells in the *Sfrp1*$^{\Delta/\Delta}$ animals with a IQ-1 pretreatment prior to the development of lethal disease. A dysfunction of HSCs can lead to a malignant transformation (Yamashita et al., 2020). Our results suggest, that the loss of *Sfrp1* in stromal cells, indirectly cause HSC dysfunction with increased differentiation. Our results thus indirectly suggest that differentiation may be required for malignancy development, a principle that was previously reported in models of MLL-AF9$^+$ or MOZ-TIF2$^+$ leukemia (Ye et al., 2015). In the latter models, differentiation through C/EBPα was required for the initial steps in leukemia development. Interestingly, C/EBPα is a direct acetylation substrate of p300 (Zaini et al., 2018) and acetylation of C/EBPα inhibits granulopoiesis (Bararia et al., 2016). These results suggest that p300 may increase differentiation while bound to β-catenin, and suggests that β-catenin may stimulate p300-mediated acetylation of substrates like C/EBPα. Thus, treatment of the *Sfrp1*$^{\Delta/\Delta}$ mice with IQ-1 prior to (overt) leukemia development (pre-leukemia) could prevent or slow down the transformation into LSCs.

6. Summary

It is known that hematopoietic stem cells (HSCs) lose their functionality over time. In parallel, increased DNA damage and differentiation can be observed and also, for example, self-renewal of stem cells is decreasing. Different niche cell populations keep stem cells dormant, limit their activation and prevent the stem cells from becoming exhausted. The interaction between hematopoietic stem cells and their microenvironment have remained poorly understood.

The previous work of the group of Prof. dr R. A. J. Oostendorp showed that if the niche is deregulated, HSCs are activated and, for example, *Sfrp1* knock-out environment fails to support the regeneration of hematopoietic stem cells with serial to repopulate secondary recipients (Renström et al., 2009). In this thesis, the role of the secreted molecule SFRP1 from the microenvironment was investigated in terms of the cellular components that are involved in HSCs regulation under normal and stress conditions like inflammation and leukemia.

In order to dissect cell specific requirements of the *Sfrp1* gene, the *Sfrp1*$^{lox/lox}$ mouse strain was established and *Sfrp1* gene was deleted in Osterix^{+} (Sp7) osteolineage cells. In the hematopoietic compartment of these mice, a decrease in myeloid progenitors (MPs) in the bone marrow (BM) was found. Although the number of primitive CD34^{-} CD48^{-} CD150^{+} HSCs (LT-HSCs) in the BM was unchanged, LT-HSCs from *Sfrp1*$^{\Delta/\Delta}$ mice failed to repopulate in wild type recipients. In single cell cultures, the LT-HSCs from *Sfrp1*$^{\Delta/\Delta}$ mice show decreased proliferation with concomitant increased differentiation into mature myeloid cells, which was associated with increased DNA damage as shown with comet assay and immunostaining for γH2A.X.

On a molecular level, it was found that LT-HSCs from *Sfrp1*$^{\Delta/\Delta}$ mice show increased β-catenin protein levels. β-catenin regulates cell differentiation and proliferation of stem cells by binding to p300 or CBP respectively (Miyabayashi et al., 2007). Interestingly, CBP protein level was unchanged in LT-HSCs from *Sfrp1*$^{\Delta/\Delta}$ mice while p300 was increased, suggesting over activation of the β-catenin/p300 complex. Indeed, blocking β-catenin/p300 binding, with specific PP2A inhibitor IQ-1, rescued not only the aberrant behavior of *Sfrp1*$^{\Delta/\Delta}$ LT-HSC *in vitro*, but also the repopulating activity of these LT-HSCs *in vivo* was restored. The results suggest that deletion of stromal SFRP1 diminishes the repopulating activity of LT-HSCs by increasing differentiation through PP2A-mediated dephosphorylation of the phospho-p300-binding site with β-catenin (Hettler et al., 2020).

Since the primary defect in *Sfrp1*$^{\Delta/\Delta}$ mice is the deletion of *Sfrp1* in osteolineage cells, it is questionable which changes in niche cells could be responsible for the observed hematopoietic defects in these mice. First analyses showed that the number of BM mesenchymal stromal cells (MSCs) is reduced, but these cells show an increased proportion of colony forming units (CFU-Fs). Furthermore, MSCs grown *ex-vivo* show increased senescence-associated β-galactosidase staining and spontaneous differentiation into adipocytes. These findings indicate altered functionality of MSCs from *Sfrp1*$^{\Delta/\Delta}$ mice. To connect the effect of primary *Sfrp1* deletion in niche cells and secondary hematopoietic decline, the transcriptome was analyzed and compared from primary sorted BM MSC. This analysis showed 208 genes to be significantly downregulated and 327 upregulated genes. Gene ontology analyses showed deregulation of endoplasmic reticulum (ER)-associated processes, immune processes, and cytokine production. Protein expression validation of some genes showed good correlation between transcriptome and protein expression for these genes. Thus, the results show deregulated expression of genes in BM MSCs from *Sfrp1*$^{\Delta/\Delta}$ mice, that could form the basis of the hematopoietic defects found in these mice.

The loss of SFRP1 in the microenvironment resulted in MSC loss, increased proliferation and differentiation, as well as cellular senescence. This could have an impact on a major function of niche, namely, modulating the activity of immune cells, which were studied by triggering immune response with Lipopolysaccharide (LPS) treatment of *Sfrp1*$^{\Delta/\Delta}$ mice and control animals. The control and *Sfrp1*$^{\Delta/\Delta}$ mice were treated with 1000 ng of LPS and 24 hours later the inflammatory molecules in peripheral blood (PB) were analyzed with cytokine beads assay. *Sfrp1*$^{+/\Delta}$ mice displayed dramatic increase of the inflammatory cytokine IL-6. In the BM, *Sfrp1*$^{\Delta/\Delta}$ niche cells spontaneously differentiate into adipocytes, and show increased senescence after passaging. But, short 24 hours after LPS treatment does not further affect niche cells from *Sfrp1*$^{\Delta/\Delta}$ mice.

Since aberrations in the microenvironment might contribute to leukemogenesis, it was determined how BCR-ABL induced leukemic cells disrupt the function of the niche. A clear difference in survival was observed. None of control animals became diseased after 350 days post transplantation, but all *Sfrp1*$^{\Delta/\Delta}$ mice died within 280 days. All diseased animals developed splenomegaly with an increase in weight and cell number. Infiltrations were also found in the lymph nodes in 6 out of 11 *Sfrp1*$^{\Delta/\Delta}$ mice.

In summary, the results demonstrate that secreted protein SFRP1 in the microenvironment is essential for the repopulating activity of hematopoietic stem cells via PP2A-mediated regulation of β-catenin/p300 and it can be shown that SFRP1 deficiency induced alterations in the bone marrow niche that enable the development of malignant cells.

7. Zusammenfassung

Es ist bekannt, dass hämatopoetische Stammzellen (HSZs) mit der Zeit ihre Funktionalität verlieren. Parallel dazu sind vermehrt DNA-Schäden und Differenzierungen zu beobachten und es nimmt auch beispielsweise die Selbsterneuerung von Stammzellen ab. Verschiedene Nischenzellpopulationen halten Stammzellen ruhend, begrenzen ihre Aktivierung und verhindern, dass die Stammzellen erschöpft sind. Die Interaktion zwischen hämatopoetischen Stammzellen und ihrer Mikroumgebung ist noch wenig verstanden.

Die bisherige Arbeit der Gruppe von Prof. dr R. A. J. Oostendorp zeigte, dass bei Deregulierung der Nische HSZs aktiviert werden und beispielsweise die *Sfrp1*-Knockout-Umgebung die Regeneration von hämatopoetischen Stammzellen mit seriellen zu repopulierenden sekundären Empfängern nicht unterstützt (Renström et al., 2009). In dieser Arbeit wurde die Rolle des sezernierten Moleküls SFRP1 aus der Mikroumgebung in Bezug auf die zellulären Komponenten untersucht, die an der HSZ-Regulation unter normalen und Stressbedingungen, wie Entzündungen und Leukämie, beteiligt sind.

Um die zellspezifischen Anforderungen des *Sfrp1*-Gens zu analysieren, wurde der *Sfrp1*$^{lox/lox}$-Mausstamm etabliert und das *Sfrp1*-Gen in Osterix^{+} (Sp7) Osteolineage-Zellen deletiert. Im hämatopoetischen Kompartiment dieser Mäuse wurde eine Abnahme der myeloischen Vorläufer (MVs) im Knochenmark (KM) gefunden. Obwohl die Anzahl der primitiven CD34^{-}CD48^{-}CD150^{+}-HSZs (LT-HSZs) im KM unverändert war, konnten sich LT-HSZs von *Sfrp1*$^{\Delta/\Delta}$ Mäusen nicht in Wildtyp-Empfängern repopulieren. In Einzelzellkulturen stellte sich heraus, dass LT-HSZs der *Sfrp1*$^{\Delta/\Delta}$ Mäuse eine verminderte Proliferation mit gleichzeitig erhöhter Differenzierung in reife myeloische Zellen zeigen, was mit einer erhöhten DNA-Schädigung verbunden war, wie durch einen Kometen-Assay und eine Immunofärbung für γH2.AX belegt wurde. Auf molekularer Ebene ergab sich, dass die LT-HSZs der *Sfrp1*$^{\Delta/\Delta}$ Mäusen einen erhöhten β-catenin-Proteingehalt aufwiesen. β-catenin reguliert die Zelldifferenzierung und Proliferation von Stammzellen durch Bindung an p300 bzw. CBP (Miyabayashi et al., 2007). Interessanterweise war der CBP-Proteingehalt in LT-HSZs der *Sfrp1*$^{\Delta/\Delta}$ Mäusen unverändert, während der p300-Proteingehalt erhöht war, was auf eine Überaktivierung der β-catenin/p300-Bindung hindeutet. Tatsächlich wurde durch die Blockierung der β-catenin/p300-Bindung mit dem spezifischen PP2A-Inhibitor IQ-1 nicht nur das veränderte Verhalten der *Sfrp1*$^{\Delta/\Delta}$ LT-HSZ *in vitro* gerettet, sondern auch die Repopulationsaktivität dieser LT-HSZs *in vivo* wiederhergestellt. Die Ergebnisse legen nahe, dass die Deletion von stromalem SFRP1 die Repopulationsaktivität von LT-HSZs verringert, indem die Differenzierung durch PP2A-vermittelte Dephosphorylierung der Phospho-p300-Bindungsstelle mit β-catenin erhöht wird (Hettler et al., 2020a).

Da der primäre Defekt bei den *Sfrp1*$^{\Delta/\Delta}$ Mäusen die Deletion von *Sfrp1* in Osteolineage-Zellen ist, ist fraglich, welche Veränderungen in den Nischenzellen für die beobachteten hämatopoetischen Defekte bei diesen Mäusen verantwortlich sein könnten. Erste Analysen zeigten, dass die Zahl der KM-MSZs reduziert ist, diese jedoch einen erhöhten Anteil an koloniebildenden Einheiten (CFU-F) aufweisen. Darüber hinaus zeigen *ex-vivo* gezüchtete MSZs eine erhöhte Seneszenz-assoziierte-Galactosidase-Färbung und eine spontane Differenzierung in Adipozyten. Diese Ergebnisse weisen auf eine veränderte Funktionalität von MSCs bei *Sfrp1*$^{\Delta/\Delta}$ Mäusen hin. Um den Effekt der primären *Sfrp1*-Deletion in Nischenzellen und des sekundären hämatopoetischen Rückgangs zu verbinden, wurde das Transkriptom von primär sortierten KM-MSZs analysiert und verglichen. Diese Analyse zeigte, dass 208 Gene signifikant herunterreguliert und 327 Gene signifikant hochreguliert waren. Genontologische Analysen zeigten eine Deregulierung von endoplasmatischen Retikulum (ER)-assoziierten Prozessen, Immunprozessen und der Zytokinproduktion. Die Validierung der Proteinexpression einiger Gene zeigte eine gute Korrelation zwischen Transkriptom und Proteinexpression. Somit zeigen die Ergebnisse eine deregulierte Expression von Genen in KM-MSZs von *Sfrp1*$^{\Delta/\Delta}$ Mäusen, die die Grundlage für die bei diesen Mäusen gefundenen hämatopoetischen Defekte bilden könnten.

Der Verlust von SFRP1 in der Mikroumgebung führte zu MSZ-Verlust, erhöhter Proliferation und Differenzierung sowie zellulärer Seneszenz. Dies könnte einen Einfluss auf eine wichtige Funktion der Nische haben, nämlich die Modulation der Aktivität von Immunzellen, die untersucht wurden, indem eine Immunantwort mit Lipopolysaccharide (LPS)-Behandlung von *Sfrp1*$^{\Delta/\Delta}$ Mäusen und Kontrolltieren ausgelöst werden konnte. Die Kontroll- und *Sfrp1*$^{\Delta/\Delta}$ Mäuse wurden mit 1000 ng LPS behandelt und 24 Stunden später die Entzündungsmoleküle im peripheren Blut (PB) mit dem Cytokine-Bead-Assay analysiert. *Sfrp1*$^{+/\Delta}$ Mäuse zeigten einen dramatischen Anstieg des entzündlichen Zytokins IL-6. Im KM differenzieren sich *Sfrp1*$^{\Delta/\Delta}$ Nischenzellen spontan zu Adipozyten und zeigen eine erhöhte Seneszenz nach mehreren Passagen. Jedoch beeinflusst die LPS-Behandlung die Nischenzellen der *Sfrp1*$^{\Delta/\Delta}$ Mäuse nicht weiter.

Da Veränderungen in der Mikroumgebung zur Leukämogenese beitragen könnten, wurde analysiert, wie BCR-ABL-induzierte Leukämiezellen die Funktion der Nische stören. Es wurde ein deutlicher Unterschied im Überleben beobachtet. Keines der Kontrolltiere erkrankte 350 Tage nach der Transplantation, aber alle *Sfrp1*$^{\Delta/\Delta}$ Mäuse starben innerhalb von 280 Tagen. Alle erkrankten Tiere entwickelten eine Splenomegalie mit Zunahme des Gewichts und der Zellzahl. Es wurden auch Infiltrationen in den Lymphknoten bei 6 von 11 *Sfrp1*$^{\Delta/\Delta}$ Mäusen gefunden.

Zusammenfassend zeigen die Ergebnisse, dass das sekretierte Protein SFRP1 in der Mikroumgebung über die PP2A-vermittelte Regulation von ß-catenin/p300 für die Repopulation von hämatopoetischen Stammzellen essentiell ist und es kann aufgezeigt werden, dass durch den SFRP1-Mangel induzierte Veränderungen in der Knochenmarknische die Entwicklung von malignen Zellen ermöglicht.

8. Appendices

8.1. List of Figures

8.2. List of Tables

9. Publications

Parts of this work have been published in the following peer-reviewed articles or are part of a submitted publication:

1. *Sandra Romero Marquez, ***Franziska Hettler**, Renate Hausinger, Christina Schreck, Theresa Landspersky, Lynette Henkel, Corinne Angerpointner, Ihsan E. Demir, Matthias Schiemann, Florian Bassermann, Katharina S. Götze, Rouzanna Istvánffy and Robert A.J. Oostendorp. (2020). Secreted factors from mouse embryonic fibroblasts maintain repopulating function of single cultured hematopoietic stem cells. *Haematologica*. doi:10.3324/haematol.2020.249102

*: SRM and FH co-first authors

2. Renate Hausinger, Marianne Hackl, Ana Jardon-Alvarez, Miriam Kehr, Sandra Romero Marquez, **Franziska Hettler**, Christian Kehr, Sandra Grziwok, Christina Schreck, Christian Peschel, Rouzanna Istvánffy, Robert A.J. Oostendorp. 2021). Cathepsin K maintains the compartment of bone marrow T lymphocytes in vivo. *Immun Inflamm Dis*, *9*(2), 521-532. doi: 10.1002/iid3.412.

Parts of this work were published in Conference Proceedings:

1. **Franziska Hettler**, Christina Schreck, Sandra Romero Marquez, Theresa Sippenauer, Franziska Koller, Ekin Demir, Florian Bassermann, Rouzanna Istvánffy, Robert Oostendorp. (2020). MICROENVIRONMENTAL SFRP1 REGULATES REPOPULATING ACTIVITY OF HEMATOPOIETIC STEM CELLS VIA PP2A-MEDIATED REGULATION OF CTNNB1/EP300. *ISEH - Experimental Hematology VIRTUAL*, Volume 88, Supplement, Page S31. Abstract: 2010. doi:https://doi.org/10.1016/j.exphem.2020.09.172.

2. **Franziska Hettler**, Christina Schreck, Sandra Romero Marquez, Theresa Sippenauer, Franziska Koller, Ekin Demir, Florian Bassermann, Rouzanna Istvánffy, Robert Oostendorp. (2020a). Stromales SFRP1 steuert das Verhalten von hämatopoetischen Stammzellen über die PP2A-vermittelte Regulation von CTNNB1 / EP300. *DGHO Jahrestagung 2020 VIRTUAL*, Abstract: 619. doi:https://www.oncoletter.ch/kongressberichte-live-webcasts/dgho-oegho-sgmo-und-sghssh-jahrestagung-2020-virtual/best-abstracts.html

10. Acknowledgments

Ich möchte mich bei allen bedanken, die einen Beitrag zu dieser Doktorarbeit geleistet haben.

Besonderer Dank gilt Herrn Prof. dr R. A. J. Oostendorp. Er gab mir für die Möglichkeit, dieses interessante und anspruchsvolle Thema im Rahmen meiner Dissertation im Labor für Stammzellphysiologie der III. Medizinischen Klinik & Poliklinik für Hämatologie und Onkologie am Klinikum rechts der Isar zu bearbeiten. Vielen Dank für die umfangreiche Unterstützung, Betreuung und wertvollen & lehrreichen Diskussionen. Ich schätze sein ständiges Feedback, seine Anleitung und seine Motivation für die Projekte sehr.

Ich danke meinem Zweitgutachter Dr. Matthias Heinig für die wertvollen wissenschaftlichen Diskussionen, Sie hatten großen Einfluss auf den Fortschritt und Erfolg meiner Projekte.

Ebenfalls möchte ich mich bei meinen Kolleginnen aus meiner Arbeitsgruppe von Robert A. J. Oostendorp für die äußerst harmonische Arbeitsatmosphäre, große Unterstützung und ständige Hilfsbereitschaft bedanken. Mein besonderer Dank geht hier vor allem an Dr. Rouzanna Istvánffy, Sandra Romero Marquez, Dr. Christina Schreck, Theresa Landspersky und Renate Hausinger die mir immer mit einem guten Rat zur Seite standen. Vielen Dank auch an das ganze Team aus der Trogerstraße 32.

Weiterhin danke ich meinen FreundInnen und besonders meiner Familie, vor allem meinen Eltern Heike und René Hettler, sowie meiner Schwester Lisa Hettler und meiner Oma Heidemarie Hettler, für ihre unermüdliche moralische Unterstützung während des Studiums, sie standen mir auch dann zur Seite, wenn ich ihnen die letzten Nerven raubte.

Ohne diese herzliche Unterstützung, wäre diese Arbeit nicht möglich gewesen.

11. References

Ackers, I., & Malgor, R. (2018). Interrelationship of canonical and non-canonical Wnt signalling pathways in chronic metabolic diseases. *Diab Vasc Dis Res, 15*(1), 3-13. doi:10.1177/1479164117738442

Agostino, M., & Pohl, S. (2019). Wnt Binding Affinity Prediction for Putative Frizzled-Type Cysteine-Rich Domains. *Int J Mol Sci, 20*(17). doi:10.3390/ijms20174168

Agostino, M., Pohl, S., & Dharmarajan, A. (2017). Structure-based prediction of Wnt binding affinities for Frizzled-type cysteine-rich domains. *J Biol Chem, 292*(27), 11218-11229. doi:10.1074/jbc.M117.786269

Aiello, F. B., Keller, J. R., Klarmann, K. D., Dranoff, G., Mazzucchelli, R., & Durum, S. K. (2007). IL-7 induces myelopoiesis and erythropoiesis. *J Immunol, 178*(3), 1553-1563. doi:10.4049/jimmunol.178.3.1553

Alsina-Sanchis, E., Mülfarth, R., Moll, I., Mogler, C., Rodriguez-Vita, J., & Fischer, A. (2021). Intraperitoneal Oil Application Causes Local Inflammation with Depletion of Resident Peritoneal Macrophages. *Mol Cancer Res, 19*(2), 288-300. doi:10.1158/1541-7786.Mcr-20-0650

Anthony, C. C., Robbins, D. J., Ahmed, Y., & Lee, E. (2020). Nuclear Regulation of Wnt/β-Catenin Signaling: It's a Complex Situation. *Genes (Basel), 11*(8). doi:10.3390/genes11080886

Araki, K., Imaizumi, T., Okuyama, K., Oike, Y., & Yamamura, K. (1997). Efficiency of recombination by Cre transient expression in embryonic stem cells: comparison of various promoters. *J Biochem, 122*(5), 977-982. doi:10.1093/oxfordjournals.jbchem.a021860

Asada, N., Takeishi, S., & Frenette, P. S. (2017). Complexity of bone marrow hematopoietic stem cell niche. *Int J Hematol, 106*(1), 45-54. doi:10.1007/s12185-017-2262-9

Audet, J., Miller, C. L., Eaves, C. J., & Piret, J. M. (2002). Common and distinct features of cytokine effects on hematopoietic stem and progenitor cells revealed by dose–response surface analysis. *Biotechnology and Bioengineering, 80*(4), 393-404. doi:https://doi.org/10.1002/bit.10399

Avantaggiati, M. L., Ogryzko, V., Gardner, K., Giordano, A., Levine, A. S., & Kelly, K. (1997). Recruitment of p300/CBP in p53-dependent signal pathways. *Cell, 89*(7), 1175-1184. doi:10.1016/s0092-8674(00)80304-9

Azbazdar, Y., Karabicici, M., Erdal, E., & Ozhan, G. (2021). Regulation of Wnt Signaling Pathways at the Plasma Membrane and Their Misregulation in Cancer. *Front Cell Dev Biol, 9*, 631623. doi:10.3389/fcell.2021.631623

Baccin, C., Al-Sabah, J., Velten, L., Helbling, P. M., Grünschläger, F., Hernández-Malmierca, P., Nombela-Arrieta, C., Steinmetz L. M., Trumpp, A., Haas, S. (2020). Combined single-cell and spatial transcriptomics reveal the molecular, cellular and spatial bone marrow niche organization. *Nat Cell Biol, 22*(1), 38-48. doi:10.1038/s41556-019-0439-6

Baharudin, R., Tieng, F. Y. F., Lee, L. H., & Ab Mutalib, N. S. (2020). Epigenetics of SFRP1: The Dual Roles in Human Cancers. *Cancers (Basel), 12*(2). doi:10.3390/cancers12020445

Bakker, S. T., & Passegué, E. (2013). Resilient and resourceful: genome maintenance strategies in hematopoietic stem cells. *Exp Hematol, 41*(11), 915-923. doi:10.1016/j.exphem.2013.09.007

Baksh, D., Boland, G. M., & Tuan, R. S. (2007). Cross-talk between Wnt signaling pathways in human mesenchymal stem cells leads to functional antagonism during osteogenic differentiation. *J Cell Biochem, 101*(5), 1109-1124. doi:10.1002/jcb.21097

Bannister, A. J., & Kouzarides, T. (1995). CBP-induced stimulation of c-Fos activity is abrogated by E1A. *Embo j, 14*(19), 4758-4762.

Bannister, A. J., Oehler, T., Wilhelm, D., Angel, P., & Kouzarides, T. (1995). Stimulation of c-Jun activity by CBP: c-Jun residues Ser63/73 are required for CBP induced stimulation in vivo and CBP binding in vitro. *Oncogene, 11*(12), 2509-2514.

Bararia, D., Kwok, H. S., Welner, R. S., Numata, A., Sárosi, M. B., Yang, H., Wee, S., Tschuri, S., Ray, D., Weigert, O., Levantini, E., Ebralidze, A. K., Gunaratne, J., Tenen, D. G. (2016) Acetylation of C/EBPα inhibits its granulopoietic function. *Nat Commun*, *7*, 10968. doi: 10.1038/ncomms10968

Barcellos-Hoff, M. H., Lyden, D., & Wang, T. C. (2013). The evolution of the cancer niche during multistage carcinogenesis. *Nat Rev Cancer, 13*(7), 511-518. doi:10.1038/nrc3536

Baryawno, N., Przybylski, D., Kowalczyk, M. S., Kfoury, Y., Severe, N., Gustafsson, K., Kokkaliaris, K. D., Mercier, F., Tabaka, M., Hofree, M., Dionne, D., Papazian, A., Lee, D., Ashenberg, D., Subramanian, A., Vaishnav, A. D., Rozenblatt-Rosen, O., Regev, A., Scadden, D. T. (2019). A Cellular Taxonomy of the Bone Marrow Stroma in Homeostasis and Leukemia. *Cell, 177*(7), 1915-1932.e1916. doi:10.1016/j.cell.2019.04.040

Batsivari, A., Haltalli, M. L. R., Passaro, D., Pospori, C., Celso, C. L., & Bonnet, D. (2020). Author Correction: Dynamic responses of the haematopoietic stem cell niche to diverse stresses. *Nat Cell Biol, 22*(2), 257-257. doi:10.1038/s41556-020-0469-0

Benjamini, Y., & Hochberg, Y. (1995). Controlling the False Discovery Rate: A Practical and Powerful Approach to Multiple Testing. *Journal of the Royal Statistical Society. Series B (Methodological), 57*(1), 289-300.

Bernardo, M. E., & Fibbe, W. E. (2013). Mesenchymal stromal cells: sensors and switchers of inflammation. *Cell Stem Cell, 13*(4), 392-402. doi:10.1016/j.stem.2013.09.006

Bhagat, T. D., Chen, S., Bartenstein, M., Barlowe, A. T., Von Ahrens, D., Choudhary, G. S., Tivnan, P., Amin, E., Marcondes, A. M., Sanders, M. A., Hoogenboezem, R. M., Kambhampati, S., Ramachandra, N., Mantzaris, I., Sukrithan, V., Laurence, R., Lopez, R.,

Bhagat, P., Giricz, O., Sohal, D., Wickrema, A., Yeung, C., Gritsman, K., Aplan, P., Hochedlinger, K., Yu, Y., Pradhan, K., Zhang, J., Greally, J. M., Mukherjee, S., Pellagatti, A., Boultwood, J., Will, B., Steidl, U., Raaijmakers, M. H. G. P., Deeg, H. J., Kharas, M. K., Verma, A. (2017). Epigenetically Aberrant Stroma in MDS Propagates Disease via Wnt/β-Catenin Activation. *Cancer Res, 77*(18), 4846-4857. doi:10.1158/0008-5472.Can-17-0282

Bhatia, R., McGlave, P. B., Dewald, G. W., Blazar, B. R., & Verfaillie, C. M. (1995). Abnormal function of the bone marrow microenvironment in chronic myelogenous leukemia: role of malignant stromal macrophages. *Blood, 85*(12), 3636-3645.

Bianco, P., Robey, P. G., Simmons, P. J. (2008) Mesenchymal stem cells: revisiting history, concepts, and assays. *Cell Stem Cell*, *2*(4), 313-9. doi: 10.1016/j.stem.2008.03.002.

Biffl, W. L., Moore, E. E., Moore, F. A., & Barnett, C. C., Jr. (1995). Interleukin-6 suppression of neutrophil apoptosis is neutrophil concentration dependent. *J Leukoc Biol, 58*(5), 582-584. doi:10.1002/jlb.58.5.582

Birbrair, A., & Frenette, P. S. (2016). Niche heterogeneity in the bone marrow. *Ann N Y Acad Sci, 1370*(1), 82-96. doi:10.1111/nyas.13016

Biunno, I., Cattaneo, M., Orlandi, R., Canton, C., Biagiotti, L., Ferrero, S., Barberis, M., Pupa, S. M., Scarpa, A., Ménard, S. (2006). SEL1L a multifaceted protein playing a role in tumor progression. *J Cell Physiol, 208*(1), 23-38. doi:10.1002/jcp.20574

Bodine, P. V., Zhao, W., Kharode, Y. P., Bex, F. J., Lambert, A. J., Goad, M. B., Gaur, T., Stein, G. S., LIan, J. B., Komm, B. S. (2004). The Wnt antagonist secreted frizzled-related protein-1 is a negative regulator of trabecular bone formation in adult mice. *Mol Endocrinol, 18*(5), 1222-1237. doi:10.1210/me.2003-0498

Boettcher, S., Ziegler, P., Schmid, M. A., Takizawa, H., van Rooijen, N., Kopf, M., Heikenwalder, M., and Manz, M. G. (2012). Cutting Edge: LPS-Induced Emergency Myelopoiesis Depends on TLR4-Expressing Nonhematopoietic Cells. *J Immunol*, *188*(12), 5824-5828; doi: https://doi.org/10.4049/jimmunol.1103253

Bonavida, B. (1991). Immunomodulatory effect of tumor necrosis factor. *Biotherapy, 3*(2), 127-133. doi:10.1007/bf02172085

Boulais, P. E., & Frenette, P. S. (2015). Making sense of hematopoietic stem cell niches. *Blood, 125*(17), 2621-2629. doi:10.1182/blood-2014-09-570192

Bovolenta, P., Esteve, P., Ruiz, J. M., Cisneros, E., & Lopez-Rios, J. (2008). Beyond Wnt inhibition: new functions of secreted Frizzled-related proteins in development and disease. *J Cell Sci, 121*(Pt 6), 737-746. doi:10.1242/jcs.026096

Bowen, M. A., Bajorath, J., D'Egidio, M., Whitney, G. S., Palmer, D., Kobarg, J., Starling, G. C., Siadak, A. W., Aruffo, A. (1997). Characterization of mouse ALCAM (CD166): the CD6-binding domain is conserved in different homologs and mediates cross-species binding. *Eur J Immunol, 27*(6), 1469-1478. doi:10.1002/eji.1830270625

Bowie, M. B., Kent, D. G., Dykstra, B., McKnight, K. D., McCaffrey, L., Hoodless, P. A., Eaves, C. J. (2007) Identification of a new intrinsically timed developmental checkpoint that reprograms key hematopoietic stem cell properties. *Proc Natl Acad Sci U S A*, *104*(14), 5878-82. doi: 10.1073/pnas.0700460104.

Brouckaert, P., Libert, C., Everaerdt, B., Takahashi, N., Cauwels, A., & Fiers, W. (1993). Tumor necrosis factor, its receptors and the connection with interleukin 1 and interleukin 6. *Immunobiology, 187*(3-5), 317-329. doi:10.1016/s0171-2985(11)80347-5

Buckley, S. M., Ulloa-Montoya, F., Abts, D., Oostendorp, R. A., Dzierzak, E., Ekker, S. C., & Verfaillie, C. M. (2011). Maintenance of HSC by Wnt5a secreting AGM-derived stromal cell line. *Exp Hematol, 39*(1), 114-123.e111-115. doi:10.1016/j.exphem.2010.09.010

Calvi, L. M., Adams, G. B., Weibrecht, K. W., Weber, J. M., Olson, D. P., Knight, M. C., Martin, R. P., Schipani, E., Divieti, P., Bringhurst, F. R., Milner, L. A., Kronenberg, H. M., Scadden, D. T. (2003). Osteoblastic cells regulate the haematopoietic stem cell niche. *Nature, 425*(6960), 841-846. doi:10.1038/nature02040

Cardano, M., Diaferia, G. R., Cattaneo, M., Dessì, S. S., Long, Q., Conti, L., Deblasio, P., Cattaneo, E., Biunno, I. (2011). mSEL-1L (Suppressor/enhancer Lin12-like) protein levels influence murine neural stem cell self-renewal and lineage commitment. *J Biol Chem, 286*(21), 18708-18719. doi:10.1074/jbc.M110.210740

Chamberlain, G., Fox, J., Ashton, B., & Middleton, J. (2007). Concise review: mesenchymal stem cells: their phenotype, differentiation capacity, immunological features, and potential for homing. *Stem Cells, 25*(11), 2739-2749. doi:10.1634/stemcells.2007-0197

Chan, K. C., Chan, L. S., Ip, J. C. Y., Lo, C., Yip, T. T. C., Ngan, R. K. C., Wong, R. N. S., Lo, K. W., Ng, W. T., Lee, A. W. M., Tsao, G. S. W., Kahn, M., Lung, M. L., Mak, N. K. (2015). Therapeutic targeting of CBP/β-catenin signaling reduces cancer stem-like population and synergistically suppresses growth of EBV-positive nasopharyngeal carcinoma cells with cisplatin. *Scientific Reports, 5*(1), 9979. doi:10.1038/srep09979

Chan, H. M., & La Thangue, N. B. (2001). p300/CBP proteins: HATs for transcriptional bridges and scaffolds. *J Cell Sci, 114*(Pt 13), 2363-2373.

Chen, J., Shi, Y., Regan, J., Karuppaiah, K., Ornitz, D. M., & Long, F. (2014). Osx-Cre targets multiple cell types besides osteoblast lineage in postnatal mice. *PLOS ONE, 9*(1), e85161. doi:10.1371/journal.pone.0085161

Cheng, G., Liu, F., Asai, T., Lai, F., Man, N., Xu, H., Chen, S., Greenblatt, S., Hamard, P. J., Ando, K., Martinez, C., Tadi, M., Wang, L., Xu, M., Yang, F. C., Shiekhattar, R., Nimer, S. D. (2017). Loss of p300 accelerates MDS-associated leukemogenesis. *Leukemia, 31*(6), 1382-1390. doi:10.1038/leu.2016.347

Cheng, T. (2008). Toward 'SMART' stem cells. *Gene Ther, 15*(2), 67-73. doi:10.1038/sj.gt.3303066

Chong, J. M., Uren, A., Rubin, J. S., & Speicher, D. W. (2002). Disulfide bond assignments of secreted Frizzled-related protein-1 provide insights about Frizzled homology and netrin modules. *J Biol Chem, 277*(7), 5134-5144. doi:10.1074/jbc.M108533200

Chrivia, J. C., Kwok, R. P., Lamb, N., Hagiwara, M., Montminy, M. R., & Goodman, R. H. (1993). Phosphorylated CREB binds specifically to the nuclear protein CBP. *Nature, 365*(6449), 855-859. doi:10.1038/365855a0

Colmone, A., Amorim, M., Pontier, A. L., Wang, S., Jablonski, E., & Sipkins, D. A. (2008). Leukemic cells create bone marrow niches that disrupt the behavior of normal hematopoietic progenitor cells. *Science, 322*(5909), 1861-1865. doi:10.1126/science.1164390

Cooper, S. J., von Roemeling, C. A., Kang, K. H., Marlow, L. A., Grebe, S. K., Menefee, M. E., Tun, H. W., Colon-Otero, G., Perez, E. A., Copland, J. A. (2012) Reexpression of tumor suppressor, sFRP1, leads to antitumor synergy of combined HDAC and methyltransferase inhibitors in chemoresistant cancers. *Mol Cancer Ther*, *11*(10), 2105-15. doi: 10.1158/1535-7163.MCT-11-0873.

Creyghton, M. P., Roël, G., Eichhorn, P. J., Hijmans, E. M., Maurer, I., Destrée, O., & Bernards, R. (2005). PR72, a novel regulator of Wnt signaling required for Naked cuticle function. *Genes Dev, 19*(3), 376-386. doi:10.1101/gad.328905

Creyghton, M. P., Roël, G., Eichhorn, P. J., Vredeveld, L. C., Destrée, O., & Bernards, R. (2006). PR130 is a modulator of the Wnt-signaling cascade that counters repression of the antagonist Naked cuticle. *Proc Natl Acad Sci U S A., 103*(14), 5397–5402. doi:10.1073/pnas.0507237103

Crippa, S., & Bernardo, M. E. (2018). Mesenchymal Stromal Cells: Role in the BM Niche and in the Support of Hematopoietic Stem Cell Transplantation. *HemaSphere, 2*(6), e151. doi:10.1097/hs9.0000000000000151
Cumano, A., & Godin, I. (2007). Ontogeny of the hematopoietic system. *Annu Rev Immunol, 25*, 745-785. doi:10.1146/annurev.immunol.25.022106.141538

Dahl, E., Wiesmann, F., Woenckhaus, M., Stoehr, R., Wild, P. J., Veeck, J., Knüchel, R., Klopocki, E., Sauter, G., Simon, R., Wieland, W. F., Walter, B., Denzinger, S., Hartmann, A., Hammerschmied, C. G. (2007). Frequent loss of SFRP1 expression in multiple human solid tumours: association with aberrant promoter methylation in renal cell carcinoma. *Oncogene, 26*(38), 5680-5691. doi:10.1038/sj.onc.1210345

Dal Porto, J. M., Gauld, S. B., Merrell, K. T., Mills, D., Pugh-Bernard, A. E., & Cambier, J. (2004). B cell antigen receptor signaling 101. *Mol Immunol, 41*(6-7), 599-613. doi:10.1016/j.molimm.2004.04.008

Daley, G. Q., Van Etten, R. A., & Baltimore, D. (1990). Induction of chronic myelogenous leukemia in mice by the P210bcr/abl gene of the Philadelphia chromosome. *Science, 247*(4944), 824-830. doi:10.1126/science.2406902

Davey, R.A., Clarke, M.V., Sastra, S., Skinner, J. P., Chiang, C., Anderson, P. H., Zajac, J. D. (2012). Decreased body weight in young Osterix-Cre transgenic mice results in delayed cortical bone expansion and accrual. *Transgenic Res*, *21*, 885–893. doi:10.1007/s11248-011-9581-z

de Bruijn, M. F., Ma, X., Robin, C., Ottersbach, K., Sanchez, M. J., & Dzierzak, E. (2002). Hematopoietic stem cells localize to the endothelial cell layer in the midgestation mouse aorta. *Immunity, 16*(5), 673-683. doi:10.1016/s1074-7613(02)00313-8

de Girolamo, L., Lucarelli, E., Alessandri, G., Avanzini, M. A., Bernardo, M. E., Biagi, E., Brini, A. T., D'Amico, G., Fagioli, F., Ferrero, I., Locatelli, F., Maccario, R., Marazzi, M., Parolini, O., Pessina, A., Torre, M. L. (2013). Mesenchymal stem/stromal cells: a new "cells as drugs" paradigm. Efficacy and critical aspects in cell therapy. *Curr Pharm Des, 19*(13), 2459-2473. doi:10.2174/1381612811319130015

Deininger, M. W., Goldman, J. M., & Melo, J. V. (2000). The molecular biology of chronic myeloid leukemia. *Blood, 96*(10), 3343-3356.

Desterke, C., Petit, L., Sella, N., Chevallier, N., Cabeli, V., Coquelin, L., Durand, C., Oostendorp, R. A. J., Isambert, H., Jaffredo, T., Charbord, P. (2020). Inferring Gene Networks in Bone Marrow Hematopoietic Stem Cell-Supporting Stromal Niche Populations. *iScience, 23*(6), 101222. doi:10.1016/j.isci.2020.101222

Dijksterhuis, J. P., Petersen, J., & Schulte, G. (2014). WNT/Frizzled signalling: receptor-ligand selectivity with focus on FZD-G protein signalling and its physiological relevance: IUPHAR Review 3. *Br J Pharmacol, 171*(5), 1195-1209. doi:10.1111/bph.12364

Dimri, G. P., Lee, X., Basile, G., Acosta, M., Scott, G., Roskelley, C., Medrano, E. E., Linskens, M., Rubelj, I., Pereira-Smith, O. (1995). A biomarker that identifies senescent human cells in culture and in aging skin in vivo. *Proc Natl Acad Sci U S A, 92*(20), 9363-9367. doi:10.1073/pnas.92.20.9363

Ding, L., & Morrison, S. J. (2013). Haematopoietic stem cells and early lymphoid progenitors occupy distinct bone marrow niches. *Nature, 495*(7440), 231-235. doi:10.1038/nature11885

Ding, L., Saunders, T. L., Enikolopov, G., & Morrison, S. J. (2012). Endothelial and perivascular cells maintain haematopoietic stem cells. *Nature, 481*(7382), 457-462. doi:10.1038/nature10783

Dolgalev, I., & Tikhonova, A. N. (2021). Connecting the Dots: Resolving the Bone Marrow Niche Heterogeneity. *Frontiers in Cell and Developmental Biology, 9*(478). doi:10.3389/fcell.2021.622519

Dominici, M., Le Blanc, K., Mueller, I., Slaper-Cortenbach, I., Marini, F., Krause, D., Deans, R., Keating, A., Prockop, D., Horwitz, E. (2006). Minimal criteria for defining multipotent mesenchymal stromal cells. The International Society for Cellular Therapy position statement. *Cytotherapy, 8*(4), 315-317. doi:10.1080/14653240600855905

Dougan, S. K., Hu, C. C., Paquet, M. E., Greenblatt, M. B., Kim, J., Lilley, B. N., Watson, N., Ploegh, H. L. (2011) Derlin-2-deficient mice reveal an essential role for protein dislocation in chondrocytes. *Mol Cell Biol*, *31*(6), 1145-59. doi: 10.1128/MCB.00967-10

Doulatov, S., Notta, F., Laurenti, E., & Dick, J. E. (2012). Hematopoiesis: a human perspective. *Cell Stem Cell, 10*(2), 120-136. doi:10.1016/j.stem.2012.01.006

Dufourcq, P., Descamps, B., Tojais, N. F., Leroux, L., Oses, P., Daret, D., Moreau, C., Lamazière, J. M. D., Couffinhal, T., Duplàa, C. (2008). Secreted frizzled-related protein-1 enhances mesenchymal stem cell function in angiogenesis and contributes to neovessel maturation. *Stem Cells, 26*(11), 2991-3001. doi:10.1634/stemcells.2008-0372

Durkin, M. E., Qian, X., Popescu, N. C., & Lowy, D. R. (2013). Isolation of Mouse Embryo Fibroblasts. *Bio Protoc, 3*(18). doi:10.21769/bioprotoc.908

Dzierzak, E., & Speck, N. A. (2008). Of lineage and legacy: the development of mammalian hematopoietic stem cells. *Nat Immunol, 9*(2), 129-136. doi:10.1038/ni1560

Dzulko, M., Pons, M., Henke, A., Schneider, G., & Krämer, O. H. (2020). The PP2A subunit PR130 is a key regulator of cell development and oncogenic transformation. *Biochim Biophys Acta Rev Cancer, 1874*(2), 188453. doi:10.1016/j.bbcan.2020.188453

Eckner, R., Ewen, M. E., Newsome, D., Gerdes, M., DeCaprio, J. A., Lawrence, J. B., & Livingston, D. M. (1994). Molecular cloning and functional analysis of the adenovirus E1A-associated 300-kD protein (p300) reveals a protein with properties of a transcriptional adaptor. *Genes Dev, 8*(8), 869-884. doi:10.1101/gad.8.8.869

Ehninger, A., & Trumpp, A. (2011). The bone marrow stem cell niche grows up: mesenchymal stem cells and macrophages move in. *J Exp Med, 208*(3), 421-428. doi:10.1084/jem.20110132

El-Badri, N. S., Wang, B. Y., Cherry, & Good, R. A. (1998). Osteoblasts promote engraftment of allogeneic hematopoietic stem cells. *Exp Hematol, 26*(2), 110-116.

El-Khoueiry, A. B., Ning, Y., Yang, D., Cole, S., Kahn, M., Zoghbi, M., Berg, J., Fujimori, M., Inada, T., Lenz, H.-J. (2013). A phase I first-in-human study of PRI-724 in patients (pts) with advanced solid tumors. *Journal of Clinical Oncology, 31*(15_suppl), 2501-2501. doi:10.1200/jco.2013.31.15_suppl.2501

Elefanty, A. G., Hariharan, I. K., & Cory, S. (1990). bcr-abl, the hallmark of chronic myeloid leukaemia in man, induces multiple haemopoietic neoplasms in mice. *Embo j, 9*(4), 1069-1078.

Emami, K. H., Nguyen, C., Ma, H., Kim, D. H., Jeong, K. W., Eguchi, M., Moon, R. T., Teo, J.-L., Kim, H. Y., Moon, S. H., Ha, J. R., Kahn, M. (2004). A small molecule inhibitor of beta-catenin/CREB-binding protein transcription [corrected]. *Proc Natl Acad Sci U S A, 101*(34), 12682-12687. doi:10.1073/pnas.0404875101

Engel, K., Rudelius, M., Slawska, J., Jacobs, L., Ahangarian Abhari, B., Altmann, B., Kurutz, J., Rathakrishnan, A., Fernández-Sáiz, V., Brunner, A., Targosz, B.-S., Loewecke, F., Gloeckner, C. J., Ueffing, M., Fulda, S., Pfreundschuh, M., Trümper, L., Klapper, W., Keller, U., Jost, P. J., Rosenwald, A., Peschel, C., Bassermann, F. (2016). USP9X stabilizes XIAP to regulate mitotic cell death and chemoresistance in aggressive B-cell lymphoma. *EMBO Molecular Medicine, 8*(8), 851-862. doi:https://doi.org/10.15252/emmm.201506047

Esplin, B. L., Shimazu, T., Welner, R. S., Garrett, K. P., Nie, L., Zhang, Q., Humphrey, M. B., Yang, Q., Borghesi, L. A., Kincade, P. W. (2011). Chronic exposure to a TLR ligand injures hematopoietic stem cells. *J Immunol, 186*(9), 5367-5375. doi:10.4049/jimmunol.1003438

Essers, M. A., Offner, S., Blanco-Bose, W. E., Waibler, Z., Kalinke, U., Duchosal, M. A., & Trumpp, A. (2009). IFNalpha activates dormant haematopoietic stem cells in vivo. *Nature, 458*(7240), 904-908. doi:10.1038/nature07815

Esteve, P., Crespo, I., Kaimakis, P., Sandonís, A., & Bovolenta, P. (2018). Sfrp1 Modulates Cell-signaling Events Underlying Telencephalic Patterning, Growth and Differentiation. *Cerebral Cortex, 29*(3), 1059-1074. doi:10.1093/cercor/bhy013

Fabre, B., Livneh, I., Ziv, T., & Ciechanover, A. (2019). Identification of proteins regulated by the proteasome following induction of endoplasmic reticulum stress. *Biochem Biophys Res Commun, 517*(2), 188-192. doi:10.1016/j.bbrc.2019.07.040

Famili, F., Brugman, M. H., Taskesen, E., Naber, B. E. A., Fodde, R., Staal, F. J. T. (2016) High Levels of Canonical Wnt Signaling Lead to Loss of Stemness and Increased Differentiation in Hematopoietic Stem Cells. *Stem Cell Reports*, *6*(5), 652-659. doi: 10.1016/j.stemcr.2016.04.009

Farhana, A., & Khan, Y. (2021). Biochemistry, Lipopolysaccharide. *StatPearls*.
Fiedler, M., Graeb, M., Mieszczanek, J., Rutherford, T. J., Johnson, C. M., & Bienz, M. (2015). An ancient Pygo-dependent Wnt enhanceosome integrated by Chip/LDB-SSDP. *Elife, 4*. doi:10.7554/eLife.09073

Finch, P. W., He, X., Kelley, M. J., Uren, A., Schaudies, R. P., Popescu, N. C., Rudikoff, S., Aaronson, S. A., Varmus, H. E., Rubin, J. S. (1997). Purification and molecular cloning of a secreted, Frizzled-related antagonist of Wnt action. *Proc Natl Acad Sci U S A, 94*(13), 6770-6775. doi:10.1073/pnas.94.13.6770

Fisher, R. A. (1948). Combining independent tests of significance. *American Statistician, 2*(5), 30.

Flach, J., Bakker, S. T., Mohrin, M., Conroy, P. C., Pietras, E. M., Reynaud, D., Alvarez, S., Diolaiti, M. E., Ugarte, F., Forsberg, E. C., Le Beau, M. M., Stohr, B. A., Méndez, J., Morrison, C. G., Passegué, E. (2014). Replication stress is a potent driver of functional decline in ageing haematopoietic stem cells. *Nature, 512*(7513), 198-202. doi:10.1038/nature13619

Fleming, H. E., Janzen, V., Lo Celso, C., Guo, J., Leahy, K. M., Kronenberg, H. M., & Scadden, D. T. (2008). Wnt signaling in the niche enforces hematopoietic stem cell quiescence and is necessary to preserve self-renewal in vivo. *Cell Stem Cell, 2*(3), 274-283. doi:10.1016/j.stem.2008.01.003

Florian, M. C., Nattamai, K. J., Dörr, K., Marka, G., Überle, B., Vas, V., Eckl, C., Andrä, I., Schiemann, M., Oostendorp, R. A. J., Scharffetter-Kochanek, K., Kestler, H. A., Zheng, Y., Geiger, H. (2013). A canonical to non-canonical Wnt signalling switch in haematopoietic stem-cell ageing. *Nature, 503*(7476), 392-396. doi:10.1038/nature12631

Frame, J. M., McGrath, K. E., & Palis, J. (2013). Erythro-myeloid progenitors: "definitive" hematopoiesis in the conceptus prior to the emergence of hematopoietic stem cells. *Blood Cells Mol Dis, 51*(4), 220-225. doi:10.1016/j.bcmd.2013.09.006

Frederiksen, H., Svaerke, C., Thomsen, R. W., Farkas, D. K., Pedersen, L., Weiss, N. S., & Sørensen, H. T. (2013). Lymph node enlargement and risk of haematological and solid cancer. *Br J Haematol, 160*(5), 599-607. doi:10.1111/bjh.12174

Friedenstein, A. J., Chailakhyan, R. K., & Gerasimov, U. V. (1987). Bone marrow osteogenic stem cells: in vitro cultivation and transplantation in diffusion chambers. *Cell Tissue Kinet, 20*(3), 263-272. doi:10.1111/j.1365-2184.1987.tb01309.x

Friedenstein, A. J., Piatetzky, S., II, & Petrakova, K. V. (1966). Osteogenesis in transplants of bone marrow cells. *J Embryol Exp Morphol, 16*(3), 381-390.

Fröbel, J., Landspersky, T., Percin, G. e., Schreck, C., Rahmig, S., Ori, A., Nowak, D., Essers, M., Waskow, C., Oostendorp, R. A. J. (2021). The Hematopoietic Bone Marrow Niche Ecosystem. *Frontiers in Cell and Developmental Biology, 9*. doi:10.3389/fcell.2021.705410

Galloway, J. L., & Zon, L. I. (2003). Ontogeny of hematopoiesis: examining the emergence of hematopoietic cells in the vertebrate embryo. *Curr Top Dev Biol, 53*, 139-158. doi:10.1016/s0070-2153(03)53004-6

Gang, E. J., Hsieh, Y. T., Pham, J., Zhao, Y., Nguyen, C., Huantes, S., Park, E., Naing, K., Klemm, L., Swaminathan, S., Conway, E. M., Pelus, L. M., Crispino, J., Mullighan, C. G., McMillan, M., Müschen, M., Kahn, M., Kim, Y. M. (2014). Small-molecule inhibition of CBP/catenin interactions eliminates drug-resistant clones in acute lymphoblastic leukemia. *Oncogene, 33*(17), 2169-2178. doi:10.1038/onc.2013.169

Gao, B., Lee, S. M., Chen, A., Zhang, J., Zhang, D. D., Kannan, K., Ortmann, R. A., Fang, D. (2008) Synoviolin promotes IRE1 ubiquitination and degradation in synovial fibroblasts from mice with collagen-induced arthritis. *EMBO Rep*, *9*(5), 480-5. doi: 10.1038/embor.2008.37

Gao, X., & Huang, L. (1995). Cationic liposome-mediated gene transfer. *Gene Ther, 2*(10), 710-722.

Garcia-Ortega, A. M., Cañete, A., Quinter, C., Silberstein, L., Piquer-Gil, M., Alvarez-Dolado, M., Dekel, B., Gottgens, B., Sánchez, M. J. (2010). Enhanced hematovascular contribution of SCL 3' enhancer expressing fetal liver cells uncovers their potential to integrate in extramedullary adult niches. *Stem Cells, 28*(1), 100-112. doi:10.1002/stem.228

Gaur, T., Lengner, C. J., Hovhannisyan, H., Bhat, R. A., Bodine, P. V., Komm, B. S., Javed, A., van Wijnen, A. J., Stein, J. L., Lian, J. B. (2005). Canonical WNT signaling promotes osteogenesis by directly stimulating Runx2 gene expression. *J Biol Chem, 280*(39), 33132-33140. doi:10.1074/jbc.M500608200

Gaur, T., Rich, L., Lengner, C. J., Hussain, S., Trevant, B., Ayers, D., Stein, J. L., Bodine, P. V. N., Komm, B. S., Stein, G. S., Lian, J. B. (2006). Secreted frizzled related protein 1 regulates Wnt signaling for BMP2 induced chondrocyte differentiation. *J Cell Physiol, 208*(1), 87-96. doi:10.1002/jcp.20637

Gayther, S. A., Batley, S. J., Linger, L., Bannister, A., Thorpe, K., Chin, S. F., Daigo, Y., Russell, P., Wilson, A., Sowter, H. M., Delhanty, J. D., Ponder, B. A., Kouzarides, T., Caldas, C. (2000). Mutations truncating the EP300 acetylase in human cancers. *Nat Genet, 24*(3), 300-303. doi:10.1038/73536

Gazit, Z., Aslan, H., Gafni, Y., Kimelman, N., Pelled, G., & Gazit, D. (2008). Mesenchymal Stem Cells. In A. Atala, R. Lanza, J. A. Thomson, & R. M. Nerem (Eds.), *Principles of Regenerative Medicine* (pp. 318-343). Academic Press.

Geiger, H., de Haan, G., & Florian, M. C. (2013). The ageing haematopoietic stem cell compartment. *Nat Rev Immunol, 13*(5), 376-389. doi:10.1038/nri3433

Gerdes, J., Lemke, H., Baisch, H., Wacker, H. H., Schwab, U., & Stein, H. (1984). Cell cycle analysis of a cell proliferation-associated human nuclear antigen defined by the monoclonal antibody Ki-67. *J Immunol, 133*(4), 1710-1715.

Gerdes, J., Schwab, U., Lemke, H., & Stein, H. (1983). Production of a mouse monoclonal antibody reactive with a human nuclear antigen associated with cell proliferation. *Int J Cancer, 31*(1), 13-20. doi:10.1002/ijc.2910310104

Geyh, S., Oz, S., Cadeddu, R. P., Fröbel, J., Brückner, B., Kündgen, A., Fenk, R., Bruns, I., Zilkens, C., Hermsen, D., Gattermann, N., Kobbe, G., Germing, U., Lyko, F., Haas, R., Schroeder, T. (2013). Insufficient stromal support in MDS results from molecular and functional deficits of mesenchymal stromal cells. *Leukemia, 27*(9), 1841-1851. doi:10.1038/leu.2013.193

Giles, R. H., Peters, D. J., & Breuning, M. H. (1998). Conjunction dysfunction: CBP/p300 in human disease. *Trends Genet, 14*(5), 178-183. doi:10.1016/s0168-9525(98)01438-3

Giordano, A., & Avantaggiati, M. L. (1999). p300 and CBP: partners for life and death. *J Cell Physiol, 181*(2), 218-230. doi:10.1002/(sici)1097-4652(199911)181:2<218::Aid-jcp4>3.0.Co;2-5

Glaeser, K., Urban, M., Fenech, E., Voloshanenko, O., Kranz, D., Lari, F., Christianson, J. C., Boutros, M. (2018). ERAD-dependent control of the Wnt secretory factor Evi. *Embo j, 37*(4). doi:10.15252/embj.201797311

Gnani, D., Crippa, S., della Volpe, L., Rossella, V., Conti, A., Lettera, E., Rivis, S., Ometti, M., Fraschini, G., Bernardo, M. E., Di Micco, R. (2019). An early-senescence state in aged mesenchymal stromal cells contributes to hematopoietic stem and progenitor cell clonogenic impairment through the activation of a pro-inflammatory program. *Aging Cell, 18*(3), e12933. doi:https://doi.org/10.1111/acel.12933

Goardon, N., Marchi, E., Atzberger, A., Quek, L., Schuh, A., Soneji, S., Woll, P., Mead, A., Alford, K. A., Rout, R., Chaudhury, S., Gilkes, A., Knapper, S., Beldjord, K., Begum, S., Rose, S., Geddes, N., Griffiths, M., Standen, G., Sternberg, A., Cavenagh, J., Hunter, H., Bowen, D., Killick, S., Robinson, L., Price, A., Macintyre, E., Virgo, P., Burnett, A., Craddock, C., Enver, T., Jacobsen, S. E. W., Porcher, C., Vyas, P. (2011). Coexistence of LMPP-like and GMP-like leukemia stem cells in acute myeloid leukemia. *Cancer Cell, 19*(1), 138-152. doi:10.1016/j.ccr.2010.12.012

Goodman, R. H., & Smolik, S. (2000). CBP/p300 in cell growth, transformation, and development. *Genes Dev, 14*(13), 1553-1577.

Goodwin, A. M., & D'Amore, P. A. (2002). Wnt signaling in the vasculature. *Angiogenesis, 5*(1-2), 1-9. doi:10.1023/a:1021563510866

Gradilla, A. C., Sanchez-Hernandez, D., Brunt, L., & Scholpp, S. (2018). From top to bottom: Cell polarity in Hedgehog and Wnt trafficking. *BMC Biol, 16*(1), 37. doi:10.1186/s12915-018-0511-x

Greenbaum, A., Hsu, Y. M., Day, R. B., Schuettpelz, L. G., Christopher, M. J., Borgerding, J. N., Nagasawa, T., Link, D. C. (2013). CXCL12 in early mesenchymal progenitors is required for haematopoietic stem-cell maintenance. *Nature, 495*(7440), 227-230. doi:10.1038/nature11926

Groffen, J., Voncken, J. W., Kaartinen, V., Morris, C., & Heisterkamp, N. (1993). Ph-positive leukemia: a transgenic mouse model. *Leuk Lymphoma, 11 Suppl 1*, 19-24. doi:10.3109/10428199309047857

Groisman, B., Shenkman, M., Ron, E., & Lederkremer, G. Z. (2011). Mannose trimming is required for delivery of a glycoprotein from EDEM1 to XTP3-B and to late endoplasmic reticulum-associated degradation steps. *J Biol Chem, 286*(2), 1292-1300. doi:10.1074/jbc.M110.154849

Gumz, M. L., Zou, H., Kreinest, P. A., Childs, A. C., Belmonte, L. S., LeGrand, S. N., Wu, K. J., Luxon, B. A., Sinha, M., Parker, A. S., Sun, L. Z., Ahlquist, D. A., Wood, C. G., Copland, J. A. (2007). Secreted frizzled-related protein 1 loss contributes to tumor phenotype of clear cell renal cell carcinoma. *Clin Cancer Res, 13*(16), 4740-4749. doi:10.1158/1078-0432.Ccr-07-0143

Guo, Z., Li, H., Li, X., Yu, X., Wang, H., Tang, P., & Mao, N. (2006). In vitro characteristics and in vivo immunosuppressive activity of compact bone-derived murine mesenchymal progenitor cells. *Stem Cells, 24*(4), 992-1000. doi:10.1634/stemcells.2005-0224

Haeckel, E. H. P. A. (1877). *Anthropogenie*: W. Engelmann.

Hanahan, D. (1983). Studies on transformation of Escherichia coli with plasmids. *J Mol Biol, 166*(4), 557-580. doi:10.1016/s0022-2836(83)80284-8

Hanahan, D., & Weinberg, R. A. (2011). Hallmarks of cancer: the next generation. *Cell, 144*(5), 646-674. doi:10.1016/j.cell.2011.02.013

Hasegawa, K., Yasuda, S. Y., Teo, J. L., Nguyen, C., McMillan, M., Hsieh, C. L., Suemori, H., Nakatsuji, N., Yamamoto, M., Miyabayashi, T., Lutzko, C., Pera, M. F., Kahn, M. (2012). Wnt signaling orchestration with a small molecule DYRK inhibitor provides long-term xeno-free human pluripotent cell expansion. *Stem Cells Transl Med, 1*(1), 18-28. doi:10.5966/sctm.2011-0033

Hausinger, R., Hackl, M., Jardon Alvarez, A., Kehr, M., Romero Marquez, S., Hettler, F., Kehr, C., Grziwok, S., Schreck, C., Peschel, C., Istvánffy, R., Oostendorp, R. A. J. (2021). Cathepsin K maintains the compartment of bone marrow T lymphocytes in vivo. *Immun Inflamm Dis*, *9*(2), 521-532. doi: 10.1002/iid3.412.

Häusler, K. D., Horwood, N. J., Chuman, Y., Fisher, J. L., Ellis, J., Martin, T. J., Rubin, J. S., Gillespie, M. T. (2004). Secreted frizzled-related protein-1 inhibits RANKL-dependent osteoclast formation. *J Bone Miner Res, 19*(11), 1873-1881. doi:10.1359/jbmr.040807

Hayashi, O., Katsube, Y., Hirose, M., Ohgushi, H., & Ito, H. (2008). Comparison of osteogenic ability of rat mesenchymal stem cells from bone marrow, periosteum, and adipose tissue. *Calcif Tissue Int, 82*(3), 238-247. doi:10.1007/s00223-008-9112-y

He, K., Xu, T., Xu, Y., Ring, A., Kahn, M., & Goldkorn, A. (2014). Cancer cells acquire a drug resistant, highly tumorigenic, cancer stem-like phenotype through modulation of the PI3K/Akt/β-catenin/CBP pathway. *Int J Cancer, 134*(1), 43-54. doi:10.1002/ijc.28341

Hecht, A., Vleminckx, K., Stemmler, M. P., van Roy, F., & Kemler, R. (2000). The p300/CBP acetyltransferases function as transcriptional coactivators of beta-catenin in vertebrates. *Embo j, 19*(8), 1839-1850. doi:10.1093/emboj/19.8.1839

Hettler, F., Schreck, C., Romero Marquez, S., Sippenauer, T., Koller, F., Demir, E., Bassermann, F., Istvanffy, R., Oostendorp, R. (2020). MICROENVIRONMENTAL SFRP1 REGULATES REPOPULATING ACTIVITY OF HEMATOPOIETIC STEM CELLS VIA PP2A-MEDIATED REGULATION OF CTNNB1/EP300. *Experimental Hematology*, Volume 88, Supplement, Page S31. Abstract: 2010. https://doi.org/10.1016/j.exphem.2020.09.172.

Hettler, F., Schreck, C., Romero Marquez, S., Sippenauer, T., Koller, F., Demir, E., Bassermann, F., Istvanffy, R., Oostendorp R. (2020a). Stromales SFRP1 steuert das Verhalten von hämatopoetischen Stammzellen über die PP2A-vermittelte Regulation von CTNNB1 / EP300. *DGHO Jahrestagung 2020 VIRTUAL*, Abstract: 619. https://www.oncoletter.ch/kongressberichte-live-webcasts/dgho-oegho-sgmo-und-sghssh-jahrestagung-2020-virtual/best-abstracts.html

Hertenstein, B., Hambach, L., Bacigalupo, A., Schmitz, N., McCann, S., Slavin, S., Gratwohl, A., Ferrant, A., Elmaagacli, A., Schwerfeger, R., Locasciulli, A., Zander, A., Bornhauser, M., Niederwieser, D., Ruutu, T. (2005). Development of leukemia in donor cells after allogeneic stem cell transplantation--a survey of the European Group for Blood and Marrow Transplantation (EBMT). *Haematologica, 90*(7), 969-975.

Heyde, A., Rohde, D., McAlpine, C. S., Zhang, S., Hoyer, F. F., Gerold, J. M., Cheek, D., Iwamoto, Y., Schloss, M. J., Vandoorne, K., Iborra-Egea, O., Muñoz-Guijosa, C., Bayes-Genis, A., Reiter, J. G., Craig, M., Swirski, F. K., Nahrendorf, M., Nowak, M. A., Naxerova, K. (2021). Increased stem cell proliferation in atherosclerosis accelerates clonal hematopoiesis. *Cell, 184*(5), 1348-1361.e1322. doi:10.1016/j.cell.2021.01.049

Higuchi, Y., Nguyen, C., Yasuda, S. Y., McMillan, M., Hasegawa, K., & Kahn, M. (2016). Specific Direct Small Molecule p300/β-Catenin Antagonists Maintain Stem Cell Potency. *Curr Mol Pharmacol, 9*(3), 272-279. doi:10.2174/1874467208666150526155146

Hirakawa, T., Nasu, K., Miyabe, S., Kouji, H., Katoh, A., Uemura, N., & Narahara, H. (2019). β-catenin signaling inhibitors ICG-001 and C-82 improve fibrosis in preclinical models of endometriosis. *Scientific Reports, 9*(1), 20056. doi:10.1038/s41598-019-56302-4

Ho, Y. H., & Méndez-Ferrer, S. (2020). Microenvironmental contributions to hematopoietic stem cell aging. *Haematologica, 105*(1), 38-46. doi:10.3324/haematol.2018.211334

Houlihan, D. D., Mabuchi, Y., Morikawa, S., Niibe, K., Araki, D., Suzuki, S., Okano, H., Matsuzaki, Y. (2012). Isolation of mouse mesenchymal stem cells on the basis of expression of Sca-1 and PDGFR-α. *Nat Protoc, 7*(12), 2103-2111. doi:10.1038/nprot.2012.125

Houshmand, M., Blanco, T. M., Circosta, P., Yazdi, N., Kazemi, A., Saglio, G., & Zarif, M. N. (2019). Bone marrow microenvironment: The guardian of leukemia stem cells. *World J Stem Cells, 11*(8), 476-490. doi:10.4252/wjsc.v11.i8.476

Hsieh, J. C., Kodjabachian, L., Rebbert, M. L., Rattner, A., Smallwood, P. M., Samos, C. H., Nusse, R., Dawid, I. B., Nathans, J. (1999). A new secreted protein that binds to Wnt proteins and inhibits their activities. *Nature, 398*(6726), 431-436. doi:10.1038/18899

Hu, J., Feng, M., Liu, Z. L., Liu, Y., Huang, Z. L., Li, H., & Feng, W. L. (2016). Potential role of Wnt/β-catenin signaling in blastic transformation of chronic myeloid leukemia: cross talk between β-catenin and BCR-ABL. *Tumour Biol*. doi:10.1007/s13277-016-5413-3

Hu, Y., & Smyth, G. K. (2009). ELDA: extreme limiting dilution analysis for comparing depleted and enriched populations in stem cell and other assays. *J Immunol Methods, 347*(1-2), 70-78. doi:10.1016/j.jim.2009.06.008

Hua, Y., Yang, Y., Li, Q., He, X., Zhu, W., Wang, J., & Gan, X. (2018). Oligomerization of Frizzled and LRP5/6 protein initiates intracellular signaling for the canonical WNT/β-catenin pathway. *J Biol Chem, 293*(51), 19710-19724. doi:10.1074/jbc.RA118.004434

Huang, J., Zhang, Y. L., Teng, X. M., Lin, Y., Zheng, D. L., Yang, P. Y., & Han, Z. G. (2007). Down-regulation of SFRP1 as a putative tumor suppressor gene can contribute to human hepatocellular carcinoma. *BMC Cancer, 7*, 126. doi:10.1186/1471-2407-7-126

Huntly, B. J., & Gilliland, D. G. (2005). Cancer biology: summing up cancer stem cells. *Nature, 435*(7046), 1169-1170. doi:10.1038/4351169a

Hwang, S. G., Yu, S. S., Ryu, J. H., Jeon, H. B., Yoo, Y. J., Eom, S. H., & Chun, J. S. (2005). Regulation of beta-catenin signaling and maintenance of chondrocyte differentiation by ubiquitin-independent proteasomal degradation of alpha-catenin. *J Biol Chem, 280*(13), 12758-12765. doi:10.1074/jbc.M413367200

Ikuta, K., & Weissman, I. L. (1992). Evidence that hematopoietic stem cells express mouse c-kit but do not depend on steel factor for their generation. *Proc Natl Acad Sci U S A, 89*(4), 1502-1506. doi:10.1073/pnas.89.4.1502

Isern, J., García-García, A., Martín, A. M., Arranz, L., Martín-Pérez, D., Torroja, C., Sánchez-Cabo, F., Méndez-Ferrer, S. (2014). The neural crest is a source of mesenchymal stem cells with specialized hematopoietic stem cell niche function. *Elife, 3*, e03696. doi:10.7554/eLife.03696

Ishitani, T., Kishida, S., Hyodo-Miura, J., Ueno, N., Yasuda, J., Waterman, M., Shibuya, H., Moon, R. T., Ninomiya-Tsuji, J., Matsumoto, K. (2003). The TAK1-NLK mitogen-activated protein kinase cascade functions in the Wnt-5a/Ca(2+) pathway to antagonize Wnt/beta-catenin signaling. *Mol Cell Biol, 23*(1), 131-139. doi:10.1128/mcb.23.1.131-139.2003

Istvanffy, R., Kröger, M., Eckl, C., Gitzelmann, S., Vilne, B., Bock, F., Graf, S., Schiemann, M., Keller, U. B., Peschel, C., Oostendorp, R. A. J. (2011). Stromal pleiotrophin regulates repopulation behavior of hematopoietic stem cells. *Blood, 118*(10), 2712-2722. doi:10.1182/blood-2010-05-287235

Iyer, N. G., Ozdag, H., & Caldas, C. (2004). p300/CBP and cancer. *Oncogene, 23*(24), 4225-4231. doi:10.1038/sj.onc.1207118

Jacob, M. C., Favre, M., & Bensa, J.-C. (1991). Membrane cell permeabilisation with saponin and multiparametric analysis by flow cytometry. *Cytometry, 12*(6), 550-558. doi:https://doi.org/10.1002/cyto.990120612

Jagannathan-Bogdan, M., & Zon, L. I. (2013). Hematopoiesis. *Development, 140*(12), 2463-2467. doi:10.1242/dev.083147

James, A. W. (2013). Review of Signaling Pathways Governing MSC Osteogenic and Adipogenic Differentiation. *Scientifica (Cairo), 2013*, 684736. doi:10.1155/2013/684736

Janssens, V., & Goris, J. (2001). Protein phosphatase 2A: a highly regulated family of serine/threonine phosphatases implicated in cell growth and signalling. *Biochem J, 353*(Pt 3), 417-439. doi:10.1042/0264-6021:3530417

Jost, E., Schmid, J., Wilop, S., Schubert, C., Suzuki, H., Herman, J. G., Osieka, R., Galm, O. (2008). Epigenetic inactivation of secreted Frizzled-related proteins in acute myeloid leukaemia. *British Journal of Haematology, 142*(5), 745-753. doi:https://doi.org/10.1111/j.1365-2141.2008.07242.x

Jrid, I., Pike-Overzet, K., Cante-Barrett, K., & Staal, F. J. (2020). Wnt Signaling In Lymphopoiesis And Hematopoiesis. *J Stem Cell Res., 1*(2), 1-27. doi:https://doi.org/10.52793/JSCR.2020.1(2)-07

Kabanov, A. V., & Kabanov, V. A. (1995). DNA complexes with polycations for the delivery of genetic material into cells. *Bioconjug Chem, 6*(1), 7-20. doi:10.1021/bc00031a002
Kahn, M. (2014). Can we safely target the WNT pathway? *Nat Rev Drug Discov, 13*(7), 513-532. doi:10.1038/nrd4233

Kaneko, M., Yasuim, S., Niinuma, Y., Arai, K., Omura, T., Okuma, Y., Nomura, Y. (2007) A different pathway in the endoplasmic reticulum stress-induced expression of human HRD1 and SEL1 genes. *FEBS Lett*, *581*(28), 5355-60. doi: 10.1016/j.febslet.2007.10.033.

Kawai, T., & Akira, S. (2010). The role of pattern-recognition receptors in innate immunity: update on Toll-like receptors. *Nat Immunol, 11*(5), 373-384. doi:10.1038/ni.1863

Kawano, Y., & Kypta, R. (2003). Secreted antagonists of the Wnt signalling pathway. *J Cell Sci, 116*(Pt 13), 2627-2634. doi:10.1242/jcs.00623

Kawasaki, H., Altieri, D. C., Lu, C. D., Toyoda, M., Tenjo, T., & Tanigawa, N. (1998). Inhibition of apoptosis by survivin predicts shorter survival rates in colorectal cancer. *Cancer Res, 58*(22), 5071-5074.

Kehr, C. (2016). Die extrinsische Rolle von Secreted frizzled-related protein 1 (Sfrp1) in kindlicher Leukämie. *Universitätsbibliothek der Technischen Universität München*.

Kelliher, M. A., McLaughlin, J., Witte, O. N., & Rosenberg, N. (1990). Induction of a chronic myelogenous leukemia-like syndrome in mice with v-abl and BCR/ABL. *Proc Natl Acad Sci U S A, 87*(17), 6649-6653. doi:10.1073/pnas.87.17.6649

Kempf, J. M., Weser, S., Bartoschek, M. D., Metzeler, K. H., Vick, B., Herold, T., Völse, K., Mattes, R., Scholz, M., Wange, L. E., Festini, M., Ugur, E., Roas, M., Weigert, O., Bultmann, S., Leonhardt, H., Schotta, G., Hiddemann, W., Jeremias, I., Spiekermann, K. (2021). Loss-of-function mutations in the histone methyltransferase EZH2 promote chemotherapy resistance in AML. *Scientific Reports, 11*(1), 5838. doi:10.1038/s41598-021-84708-6

Kfoury, Y., & Scadden, David T. (2015). Mesenchymal Cell Contributions to the Stem Cell Niche. *Cell Stem Cell, 16*(3), 239-253. doi:https://doi.org/10.1016/j.stem.2015.02.019

Kiel, M. J., Yilmaz, O. H., Iwashita, T., Yilmaz, O. H., Terhorst, C., & Morrison, S. J. (2005). SLAM family receptors distinguish hematopoietic stem and progenitor cells and reveal endothelial niches for stem cells. *Cell, 121*(7), 1109-1121. doi:10.1016/j.cell.2005.05.026

Kim, H. S., Shin, J., Kim, S. H., Chun, H. S., Kim, J. D., Kim, Y. S., Kim, M. J., Rhee, M., Yeo, S. Y., Huh, T. L. (2007). Eye field requires the function of Sfrp1 as a Wnt antagonist. *Neurosci Lett, 414*(1), 26-29. doi:10.1016/j.neulet.2006.12.027

Kim, I., Saunders, T. L., Morrison, S. J. (2007) Sox17 dependence distinguishes the transcriptional regulation of fetal from adult hematopoietic stem cells. *Cell, 130*(3), 470-83. doi: 10.1016/j.cell.2007.06.011.

Kimelman, D., & Xu, W. (2006). β-Catenin destruction complex: insights and questions from a structural perspective. *Oncogene, 25*(57), 7482-7491. doi:10.1038/sj.onc.1210055

Ko, J., Ryu, K. S., Lee, Y. H., Na, D. S., Kim, Y. S., Oh, Y. M., Kim, I. S., Kim, J. W. (2002). Human secreted frizzled-related protein is down-regulated and induces apoptosis in human cervical cancer. *Exp Cell Res, 280*(2), 280-287. doi:10.1006/excr.2002.5649

Kode, A., Manavalan, J. S., Mosialou, I., Bhagat, G., Rathinam, C. V., Luo, N., Khiabanian, H., Lee, A., Murty, V. V., Friedman, R., Brum, A., Park, D., Galili, N., Mukherjee, S., Teruya-Feldstein, J., Raza, A., Rabadan, R., Berman, E., Kousteni, S. (2014). Leukaemogenesis induced by an activating β-catenin mutation in osteoblasts. *Nature, 506*(7487), 240-244. doi:10.1038/nature12883

Komiya, Y., & Habas, R. (2008). Wnt signal transduction pathways. *Organogenesis, 4*(2), 68-75. doi:10.4161/org.4.2.5851

Korn, C., & Méndez-Ferrer, S. (2017). Myeloid malignancies and the microenvironment. *Blood, 129*(7), 811-822. doi:10.1182/blood-2016-09-670224

Kouadjo, K. E., Nishida, Y., Cadrin-Girard, J. F., Yoshioka, M., & St-Amand, J. (2007). Housekeeping and tissue-specific genes in mouse tissues. *BMC Genomics, 8*, 127. doi:10.1186/1471-2164-8-127

Krause, D. S., Fulzele, K., Catic, A., Sun, C. C., Dombkowski, D., Hurley, M. P., Lezeau, S., Attar, E., Wu, J. Y., Lin, H. Y., Divieti-Pajevic, P., Hasserjian, R. P., Schipani, E., Van Etten, R. A., Scadden, D. T. (2013). Differential regulation of myeloid leukemias by the bone marrow microenvironment. *Nat Med, 19*(11), 1513-1517. doi:10.1038/nm.3364

Kreso, A., & Dick, J. E. (2014). Evolution of the cancer stem cell model. *Cell Stem Cell, 14*(3), 275-291. doi:10.1016/j.stem.2014.02.006

Krizhanovsky, V., Yon, M., Dickins, R. A., Hearn, S., Simon, J., Miething, C., Yee, H., Zender, L., Lowe, S. W. (2008). Senescence of activated stellate cells limits liver fibrosis. *Cell, 134*(4), 657-667. doi:10.1016/j.cell.2008.06.049

Kuhn, P. H., Koroniak, K., Hogl, S., Colombo, A., Zeitschel, U., Willem, M., Volbracht, C., Schepers, U., Imhof, A., Hoffmeister, A., Haass, C., Roßner, S., Bräse, S., Lichtenthaler, S. F. (2012). Secretome protein enrichment identifies physiological BACE1 protease substrates in neurons. *Embo j, 31*(14), 3157-3168. doi:10.1038/emboj.2012.173

Kung, A. L., Rebel, V. I., Bronson, R. T., Ch'ng, L. E., Sieff, C. A., Livingston, D. M., & Yao, T. P. (2000). Gene dose-dependent control of hematopoiesis and hematologic tumor suppression by CBP. *Genes Dev, 14*(3), 272-277.

Kunisaki, Y., Bruns, I., Scheiermann, C., Ahmed, J., Pinho, S., Zhang, D., Mizoguchi, T., Wei, Q., Lucas, D., Ito, K., Mar, J. C., Bergman, A., Frenette, P. S. (2013). Arteriolar niches maintain haematopoietic stem cell quiescence. *Nature, 502*(7473), 637-643. doi:10.1038/nature12612

Kwon, C., Arnold, J., Hsiao, E. C., Taketo, M. M., Conklin, B. R., & Srivastava, D. (2007). Canonical Wnt signaling is a positive regulator of mammalian cardiac progenitors. *Proc Natl Acad Sci U S A, 104*(26), 10894-10899. doi:10.1073/pnas.0704044104
Labat-Moleur, F., Steffan, A. M., Brisson, C., Perron, H., Feugeas, O., Furstenberger, P., Oberling, F., Brambilla, E., Behr, J. P. (1996). An electron microscopy study into the mechanism of gene transfer with lipopolyamines. *Gene Ther, 3*(11), 1010-1017.

Ladikou, E. E., Sivaloganathan, H., Pepper, A., & Chevassut, T. (2020). Acute Myeloid Leukaemia in Its Niche: the Bone Marrow Microenvironment in Acute Myeloid Leukaemia. *Curr Oncol Rep, 22*(3), 27. doi:10.1007/s11912-020-0885-0

Laird, D. J., von Andrian, U. H., & Wagers, A. J. (2008). Stem cell trafficking in tissue development, growth, and disease. *Cell, 132*(4), 612-630. doi:10.1016/j.cell.2008.01.041

Lane, S. W., Wang, Y. J., Lo Celso, C., Ragu, C., Bullinger, L., Sykes, S. M., Ferraro, F., Shterental, S., Lin, C. P., Gilliland, D. G., Scadden, D. T., Armstrong, S. A., Williams, D. A. (2011). Differential niche and Wnt requirements during acute myeloid leukemia progression. *Blood, 118*(10), 2849-2856. doi:10.1182/blood-2011-03-345165

Ledran, M. H., Krassowska, A., Armstrong, L., Dimmick, I., Renström, J., Lang, R., Yung, S., Santibanez-Coref, M., Dzierzak, E., Stojkovic, M., Oostendorp, R. A. J., Forrester, L., Lako, M. (2008). Efficient hematopoietic differentiation of human embryonic stem cells on stromal cells derived from hematopoietic niches. *Cell Stem Cell, 3*(1), 85-98. doi:10.1016/j.stem.2008.06.001

Lee, J. G., Takahama, S., Zhang, G., Tomarev, S. I., & Ye, Y. (2016). Unconventional secretion of misfolded proteins promotes adaptation to proteasome dysfunction in mammalian cells. *Nat Cell Biol, 18*(7), 765-776. doi:10.1038/ncb3372

Leimeister, C., Bach, A., & Gessler, M. (1998). Developmental expression patterns of mouse sFRP genes encoding members of the secreted frizzled related protein family. *Mech Dev, 75*(1-2), 29-42. doi:10.1016/s0925-4773(98)00072-0

Leimkühler, N. B., & Schneider, R. K. (2019). Inflammatory bone marrow microenvironment. *Hematology Am Soc Hematol Educ Program, 2019*(1), 294-302. doi:10.1182/hematology.2019000045

Lemus, L., & Goder, V. (2014). Regulation of Endoplasmic Reticulum-Associated Protein Degradation (ERAD) by Ubiquitin. *Cells, 3*(3), 824-847. doi:10.3390/cells3030824

Lesur, O., Kokis, A., Hermans, C., Fülöp, T., Bernard, A., & Lane, D. (2000). Interleukin-2 involvement in early acute respiratory distress syndrome: relationship with polymorphonuclear neutrophil apoptosis and patient survival. *Crit Care Med, 28*(12), 3814-3822. doi:10.1097/00003246-200012000-00010

Li, H., Dai, K., Tang, T., Zhang, X., Yan, M., & Lou, J. (2007). Bone regeneration by implantation of adipose-derived stromal cells expressing BMP-2. *Biochem Biophys Res Commun, 356*(4), 836-842. doi:10.1016/j.bbrc.2007.02.165

Li, S., Ilaria, R. L., Jr., Million, R. P., Daley, G. Q., & Van Etten, R. A. (1999). The P190, P210, and P230 forms of the BCR/ABL oncogene induce a similar chronic myeloid leukemia-like syndrome in mice but have different lymphoid leukemogenic activity. *J Exp Med, 189*(9), 1399-1412. doi:10.1084/jem.189.9.1399

Li, W., Johnson, S. A., Shelley, W. C., Ferkowicz, M., Morrison, P., Li, Y., & Yoder, M. C. (2003). Primary endothelial cells isolated from the yolk sac and para-aortic splanchnopleura support the expansion of adult marrow stem cells in vitro. *Blood, 102*(13), 4345-4353. doi:10.1182/blood-2003-03-0729

Liang, C. C., Park, A. Y., & Guan, J. L. (2007). In vitro scratch assay: a convenient and inexpensive method for analysis of cell migration in vitro. *Nat Protoc, 2*(2), 329-333. doi:10.1038/nprot.2007.30

Liang, C. J., Wang, Z. W., Chang, Y. W., Lee, K. C., Lin, W. H., & Lee, J. L. (2019). SFRPs Are Biphasic Modulators of Wnt-Signaling-Elicited Cancer Stem Cell Properties beyond Extracellular Control. *Cell Rep, 28*(6), 1511-1525.e1515. doi:10.1016/j.celrep.2019.07.023

Liang, H., Chen, Q., Coles, A. H., Anderson, S. J., Pihan, G., Bradley, A., Gerstein, R., Jurecic, R., Jones, S. N. (2003). Wnt5a inhibits B cell proliferation and functions as a tumor suppressor in hematopoietic tissue. *Cancer Cell, 4*(5), 349-360. doi:10.1016/s1535-6108(03)00268-x

Lill, N. L., Grossman, S. R., Ginsberg, D., DeCaprio, J., & Livingston, D. M. (1997). Binding and modulation of p53 by p300/CBP coactivators. *Nature, 387*(6635), 823-827. doi:10.1038/42981

Littlefield, J. W. (1982). NIH 3T3 cell line. *Science, 218*(4569), 214-216. doi:10.1126/science.218.4569.214-b

Liu, T. H., Raval, A., Chen, S. S., Matkovic, J. J., Byrd, J. C., & Plass, C. (2006). CpG island methylation and expression of the secreted frizzled-related protein gene family in chronic lymphocytic leukemia. *Cancer Res, 66*(2), 653-658. doi:10.1158/0008-5472.Can-05-3712

Liu, W., Tolar, P., Song, W., & Kim, T. J. (2020). Editorial: BCR Signaling and B Cell Activation. *Frontiers in Immunology, 11*(45). doi:10.3389/fimmu.2020.00045

Liu, X., Wang, L., Zhao, K., Thompson, P. R., Hwang, Y., Marmorstein, R., & Cole, P. A. (2008). The structural basis of protein acetylation by the p300/CBP transcriptional coactivator. *Nature, 451*(7180), 846-850. doi:10.1038/nature06546

Lo Celso, C., & Scadden, D. T. (2011). The haematopoietic stem cell niche at a glance. *J Cell Sci, 124*(Pt 21), 3529-3535. doi:10.1242/jcs.074112

Loeffler, M., & Roeder, I. (2002). Tissue stem cells: definition, plasticity, heterogeneity, self-organization and models--a conceptual approach. *Cells Tissues Organs, 171*(1), 8-26. doi:10.1159/000057688

Loghavi, S., Kutok, J. L., & Jorgensen, J. L. (2015). B-acute lymphoblastic leukemia/lymphoblastic lymphoma. *Am J Clin Pathol, 144*(3), 393-410. doi:10.1309/ajcpan7bh5dnywzb

Lopez-Rios, J., Esteve, P., Ruiz, J. M., & Bovolenta, P. (2008). The Netrin-related domain of Sfrp1 interacts with Wnt ligands and antagonizes their activity in the anterior neural plate. *Neural Development, 3*(1), 19. doi:10.1186/1749-8104-3-19

Love, M. I., Huber, W., & Anders, S. (2014). Moderated estimation of fold change and dispersion for RNA-seq data with DESeq2. *Genome Biol, 15*(12), 550. doi:10.1186/s13059-014-0550-8

Luis, T. C., Naber, B. A., Roozen, P. P., Brugman, M. H., de Haas, E. F., Ghazvini, M., Fibbe, W. E., van Dongen, J. J., Fodde, R., Staal, F.J. (2011) Canonical wnt signaling regulates hematopoiesis in a dosage-dependent fashion. *Cell Stem Cell*, *9*(4), 345-56. doi: 10.1016/j.stem.2011.07.017.

Luis, T. C., Ichii, M., Brugman, M. H., Kincade, P., & Staal, F. J. (2012). Wnt signaling strength regulates normal hematopoiesis and its deregulation is involved in leukemia development. *Leukemia, 26*(3), 414-421. doi:10.1038/leu.2011.387

Luskey, B. D., Rosenblatt, M., Zsebo, K., & Williams, D. A. (1992). Stem cell factor, interleukin-3, and interleukin-6 promote retroviral-mediated gene transfer into murine hematopoietic stem cells. *Blood, 80*(2), 396-402.

Lutze, G., Haarmann, A., Demanou Toukam, J. A., Buttler, K., Wilting, J., & Becker, J. (2019). Non-canonical WNT-signaling controls differentiation of lymphatics and extension lymphangiogenesis via RAC and JNK signaling. *Scientific Reports, 9*(1), 4739. doi:10.1038/s41598-019-41299-7

Lutzny, G., Kocher, T., Schmidt-Supprian, M., Rudelius, M., Klein-Hitpass, L., Finch, A. J., Dürig, J., Wagner, M., Haferlach, C., Kohlmann, A., Schnittger, S., Seifert, M., Wanninger, S., Zaborsky, N., Oostendorp, R., Ruland, J., Leitges, M., Kuhnt, T., Schäfer, Y., Lampl, B., Peschel, C., Egle, A., Ringshausen, I. (2013). Protein kinase c-β-dependent activation of NF-κB in stromal cells is indispensable for the survival of chronic lymphocytic leukemia B cells in vivo. *Cancer Cell, 23*(1), 77-92. doi:10.1016/j.ccr.2012.12.003

Ma, H., Nguyen, C., Lee, K. S., & Kahn, M. (2005). Differential roles for the coactivators CBP and p300 on TCF/beta-catenin-mediated survivin gene expression. *Oncogene, 24*(22), 3619-3631. doi:10.1038/sj.onc.1208433

Ma, Q., Jones, D., Borghesani, P. R., Segal, R. A., Nagasawa, T., Kishimoto, T., Broson, R. T., Springer, T. A. (1998). Impaired B-lymphopoiesis, myelopoiesis, and derailed cerebellar neuron migration in CXCR4- and SDF-1-deficient mice. *Proc Natl Acad Sci U S A, 95*(16), 9448-9453. doi:10.1073/pnas.95.16.9448

MacDonald, B. T., Tamai, K., & He, X. (2009). Wnt/beta-catenin signaling: components, mechanisms, and diseases. *Dev Cell, 17*(1), 9-26. doi:10.1016/j.devcel.2009.06.016

Macosko, E. Z., Basu, A., Satija, R., Nemesh, J., Shekhar, K., Goldman, M., Tirosh, I., Bialas, A. R., Kamitaki, N., Martersteck, E. M., Trombetta, J. J., Weitz, D. A., Sanes, J. R., Shalek, A. K., Regev, A., McCarroll, S. A. (2015). Highly Parallel Genome-wide Expression Profiling of Individual Cells Using Nanoliter Droplets. *Cell, 161*(5), 1202-1214. doi:10.1016/j.cell.2015.05.002

Maeda, K., Kobayashi, Y., Udagawa, N., Uehara, S., Ishihara, A., Mizoguchi, T., Kikuchi, Y., Takada, I., Kato, S., Kani, S., Nishita, M., Marumo, K., Martin, T. J., Minami, Y., Takahashi, N. (2012). Wnt5a-Ror2 signaling between osteoblast-lineage cells and osteoclast precursors enhances osteoclastogenesis. *Nat Med, 18*(3), 405-412. doi:10.1038/nm.2653

Maehle, A. H. (2011). Ambiguous cells: the emergence of the stem cell concept in the nineteenth and twentieth centuries. *Notes Rec R Soc Lond, 65*(4), 359-378. doi:10.1098/rsnr.2011.0023

Mangolini, M., Götte, F., Moore, A., Ammon, T., Oelsner, M., Lutzny-Geier, G., Klein-Hitpass, L., Williamson, J. C., Lehner, P. J., Dürig, J., Möllmann, M., Rásó-Barnett, L., Hughes, K., Santoro, A., Méndez-Ferrer, S., Oostendorp, R. A. J., Zimber-Strobl, U., Peschel, C., Hodson, D. J., Schmidt-Supprian, M., Ringshausen, I. (2018). Notch2 controls non-autonomous Wnt-signalling in chronic lymphocytic leukaemia. *Nat Commun, 9*(1), 3839. doi:10.1038/s41467-018-06069-5

Marquez Romero, S., Hettler, F., Hausinger, R., Schreck, C., Landspersky, T., Henkel, L., Angepointner, C., Demir, I. E., Schiemann, M., Bassermann, F., Götze, K. S., Istvánffy, R., Oostendorp, R. A. J. (2020). Secreted factors from mouse embryonic fibroblasts maintain repopulating function of single cultured hematopoietic stem cells. *Haematologica*. doi:10.3324/haematol.2020.249102

Marzio, G., Wagener, C., Gutierrez, M. I., Cartwright, P., Helin, K., & Giacca, M. (2000). E2F family members are differentially regulated by reversible acetylation. *J Biol Chem, 275*(15), 10887-10892. doi:10.1074/jbc.275.15.10887

McCarthy, K. F., Ledney, G. D., & Mitchell, R. (1977). A DEFICIENCY OF HEMATOPOIETIC STEM CELLS IN STEEL MICE. *Cell Proliferation, 10*(2), 121-126. doi:https://doi.org/10.1111/j.1365-2184.1977.tb00137.x

McGrath, K. E., Frame, J. M., Fegan, K. H., Bowen, J. R., Conway, S. J., Catherman, S. C., Kingsley, P. D., Koniski, A. D., Palis, J. (2015). Distinct Sources of Hematopoietic Progenitors Emerge before HSCs and Provide Functional Blood Cells in the Mammalian Embryo. *Cell Rep, 11*(12), 1892-1904. doi:10.1016/j.celrep.2015.05.036

McGrath, K. E., Frame, J. M., Fromm, G. J., Koniski, A. D., Kingsley, P. D., Little, J., Bulger, M., Palis, J. (2011). A transient definitive erythroid lineage with unique regulation of the β-globin locus in the mammalian embryo. *Blood, 117*(17), 4600-4608. doi:10.1182/blood-2010-12-325357

Medvinsky, A., Rybtsov, S., & Taoudi, S. (2011). Embryonic origin of the adult hematopoietic system: advances and questions. *Development, 138*(6), 1017-1031. doi:10.1242/dev.040998

Medyouf, H., Mossner, M., Jann, J. C., Nolte, F., Raffel, S., Herrmann, C., Lier, A., Eisen, C., Nowak, V., Zens, B., Müdder, K., Klein, C., Obländer, J., Fey, S., Vogler, J., Fabarius, A., Riedl, E., Roehl, H., Kohlmann, A., Staller, M., Haferlach, C., Müller, N., John, T., Platzbecker, U., Metzgeroth, G., Hofmann, W.-K., Trumpp, A., Nowak, D. (2014). Myelodysplastic cells in patients reprogram mesenchymal stromal cells to establish a transplantable stem cell niche disease unit. *Cell Stem Cell, 14*(6), 824-837. doi:10.1016/j.stem.2014.02.014

Mendelson, A., & Frenette, P. S. (2014). Hematopoietic stem cell niche maintenance during homeostasis and regeneration. *Nat Med, 20*(8), 833-846. doi:10.1038/nm.3647

Méndez-Ferrer, S., Michurina, T. V., Ferraro, F., Mazloom, A. R., Macarthur, B. D., Lira, S. A., Scadden, D. T., Ma'ayan, A., Enikolopov, G. N., Frenette, P. S. (2010). Mesenchymal and haematopoietic stem cells form a unique bone marrow niche. *Nature, 466*(7308), 829-834. doi:10.1038/nature09262

Mercier, F. E., Ragu, C., & Scadden, D. T. (2011). The bone marrow at the crossroads of blood and immunity. *Nat Rev Immunol, 12*(1), 49-60. doi:10.1038/nri3132

Meusser, B., Hirsch, C., Jarosch, E., & Sommer, T. (2005). ERAD: the long road to destruction. *Nat Cell Biol, 7*(8), 766-772. doi:10.1038/ncb0805-766

Mi, H., Poudel, S., Muruganujan, A., Casagrande, J. T., & Thomas, P. D. (2016). PANTHER version 10: expanded protein families and functions, and analysis tools. *Nucleic Acids Res, 44*(D1), D336-342. doi:10.1093/nar/gkv1194

Miething, C., Mugler, C., Grundler, R., Hoepfl, J., Bai, R. Y., Peschel, C., & Duyster, J. (2003). Phosphorylation of tyrosine 393 in the kinase domain of Bcr-Abl influences the sensitivity towards imatinib in vivo. *Leukemia, 17*(9), 1695-1699. doi:10.1038/sj.leu.2403040

Miller, D. G., Adam, M. A., & Miller, A. D. (1990). Gene transfer by retrovirus vectors occurs only in cells that are actively replicating at the time of infection. *Mol Cell Biol, 10*(8), 4239-4242. doi:10.1128/mcb.10.8.4239-4242.1990

Milosevic, J. D., & Kralovics, R. (2013). Genetic and epigenetic alterations of myeloproliferative disorders. *Int J Hematol, 97*(2), 183-197. doi:10.1007/s12185-012-1235-2

Mishra, P. J., Mishra, P. J., Humeniuk, R., Medina, D. J., Alexe, G., Mesirov, J. P., Ganesan, S., Glod, J. W., Banerjee, D. (2008). Carcinoma-associated fibroblast-like differentiation of human mesenchymal stem cells. *Cancer Res, 68*(11), 4331-4339. doi:10.1158/0008-5472.Can-08-0943

Mitani, K., Sato, Y., Tojo, A., Ishikawa, F., Kobayashi, Y., Miura, Y., Miyazono, K., Urabe, A., Takaku, F. (1990). Philadelphia chromosome positive B-cell type malignant lymphoma expressing an aberrant 190 kDa bcr-abl protein. *British Journal of Haematology, 76*(2), 221-225. doi:https://doi.org/10.1111/j.1365-2141.1990.tb07875.x

Miyabayashi, T., Teo, J. L., Yamamoto, M., McMillan, M., Nguyen, C., & Kahn, M. (2007). Wnt/beta-catenin/CBP signaling maintains long-term murine embryonic stem cell pluripotency. *Proc Natl Acad Sci U S A, 104*(13), 5668-5673. doi:10.1073/pnas.0701331104

Miyabayashi, T., Yamamoto, M., Sato, A., Sakano, S., & Takahashi, Y. (2008). Indole derivatives sustain embryonic stem cell self-renewal in long-term culture. *Biosci Biotechnol Biochem, 72*(5), 1242-1248. doi:10.1271/bbb.70717

Mizoguchi, T., Pinho, S., Ahmed, J., Kunisaki, Y., Hanoun, M., Mendelson, A., Ono, N., Kronenberg, H. M., Frenette, P. S. (2014) Osterix marks distinct waves of primitive and definitive stromal progenitors during bone marrow development. *Dev Cell*, 29(3), 340-9. doi: 10.1016/j.devcel.2014.03.013.

Moerman, E. J., Teng, K., Lipschitz, D. A., & Lecka-Czernik, B. (2004). Aging activates adipogenic and suppresses osteogenic programs in mesenchymal marrow stroma/stem cells: the role of PPAR-gamma2 transcription factor and TGF-beta/BMP signaling pathways. *Aging Cell, 3*(6), 379-389. doi:10.1111/j.1474-9728.2004.00127.x

Morikawa, S., Mabuchi, Y., Kubota, Y., Nagai, Y., Niibe, K., Hiratsu, E., Suzuki, S., Miyauchi-Hara, C., Nagoshi, N., Sunabori, T., Shimmura, S., Miyawaki, A., Nakagawa, T., Suda, T., Okano, H., Matsuzaki, Y. (2009). Prospective identification, isolation, and systemic transplantation of multipotent mesenchymal stem cells in murine bone marrow. *J Exp Med, 206*(11), 2483-2496. doi:10.1084/jem.20091046

Morrison, S. J., & Kimble, J. (2006). Asymmetric and symmetric stem-cell divisions in development and cancer. *Nature, 441*(7097), 1068-1074. doi:10.1038/nature04956

Morrison, S. J., & Scadden, D. T. (2014). The bone marrow niche for haematopoietic stem cells. *Nature, 505*(7483), 327-334. doi:10.1038/nature12984

Morrison, S. J., & Spradling, A. C. (2008). Stem cells and niches: mechanisms that promote stem cell maintenance throughout life. *Cell, 132*(4), 598-611. doi:10.1016/j.cell.2008.01.038

Morse, H. C., 3rd, Anver, M. R., Fredrickson, T. N., Haines, D. C., Harris, A. W., Harris, N. L., Jaffe, E. S., Kogan, S. C., MacLennan, I. C. M., Pattengale, P. K., Ward, J. M. (2002). Bethesda proposals for classification of lymphoid neoplasms in mice. *Blood, 100*(1), 246-258. doi:10.1182/blood.v100.1.246

Mosteo, L., Storer, J., Batta, K., Searle, E. J., Duarte, D., & Wiseman, D. H. (2021). The Dynamic Interface Between the Bone Marrow Vascular Niche and Hematopoietic Stem Cells in Myeloid Malignancy. *Frontiers in Cell and Developmental Biology, 9*(418). doi:10.3389/fcell.2021.635189

Moxey-Mims, M. M., Simms, H. H., Frank, M. M., Lin, E. Y., & Gaither, T. A. (1991). The effects of IL-1, IL-2, and tumor necrosis factor on polymorphonuclear leukocyte Fc gamma receptor-mediated phagocytosis. IL-2 down-regulates the effect of tumor necrosis factor. *J Immunol, 147*(6), 1823-1830.

Mumby, M. C., & Walter, G. (1993). Protein serine/threonine phosphatases: structure, regulation, and functions in cell growth. *Physiol Rev, 73*(4), 673-699. doi:10.1152/physrev.1993.73.4.673

Muraglia, A., Cancedda, R., & Quarto, R. (2000). Clonal mesenchymal progenitors from human bone marrow differentiate in vitro according to a hierarchical model. *J Cell Sci, 113 (Pt 7)*, 1161-1166.

Muroyama, Y., Kondoh, H., & Takada, S. (2004). Wnt proteins promote neuronal differentiation in neural stem cell culture. *Biochem Biophys Res Commun, 313*(4), 915-921. doi:10.1016/j.bbrc.2003.12.023

Müller, A. M., Medvinsky, A., Strouboulis, J., Grosveld, F., Dzierzak, E. (1994) Development of hematopoietic stem cell activity in the mouse embryo. *Immunity*, *1*(4), 291-301. doi: 10.1016/1074-7613(94)90081-7.

Naito, A. T., Shiojima, I., Akazawa, H., Hidaka, K., Morisaki, T., Kikuchi, A., & Komuro, I. (2006). Developmental stage-specific biphasic roles of Wnt/beta-catenin signaling in cardiomyogenesis and hematopoiesis. *Proc Natl Acad Sci U S A, 103*(52), 19812-19817. doi:10.1073/pnas.0605768103

Nakajima, H., Ito, M., Morikawa, Y., Komori, T., Fukuchi, Y., Shibata, F., Okamoto, S., Kitamura, T. (2009). Wnt modulators, SFRP-1, and SFRP-2 are expressed in osteoblasts and differentially regulate hematopoietic stem cells. *Biochem Biophys Res Commun, 390*(1), 65-70. doi:https://doi.org/10.1016/j.bbrc.2009.09.067

Nakamura, Y., Arai, F., Iwasaki, H., Hosokawa, K., Kobayashi, I., Gomei, Y., Matsumoto, Y., Yoshihara, H., Suda, T. (2010). Isolation and characterization of endosteal niche cell populations that regulate hematopoietic stem cells. *Blood, 116*(9), 1422-1432. doi:10.1182/blood-2009-08-239194

Neal, S., Duttke, S. H., & Hampton, R. Y. (2019). Assays for protein retrotranslocation in ERAD. *Methods Enzymol, 619*, 1-26. doi:10.1016/bs.mie.2019.01.002

Negahdaripour, M., Nezafat, N., & Ghasemi, Y. (2016). A panoramic review and in silico analysis of IL-11 structure and function. *Cytokine Growth Factor Rev, 32*, 41-61. doi:10.1016/j.cytogfr.2016.06.002

Nemeth, M. J., Topol, L., Anderson, S. M., Yang, Y., & Bodine, D. M. (2007). Wnt5a inhibits canonical Wnt signaling in hematopoietic stem cells and enhances repopulation. *Proc Natl Acad Sci U S A, 104*(39), 15436-15441. doi:10.1073/pnas.0704747104

Neuber, O., Jarosch, E., Volkwein, C., Walter, J., & Sommer, T. (2005). Ubx2 links the Cdc48 complex to ER-associated protein degradation. *Nat Cell Biol, 7*(10), 993-998. doi:10.1038/ncb1298

Neumann, E. (1868). *Zentralbl. f. d. mediz. Wiss., 44*, 689.

Nowell, P. C., & Hungerford, D. A. (1960a). Chromosome studies on normal and leukemic human leukocytes. *J Natl Cancer Inst, 25*, 85-109.

Nowell, P. C., & Hungerford, D. A. (1960b). A minute chromosome in human chronic granulocytic leukemia. *Science, 132*, 1497.

Nygren, M. K., Døsen, G., Hystad, M. E., Stubberud, H., Funderud, S., & Rian, E. (2007). Wnt3A activates canonical Wnt signalling in acute lymphoblastic leukaemia (ALL) cells and inhibits the proliferation of B-ALL cell lines. *British Journal of Haematology, 136*(3), 400-413. doi:https://doi.org/10.1111/j.1365-2141.2006.06442.x

Ohlstein, B., Kai, T., Decotto, E., & Spradling, A. (2004). The stem cell niche: theme and variations. *Curr Opin Cell Biol, 16*(6), 693-699. doi:10.1016/j.ceb.2004.09.003

Ohneda, O., Fennie, C., Zheng, Z., Donahue, C., La, H., Villacorta, R., Cairns, B., Lasky, L. A. (1998). Hematopoietic Stem Cell Maintenance and Differentiation Are Supported by Embryonic Aorta-Gonad-Mesonephros Region–Derived Endothelium. *Blood, 92*(3), 908-919. doi:10.1182/blood.V92.3.908

Oike, Y., Takakura, N., Hata, A., Kaname, T., Akizuki, M., Yamaguchi, Y., Yasue, H., Araki, K., Yamamura, K., Suda, T. (1999). Mice homozygous for a truncated form of CREB-binding protein exhibit defects in hematopoiesis and vasculo-angiogenesis. *Blood, 93*(9), 2771-2779.

Oostendorp, R. A., Harvey, K. N., Kusadasi, N., de Bruijn, M. F., Saris, C., Ploemacher, R. E., Medvinsky, A. L., Dzierzak, E. A. (2002). Stromal cell lines from mouse aorta-gonads-mesonephros subregions are potent supporters of hematopoietic stem cell activity. *Blood, 99*(4), 1183-1189. doi:10.1182/blood.v99.4.1183

Oostendorp, R. A., Medvinsky, A. J., Kusadasi, N., Nakayama, N., Harvey, K., Orelio, C., Ottersbach, K., Covey, T., Ploemacher, R. E., Saris, C., Dzierzak, E. (2002a). Embryonal subregion-derived stromal cell lines from novel temperature-sensitive SV40 T antigen transgenic mice support hematopoiesis. *J Cell Sci, 115*(Pt 10), 2099-2108.

Oostendorp, R. A., Robin, C., Steinhoff, C., Marz, S., Bräuer, R., Nuber, U. A., Dzierzak, E. A., Peschel, C. (2005). Long-term maintenance of hematopoietic stem cells does not require contact with embryo-derived stromal cells in cocultures. *Stem Cells, 23*(6), 842-851. doi:10.1634/stemcells.2004-0120

Orkin, S. H., & Zon, L. I. (2008). Hematopoiesis: an evolving paradigm for stem cell biology. *Cell, 132*(4), 631-644. doi:10.1016/j.cell.2008.01.025

Osawa, M., Hanada, K., Hamada, H., & Nakauchi, H. (1996). Long-term lymphohematopoietic reconstitution by a single CD34-low/negative hematopoietic stem cell. *Science, 273*(5272), 242-245. doi:10.1126/science.273.5272.242

Otero, J. J., Fu, W., Kan, L., Cuadra, A. E., & Kessler, J. A. (2004). Beta-catenin signaling is required for neural differentiation of embryonic stem cells. *Development, 131*(15), 3545-3557. doi:10.1242/dev.01218

Otsuru, S., Tamai, K., Yamazaki, T., Yoshikawa, H., & Kaneda, Y. (2007). Bone marrow-derived osteoblast progenitor cells in circulating blood contribute to ectopic bone formation in mice. *Biochem Biophys Res Commun, 354*(2), 453-458. doi:10.1016/j.bbrc.2006.12.226

Palis, J., Robertson, S., Kennedy, M., Wall, C., & Keller, G. (1999). Development of erythroid and myeloid progenitors in the yolk sac and embryo proper of the mouse. *Development, 126*(22), 5073-5084.

Palis, J., & Yoder, M. C. (2001). Yolk-sac hematopoiesis: the first blood cells of mouse and man. *Exp Hematol, 29*(8), 927-936. doi:10.1016/s0301-472x(01)00669-5

Pao, G. M., Janknecht, R., Ruffner, H., Hunter, T., & Verma, I. M. (2000). CBP/p300 interact with and function as transcriptional coactivators of BRCA1. *Proc Natl Acad Sci U S A, 97*(3), 1020-1025. doi:10.1073/pnas.97.3.1020

Parekh, S., Ziegenhain, C., Vieth, B., Enard, W., & Hellmann, I. (2016). The impact of amplification on differential expression analyses by RNA-seq. *Scientific Reports, 6*(1), 25533. doi:10.1038/srep25533

Parker, T. W., & Neufeld, K. L. (2020). APC controls Wnt-induced β-catenin destruction complex recruitment in human colonocytes. *Scientific Reports, 10*(1), 2957. doi:10.1038/s41598-020-59899-z

Partanen, A., Motoyama, J., & Hui, C. C. (1999). Developmentally regulated expression of the transcriptional cofactors/histone acetyltransferases CBP and p300 during mouse embryogenesis. *Int J Dev Biol, 43*(6), 487-494.

Passegué, E., Jamieson, C. H., Ailles, L. E., & Weissman, I. L. (2003). Normal and leukemic hematopoiesis: are leukemias a stem cell disorder or a reacquisition of stem cell characteristics? *Proc Natl Acad Sci U S A, 100 Suppl 1*(Suppl 1), 11842-11849. doi:10.1073/pnas.2034201100

Patel, Alam, A., Pant, R., & Chattopadhyay, S. (2019). Wnt Signaling and Its Significance Within the Tumor Microenvironment: Novel Therapeutic Insights. *Frontiers in Immunology, 10*(2872). doi:10.3389/fimmu.2019.02872

Patel, Huang, S. M., Baglia, L. A., & McCance, D. J. (1999). The E6 protein of human papillomavirus type 16 binds to and inhibits co-activation by CBP and p300. *Embo j, 18*(18), 5061-5072. doi:10.1093/emboj/18.18.5061

Pathak, P., Li, Y., Gray, B. A., May, W. S., Jr., & Markham, M. J. (2017). Synchronous Occurrence of Chronic Myeloid Leukemia and Mantle Cell Lymphoma. *Case Rep Hematol, 2017*, 7815095. doi:10.1155/2017/7815095

Paul, S. R., Bennett, F., Calvetti, J. A., Kelleher, K., Wood, C. R., O'Hara, R. M., Jr., Leary, A. C., Sibley, B., Clark, S. C., Williams, D. A. (1990). Molecular cloning of a cDNA encoding interleukin 11, a stromal cell-derived lymphopoietic and hematopoietic cytokine. *Proc Natl Acad Sci U S A, 87*(19), 7512-7516. doi:10.1073/pnas.87.19.7512

Pear, W. S., Nolan, G. P., Scott, M. L., & Baltimore, D. (1993). Production of high-titer helper-free retroviruses by transient transfection. *Proc Natl Acad Sci U S A, 90*(18), 8392-8396. doi:10.1073/pnas.90.18.8392

Peifer, M., & Polakis, P. (2000). Wnt signaling in oncogenesis and embryogenesis--a look outside the nucleus. *Science, 287*(5458), 1606-1609. doi:10.1126/science.287.5458.1606

Peng, X., Yang, L., Chang, H., Dai, G., Wang, F., Duan, X., Guo, L., Zhang, Y., Chen, G. (2014). Wnt/β-Catenin Signaling Regulates the Proliferation and Differentiation of Mesenchymal Progenitor Cells through the p53 Pathway. *PLOS ONE, 9*(5), e97283. doi:10.1371/journal.pone.0097283

Péterfy, M., Ben-Zeev, O., Mao, H. Z., Weissglas-Volkov, D., Aouizerat, B. E., Pullinger, C. R., Frost, P. H., Kane, J. P., Malloy, M. J., Reue, K., Pajukanta, P., Doolittle, M. H. (2007). Mutations in LMF1 cause combined lipase deficiency and severe hypertriglyceridemia. *Nat Genet, 39*(12), 1483-1487. doi:10.1038/ng.2007.24

Pettitt, S. J., Liang, Q., Rairdan, X. Y., Moran, J. L., Prosser, H. M., Beier, D. R., Lloyd, K. C., Bradley, A., Skarnes, W. C. (2009). Agouti C57BL/6N embryonic stem cells for mouse genetic resources. *Nat Methods, 6*(7), 493-495. doi:10.1038/nmeth.1342

Phillips, M. J., & Voeltz, G. K. (2016). Structure and function of ER membrane contact sites with other organelles. *Nat Rev Mol Cell Biol, 17*(2), 69-82. doi:10.1038/nrm.2015.8

Picelli, S., Björklund Å, K., Faridani, O. R., Sagasser, S., Winberg, G., & Sandberg, R. (2013). Smart-seq2 for sensitive full-length transcriptome profiling in single cells. *Nat Methods, 10*(11), 1096-1098. doi:10.1038/nmeth.2639

Pietras, E. M., Warr, M. R., & Passegué, E. (2011). Cell cycle regulation in hematopoietic stem cells. *J Cell Biol, 195*(5), 709-720. doi:10.1083/jcb.201102131

Pitchford, S. C., Furze, R. C., Jones, C. P., Wengner, A. M., & Rankin, S. M. (2009). Differential mobilization of subsets of progenitor cells from the bone marrow. *Cell Stem Cell, 4*(1), 62-72. doi:10.1016/j.stem.2008.10.017

Pittenger, M. F., Mackay, A. M., Beck, S. C., Jaiswal, R. K., Douglas, R., Mosca, J. D., Moorman, M. A., Simonetti, D. W., Marshak, D. R. (1999). Multilineage potential of adult human mesenchymal stem cells. *Science, 284*(5411), 143-147. doi:10.1126/science.284.5411.143

Pouponnot, C., Jayaraman, L., & Massagué, J. (1998). Physical and functional interaction of SMADs and p300/CBP. *J Biol Chem, 273*(36), 22865-22868. doi:10.1074/jbc.273.36.22865

Qiu, L. Q., Lai, W. S., Stumpo, D. J., & Blackshear, P. J. (2016). Mouse Embryonic Fibroblast Cell Culture and Stimulation. *Bio Protoc, 6*(13). doi:10.21769/BioProtoc.1859

Raaijmakers, M. H., Mukherjee, S., Guo, S., Zhang, S., Kobayashi, T., Schoonmaker, J. A., Ebert, B. L., Al-Shahrour, F., Hasserjian, R. P., Scadden, E. O., Aung, Z., Matza, M., Merkenschlager, M., Lin, C., Rommens, J. M., Scadden, D. T. (2010). Bone progenitor dysfunction induces myelodysplasia and secondary leukaemia. *Nature, 464*(7290), 852-857. doi:10.1038/nature08851

Rafii, S., Mohle, R., Shapiro, F., Frey, B. M., & Moore, M. A. (1997). Regulation of hematopoiesis by microvascular endothelium. *Leuk Lymphoma, 27*(5-6), 375-386. doi:10.3109/10428199709058305

Raitano, A. B., Whang, Y. E., & Sawyers, C. L. (1997). Signal transduction by wild-type and leukemogenic Abl proteins. *Biochim Biophys Acta, 1333*(3), F201-216. doi:10.1016/s0304-419x(97)00023-1

Rao, T. P., & Kühl, M. (2010). An Updated Overview on Wnt Signaling Pathways. *Circulation Research, 106*(12), 1798-1806. doi:doi:10.1161/CIRCRESAHA.110.219840
Rebel, V. I., Kung, A. L., Tanner, E. A., Yang, H., Bronson, R. T., & Livingston, D. M. (2002). Distinct roles for CREB-binding protein and p300 in hematopoietic stem cell self-renewal. *Proc Natl Acad Sci U S A, 99*(23), 14789-14794. doi:10.1073/pnas.232568499

Reckel, S., Hamelin, R., Georgeon, S., Armand, F., Jolliet, Q., Chiappe, D., Moniatte, M., Hantschel, O. (2017). Differential signaling networks of Bcr–Abl p210 and p190 kinases in leukemia cells defined by functional proteomics. *Leukemia, 31*(7), 1502-1512. doi:10.1038/leu.2017.36

Reins, J., Mossner, M., Neumann, M., Platzbecker, U., Schumann, C., Thiel, E., & Hofmann, W. K. (2010). Transcriptional down-regulation of the Wnt antagonist SFRP1 in haematopoietic cells of patients with different risk types of MDS. *Leuk Res, 34*(12), 1610-1616. doi:10.1016/j.leukres.2010.04.013

Ren, R. (2005). Mechanisms of BCR-ABL in the pathogenesis of chronic myelogenous leukaemia. *Nat Rev Cancer, 5*(3), 172-183. doi:10.1038/nrc1567

Renström, J., Istvanffy, R., Gauthier, K., Shimono, A., Mages, J., Jardon-Alvarez, A., Kröger, M., Schiemann, M., Busch, D. H., Esposito, I., Lang, R., Peschel, C., Oostendorp, R. A. J. (2009). Secreted frizzled-related protein 1 extrinsically regulates cycling activity and maintenance of hematopoietic stem cells. *Cell Stem Cell, 5*(2), 157-167. doi:10.1016/j.stem.2009.05.020

Reya, T., & Clevers, H. (2005). Wnt signalling in stem cells and cancer. *Nature, 434*(7035), 843-850. doi:10.1038/nature03319

Reya, T., Duncan, A. W., Ailles, L., Domen, J., Scherer, D. C., Willert, K., Hintz, L., Nusse, R., Weissman, I. L. (2003). A role for Wnt signalling in self-renewal of haematopoietic stem cells. *Nature, 423*(6938), 409-414. doi:10.1038/nature01593

Reya, T., Morrison, S. J., Clarke, M. F., & Weissman, I. L. (2001). Stem cells, cancer, and cancer stem cells. *Nature, 414*(6859), 105-111. doi:10.1038/35102167

Rieger, M. E., Zhou, B., Solomon, N., Sunohara, M., Li, C., Nguyen, C., Liu, Y., Pan, J.-H., Minoo, P., Crandall, E. D., Brody, S. L., Kahn, M., Borok, Z. (2016). p300/β-Catenin Interactions Regulate Adult Progenitor Cell Differentiation Downstream of WNT5a/Protein Kinase C (PKC). *J Biol Chem, 291*(12), 6569-6582. doi:10.1074/jbc.M115.706416

Rifkind , R. A., Chui , D., & Epler , H. (1969). AN ULTRASTRUCTURAL STUDY OF EARLY MORPHOGENETIC EVENTS DURING THE ESTABLISHMENT OF FETAL HEPATIC ERYTHROPOIESIS. *Journal of Cell Biology, 40*(2), 343-365. doi:10.1083/jcb.40.2.343

Robert, A. W., Marcon, B. H., Dallagiovanna, B., & Shigunov, P. (2020). Adipogenesis, Osteogenesis, and Chondrogenesis of Human Mesenchymal Stem/Stromal Cells: A Comparative Transcriptome Approach. *Front Cell Dev Biol, 8*, 561. doi:10.3389/fcell.2020.00561

Robinson, M. D., McCarthy, D. J., & Smyth, G. K. (2010). edgeR: a Bioconductor package for differential expression analysis of digital gene expression data. *Bioinformatics, 26*(1), 139-140. doi:10.1093/bioinformatics/btp616

Robinson, M. D., & Oshlack, A. (2010). A scaling normalization method for differential expression analysis of RNA-seq data. *Genome Biol, 11*(3), R25. doi:10.1186/gb-2010-11-3-r25

Rodda, S. J., & McMahon, A. P. (2006). Distinct roles for Hedgehog and canonical Wnt signaling in specification, differentiation and maintenance of osteoblast progenitors. *Development, 133*(16), 3231-3244. doi:10.1242/dev.02480

Rodriguez, S., Chora, A., Goumnerov, B., Mumaw, C., Goebel, W. S., Fernandez, L., Baydoun, H., HogenEsch, H., Dombkowski, D. M., Karlewicz, C. A., Rice, S., Rahme, L. G., Carlesso, N. (2009). Dysfunctional expansion of hematopoietic stem cells and block of myeloid differentiation in lethal sepsis. *Blood, 114*(19), 4064-4076. doi:10.1182/blood-2009-04-214916

Rogers, K. (2020). Endoplasmic reticulum. *Encyclopedia Britannica*.

Román-Gómez, J., Cordeu, L., Agirre, X., Jiménez-Velasco, A., San José-Eneriz, E., Garate, L., Calasanz, M. J., Heiniger, A., Torres, A., Prosper, F. (2007). Epigenetic regulation of Wnt-signaling pathway in acute lymphoblastic leukemia. *Blood, 109*(8), 3462-3469. doi:10.1182/blood-2006-09-047043

Rosnet, O., Bühring, H. J., Marchetto, S., Rappold, I., Lavagna, C., Sainty, D., Arnoulet, C., Chabannon, C., Kanz, L., Hannum, C., Birnbaum, D. (1996). Human FLT3/FLK2 receptor tyrosine kinase is expressed at the surface of normal and malignant hematopoietic cells. *Leukemia, 10*(2), 238-248.

Ross, S. E., Hemati, N., Longo, K. A., Bennett, C. N., Lucas, P. C., Erickson, R. L., & MacDougald, O. A. (2000). Inhibition of adipogenesis by Wnt signaling. *Science, 289*(5481), 950-953. doi:10.1126/science.289.5481.950

Roth, J. F., Shikama, N., Henzen, C., Desbaillets, I., Lutz, W., Marino, S., Wittwer, J., Schorle, H., Gassmann, M., Eckner, R. (2003). Differential role of p300 and CBP acetyltransferase during myogenesis: p300 acts upstream of MyoD and Myf5. *Embo j, 22*(19), 5186-5196. doi:10.1093/emboj/cdg473

Rowley, J. D. (1973). Letter: A new consistent chromosomal abnormality in chronic myelogenous leukaemia identified by quinacrine fluorescence and Giemsa staining. *Nature, 243*(5405), 290-293. doi:10.1038/243290a0

Ruf, F., Schreck, C., Wagner, A., Grziwok, S., Pagel, C., Romero, S., Kieslinger, M., Shimono, A., Peschel, C., Götze, K.S., Istvanffy, R., Oostendorp, R. A. J. (2016). Loss of Sfrp2 in the Niche Amplifies Stress-Induced Cellular Responses, and Impairs the In Vivo

Regeneration of the Hematopoietic Stem Cell Pool. *Stem Cells, 34*(9), 2381-2392. doi:https://doi.org/10.1002/stem.2416

Sadowski, P. D. (1995). The Flp recombinase of the 2-microns plasmid of Saccharomyces cerevisiae. *Prog Nucleic Acid Res Mol Biol, 51*, 53-91.

Sands, M. S., & Barker, J. E. (1999). Percutaneous intravenous injection in neonatal mice. *Lab Anim Sci, 49*(3), 328-330.

Santaguida, M., Schepers, K., King, B., Sabnis, A. J., Forsberg, E. C., Attema, J. L., Braun, B.S., Passegué, E. (2009). JunB protects against myeloid malignancies by limiting hematopoietic stem cell proliferation and differentiation without affecting self-renewal. *Cancer Cell, 15*(4), 341-352. doi:10.1016/j.ccr.2009.02.016

Sasaki, T., & Kahn, M. (2014). Inhibition of β-catenin/p300 interaction proximalizes mouse embryonic lung epithelium. *Translational Respiratory Medicine, 2*(1), 8. doi:10.1186/s40247-014-0008-1

Sato, N., Meijer, L., Skaltsounis, L., Greengard, P., & Brivanlou, A. H. (2004). Maintenance of pluripotency in human and mouse embryonic stem cells through activation of Wnt signaling by a pharmacological GSK-3-specific inhibitor. *Nat Med, 10*(1), 55-63. doi:10.1038/nm979

Satoh, W., Gotoh, T., Tsunematsu, Y., Aizawa, S., & Shimono, A. (2006). Sfrp1 and Sfrp2 regulate anteroposterior axis elongation and somite segmentation during mouse embryogenesis. *Development, 133*(6), 989-999. doi:10.1242/dev.02274

Sauer, B., & Henderson, N. (1988). Site-specific DNA recombination in mammalian cells by the Cre recombinase of bacteriophage P1. *Proc Natl Acad Sci U S A, 85*(14), 5166-5170. doi:10.1073/pnas.85.14.5166

Schenke-Layland K, Nsair A, Van Handel B, Angelis E, Gluck JM, Votteler M, Goldhaber, J. I., Mikkola, H. K., Kahn, M., WR, M. (2011). Recapitulation of the embryonic cardiovascular progenitor cell niche. *Biomaterials, 32*(11), 2748-2756. doi:10.1016/j.biomaterials.2010.12.046

Schepers, K., Campbell, T. B., & Passegué, E. (2015). Normal and leukemic stem cell niches: insights and therapeutic opportunities. *Cell Stem Cell, 16*(3), 254-267. doi:10.1016/j.stem.2015.02.014

Schofield, R. (1978). The relationship between the spleen colony-forming cell and the haemopoietic stem cell. *Blood Cells, 4*(1-2), 7-25.

Schreck, Istvánffy, R., Ziegenhain, C., Sippenauer, T., Ruf, F., Henkel, L., Gärtner, F., Vieth, B., Florian, M. C., Mende, N., Taubenberger, A., Prendergast, A., Wagner, A., Pagel, C., Grziwok, S., Götze, K. S., Guck, J., Dean, D. C., Massberg, S., Essers, M., Waskow, C., Geiger, H., Schiemann, M., Peschel, C., Enard, W., Oostendorp, R. A. J. (2017). Niche WNT5A regulates the actin cytoskeleton during regeneration of hematopoietic stem cells. *J Exp Med, 214*(1), 165-181. doi:10.1084/jem.20151414

Schreck, C., Bock, F., Grziwok, S., Oostendorp, R. A. J., & Istvánffy, R. (2014). Regulation of hematopoiesis by activators and inhibitors of Wnt signaling from the niche. *Annals of the New York Academy of Sciences, 1310*(1), 32-43. doi:https://doi.org/10.1111/nyas.12384

Schuberth, C., & Buchberger, A. (2005). Membrane-bound Ubx2 recruits Cdc48 to ubiquitin ligases and their substrates to ensure efficient ER-associated protein degradation. *Nat Cell Biol, 7*(10), 999-1006. doi:10.1038/ncb1299

Schwarting, R., Gerdes, J., Niehus, J., Jaeschke, L., & Stein, H. (1986). Determination of the growth fraction in cell suspensions by flow cytometry using the monoclonal antibody Ki-67. *J Immunol Methods, 90*(1), 65-70. doi:10.1016/0022-1759(86)90384-4

Schwartzberg, P. L., Stall, A. M., Hardin, J. D., Bowdish, K. S., Humaran, T., Boast, S., Harbison, M. L., Robertson, E. J., Goff, S. P. (1991). Mice homozygous for the ablm1 mutation show poor viability and depletion of selected B and T cell populations. *Cell, 65*(7), 1165-1175. doi:10.1016/0092-8674(91)90012-n

Seeliger, B., Wilop, S., Osieka, R., Galm, O., & Jost, E. (2009). CpG island methylation patterns in chronic lymphocytic leukemia. *Leuk Lymphoma, 50*(3), 419-426. doi:10.1080/10428190902756594

Seita, J., & Weissman, I. L. (2010). Hematopoietic stem cell: self-renewal versus differentiation. *Wiley Interdiscip Rev Syst Biol Med, 2*(6), 640-653. doi:10.1002/wsbm.86

Sekiya, M., Maruko-Otake, A., Hearn, S., Sakakibara, Y., Fujisaki, N., Suzuki, E., Ando, K., Iijima, K. M. (2017). EDEM Function in ERAD Protects against Chronic ER Proteinopathy and Age-Related Physiological Decline in Drosophila. *Dev Cell, 41*(6), 652-664.e655. doi:10.1016/j.devcel.2017.05.019

Sesler, C. L., & Zayzafoon, M. (2013). NFAT signaling in osteoblasts regulates the hematopoietic niche in the bone microenvironment. *Clin Dev Immunol, 2013*, 107321. doi:10.1155/2013/107321

Sha, H., Sun, S., Francisco, A. B., Ehrhardt, N., Xue, Z., Liu, L., Lawrence, P., Mattijssen, F., Guber, R. D., Panhwar, M. S., Brenna, J. T., Shi, H., Xue, B., Kersten, S., Bensadoun, A., Péterfy, M., Long, Q., Qi, L. (2014). The ER-associated degradation adaptor protein Sel1L regulates LPL secretion and lipid metabolism. *Cell Metab, 20*(3), 458-470. doi:10.1016/j.cmet.2014.06.015

Shi, Y. (2009). Serine/threonine phosphatases: mechanism through structure. *Cell, 139*(3), 468-484. doi:10.1016/j.cell.2009.10.006

Shirasaki, R., Tashiro, H., Oka, Y., Matsuo, T., Yamamoto, T., Sugao, T., Akiyama, N., Shirafuji, N. (2012). Chronic Myelogenous Leukemia Cells Contribute to the Stromal Myofibroblasts in Leukemic NOD/SCID Mouse In Vivo. *J Oncol, 2012*, 901783. doi:10.1155/2012/901783

Shizuru, J. A., Negrin, R. S., & Weissman, I. L. (2005). Hematopoietic stem and progenitor cells: clinical and preclinical regeneration of the hematolymphoid system. *Annu Rev Med, 56*, 509-538. doi:10.1146/annurev.med.54.101601.152334

Short, B., Brouard, N., Driessen, R., & Simmons, P. J. (2001). Prospective isolation of stromal progenitor cells from mouse BM. *Cytotherapy, 3*(5), 407-408. doi:10.1080/146532401753277265

Skarnes, W. C., Rosen, B., West, A. P., Koutsourakis, M., Bushell, W., Iyer, V., Mujica, A. O., Thomas, M., Harrow, J., Cox, T., Jackson, D., Severin, J., Biggs, P., Fu, J., Nefedov, M., de Jong, P. J., Stewart, A. F., Bradley, A. (2011). A conditional knockout resource for the genome-wide study of mouse gene function. *Nature, 474*(7351), 337-342. doi:10.1038/nature10163

Sode, M., Burghardt, A. J., Kazakia, G. J., Link, T. M., & Majumdar, S. (2010). Regional variations of gender-specific and age-related differences in trabecular bone structure of the distal radius and tibia. *Bone, 46*(6), 1652-1660. doi:10.1016/j.bone.2010.02.021

Staal, F. J., & Clevers, H. (2000). Tcf/Lef transcription factors during T-cell development: unique and overlapping functions. *Hematol J, 1*(1), 3-6. doi:10.1038/sj.thj.6200001

Staal, F. J., Luis, T. C., & Tiemessen, M. M. (2008). WNT signalling in the immune system: WNT is spreading its wings. *Nat Rev Immunol, 8*(8), 581-593. doi:10.1038/nri2360

Stagg, J., Pommey, S., Eliopoulos, N., & Galipeau, J. (2006). Interferon-gamma-stimulated marrow stromal cells: a new type of nonhematopoietic antigen-presenting cell. *Blood, 107*(6), 2570-2577. doi:10.1182/blood-2005-07-2793

Stamos, J. L., & Weis, W. I. (2013). The β-catenin destruction complex. *Cold Spring Harb Perspect Biol, 5*(1), a007898. doi:10.1101/cshperspect.a007898

Stenderup, K., Justesen, J., Clausen, C., & Kassem, M. (2003). Aging is associated with decreased maximal life span and accelerated senescence of bone marrow stromal cells. *Bone, 33*(6), 919-926. doi:10.1016/j.bone.2003.07.005

Sternberg, N., & Hamilton, D. (1981). Bacteriophage P1 site-specific recombination. I. Recombination between loxP sites. *J Mol Biol, 150*(4), 467-486. doi:10.1016/0022-2836(81)90375-2

Sugimura, R., & Li, L. (2010). Noncanonical Wnt signaling in vertebrate development, stem cells, and diseases. *Birth Defects Res C Embryo Today, 90*(4), 243-256. doi:10.1002/bdrc.20195

Sugiyama, T., Kohara, H., Noda, M., & Nagasawa, T. (2006). Maintenance of the hematopoietic stem cell pool by CXCL12-CXCR4 chemokine signaling in bone marrow stromal cell niches. *Immunity, 25*(6), 977-988. doi:10.1016/j.immuni.2006.10.016

Sun, S., Shi, G., Han, X., Francisco, A. B., Ji, Y., Mendonça, N., Liu, X., Locasale, J. W., Simpson, K. W., Duhamel, G. E., Kersten, S., Yates III, J. R., Long, Q., Qi, L. (2014). Sel1L is indispensable for mammalian endoplasmic reticulum-associated degradation, endoplasmic reticulum homeostasis, and survival. *Proceedings of the National Academy of Sciences, 111*(5), E582-E591. doi:10.1073/pnas.1318114111

Szade, K., Gulati, G. S., Chan, C. K. F., Kao, K. S., Miyanishi, M., Marjon, K. D., Sinha, R., George, B. M., Chen, J. Y., Weissman, I. L. (2018). Where Hematopoietic Stem Cells Live: The Bone Marrow Niche. *Antioxid Redox Signal, 29*(2), 191-204. doi:10.1089/ars.2017.7419

Szulc, P., Naylor, K., Pickering, M. E., Hoyle, N., Eastell, R., & Leary, E. (2018). [Use of CTX-I and PINP as bone turnover markers: National Bone Health Alliance recommendations to standardize sample handling and patient preparation to reduce pre-analytical variability]. *Ann Biol Clin (Paris), 76*(4), 373-391. doi:10.1684/abc.2018.1363

Taichman, R. S., & Emerson, S. G. (1998). The role of osteoblasts in the hematopoietic microenvironment. *Stem Cells, 16*(1), 7-15. doi:10.1002/stem.160007

Taichman, R. S., Reilly, M. J., & Emerson, S. G. (2000). The Hematopoietic Microenvironment: Osteoblasts and The Hematopoietic Microenvironment. *Hematology, 4*(5), 421-426.

Tak, T., van Groenendael, R., Pickkers, P., & Koenderman, L. (2017). Monocyte Subsets Are Differentially Lost from the Circulation during Acute Inflammation Induced by Human Experimental Endotoxemia. *J Innate Immun, 9*(5), 464-474. doi:10.1159/000475665

Takada, T., Yagi, Y., Maekita, T., Imura, M., Nakagawa, S., Tsao, S. W., Miyamoto, K., Yoshino, O., Yasugi, T., Taketani, Y., Ushijima, T. (2004). Methylation-associated silencing of the Wnt antagonist SFRP1 gene in human ovarian cancers. *Cancer Sci, 95*(9), 741-744. doi:10.1111/j.1349-7006.2004.tb03255.x

Takemaru, K.-I., & Moon, R. T. (2000). The Transcriptional Coactivator Cbp Interacts with β-Catenin to Activate Gene Expression. *Journal of Cell Biology, 149*(2), 249-254. doi:10.1083/jcb.149.2.249

Takizawa, H., & Manz, M. G. (2017). Impact of inflammation on early hematopoiesis and the microenvironment. *Int J Hematol, 106*(1), 27-33. doi:10.1007/s12185-017-2266-5

Takubo, K., Morikawa, T., & Kobayashi, H. (2017). Abnormal hematopoiesis and hematopoietic stem cell niche. *Rinsho Ketsueki, 58*(10), 1844-1850. doi:10.11406/rinketsu.58.1844

Teo, J. L., & Kahn, M. (2010). The Wnt signaling pathway in cellular proliferation and differentiation: A tale of two coactivators. *Adv Drug Deliv Rev, 62*(12), 1149-1155. doi:10.1016/j.addr.2010.09.012

Teo, J. L., Ma, H., Nguyen, C., Lam, C., & Kahn, M. (2005). Specific inhibition of CBP/beta-catenin interaction rescues defects in neuronal differentiation caused by a presenilin-1 mutation. *Proc Natl Acad Sci U S A, 102*(34), 12171-12176. doi:10.1073/pnas.0504600102

Thorrez, L., Van Deun, K., Tranchevent, L. C., Van Lommel, L., Engelen, K., Marchal, K., Moreau, Y., Mechelen, I. V., Schuit, F. (2008). Using ribosomal protein genes as reference: a tale of caution. *PLOS ONE, 3*(3), e1854. doi:10.1371/journal.pone.0001854

Tikhonova, A. N., Dolgalev, I., Hu, H., Sivaraj, K. K., Hoxha, E., Cuesta-Domínguez, Á., Pinho, S., Akhmetzyanova, I., Gao, J., Witkowski, M., Guillamot, M., Gutkin, M. C., Zhang, Y., Marier, C., Diefenbach, C., Kousteni, S., Heguy, A., Zhong, H., Fooksman, D. R., Butler, J. M., Economides, A., Frenette, P.S., Adams, R. H., Satija, R., Tsirigos, A., Aifantis, I. (2019). The bone marrow microenvironment at single-cell resolution. *Nature, 569*(7755), 222-228. doi:10.1038/s41586-019-1104-8

To, K. F., Chan, M. W., Leung, W. K., Yu, J., Tong, J. H., Lee, T. L., Chan, F. K., Sung, J. J. (2001). Alterations of frizzled (FzE3) and secreted frizzled related protein (hsFRP) expression in gastric cancer. *Life Sci, 70*(4), 483-489. doi:10.1016/s0024-3205(01)01422-9

Topol, L., Jiang, X., Choi, H., Garrett-Beal, L., Carolan, P. J., & Yang, Y. (2003). Wnt-5a inhibits the canonical Wnt pathway by promoting GSK-3-independent beta-catenin degradation. *J Cell Biol, 162*(5), 899-908. doi:10.1083/jcb.200303158

Trevant, B., Gaur, T., Hussain, S., Symons, J., Komm, B. S., Bodine, P. V., Stein, G. S., Lian, J. B. (2008). Expression of secreted frizzled related protein 1, a Wnt antagonist, in brain, kidney, and skeleton is dispensable for normal embryonic development. *J Cell Physiol, 217*(1), 113-126. doi:10.1002/jcp.21482

Turashvili, G., Bouchal, J., Burkadze, G., & Kolar, Z. (2006). Wnt signaling pathway in mammary gland development and carcinogenesis. *Pathobiology, 73*(5), 213-223. doi:10.1159/000098207

Tybulewicz, V. L., Crawford, C. E., Jackson, P. K., Bronson, R. T., & Mulligan, R. C. (1991). Neonatal lethality and lymphopenia in mice with a homozygous disruption of the c-abl proto-oncogene. *Cell, 65*(7), 1153-1163. doi:10.1016/0092-8674(91)90011-m

Ugai, H., Uchida, K., Kawasaki, H., Yokoyama, K. K. (1999) The coactivators p300 and CBP have different functions during the differentiation of F9 cells. *J Mol Med (Berl)*, *77*(6), 481-94. doi: 10.1007/s001099900021

Ugolini, F., Adélaïde, J., Charafe-Jauffret, E., Nguyen, C., Jacquemier, J., Jordan, B., Birnbaum, D., Pébusque, M. J. (1999). Differential expression assay of chromosome arm 8p genes identifies Frizzled-related (FRP1/FRZB) and Fibroblast Growth Factor Receptor 1 (FGFR1) as candidate breast cancer genes. *Oncogene, 18*(10), 1903-1910. doi:10.1038/sj.onc.1202739

van de Wetering, M., Sancho, E., Verweij, C., de Lau, W., Oving, I., Hurlstone, A., van der Horn, K., Batlle, E., Coudreuse, D., Haramis, A. P., Tjon-Pon-Fong, M., Moerer, P., van den Born, M., Soete, G., Pals, S., Eilers, M., Medema, R., Clevers, H. (2002). The beta-catenin/TCF-4 complex imposes a crypt progenitor phenotype on colorectal cancer cells. *Cell, 111*(2), 241-250. doi:10.1016/s0092-8674(02)01014-0

Vincent, K. M., & Postovit, L.-M. (2017). A pan-cancer analysis of secreted Frizzled-related proteins: re-examining their proposed tumour suppressive function. *Scientific Reports, 7*(1), 42719. doi:10.1038/srep42719

Visweswaran, M., Schiefer, L., Arfuso, F., Dilley, R. J., Newsholme, P., & Dharmarajan, A. (2015). Wnt Antagonist Secreted Frizzled-Related Protein 4 Upregulates Adipogenic Differentiation in Human Adipose Tissue-Derived Mesenchymal Stem Cells. *PLOS ONE, 10*(2), e0118005. doi:10.1371/journal.pone.0118005

Voncken, J. W., van Schaick, H., Kaartinen, V., Deemer, K., Coates, T., Landing, B., Pattengale, P., Dorseuil, O., Bokoch, G. M., Groffen, J., Heisterkamp, N. (1995). Increased neutrophil respiratory burst in bcr-null mutants. *Cell, 80*(5), 719-728. doi:10.1016/0092-8674(95)90350-x

Waclawiczek, A., Hamilton, A., Rouault-Pierre, K., Abarrategi, A., Albornoz, M. G., Miraki-Moud, F., Bah, N., Gribben, J., Fitzgibbon, J., Taussig, D., Bonnet, D. (2020). Mesenchymal niche remodeling impairs hematopoiesis via stanniocalcin 1 in acute myeloid leukemia. *J Clin Invest, 130*(6), 3038-3050. doi:10.1172/jci133187

Walter, D., Lier, A., Geiselhart, A., Thalheimer, F. B., Huntscha, S., Sobotta, M. C., Moehrle, B., Brocks, D., Bayindir, I., Kaschutnig, P., Muedder, K., Klein, C., Jauch, A., Schroeder, T., Geiger, H., Dick, T. P., Holland-Letz, T., Schmezer, P., Lane, S. W., Rieger, M. A., Essers, M. A. G., Williams, D. A., Trumpp, A., Milsom, M. D. (2015). Exit from dormancy provokes DNA-damage-induced attrition in haematopoietic stem cells. *Nature, 520*(7548), 549-552. doi:10.1038/nature14131

Wang, J. Y. (2014). The capable ABL: what is its biological function? *Mol Cell Biol, 34*(7), 1188-1197. doi:10.1128/mcb.01454-13

Wang, Y., Krivtsov, A. V., Sinha, A. U., North, T. E., Goessling, W., Feng, Z., Zon, L. I., Armstrong, S. A. (2010). The Wnt/beta-catenin pathway is required for the development of leukemia stem cells in AML. *Science, 327*(5973), 1650-1653. doi:10.1126/science.1186624

Ward, J. M. (2006). Lymphomas and leukemias in mice. *Exp Toxicol Pathol, 57*(5-6), 377-381. doi:10.1016/j.etp.2006.01.007

Warde-Farley, D., Donaldson, S. L., Comes, O., Zuberi, K., Badrawi, R., Chao, P., Franz, M., Grouios, C., Kazi, F., Lopes, C. T., Maitland, A., Mostafavi, S., Montojo, J., Shao, Q., Wright, G., Bader G. D., Morris, Q. (2010). The GeneMANIA prediction server: biological network integration for gene prioritization and predicting gene function. *Nucleic Acids Res, 38*(Web Server issue), W214-220. doi:10.1093/nar/gkq537

Wei, C., Zeff, R., & Goldschneider, I. (2000). Murine pro-B cells require IL-7 and its receptor complex to up-regulate IL-7R alpha, terminal deoxynucleotidyltransferase, and c mu expression. *J Immunol, 164*(4), 1961-1970. doi:10.4049/jimmunol.164.4.1961

Weidner, H., Baschant, U., Lademann, F., Ledesma Colunga,, M. G., Balaian, E.,2 Hofbauer, C., Misof, B. M., Roschger, P., Blouin, S., Richards, W. G., Platzbecker, U., Hofbauer, L. C., Rauner, M. (2020). *JCI Insight*, *5*(15), e137062. https://doi.org/10.1172/jci.insight.137062.

Weissman, I. L., Anderson, D. J., & Gage, F. (2001). Stem and progenitor cells: origins, phenotypes, lineage commitments, and transdifferentiations. *Annu Rev Cell Dev Biol, 17*, 387-403. doi:10.1146/annurev.cellbio.17.1.387

Welch, J. S., Ley, T. J., Link, D. C., Miller, C. A., Larson, D. E., Koboldt, D. C., Wartman, L. D., Lamprecht, T. L., Liu, F., Xia, J., Kandoth, C., Fulton, R. S., McLellan, M. D., Dooling, D. J., Wallis, J. W., Chen, K., Harris, C. C., Schmidt, H. K., Kalicki-Veizer, J. M., Lu, C., Zhang, Q., Lin, L., O'Laughlin, M. D., McMichael, J. F., Delehaunty, K. D., Fulton, L.A., Magrini, V. J., McGrath, S. D., Demeter, R. T., Vickery, T. L., Hundal, J., Cook, L. L., Swift, G. W., Reed, J. P., Alldredge, P. A., Wylie, T. N., Walker, J. R., Watson, M. A., Heath, S. E., Shannon, W. D., Varghese, N., Nagarajan, R., Payton, J. E., Baty, J. D., Kulkarni, S., Klco, J. M., Tomasson, M. H., Westervelt, P., Walter, M. J., Graubert, T. A., DiPersio, J. F., Ding, L., Mardis, E. R., Wilson, R. K. (2012). The origin and evolution of mutations in acute myeloid leukemia. *Cell, 150*(2), 264-278. doi:10.1016/j.cell.2012.06.023

Wend, P., Fang, L., Zhu, Q., Schipper, J. H., Loddenkemper, C., Kosel, F., Brinkmann, V., Eckert, K., Hindersin, S., Holland, J.D., Lehr, S., Kahn, M., Ziebold, U., Birchmeier, W. (2013). Wnt/β-catenin signalling induces MLL to create epigenetic changes in salivary gland tumours. *Embo j, 32*(14), 1977-1989. doi:10.1038/emboj.2013.127

West, L. J., Morris, P. J., & Wood, K. J. (1994). Fetal liver haematopoietic cells and tolerance to organ allografts. *Lancet, 343*(8890), 148-149. doi:10.1016/s0140-6736(94)90936-9

Willert, K., Brown, J. D., Danenberg, E., Duncan, A. W., Weissman, I. L., Reya, T., Yates 3rd, J. R., Nusse, R. (2003). Wnt proteins are lipid-modified and can act as stem cell growth factors. *Nature, 423*(6938), 448-452. doi:10.1038/nature01611

Williams, R. T., & Sherr, C. J. (2007). The ARF tumor suppressor in acute leukemias: insights from mouse models of Bcr-Abl-induced acute lymphoblastic leukemia. *Adv Exp Med Biol, 604*, 107-114. doi:10.1007/978-0-387-69116-9_9

Wilson, A., Laurenti, E., Oser, G., van der Wath, R. C., Blanco-Bose, W., Jaworski, M., Offner, S., Dunant, C. F., Eshkind, L., Bockamp, E., Lió, P., Macdonald, H. R., Trumpp, A. (2008). Hematopoietic stem cells reversibly switch from dormancy to self-renewal during homeostasis and repair. *Cell, 135*(6), 1118-1129. doi:10.1016/j.cell.2008.10.048

Wilson, A., Oser, G. M., Jaworski, M., Blanco-Bose, W. E., Laurenti, E., Adolphe, C., Essers, M. A., Macdonald, H. R., Trumpp, A. (2007). Dormant and self-renewing hematopoietic stem cells and their niches. *Ann N Y Acad Sci, 1106*, 64-75. doi:10.1196/annals.1392.021

Wilson, A., Shehadeh, L. A., Yu, H., & Webster, K. A. (2010). Age-related molecular genetic changes of murine bone marrow mesenchymal stem cells. *BMC Genomics, 11*(1), 229. doi:10.1186/1471-2164-11-229

Wilson, A., & Trumpp, A. (2006). Bone-marrow haematopoietic-stem-cell niches. *Nat Rev Immunol, 6*(2), 93-106. doi:10.1038/nri1779

Winkler, I. G., Sims, N. A., Pettit, A. R., Barbier, V., Nowlan, B., Helwani, F., Poulton, I. J., van Rooijen, N., Alexander, K. A., Raggatt, L. J., Lévesque, J. P. (2010). Bone marrow macrophages maintain hematopoietic stem cell (HSC) niches and their depletion mobilizes HSCs. *Blood, 116*(23), 4815-4828. doi:10.1182/blood-2009-11-253534

Wiseman, D. H. (2011). Donor cell leukemia: a review. *Biol Blood Marrow Transplant, 17*(6), 771-789. doi:10.1016/j.bbmt.2010.10.010

Wohrer, S., Knapp, D. J., Copley, M. R., Benz, C., Kent, D. G., Rowe, K., Babovic, S., Mader, H., Oostendorp, R. A. J., Eaves, C. J. (2014). Distinct stromal cell factor combinations can separately control hematopoietic stem cell survival, proliferation, and self-renewal. *Cell Rep, 7*(6), 1956-1967. doi:10.1016/j.celrep.2014.05.014
Wolf, L. M., Lambert, A. M., Haenlin, J., & Boutros, M. (2021). EVI/WLS function is regulated by ubiquitination and linked to ER-associated degradation by ERLIN2. *J Cell Sci*. doi:10.1242/jcs.257790

Woll, P. S., Kjällquist, U., Chowdhury, O., Doolittle, H., Wedge, D. C., Thongjuea, S., Erlandsson, R., Ngara, M., Anderson, K., Deng, Q., Mead, A. J., Stenson, L., Giustacchini, A., Duarte, S., Giannoulatou, E., Taylor, S., Karimi, M., Scharenberg, C., Mortera-Blanco, T., Macaulay, I. C., Clark, S.-A., Dybedal, I., Josefsen, D., Fenaux, P., Hokland, P., Holm, M. S., Cazzola, M., Malcovati, L., Tauro, S., Bowen, D., Boultwood, J., Pellagatti, A., Pimanda, J. E., Unnikrishnan, A., Vyas, P., Göhring, G., Schlegelberger, B., Tobiasson, M., Kvalheim, G., Constantinescu, S. N., Nerlov, C., Nilsson, L., Campbell, P. J., Sandberg, R., Papaemmanuil, E., Hellström-Lindberg, E., Linnarsson, S., Jacobsen, S. E. W. (2014). Myelodysplastic syndromes are propagated by rare and distinct human cancer stem cells in vivo. *Cancer Cell, 25*(6), 794-808. doi:10.1016/j.ccr.2014.03.036

Woll, P. S., Morris, J. K., Painschab, M. S., Marcus, R. K., Kohn, A. D., Biechele, T. L., Moon, R. T., Kaufman, D. S. (2008). Wnt signaling promotes hematoendothelial cell development from human embryonic stem cells. *Blood, 111*(1), 122-131. doi:10.1182/blood-2007-04-084186

Wolock, S. L., Krishnan, I., Tenen, D. E., Matkins, V., Camacho, V., Patel, S., Agarwal, P., Bhatia, R., Tenen, D. G., Klein, A. M., Welner, R. S. (2019). Mapping Distinct Bone Marrow Niche Populations and Their Differentiation Paths. *Cell Rep, 28*(2), 302-311.e305. doi:10.1016/j.celrep.2019.06.031

Wong, H. C., Bourdelas, A., Krauss, A., Lee, H. J., Shao, Y., Wu, D., Mlodzik, M., Shi, D.-L., Zheng, J. (2003). Direct binding of the PDZ domain of Dishevelled to a conserved internal sequence in the C-terminal region of Frizzled. *Mol Cell, 12*(5), 1251-1260. doi:10.1016/s1097-2765(03)00427-1

Xu, L., Liu, X., Peng, F., Zhang, W., Zheng, L., Ding, Y., Gu, T., Lv, K., Wang, J., Ortinau, L., Hu, T., Shi, X., Shi, G., Shang, G., Sun, S., Iwawaki, T., Ji, Y., Li, W., Rosen, J. M., Zhang, X. H., Park, D., Adoro, S., Catic, A., Tong, W., Qi, L., Nakada, D., Chen, X. (2020) Protein quality control through endoplasmic reticulum-associated degradation maintains haematopoietic stem cell identity and niche interactions. *Nat Cell Biol*, *22*(10), 1162-1169. doi: 10.1038/s41556-020-00581-x

Yamashita, M., Dellorusso, P. V., Olson, O. C., & Passegué, E. (2020). Dysregulated haematopoietic stem cell behaviour in myeloid leukaemogenesis. *Nat Rev Cancer, 20*(7), 365-382. doi:10.1038/s41568-020-0260-3

Yang, W., Zhang, S., Ou, T., Jiang, H., Jia, D., Qi, Z., Zou, Y., Qian, J., Sun, A., Ge, J. (2020). Interleukin-11 regulates the fate of adipose-derived mesenchymal stem cells via STAT3 signalling pathways. *Cell Prolif, 53*(5), e12771. doi:10.1111/cpr.12771

Yao, T. P., Oh, S. P., Fuchs, M., Zhou, N. D., Ch'ng, L. E., Newsome, D., Bronson, R. T., Livingston, D. M., Eckner, R. (1998). Gene dosage-dependent embryonic development and proliferation defects in mice lacking the transcriptional integrator p300. *Cell, 93*(3), 361-372. doi:10.1016/s0092-8674(00)81165-4

Yao, W., Cheng, Z., Shahnazari, M., Dai, W., Johnson, M. L., & Lane, N. E. (2010). Overexpression of secreted frizzled-related protein 1 inhibits bone formation and attenuates parathyroid hormone bone anabolic effects. *J Bone Miner Res, 25*(2), 190-199. doi:10.1359/jbmr.090719

Ye, M., Zhang, H., Yang, H., Koche, R., Staber, P. B., Cusan, M., Levantini, E., Welner, R. S., Bach, C. S., Zhang, J., Krivtsov, A. V., Armstrong, S. A., Tenen, D. G. (2015) Hematopoietic Differentiation Is Required for Initiation of Acute Myeloid Leukemia. *Cell Stem Cell*, *17*(5), 611-23. doi: 10.1016/j.stem.2015.08.011

Yoder, M. C., Cumming, J. G., Hiatt, K., Mukherjee, P., & Williams, D. A. (1996). A novel method of myeloablation to enhance engraftment of adult bone marrow cells in newborn mice. *Biol Blood Marrow Transplant, 2*(2), 59-67.

Yokota, T., Oritani, K., Garrett, K. P., Kouro, T., Nishida, M., Takahashi, I., Ichii, M., Satoh, Y., Kincade, P. W., Kanakura, Y. (2008). Soluble frizzled-related protein 1 is estrogen inducible in bone marrow stromal cells and suppresses the earliest events in lymphopoiesis. *J Immunol, 181*(9), 6061-6072. doi:10.4049/jimmunol.181.9.6061

Yokota, T., Oritani, K., Sudo, T., Ishibashi, T., Doi, Y., Habuchi, Y., Ichii, M., Fukushima, K., Okuzaki, D., Tomizuka, K., Yamawaki, K., Kakitani, M., Shimono, A., Morii, E., Kincade, P. W., Kanakura, Y. (2015). Estrogen-inducible sFRP5 inhibits early B-lymphopoiesis in vivo, but not during pregnancy. *Eur J Immunol, 45*(5), 1390-1401. doi:https://doi.org/10.1002/eji.201444939

Yoshino, K., Rubin, J. S., Higinbotham, K. G., Uren, A., Anest, V., Plisov, S. Y., & Perantoni, A. O. (2001). Secreted Frizzled-related proteins can regulate metanephric development. *Mech Dev, 102*(1-2), 45-55. doi:10.1016/s0925-4773(01)00282-9

Yu, G., Wang, L. G., Han, Y., & He, Q. Y. (2012). clusterProfiler: an R package for comparing biological themes among gene clusters. *Omics, 16*(5), 284-287. doi:10.1089/omi.2011.0118

Yuan, Y., Niu, C. C., Deng, G., Li, Z. Q., Pan, J., Zhao, C., Yang, Z. L., Si, W. K. (2011). The Wnt5a/Ror2 noncanonical signaling pathway inhibits canonical Wnt signaling in K562 cells. *Int J Mol Med, 27*(1), 63-69. doi:10.3892/ijmm.2010.560

Yücel, G., Zhao, Z., El-Battrawy, I., Lan, H., Lang, S., Li, X., Buljubasic, F., Zimmermann, W.-H., Cyganek, L., Utikal, J., Ravens, U., Wieland, T., Borggrefe, M., Zhou, X.-B., Akin, I. (2017). Lipopolysaccharides induced inflammatory responses and electrophysiological dysfunctions in human-induced pluripotent stem cell derived cardiomyocytes. *Scientific Reports, 7*(1), 2935. doi:10.1038/s41598-017-03147-4

Zaini, M. A., Müller, C., de Jong, T. V., Ackermann, T., Hartleben, G., Kortman, G., Gührs, K. H., Fusetti, F., Krämer, O. H., Guryev, V., Calkhoven, C. F. (2018) A p300 and SIRT1 Regulated Acetylation Switch of C/EBPα Controls Mitochondrial Function. *Cell Rep*, *22*(2), 497-511. doi: 10.1016/j.celrep.2017.12.061

Zambetti, N. A., Ping, Z., Chen, S., Kenswil, K. J. G., Mylona, M. A., Sanders, M. A., Hoogenboezem, R. M., Bindels, E. M. J., Adisty, M. N., Van Strien, P. M. H., van der Leije, C. S., Westers, T. M., Cremers, E. M. P., Milanese, C., Mastroberardino, P. G., van Leeuwen, J. P. T. M., van der Eerden, B. C. J., Touw, I. P., Kuijpers, T. W., Kanaar, R., van de Loosdrecht, A. A., Vogl, T., Raaijmakers, M. H. G. P. (2016). Mesenchymal Inflammation Drives Genotoxic Stress in Hematopoietic Stem Cells and Predicts Disease Evolution in Human Pre-leukemia. *Stem Cell Research, 19*(5), 613-627. doi:https://doi.org/10.1016/j.stem.2016.08.021

Zechner, D., Fujita, Y., Hülsken, J., Müller, T., Walther, I., Taketo, M. M., Crenshaw 3rd, E. B., Birchmeier, W., Birchmeier, C. (2003). beta-Catenin signals regulate cell growth and the balance between progenitor cell expansion and differentiation in the nervous system. *Dev Biol, 258*(2), 406-418. doi:10.1016/s0012-1606(03)00123-4

Zeng, L., Zhang, Q., Gerona-Navarro, G., Moshkina, N., & Zhou, M. M. (2008). Structural basis of site-specific histone recognition by the bromodomains of human coactivators PCAF and CBP/p300. *Structure, 16*(4), 643-652. doi:10.1016/j.str.2008.01.010

Zeng, W., Wharton, K. A., Jr., Mack, J. A., Wang, K., Gadbaw, M., Suyama, K., Klein, P. S., Scott, M. P. (2000). naked cuticle encodes an inducible antagonist of Wnt signalling. *Nature, 403*(6771), 789-795. doi:10.1038/35001615

Zhang, J., Niu, C., Ye, L., Huang, H., He, X., Tong, W. G., Ross, J., Haug, J., Johnson, T., Feng, J. Q., Harris, S., Wiedemann, L. M., Mishina, Y., Li, L. (2003). Identification of the haematopoietic stem cell niche and control of the niche size. *Nature, 425*(6960), 836-841. doi:10.1038/nature02041

Zhao, C., Blum, J., Chen, A., Kwon, H. Y., Jung, S. H., Cook, J. M., Lagoo, A., Reya, T. (2007). Loss of beta-catenin impairs the renewal of normal and CML stem cells in vivo. *Cancer Cell, 12*(6), 528-541. doi:10.1016/j.ccr.2007.11.003

Zhao, C., Wu, M., Zeng, N., Xiong, M., Hu, W., Lv, W., Yi, Y., Zhang, Q., Wu, Y. (2020). Cancer-associated adipocytes: emerging supporters in breast cancer. *J Exp Clin Cancer Res, 39*(1), 156. doi:10.1186/s13046-020-01666-z

Zhao, Y., Wu, K., Nguyen, C., Smbatyan, G., Melendez, E., Higuchi, Y., Chen, Y., Kahn, M. (2017). Small molecule p300/catenin antagonist enhances hematopoietic recovery after radiation. *PLOS ONE, 12*(5), e0177245. doi:10.1371/journal.pone.0177245

Zheng, H., Martin, J. A., Duwayri, Y., Falcon, G., & Buckwalter, J. A. (2007). Impact of Aging on Rat Bone Marrow-Derived Stem Cell Chondrogenesis. *The Journals of Gerontology: Series A, 62*(2), 136-148. doi:10.1093/gerona/62.2.136

Zhong, L., Yao, L., Tower, R. J., Wei, Y., Miao, Z., Park, J., Shrestha, R., Wang, L., Yu, W., Holdreith, N., Huang, X., Zhang, Y., Tong, W., Gong, Y., Ahn, J., Susztak, K., Dyment, N., Li, M., Long, F., Chen, C., Seale, P., Qin, L. (2020). Single cell transcriptomics identifies a unique adipose lineage cell population that regulates bone marrow environment. *Elife, 9*. doi:10.7554/eLife.54695

Zhong, X., & Jin, Y. (2009). Critical roles of coactivator p300 in mouse embryonic stem cell differentiation and Nanog expression. *J Biol Chem, 284*(14), 9168-9175. doi:10.1074/jbc.M805562200

Zhou, Z., Wang, J., Han, X., Zhou, J., & Linder, S. (1998). Up-regulation of human secreted frizzled homolog in apoptosis and its down-regulation in breast tumors. *Int J Cancer, 78*(1), 95-99. doi:10.1002/(sici)1097-0215(19980925)78:1<95::aid-ijc15>3.0.co;2-4

Zhu, H., Guo, Z. K., Jiang, X. X., Li, H., Wang, X. Y., Yao, H. Y., Zhang, Y., Mao, N. (2010). A protocol for isolation and culture of mesenchymal stem cells from mouse compact bone. *Nat Protoc, 5*(3), 550-560. doi:10.1038/nprot.2009.238

Zi, X., Guo, Y., Simoneau, A. R., Hope, C., Xie, J., Holcombe, R. F., & Hoang, B. H. (2005). Expression of Frzb/secreted Frizzled-related protein 3, a secreted Wnt antagonist, in human androgen-independent prostate cancer PC-3 cells suppresses tumor growth and cellular invasiveness. *Cancer Res, 65*(21), 9762-9770. doi:10.1158/0008-5472.Can-05-0103